

*Contrails*



**A DESIGN PROCEDURE AND HANDLING-QUALITY  
CRITERIA FOR LATERAL-DIRECTIONAL  
FLIGHT CONTROL SYSTEMS**

*GUNTER STEIN  
ALLEN H. HENKE*

71-26,774

Approved for public release; distribution unlimited.

## FOREWORD

The present study is part of a U.S. Air Force research program to design practical, optimal aircraft flight control systems which are based on handling-quality criteria and verified by a simulation program. The principal investigators were G. Stein and A.H. Henke of Honeywell Inc. Systems and Research Center. The project engineers were P. Pietrzak and Lt. K. Bassett of the Flight Control Division of the Air Force Flight Dynamics Laboratory whose valuable assistance in monitoring the work and whose help, especially during the WPAFB simulations, were greatly appreciated. Lt. Bassett was preceded by Maj. R. Lorenzetti, Lt. Col. W. Knox, and Duane Rubertus. Their help is also gratefully acknowledged. The results were gathered under Project Nos. 8219, and 8225, Contract No. F33615-70-C-1190, sponsored by the Air Force Flight Dynamics Laboratory.

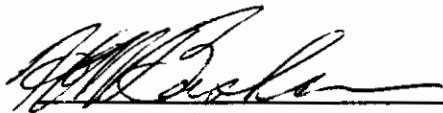
The authors gratefully acknowledge the assistance of E.D. Skelley of Honeywell Systems and Research Center whose contributions to the planning and execution of the simulation efforts at both Honeywell and WPAFB significantly contributed to the success of this program.

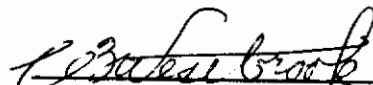
Further, we are indebted to R. Haas and Capt. F. Unfried for providing excellent support and technical expertise during the simulation effort at WPAFB. Their assistance was invaluable.

Finally, we acknowledge our appreciation to the willing and capable subjects who supplied us with their valuable time and talents: Major R. Keller (4950 TW/FTFF), Major W. Schob (ASD/YFT), R. Stewart (Honeywell), R. Pratt (Northwest Airlines), T. Higgins (Northwest Airlines), Major J. Smith (TACSO-A), Major R. Ettinger (4950 TW/FTFF), Lt. Col. T. Hosch (FTD/PDXD), and Capt. D. Zieg (4950 TW/FTFF).

The manuscript was released by the authors in October 1970. The number assigned to this report by Honeywell Systems and Research Center is 12212-FR.

This technical report has been reviewed and is approved.

  
H. W. Basham  
Chief-Control Elements Branch  
Flight Control Division  
AFFDL

  
C. B. Westbrook  
Chief-Control Criteria Branch  
Flight Control Division  
AFFDL

## ABSTRACT

This program develops a practical design procedure for aircraft augmentation systems based on quadratic optimal control technology and handling-quality-oriented cost functionals. The procedure is applied to the design of a lateral-directional control system for the F4C aircraft. The design criteria, design procedure, and final control system are validated with a program of formal pilot evaluation experiments. These use 5 x 2 x 3 mixed-design analysis of variance. A reformulated optimal model-following control problem is used as the cornerstone for the procedure. Design criteria are expressed as model differential equations satisfying available handling-quality data. The reformulation includes optimality over multiple flight conditions and constant gain and measurement realizability constraints. A computational algorithm is developed to solve the new optimization problem. The algorithm successfully handled 20th-order F4C lateral-axes dynamics and optimized five flight conditions simultaneously. The results of the validation experiments were fully positive with strong correlation between performance and pilot opinion data.

# *Contrails*



# Contrails

## TABLE OF CONTENTS

		Page
SECTION I	INTRODUCTION AND SUMMARY	1
	The Design Procedure	1
	Validation Procedure	3
	Summary of Results	4
	Outline of the Report	5
SECTION II	DESIGN CRITERIA	7
	Philosophy	7
	Handling-Quality Models	9
	The Model Form	9
	Specifications	11
	Numerical Values for the F4C Lateral Axes	15
SECTION III	DESIGN MECHANICS	22
	Optimal Model-Following Control	22
	Practical Model-Following Control	25
	Problem Reformulation	26
	Necessary Conditions of Optimality	27
	Computational Solutions	29
SECTION IV	LATERAL-AXIS DESIGNS FOR THE F4C	33
	Mathematical Models	33
	Rigid Body	34
	Approximated Flexure	45
	Actuators and Servos	46
	Sensors	49
	Gust Model	51
	Handling-Quality Models	52
	Command Models	55
	Optimal Model-Following Designs	57
	Baseline Designs at FC(2)	59
	Command Bandwidth Study	71
	Other Optimal Controllers	71
	Performance Sensitivity	86
	Gain Sensitivity	86
	Practical Controller Designs	91
	Single-Flight-Condition Cases	94
	Multiple-Flight-Condition Cases	97
	Hindsight and Interpretations	120

# Contrails

## TABLE OF CONTENTS -- CONTINUED

	Page	
SECTION V	VALIDATION METHOD	123
	Introduction	123
	The Experimental Design	123
	Independent Variables	124
	Dependent Variables	125
	The Task	127
	Subjects	128
	Simulation Equipment	129
	The WPAFB Simulation	130
	Minneapolis Simulation	134
	Validation Procedure	139
	Familiarization	139
	Phase I - Performance Data Collection	140
	Phase II - Rating Scale Collection	141
	Minneapolis/WPAFB Procedural Differences	141
SECTION VI	RESULTS OF VALIDATION PROGRAM	142
	Method of Analysis	
	Data Sources	143
	A Qualitative Look at the Data	145
	Lateral Error at WPAFB	145
	Cooper-Harper Ratings at WPAFB	148
	Quantitative Analysis	150
	Lateral Error at WPAFB	150
	Cooper-Harper Data at WPAFB	154
	Other Data Sources	156
	Summary of Results	167
SECTION VII	CONCLUSIONS	169
APPENDIX I	HANDLING-QUALITIES DATA	171
APPENDIX II	EVALUATION OF $\partial J / \partial K^1$ , $\partial^2 J / \partial K^1 \partial K^{1T}$ , AND $\partial^2 J / \partial K^1 \partial \lambda$	180
APPENDIX III	BENDING MODE EQUATIONS	185
APPENDIX IV	TRANSFORMATION MATRICES $T_{rb}$ , FOR THE AIRFRAME	192
APPENDIX V	QUALITATIVE CHARACTERISTICS AND FORMAL EXPERIMENTAL TRIALS OF PRACTICAL CONTROLLER 7	194
APPENDIX VI	GENERATION OF FLIGHT PROFILES, LONGITUDINAL-LATERAL COMMAND EQUATIONS, AND LISTING OF FLIGHT PROFILES	212

TABLE OF CONTENTS -- CONCLUDED

		Page
APPENDIX VII	TRANSIENT RESPONSES OF THE WPAFB AND MINNEAPOLIS SIMULATIONS	216
APPENDIX VIII	TRAINING TRIAL SEQUENCES FOR MINNEAPOLIS AND WPAFB (3 SUBJECTS)	232
APPENDIX IX	DATA TRIAL SEQUENCES FOR MINNEAPOLIS AND WPAFB (3 SUBJECTS)	233
APPENDIX X	EXPERIENCE QUESTIONNAIRE, AND GLOBAL AND COOPER -HARPER RATING SCALES AD- MINISTERED TO ALL SUBJECTS AT MINNEAPOLIS, WPAFB (3SUBJECTS), AND WPAFB (4 SUBJECTS)	236
APPENDIX XI	RAW RATING DATA	241
REFERENCES		244

## LIST OF ILLUSTRATIONS

Figure		Page
1	Step Responses -- Model 1	17
2	Step Responses -- Model 2	17
3	Step Responses -- Model 3	18
4	Step Responses -- Model 4	18
5	Zero-Pole Relationships -- Free Airframe	21
6	Zero-Pole Relationships of the Models	21
7	Model-Following Structure	24
8	Flow Diagram for Computational Algorithm	32
9	Step Responses -- Free Aircraft (Flight Condition 1, Mach 0.2, Sea Level, Power Approach)	39
10	Step Responses -- Free Aircraft (Flight Condition 2, Mach 0.5, h = 5000 Feet)	39
11	Step Responses -- Free Aircraft (Flight Condition 3, Mach 1.2, h = 5000 Feet)	40
12	Step Responses -- Free Aircraft (Flight Condition 4, Mach 0.9, h = 15,000 Feet)	40
13	Step Responses -- Free Aircraft (Flight Condition 5, Mach 0.5, h = 25,000 Feet)	41
14	Step Responses -- Free Aircraft (Flight Condition 6, Mach 1.5, h = 25,000 Feet)	41
15	Step Responses -- Free Aircraft (Flight Condition 7, Mach 1.2, h = 35,000 Feet)	42
16	Step Responses -- Free Aircraft (Flight Condition 8, Mach 0.9, h = 45,000 Feet)	42
17	Step Responses -- Free Aircraft (Flight Condition 9, Mach 2.15, h = 45,000 Feet)	43
18	Step Responses -- Free Aircraft (Flight Condition 10, Mach 0.9, h = 35,000 Feet, Weight = 53,741 Pounds)	43
19	Step Responses -- Free Aircraft (Flight Condition 11, Mach 0.85, h = 5000 Feet, Weight = 53,741 Pounds)	44
20	Effective Lateral Actuator Deflections at FC(3)	48
21	Autocorrelation of r(t)	57
22	Step Responses -- Run 7 -- 0.177-Rad Rudder Command	64
23	Step Responses -- Run 7 -- 0.250-Rad Lateral Command	66

## LIST OF ILLUSTRATIONS -- CONTINUED

24	Step Responses -- Run 7 -- 0.0177-Rad Rudder Command	68
25	Step Responses -- Run 7 -- 0.025-Rad Lateral Command	70
26	RMS Response Ratios versus Command Bandwidth	72
27	Surface Rate versus Command Bandwidth	72
28	Steady-State Errors for Lateral Step versus Command Bandwidth	73
29	Step Responses -- Optimal Quadratic Controller (Flight Condition 1, Model 4)	75
30	Step Responses -- Optimal Quadratic Controller (Flight Condition 2, Model 4, Minneapolis Simulation)	78
31	Step Responses -- Optimal Quadratic Controller (Flight Condition 3, Model 4, Minneapolis Simulation)	78
32	Step Responses -- Optimal Quadratic Controller (Flight Condition 4, Model 4, Minneapolis Simulation)	79
33	Step Responses -- Optimal Quadratic Controller (Flight Condition 5, Model 4, Minneapolis Simulation)	79
34	Step Responses -- Optimal Quadratic Controller (Flight Condition 6, Model 4, Minneapolis Simulation)	80
35	Step Responses -- Optimal Quadratic Controller (Flight Condition 7, Model 4, Minneapolis Simulation)	80
36	Step Responses -- Optimal Quadratic Controller (Flight Condition 8, Model 4, Minneapolis Simulation)	81
37	Step Responses -- Optimal Quadratic Controller (Flight Condition 9, Model 4, Minneapolis Simulation)	81
38	Step Responses -- Optimal Quadratic Controller (Flight Condition 10, Model 4, Minneapolis Simulation)	82
39	Step Responses -- Optimal Quadratic Controller (Flight Condition 11, Model 4, Minneapolis Simulation)	82
40	Step Responses -- Optimal Quadratic Controller (Flight Condition 2, Model 1, Minneapolis Simulation)	83
41	Step Responses -- Optimal Quadratic Controller (Flight Condition 3, Model 1, Minneapolis Simulation)	83
42	Step Responses -- Optimal Quadratic Controller (Flight Condition 2, Model 2, Minneapolis Simulation)	84
43	Step Responses -- Optimal Quadratic Controller (Flight Condition 3, Model 2, Minneapolis Simulation)	84
44	Step Responses -- Optimal Quadratic Controller (Flight Condition 2, Model 3, Minneapolis Simulation)	85

# Contrails

## LIST OF ILLUSTRATIONS -- CONTINUED

45	Step Responses -- Optimal Quadratic Controller (Flight Condition 3, Model 3, Minneapolis Simulation)	85
46	Performance Sensitivity of Optimal Controller (0.1-Rad RMS Rudder Command)	87
47	Performance Sensitivity of Optimal Controllers (0.1-Rad RMS Lateral Command)	88
48	Performance Sensitivity of Optimal Controller (6-Ft/Sec RMS Lateral Gust)	89
49	Gain Sensitivity	92
50	Structure of the Practical Gain Matrix, $[K^1(\lambda) + K^3] M + \lambda K^2, \lambda = 0$	95
51	Gain Structure of Single-Flight-Condition Practical Controllers	95
52	Typical Cost History for Computation of Practical Controller (PC4)	97
53	Lambda-Histories of Costs for Practical Controller Computation (PC6)	99
54	Performance Sensitivity of PC6 (0.1-Rad RMS Rudder Command)	100
55	Performance Sensitivity of PC6 (0.1-Rad RMS Lateral Command)	101
56	Step Responses -- PC6 at Flight Condition 2, Minneapolis Simulation	103
57	Step Responses -- PC6 at Flight Condition 4, Minneapolis Simulation	104
58	Step Responses -- PC6 at Flight Condition 9, Minneapolis Simulation	105
59	Roots of Optimally-Controlled Aircraft	106
60	Roots of Practical Controller	108
61	Gain Structure for PC7, $[K^1(\lambda) + K^3] M, \lambda = 0$	108
62	Performance Sensitivity of PC7 (0.1-Rad RMS Rudder Command)	109
63	Performance Sensitivity of PC7 (0.1-Rad RMS Lateral Command)	110
64	Step Responses -- PC7 at Flight Condition 1	111
65	Step Responses -- PC7 at Flight Condition 2, Minneapolis Simulation	115



## LIST OF ILLUSTRATIONS -- CONTINUED

66	Step Responses -- PC7 at Flight Condition 3, Minneapolis Simulation	115
67	Step Responses -- PC7 at Flight Condition 4, Minneapolis Simulation	116
68	Step Responses -- PC7 at Flight Condition 5, Minneapolis Simulation	116
69	Step Responses -- PC7 at Flight Condition 6, Minneapolis Simulation	117
70	Step Responses -- PC7 at Flight Condition 7, Minneapolis Simulation	117
71	Step Responses -- PC7 at Flight Condition 8, Minneapolis Simulation	118
72	Step Responses -- PC7 at Flight Condition 9, Minneapolis Simulation	118
73	Step Responses -- PC7 at Flight Condition 10, Minneapolis Simulation	119
74	Step Responses -- PC7 at Flight Condition 11, Minneapolis Simulation	119
75	Experimental Design	124
76	Typical Flight Profile	128
77	WPAFB Simulation Block Diagram	131
78	Cockpit of AFFDL Moving Base Simulator	132
79	Navigation Error Display, WPAFB	133
80	Minneapolis Simulation Block Diagram	136
81	Cockpit of Minneapolis Simulator	137
82	Navigation Error Display	138
83	Histogram of Lateral RMS Error at WPAFB	146
84	Histogram of Cooper-Harper Ratings at WPAFB (3 Subjects)	149
85	Mean RMS Lateral Errors at WPAFB	149
86	Graphical Interpretation of Individual Comparisons	154
87	Mean Cooper-Harper Ratings at WPAFB (3 Subjects)	154
88	Mean RMS Lateral Error at Minneapolis	158
89	Mean RMS Altitude Errors at WPAFB and Minneapolis	158
90	Mean RMS Velocity Errors at WPAFB and Minneapolis	159

## LIST OF ILLUSTRATIONS -- CONTINUED

91	Mean Cooper-Harper (C-H) Ratings at WPAFB (4 Subjects) and Minneapolis	159
92	Mean Global "Handling-Quality (HQ)" Ratings at WPAFB (3 Subjects) and Minneapolis	160
93	Mean Global "Demand-on-Pilot (DOP)" Ratings at WPAFB (3 Subjects) and Minneapolis	160
94	Mean Global DOP and HQ Ratings at WPAFB (4 Subjects)	161
95	Mean RMS Lateral Commands and Rudder Commands at WPAFB	161
96	Illustration of A x B Interaction - Lateral Error, WPAFB	165
97	Illustration of A x C Interaction	166
98	Rating/Performance Relationship	168
99	Data for Handling-Quality Parameters $s_1$ and $s_2$ (Taken from Ref. 2)	172
100	Data for Handling-Quality Parameters $s_1$ and $s_2$ (Taken from Ref. 6)	173
101	Data for Handling-Quality Parameter $s_3$ (Taken from Ref. 2)	175
102	Data for Handling-Quality Parameter $s_3$ (Taken from Ref. 2)	176
103	Data for Handling-Quality Parameter $s_5$ (Taken from Ref. 2)	177
104	Data for Handling-Quality Parameters $s_6$ and $s_7$ (Taken from Ref. 2)	178
105	Data for Handling-Quality Parameter $s_8$ Sideslip Specification (Taken from Ref. 1)	179
106	Demonstration Flights -- Flight Condition 2	195
107	Demonstration Flights -- Flight Condition 3	196
108	Demonstration Flights -- Flight Condition 4	197
109	Demonstration Flights -- Flight Condition 5	197
110	Demonstration Flights -- Flight Condition 6	198
111	Demonstration Flights -- Flight Condition 7	199
112	Demonstration Flights -- Flight Condition 8	200
113	Demonstration Flights -- Flight Condition 9	201
114	Demonstration Flights -- Flight Condition 10	201
115	Demonstration Flights -- Flight Condition 11	202
116	Practical Controller with Bank Angle Hold Loop ( $\pm 30$ -Deg Bank Angle Commands)	203



## LIST OF ILLUSTRATIONS -- CONTINUED

117	Practical Controller with Sensor Noise (2 Ft/Sec <sup>2</sup> RMS Accelerometer, 0.05 Rad/Sec RMS Rate Gyros) -- WPAFB	205
118	Formal Data Trials -- Subject D. S. at Minneapolis, Model 1; Low Speed	206
119	Formal Data Trials -- Subject D. S. at Minneapolis, Model 1, High Speed	206
120	Formal Data Trials -- Subject D. S. at Minneapolis, Model 5, Low Speed	207
121	Formal Data Trials -- Subject D. S. at Minneapolis, Model 5, High Speed	207
122	Formal Data Trials -- Subject D. S. at Minneapolis, Model 3, Low Speed	208
123	Formal Data Trials -- Subject D. S. at Minneapolis, Model 3, High Speed	208
124	Formal Data Trials -- Subject R. K. at WPAFB, Model 5, High Speed	209
125	Formal Data Trials -- Subject R. K. at WPAFB, Model 5, Low Speed	209
126	Formal Data Trials -- Subject R. K. at WPAFB, Model 1, High Speed	210
127	Formal Data Trials -- Subject R. K. at WPAFB, Model 1, Low Speed	210
128	Formal Data Trials -- Subject R. K. at WPAFB, Model 3, High Speed	211
129	Formal Data Trials -- Subject R. K. at WPAFB, Model 3, Low Speed	211
130	WPAFB Simulation -- Free Aircraft, Flight Condition 2	216
131	WPAFB Simulation -- Free Aircraft, Flight Condition 3	216
132	WPAFB Simulation -- Free Aircraft, Flight Condition 4	217
133	WPAFB Simulation -- Free Aircraft, Flight Condition 5	217
134	WPAFB Simulation -- Free Aircraft, Flight Condition 6	218
135	WPAFB Simulation -- Free Aircraft, Flight Condition 7	218
136	WPAFB Simulation -- Free Aircraft, Flight Condition 8	219
137	WPAFB Simulation -- Free Aircraft, Flight Condition 9	219
138	WPAFB Simulation -- Free Aircraft, Flight Condition 10	220
139	WPAFB Simulation -- Free Aircraft, Flight Condition 11	220

## LIST OF ILLUSTRATIONS -- CONTINUED

140	WPAFB Simulation -- Controlled Aircraft, Flight Condition 2, Model 1	221
141	WPAFB Simulation -- Controlled Aircraft, Flight Condition 2, Model 2	221
142	WPAFB Simulation -- Controlled Aircraft, Flight Condition 2, Model 3	222
143	WPAFB Simulation -- Controlled Aircraft, Flight Condition 2, Model 4	222
144	WPAFB Simulation -- Controlled Aircraft, Flight Condition 2, Model 4, Practical Controller	223
145	WPAFB Simulation -- Controlled Aircraft, Flight Condition 3, Model 1	223
146	WPAFB Simulation -- Controlled Aircraft, Flight Condition 3, Model 2	224
147	WPAFB Simulation -- Controlled Aircraft, Flight Condition 3, Model 3	224
148	WPAFB Simulation -- Controlled Aircraft, Flight Condition 3, Model 4	225
149	WPAFB Simulation -- Controlled Aircraft, Flight Condition 3, Model 4, Practical Controller	225
150	Minneapolis Simulation -- Free Aircraft, Flight Condition 2	226
151	Minneapolis Simulation -- Free Aircraft, Flight Condition 3	226
152	Minneapolis Simulation -- Free Aircraft, Flight Condition 4	227
153	Minneapolis Simulation -- Free Aircraft, Flight Condition 5	227
154	Minneapolis Simulation -- Free Aircraft, Flight Condition 6	228
155	Minneapolis Simulation -- Free Aircraft, Flight Condition 7	228
156	Minneapolis Simulation -- Free Aircraft, Flight Condition 8	229
157	Minneapolis Simulation -- Free Aircraft, Flight Condition 9	229
158	Minneapolis Simulation -- Free Aircraft, Flight Condition 10	230

## LIST OF ILLUSTRATIONS -- CONCLUDED

159	Minneapolis Simulation -- Free Aircraft, Flight Condition 11	230
160	Minneapolis Simulation -- Controlled Aircraft, Flight Condition 2, Pitch Transient Response (Stick Input = 1.4 Deg of Step Stabilator)	231
161	Minneapolis Simulation -- Controlled Aircraft, Flight Condition 3, Pitch Transient Response (Stick Input = 1.4 Deg of Step Stabilator)	231

# Contrails

## LIST OF TABLES

Table		Page
I	Frequency-Domain Representation of Models	10
II	Parameters Which Specify Free Model Coefficients	12
III	Numerical Values for Parameters 1 through 11	16
IV	Model Coefficients	16
V	Steady-State Roll Rates and Sideslip for Free Airframe	21
VI	Flight Conditions	36
VII	Coefficients for Rigid-Body Equations	37
VIII	Handling-Quality Characteristics for the Unaugmented Aircraft	38
IX	Maximum Surface Deflections	48
X	Reduced-Order Models	54
XI	Command Magnitudes	58
XII	Iterations for Baseline Design Quadratic Weights and RMS Responses	62
XIII	Rigid-Body Feedback Gains for Baseline Design Iterations	63
XIV	Command Feedforward Gains as a Function of $\omega_o$ [FC(2), Q, R from Run 7]	73
XV	Quadratic Weights for All Flight Conditions	74
XVI	Gain Summary	90
XVII	RMS Performance of Single-Flight-Condition Practical Controllers for Flight Condition 2	96
XVIII	Maximum Deterioration Ratios, PC6	102
XIX	Maximum Deterioration Ratios, PC7	107
XX	Breakdown of Quadratic Cost Components for Flight Condition 2	121
XXI	Subject Data for Pilots Who Participated in Performance Data Sessions	128
XXII	Subject Data for Pilots who Rated Models at WPAFB	129
XXIII	Cockpit Control Summary -- WPAFB Simulation	133
XXIV	Cockpit Control Summary -- Minneapolis Simulation	138
XXV	Analysis of Variance of WPAFB Lateral Error Data	152
XXVI	Individual Comparisons (Scheffe) of WPAFB Lateral Error Data	153

## LIST OF TABLES -- CONCLUDED

Table		Page
XXVII	Analysis of Variance of WPAFB Cooper-Harper Data (3 Subjects)	157
XXVIII	Individual Comparisons of WPAFB Cooper-Harper Data (3 Subjects)	157
XXIX	Summary of Levels of Significance for Main Effects and Interactions of the Dependent Variable Analysis of Variance	162
XXX	Summary of Levels of Significance for Individual Orthogonal Comparisons of all Pairs of Systems	163
XXXI	Rank-Order of Systems for Main Data Sources	167
XXXII	Low-Speed Flight Profiles	215
XXXIII	High-Speed Flight Profiles	215
XXXIV	Training Trial Sequences for Minneapolis	232
XXXV	Training Trial Sequences for WPAFB	232
XXXVI	Data Session Sequences for Subject W. S. at WPAFB	233
XXXVII	Data Session Sequences for Subject R. K. at WPAFB	233
XXXVIII	Data Session Sequences for Subject D. S. at WPAFB	234
XXXIX	Data Session Sequences for Subject D. S. at Minneapolis	234
XL	Data Session Sequences for Subject R. P. at Minneapolis	235
XLI	Data Session Sequences for Subject T. H. at Minneapolis	235
XLII	Raw Pilot Rating Data -- WPAFB (3 Subjects) (Two Observations/System, Speed, Subject)	241
XLIII	Raw Pilot Rating Data -- Minneapolis (3 Subjects) (Two Observations/System, Speed, Subject)	242
XLIV	Raw Pilot Rating Data -- WPAFB (4 Subjects) (Two Observations/System, Speed, Subject)	243

## LIST OF SYMBOLS

$a, \dot{a}$	Accelerometer state variables
$a_y$	Lateral acceleration at the center of gravity (ft/sec <sup>2</sup> )
$E\{\cdot\}$	Mathematical expectation
$E_h, E_v, E_y$	Altitude (ft), velocity (ft/sec), and lateral (ft) errors
$\bar{E}_h, \bar{E}_v, \bar{E}_y$	RMS altitude (ft), velocity (ft/sec), and lateral (ft) errors
$E^{ij}$	Partial derivative of gain matrix with respect to $(K^1)_{ij}$
F	1) System matrix 2) F-statistic
G	Input distribution matrix
g	Gravitational acceleration (32.2 ft/sec <sup>2</sup> )
H	1) Output matrix 2) Hamiltonian
h	Altitude (ft)
J	Performance index
$K, K^1, K^2, K^3, K^p, K^c$	Controller gains, gains to be retained, gains to be discarded, preselected gains, predicted gains, corrected gains
$L_p, L_r, L_\beta, L_{\delta R}, L_{\delta AS}$	Coefficients of linearized roll rate equation in stability coordinates with product of inertia terms included (units, respectively, are rad/sec <sup>2</sup> per rad/sec; rad/sec; rad; rad; and rad)
$t_1, t_2, \dots, t_8$	Distances on pole-zero plot of roll rate due to aileron transfer function
$l$	Number of gains to be retained

## LIST OF SYMBOLS -- CONTINUED

M	1) Measurement matrix 2) Mach number
m	Dimension of control vector, u
$N_p, N_r, N_\beta, N_{\delta R}, N_{\delta AS}$	Coefficients of linearized yaw rate equation in stability coordinates with product of inertia terms included (units, respectively, are rad/sec <sup>2</sup> per rad/sec; rad/sec; rad; rad; and rad)
n	Dimension of state vector, x
P	Riccati matrix
p	1) Roll rate (rad/sec) 2) Probability density function 3) Number of plants for multiplant optimization
$p_{se}$	Sensed roll rate (rad/sec)
Q	Matrix of quadratic weights on state variables
$Q_{11}, Q_{22}, \dots, Q_{44}$	Components of Q
q	Dynamic pressure (lb/ft <sup>2</sup> )
R	1) Matrix of quadratic weights on control variables 2) Radius of turn (ft)
$R_{11}, R_{22}$	Components of weighting matrix, R
r	1) Yaw rate (rad/sec) 2) Dimension of disturbance vector, $\eta$
$r_{se}$	Sensed yaw rate (rad/sec)
S	Costate matrix
$s_1, s_2, \dots, s_{11}$	Handling-quality parameters



# Contrails

## LIST OF SYMBOLS -- CONTINUED

Trace {A}	Sum of diagonal elements of matrix A
T	Transformation matrix
T(i, j)	Profile matrix
T <sub>R</sub> , T <sub>s</sub>	Roll time constant, spiral time constant (sec)
T <sub>1/2</sub> , T <sub>2</sub>	Time to one-half amplitude, time to double amplitude (sec)
U <sub>o</sub>	Nominal velocity (ft/sec)
u <sub>p</sub>	Plant control vector (servo inputs) with components (u <sub>pR</sub> , u <sub>pAS</sub> )
u <sub>m</sub>	Command model state vector with components (u <sub>mR</sub> , u <sub>mAS</sub> )
v	Velocity component along y-stability axis (ft/sec)
v <sub>g</sub>	Lateral gust (ft/sec)
W	Composite quadratic weighting matrix
X	1) State covariance matrix 2) Aircraft position along x-earth-fixed axis (ft)
x	Composite state vector composed of subvectors (x <sub>p</sub> , x <sub>m</sub> , u <sub>m</sub> )
x <sub>p</sub>	Plant state vector composed of subvectors (x <sub>rb</sub> , x <sub>f</sub> , x <sub>as</sub> , x <sub>se</sub> , x <sub>w</sub> )
x <sub>rb</sub>	Rigid-body state variables (p, r, β, φ)
x <sub>f</sub>	Flexure mode state variables (ξ, ξ̇)
x <sub>as</sub>	Actuator/servo state variables (δ <sub>R</sub> , δ <sub>AS</sub> , γ <sub>1</sub> , γ <sub>2</sub> , γ <sub>3</sub> , γ <sub>4</sub> )



## LIST OF SYMBOLS -- CONTINUED

$x_{se}$	Sensor state variables ( $a, \dot{a}$ )
$x_w$	Gust model state variables ( $v_g$ )
$x_m$	Handling-quality model state variables ( $p_m, r_m, \beta_m, \phi_m$ )
$x_o$	Accelerometer location along x-body axis (ft)
Y	Aircraft position along y-earth-fixed axis (ft)
$Y_p, Y_r, Y_\beta, Y_\phi, Y_{\delta R}, Y_{\delta AS}$	Coefficients of linearized sideslip equation in stability coordinates (units, respectively, are rad/sec per rad/sec; rad/sec; rad; rad; rad; and rad)
y	Vector of measured signals with components ( $p_{se}, r_{se}, a, \phi, \tilde{x}_m, u_m$ )
z	Spiral mode
$z_o$	Accelerometer location along z-body axis (ft)
GREEK	
$\alpha_{wL}$	Angle of attack of water line (rad)
$\alpha_1, \alpha_2, \dots, \alpha_p$	Weighting coefficients in composite performance index
$\beta$	Angle of sideslip (rad)
$\Gamma$	Disturbance distribution matrix
$\gamma_1, \gamma_2, \dots, \gamma_4$	Servo state variables
$\Delta\beta$	Sideslip increment (rad)
$\Delta\lambda$	Numerical integration step size

## LIST OF SYMBOLS -- CONTINUED

$\delta_{AS}, \delta_R$	Surface deflection, lateral, rudder (rad)
$\delta(t - \tau)$	Dirac delta function
$\delta_{PAS}, \delta_{PR}, \delta_{PT}$	Pilot commands, lateral, rudder, throttle (rad)
$\bar{\delta}_{PAS}, \bar{\delta}_{PR}$	RMS pilot commands, lateral, rudder (rad)
$\epsilon$	Convergence criterion for Newton Raphson corrector
$\zeta$	Damping ratio
$\eta$	White noise vector consisting of subvectors ( $\eta_p, \eta_u$ ) and components ( $\eta_w, \eta_R, \eta_{AS}$ ) and having correlation function $E \{ \eta(t) \eta^T(\tau) \} = I \delta(t - \tau)$
$\lambda$	1) Scalar integration parameter 2) Left eigenvector of matrix F
$\mu$	Dimension of measurement vector, y
$\nu$	Right eigenvector of matrix F
$\xi$	Amplitude of first asymmetric flexure mode
$\dot{\xi}$	Amplitude rate of first asymmetric flexure mode
$\sigma_{AS}, \sigma_R, \sigma_{vg}$	RMS lateral command, rudder command, and gust magnitude
$\phi$	Bank angle (rad)
$\psi$	Heading angle (rad)
$\psi_\beta$	Phase angle of dutch roll component of sideslip (rad)
$\omega$	Frequency (rad/sec)
$\omega_o, \omega_i$	Command bandwidth, input bandwidth (rad/sec)
$\omega_c$	Cutoff frequency (rad/sec)

## SUBSCRIPTS

A	Aileron
AS	Lateral (aileron/spoiler)
as	Actuator/servo
avg	Average component
d	dutch roll
f	Flexure
m	Model
max	Maximum
min	Minimum
osc	Oscillatory component
p	Plant
R	Rudder
rb	Rigid body
s	Spiral mode
ss	Steady state
SP	Spoiler
S	Stabilator
se	Sensor
T, T1, T2	Throttle, Engine 1, Engine 2
u	Command model
w	Gust model
$\phi$	Numerator, roll rate-due-to-aileron

## SUPERSCRIPTS

*	Quadratic optimal, no practicality constraints
~	Spiral mode removed

# *Contrails*

## SECTION I INTRODUCTION AND SUMMARY

The work reported here is concerned with two problems in the area of optimal control and its application to the design of augmentation systems for fighter aircraft:

- Specification of performance criteria in terms of handling-quality requirements of the controlled vehicle
- Formulation (and solution) of the optimization problem such that practical control systems are obtained.

These problems have long frustrated efforts of flight control designers to exploit performance improvements and time savings offered by mathematical optimization. Even for simple performance criteria and system representations (notably quadratic cost functions and linear systems), optimization methods produce controllers too complex for flight control mechanization. When the varied requirements of handling qualities (MIL-F8785B) are imposed as criteria, the methods seem inapplicable altogether.

The objectives of this program were to alleviate these difficulties. Specifically, the objectives were: 1) to develop a practical controller design procedure based on quadratic optimal control technology and handling-quality-oriented cost functionals; 2) to apply the procedure to the design of a lateral-directional control system for the F4C aircraft; and 3) to validate the design criteria, design procedure, and final control system with a program of formal pilot evaluation experiments. These objectives were fully achieved.

### THE DESIGN PROCEDURE

A reformulated optimal model-following control problem is used as the cornerstone of the design procedure. Design criteria are expressed as systems of model differential equations which satisfy available handling-quality data. Standard quadratic functions of model-following errors (plus other selected states and controls) are then used as the mathematical performance index.

# Contrails

The control problem was reformulated to impose optimality over multiple flight conditions, with fixed-gain constraints and measurement realizability constraints on the control system. In effect, these are constraints on the structure of the controller. They eliminate two of the outstanding ailments of conventional optimal controllers -- full-state measurement and extensive gain variation over the flight envelope. While we recognize that practicality has many ramifications, any control system which overcomes these two factors is here called a "practical" system. This may be taken as an informal definition. However, it should not be construed to imply that all complexity aside from gain variation and sensor complements may go unchecked.

Unfortunately, the reformulated optimization problem does not yield closed-form solutions. Controllers must be obtained computationally, and a new algorithm was developed for this purpose. This algorithm has successfully computed practical controllers for 20th-order dynamic models of the F4C lateral-directional axes, optimizing over five diverse flight conditions simultaneously. Depending on details of the formulation, computation times of 6 to 15 minutes were required on present-generation digital machines.

An abbreviated breakdown of the design procedure is given below:

- Step 1. Construction of Handling Quality Models -- Data from Military Specification MIL-F-8785 (Ref. 1) and the backup document which supports it (Ref. 2) are used to define a system of differential equations having the same structural form and the desired handling qualities of the augmented aircraft.
- Step 2. Mathematical Modeling of the Vehicle -- Linear equations of motion are defined for all flight conditions of interest. Dynamics include rigid body, flexure (if important to the control problem), actuators, servos, sensors for an assumed complement of measurements, disturbances, and commands.
- Step 3. Computation of Optimal Quadratic Controllers -- Conventional (full-state feedback) optimal controllers are computed for each flight condition. These serve to determine weights for the model-following performance index as a function of flight condition and to establish lower-performance bounds, performance and gain sensitivities over the flight envelope, and critical flight conditions. They also provide a starting point for the computational algorithm used in Step 4.

# Contrails

- Step 4. Computation of Practical Controllers -- A single practical controller is computed for selected critical flight conditions using the newly developed computational algorithm. The result is checked at all remaining flight conditions and performance comparisons are made with the optimal controllers of Step 3.

Step 4 may be iterated repeatedly to investigate simpler or more complicated controller structures (compared with the structure specified by the assumed measurement complement, Step 2). For each iteration, the practical controller will be optimal with respect to the model-following performance index and the structural constraints.

These steps were carried out for the F4C lateral-directional axes, and the resulting control systems were evaluated with formal piloted validation experiments.

## VALIDATION PROCEDURE

The purpose of the validation program was threefold -- to validate the design criteria, to validate the design procedure, and to evaluate the practical F4C lateral-directional control system. The program was therefore designed to examine the following three propositions:

- 1) It is meaningful to express handling-quality requirements in the form of models for the controller/vehicle combination.
- 2) It is possible to cause the aircraft to follow these models (with available control authority) at least to the extent that the controlled aircraft takes on their handling-quality properties.
- 3) The required level of model-following can be achieved with a practical controller.

The experimental protocol used consists of a 5 x 2 x 3 mixed design analysis of variance in which five different controlled aircraft systems are evaluated at two flight conditions each flown by three pilot/subjects. The five aircraft systems were constructed as follows.

Systems 1 through 4 consisted of the F4C aircraft controlled by conventional optimal controllers (full-state measurement, flight-condition-dependent) which were designed to follow four different handling-quality



models. Model 1 was deliberately constructed to exhibit poor predicted handling qualities, model 2 was constructed to exhibit somewhat better handling qualities, model 3 still better, and model 4 was constructed to exhibit excellent predicted handling qualities. System 5 consisted of the same aircraft controlled by a practical controller (constant gain, realizable measurements) designed to follow model 4.

On a predicted basis, therefore (and assuming our propositions are true), dependent measures collected in the experiment should exhibit an ascending order of goodness for systems 1 through 4. System 5 should fall somewhere in between, hopefully close to system 4. In analysis-of-variance jargon, we would say that the main effect of systems should exhibit the rank ordering 1, 2, 3, 5, 4.

Two types of dependent measures were taken -- objective performance measures in a pilot navigation task, and subjective rating data of both Cooper-Harper and Global varieties.

The experiment was conducted on a fixed-base simulator at Honeywell Inc., Minneapolis, Minnesota, and later completely replicated on a limited moving-base simulator at the Air Force Flight Dynamics Laboratory.

## SUMMARY OF RESULTS

The findings of the validation program support the three propositions in a near-perfect fashion. The rank ordering of systems 1 through 4 came out 1, 2, 3, 4 for both rating and performance data. In the case of rating data, these rankings are significant for all pairs, and for performance data they are significant for all but adjacent pairs.

The ranking of system 5 shows an ordering of 5 better than 4 for rating data and 4 better than 5 for performance data. However, neither of these differences is statistically significant. From the point of view of pilot ratings, as well as performance data, therefore, the practical controller flies as well as the optimal controller.

From the two kinds of data gathered we can give the following interpretation to the rank ordering of systems. First, pilot acceptance follows the predicted trends. These are by no means linear; i. e., system 1 is not twice as bad as system 2 and system 3 is not twice as bad as system 4, but then no such relationship was predicted. Secondly, pilot acceptance is consonant with pilot performance. Within the resolution of the



experiments, the rank ordering of systems is the same whether based on rating data or based on performance data. Such strong correlations are not frequently seen in the literature. However, we feel that our procedures are sound and the correlations are valid.

## OUTLINE OF THE REPORT

Details of the program are discussed in Sections II through VII.

The construction of handling-quality models is described in Section II, which gives some philosophical background for the notion of models and develops the parameters and equations necessary to define them for the lateral axes of a fighter aircraft. In essence, 11 different handling-quality parameters are chosen from specification MIL-F-8785 and its backup document to uniquely specify the model differential equations. Four models with monotonically ascending handling-quality goodness are developed.

Section III elaborates on Steps 3 and 4 of the design procedure, the mechanics of design. The conventional quadratic optimal model-following control problem is discussed, together with some of the properties of its solution. The problem is then reformulated to include optimality over multiple flight conditions, constant gains, and realistic sensor complements. Necessary conditions of optimality for the new problem are derived and a computational algorithm is presented for their solution.

The F4C lateral axes design problem is discussed in Section IV, which begins with a detailed account of the mathematical models used for the design computations. Twentieth-order dynamics were used with four rigid-body states, two states for the first asymmetric flexure mode, six states for actuator and servos, two accelerometer states, three model states, and one state each for lateral gusts, rudder commands, and lateral commands. Conventional optimal controllers are then designed for 11 flight conditions. The performance sensitivity and gain sensitivity of these controllers are explored in detail. This is followed by a description of several practical controller designs. The first few are practical controllers for a single flight condition. They were computed to debug the design algorithm and to explore several choices of sensor complements. Two practical controllers are then described for five flight conditions treated simultaneously. Because of improperly-chosen command magnitudes, the first controller turned out to be unacceptable (too little dutch roll damping). The second controller was flown in the validation program.

# *Contrails*

Details of the validation procedure are discussed in Section V. This section covers the experimental design, independent and dependent variables, task considerations, qualifications and experience of pilot/subjects, and the manner in which the experiments were conducted.

Section VI presents results of the validation program. From the outset, all measurements are treated as samples from statistical distributions. A qualitative look at these distributions is provided by histograms of several performance and rating scores. These highlight the kinds of differences exhibited by the five systems which were evaluated. Analyses of variance and orthogonal comparisons are then presented for several variables -- lateral errors, altitude errors, velocity errors, and rating data for both the WPAFB and the Minneapolis simulation. Analyses for the main effect of models, flight condition, and subjects are included. Finally, two secondary indicators -- rms stick and rudder deflection -- are investigated.

Some final conclusions and recommendations are made in Section VII.

## SECTION II DESIGN CRITERIA

The first step of the design procedure developed in this program is to specify handling-quality-oriented design criteria which are usable within the framework of quadratic optimal control technology. Such criteria are developed in this section.

### PHILOSOPHY

Handling-quality considerations are important to flight control design because augmentation systems function primarily to make aircraft more compatible with the characteristics of pilots. Implicitly or explicitly, therefore, we are not dealing solely with machines and hardware but with the celebrated pilot/vehicle system. This system is distinguished by an interface between two quite different types of subsystems. The first is the machine which can be accurately modeled and manipulated at will. Its input and output channels carry known kinds and quantities of information whose interrelations are known. The second is the man who, on a comparative basis, can be modeled and/or manipulated in only very limited ways. His input channels carry poorly defined kinds and quantities of information whose relationships to outputs are poorly understood. It is only because we restrict them to stick displacements or pedal forces that the outputs themselves are well defined. Nevertheless, it is the second subsystem which must determine criteria for the design of the first.

Two approaches have been followed in the past to explore the interface of man and machine. The first is empirical. It consists of measuring the suitability of many different kinds of aircraft configurations to the needs of the pilot and his mission. This amounts to constructing a huge catalog or table of empirical data which has as its independent variable the vehicle configuration and as its dependent variable the configuration's suitability to the man. The independent variable is expressed parametrically in terms of such things as coefficients of its small perturbation differential equations, characteristics of its force-feel system, parameters of the display system, etc.<sup>1</sup> The dependent variable is typically expressed as a subjective pilot rating assigned by a small number of pilot/subjects after experimental evaluation trials using the configuration. Occasionally, these ratings are augmented with objective measures of performance achieved by the subjects during the trials.

---

<sup>1</sup>While a large number of parameters have been empirically investigated, we are concerned in augmentation system design and in this report primarily with the first item mentioned above -- parameters of the differential equations.

# Contrails

The catalog is compiled in the forward direction, i. e. , a configuration is specified and its suitability evaluated and recorded. To some extent, however, it is usable in the reverse direction. We can enter with a specified suitability level and come out with ranges of machine parameters which fall at or below it. In essence, this is the process by which current handling-quality specifications were generated (Ref. 1, 2). It can also be used to construct ideal configurations (handling-quality models) for the vehicle subsystem (the controlled aircraft). In an optimal model-following control formulation, such models represent meaningful design criteria.

The second approach to the study of the man/machine interface treats the pilot not as the external judge and evaluator but rather as an integral part of the overall control loop. The loop is analyzed by representing the pilot in terms of mathematical models which are compatible with our descriptions of the machine. These models are assumed mathematical structures (e. g. , integral or differential equations, time delays, etc.) whose parameters are fitted to experimental records of the pilot's input/output activity in the loop. Needless to say, they match only limited elements of his behavior and are crucially dependent upon the details of the control loop for which they were fitted. Even for the much explored quasi-linear pilot models (Ref. 3, 4), the manner in which the experimental fit changes with the overall loop situation is described by essentially verbal adjustment rules.

In principle, of course, pilot modeling represents a powerful approach to the analysis of pilot/vehicle systems. Models are condensed expressions of reams of experimental data and permit interpolation, extrapolation, and prediction of a quality no table can match. With a reasonably general pilot model, properties of the pilot/vehicle system would be well defined, and, with regard to our interest in this section, criteria for the design of augmentation subsystems could be readily determined from its overall mission and performance goals.

In an optimization framework, a natural approach to design would be to optimize the entire system, pilot model and all, for some overall performance measure. This requires a very general model, however, since the optimization might well settle on a control loop situation which is significantly different from that for which the pilot model was experimentally fitted. More simply, we must be sure that the model remains valid under severe manipulation. The judgment made in this report is that, at present levels of sophistication, pilot models fall short of this requirement. The designs carried out in Ref. 5, for example, tend to support this. In consequence, we have used the first approach to the man/machine problem and have constructed handling-quality models for the F4C lateral-directional axes. These were used as design criteria in an optimal model-following control formulation. Our decision is an interim one, subject to change as the sophistication of pilot models grows.



## HANDLING-QUALITY MODELS

In constructing ideal vehicle configurations for the design of practical controllers and for the criteria/controller validation experiments, we are asking for the best set of machine dynamics for a man/machine system intended to perform the various missions of a fighter aircraft. In addition, we are asking for the ability to identify other sets of dynamics which exhibit monotonically decreasing goodness. If no restrictions are placed upon the class of dynamics from which to choose, satisfactory answers to these questions are difficult to obtain. The catalog mentioned above has few entries for arbitrary configurations. On the other hand, if the class is restricted to "aircraft dynamics," then there are many catalog entries with which to answer the questions. We therefore chose aircraft dynamics.

### The Model Form

Accordingly, our models for the lateral-directional axes are fourth-order linear differential equations with two real poles (spiral and roll subsidence), two complex conjugate poles (dutch roll), and the following general time-domain structure:

$$\frac{d}{dt} \begin{bmatrix} p_m \\ r_m \\ \beta_m \\ \phi_m \end{bmatrix} = \begin{bmatrix} L_p & L_r & L_\beta & 0 \\ N_p & N_r & N_\beta & 0 \\ Y_p & Y_r & Y_\beta & Y_\phi \\ 1 & 0 & 0 & 0 \end{bmatrix} \begin{bmatrix} p_m \\ r_m \\ \beta_m \\ \phi_m \end{bmatrix} + \begin{bmatrix} L_{\delta R} & L_{\delta AS} \\ N_{\delta R} & N_{\delta AS} \\ Y_{\delta R} & Y_{\delta AS} \\ 0 & 0 \end{bmatrix} \begin{bmatrix} \delta_R \\ \delta_{AS} \end{bmatrix} - \begin{bmatrix} L_\beta \\ N_\beta \\ Y_\beta \\ 0 \end{bmatrix} \frac{v_g}{U_o} \quad (1)$$

Note that the coefficients of this equation are not given in conventional notation (Ref. 2). Instead, they are defined in the symbol table to correspond to our F4 data source, Ref. 22.

The frequency-domain equivalent of Equation (1) is summarized in Table I.

To correspond to the actual aircraft, certain of the coefficients in this structure will have nearly constant known values:

$$\begin{aligned} Y_p &\doteq 0, & Y_{\delta R} &\doteq 0, & Y_{\delta AS} &\doteq 0 \\ Y_r &\doteq -1, & Y_\phi &= g/U_o \end{aligned}$$

This leaves 11 free coefficients which must be specified.

Table I. Frequency-Domain Representation of Models

Denominator for All Transfer Functions:	
	$\left(s + \frac{1}{T_s}\right) \left(s + \frac{1}{T_R}\right) \left(s^2 + 2\zeta_d \omega_d s + \omega_d^2\right)$ $\frac{1}{T_R} \approx -L_p + \frac{L_\beta}{N_\beta} \left(N_p - \frac{g}{U_o}\right) \quad \omega_d^2 \approx N_\beta + N_r Y_\beta$ $\frac{1}{T_s} \approx \frac{g}{U_o} T_R \left(-L_r + N_r \frac{L_\beta}{N_\beta}\right) \quad 2\zeta_d \omega_d \approx -Y_\beta - N_r - \frac{L_\beta}{N_\beta} \left(N_p - \frac{g}{U_o}\right)$
Numerators for Control Inputs: $u = \delta_R, \delta_{AS}$	
$\frac{p}{u}$	$L_u s \left[ s^2 + \left(\frac{N_u}{L_u} L_r - N_r - Y_\beta\right) s + N_\beta + N_r Y_\beta - \frac{N_u}{L_u} (L_r Y_\beta + L_\beta) \right]$
$\frac{r}{u}$	$N_u \left[ s^3 + \left(\frac{L_u}{N_u} N_p - L_p - Y_\beta\right) s^2 + Y_\beta \left(L_p - \frac{L_u}{N_u} N_p\right) s + \frac{g}{U_o} \left(\frac{L_u}{N_u} N_\beta - L_\beta\right) \right]$
$\frac{\beta}{u}$	$-N_u \left\{ s^2 + \left[\frac{L_u}{N_u} \left(N_p - \frac{g}{U_o}\right) - L_p\right] s + \frac{g}{U_o} \left(\frac{L_u}{N_u} N_r - L_r\right) \right\}$
Numerators for Lateral Gust Input:	
$\frac{p}{v_g}$	$-\frac{1}{U_o} s^2 [L_\beta s + N_\beta L_r - L_\beta N_r]$
$\frac{r}{v_g}$	$-\frac{1}{U_o} s^2 [N_\beta s + L_\beta N_p - N_\beta L_p]$
$\frac{\beta}{v_g}$	$-\frac{1}{U_o} \left\{ Y_\beta s^3 - [N_\beta + Y_\beta (N_r + L_p)] s^2 + [N_\beta L_p + Y_\beta (L_p N_r - N_p L_r) - L_\beta (N_p - \frac{g}{U_o})] s + \frac{g}{U_o} [N_\beta L_r - L_\beta N_r] \right\}$
$(\beta \hat{=} v/U_o. \text{ Both } v \text{ and } v_g \text{ are inertial velocity components measured in stability axes.})$	

## Specifications

The recently-updated Military Specification, MIL-F-8785 (Ref. 1), and the handling-quality data which support it (Ref. 2) provide a data summary for the task of specifying the remaining coefficients. It is reasonable to assume that this summary is based upon enough careful analysis of the numerous sources of raw handling-quality data and enough consideration of various expert opinions to have isolated the results of the most reliable experiments and studies pertinent to any particular specification.

Eleven handling-quality parameters were taken from Refs. 1 and 2 which implicitly define the remaining coefficients of Equation (1). These are summarized in Table II, together with their approximate literal expressions. They are the end results of several iterations through the available data, each iteration guided by the objective of uniquely specifying the free coefficients. It is quite possible to find additional conditions. However, these will either be redundant or they will over-specify the free coefficients (i. e., there will be no single set of coefficients which satisfies all conditions). The particular parameters chosen for Table II are discussed briefly below.

Parameters  $s_1$  and  $s_2$ : Dutch Roll Frequency ( $\omega_d^2$ ) and Damping ( $2\zeta_d\omega_d$ ) -- These parameters are self-explanatory. They specify the model's dutch roll mode characteristics and correspond to paragraph 3.3.1.1 of Ref. 1. Their literal expressions can be taken directly from Table I.

Parameter  $s_3$ : Roll Time Constant ( $1/T_R$ ) -- This parameter corresponds to paragraph 3.3.1.2 of Ref. 1. Its literal expression is again given in Table I.

Parameter  $s_4$ : Spiral Time Constant ( $1/T_S$ ) -- This corresponds to paragraph 3.3.1.3 of Ref. 1 and appears to be a very insensitive condition (i. e., everything from mildly unstable,  $T_2 \leq 12$  sec, to stable,  $T_{1/2} \geq 10$ , is acceptable). The literal expression is given in Table I.

Parameter  $s_5$ : Dihedral Effect ( $L_\beta$ ) -- Among the data of Ref. 2 which support the roll time constant specification is a set of curves relating optimum values of  $L_\beta$  to  $T_R$  [Figures 4 (3.3.1.2), 5 (3.3.1.2), and 1 (3.3.6.3), on pages 212 and 353]. These curves were gathered for power approach configurations and do not necessarily specify desirable  $L_\beta$  values for other situations. Alternative specifications on  $L_\beta$ , however, are only implicit and do not serve to uniquely define this parameter. For example, paragraph 3.3.2.1 of Ref. 1 on lateral-directional response to atmospheric turbulence places implicit but nonnumerical restrictions on  $L_\beta$  (roll rate and bank angle responses to atmospheric turbulence are proportional to  $L_\beta$ , as evidenced in Table I). Similarly, paragraph 3.3.6.3.2 places "soft" upper bounds on  $L_\beta$ , again failing to specify the parameter uniquely.

# Contrails

Table II. Parameters Which Specify Free Model Coefficients

Parameter	Literal Expression	F-8785 Paragraph
$s_1 = \omega_d^2$	$= N_\beta + N_r Y_\beta$	3.3.1.1
$s_2 = 2\zeta_d \omega_d$	$= - \left[ Y_\beta + N_r + \frac{L_\beta}{N_\beta} \left( N_p - \frac{g}{U_o} \right) \right]$	3.3.1.1
$s_3 = 1/T_R$	$= - L_p + \frac{L_\beta}{N_\beta} \left( N_p - \frac{g}{U_o} \right)$	3.3.1.2
$s_4 = 1/T_s$	$= T_R \frac{g}{U_o} \left( -L_r + \frac{L_\beta}{N_\beta} N_r \right)$	3.3.1.3
$s_5 = L_\beta$		Ref. 2 data
$s_6 = \left( \omega_\phi / \omega_d \right)^2$	$= 1 - \frac{L_\beta}{N_\beta} \frac{N_{\delta AS}}{L_{\delta AS}}$	3.3.2.2
$s_7 = 2 \left( \zeta_\phi \omega_\phi - \zeta_d \omega_d \right)$	$= \frac{L_\beta}{N_\beta} \left( N_p - \frac{g}{U_o} \right) + \frac{N_{\delta AS}}{L_{\delta AS}} L_r$	3.3.2.2
$s_8 = \Delta \beta_{\max}$	$L_{\delta AS} \delta_{AS \max} \frac{T_R}{\omega_d^2} \left[ 2 \frac{g}{U_o} \left( \frac{N_{\delta AS}}{L_{\delta AS}} L_r - N_r \right) + \frac{N_{\delta AS}}{L_{\delta AS}} L_p - N_p + \frac{g}{U_o} \right]$	3.3.2.4
$s_9 = \left. \frac{p}{\delta_{AS}} \right _{ss}$	$= L_{\delta AS} T_R s_6$	airframe
$s_{10} = \left. \frac{\beta}{\delta_R} \right _{ss}$	$= N_{\delta R} / \omega_d^2$	airframe
$s_{11} = \left. \frac{p}{\delta_R} \right _{ss}$	$= T_R \left( L_{\delta R} - N_{\delta R} \frac{L_\beta}{N_\beta} \right)$	3.3.4.5



# Contrails

So, the above  $L_\beta$  versus  $T_R$  data provide perhaps the only explicit definition of  $L_\beta$ , and we have elected to use it.

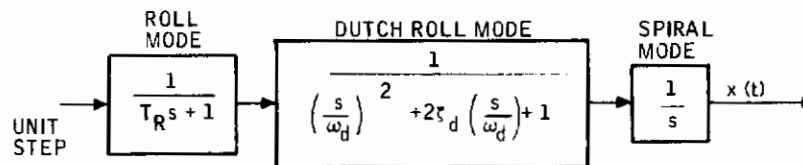
Parameters  $s_6$  and  $s_7$ : Zeros of  $p/\delta_{AS}[(\omega_\phi/\omega_d)^2, 2(\zeta_\phi\omega_\phi - \zeta_\beta\omega_d)]$  -- These two parameters specify the geometric location of the complex conjugate zeros with respect to the dutch roll poles of the roll-rate-due-to-aileron transfer function. They determine the amount of roll rate oscillation and are indirectly related to the difficulty of turn coordination (through a "relatively unique" relationship between sideslip phase,  $\psi_\beta$ , and angular zero positions with respect to dutch roll poles, which is developed in Ref. 2). In the military specification (Ref. 1),  $s_6$  and  $s_7$  are specified only implicitly by the  $p_{osc}/p_{avg}$  requirements of paragraph 3.3.2.2. This is done to avoid the difficulty of measuring zero locations in flight tests. Since we are not restricted by such limitations, the zero locations can be specified explicitly. Literal expressions for  $s_6$  and  $s_7$  can be derived from the roll-rate-due-to-aileron numerator and denominator of Table I (Ref. 6).

Parameter  $s_8$ : Sideslip Increment ( $\Delta\beta$ ) -- The maximum sideslip increment which occurs during the first few seconds of a rolling maneuver is restricted in paragraph 3.3.2.4 of Ref. 1. A literal expression for this specification was developed as follows.

From Table I, the sideslip response to a maximum step aileron command is given by ( $1/T_S = 0$ )

$$\beta(t) = -\frac{T_R}{\omega_d^2} L_{\delta AS} \delta_{AS_{max}} \left[ \frac{N_{\delta AS}}{L_{\delta AS}} \ddot{x} + \left( N_p - \frac{g}{U_0} - \frac{N_{\delta AS}}{L_{\delta AS}} L_p \right) \dot{x} + \frac{g}{U_0} \left( N_r - \frac{N_{\delta AS}}{L_{\delta AS}} L_r \right) x \right] \quad (2)$$

where  $x(t)$  is the step response of the following dynamic system:



So an exact literal expression for the maximum sideslip increment can be obtained by computing  $x(t)$ ,  $\dot{x}(t)$ , and  $\ddot{x}(t)$  as functions of  $s_1$ ,  $s_2$  and  $s_3$  alone, substituting these into Equation (2), and maximizing over  $0 \leq t \leq 2$ . The resulting expression, however, will be quite complex. Instead, some approximations were used. Note first that the coefficients of  $x$  and  $\dot{x}$  in Equation (2) are generally of the same sign and that the coefficient of  $\ddot{x}$  is small. In addition, if the diagram above represents a stable system, then we know from the response characteristics of each block that

$$\begin{aligned}
 0 &\leq x(t) \leq t + \frac{1}{\omega_d} \\
 0 &\leq \dot{x}(t) \leq 2, \quad \lim_{t \rightarrow \infty} \dot{x}(t) = 1 \\
 -\omega_d &\leq \ddot{x}(t) \leq \omega_d, \quad \lim_{t \rightarrow \infty} \ddot{x}(t) = 0
 \end{aligned} \tag{3}$$

These expressions hold for all  $t$ , including the initial oscillatory transients. Moreover, for reasonable model parameters ( $\omega_d$ ,  $\zeta_d$ ,  $T_R$ ,  $N_{\delta AS}$ ,  $L_{\delta AS}$ , etc.), the first two inequalities will actually be closer to  $0 \leq x \leq t$  and  $0 \leq \dot{x} \leq 1$ . So the maximum sideslip increment ( $\Delta\beta$ ) occurring during the first two seconds of response can be adequately approximated by

$$\Delta\beta \doteq \frac{T_R}{\omega_d} L_{\delta AS} \delta_{AS} \max \left[ \left( \frac{N_{\delta AS}}{L_{\delta AS}} L_p - N_p + \frac{g}{U_o} \right) + 2 \frac{g}{U_o} \left( \frac{N_{\delta AS}}{L_{\delta AS}} L_r - N_r \right) \right] \tag{4}$$

This is the literal expression used in Table II. Note that it is often possible to simplify  $\Delta\beta$  still further when either the constant or the ramp term in Equation (4) dominates.

Parameters  $s_9$  and  $s_{10}$ : Steady-State Roll Rate Due to Aileron ( $p/\delta_{AS}|_{SS}$ ); Steady-State Sideslip Due to Rudder ( $\beta/\delta_R|_{SS}$ ) -- These parameters should simply reflect the basic steady-state roll rate and sideslip characteristics of the free aircraft. They should not be confused with stick sensitivity or rudder sensitivity conditions. The latter must be determined from pilot rating data which relate optimal sensitivities to roll time constants and other handling-quality parameters. They are not needed for model-following design, only for final system mechanization.

Parameters  $s_{11}$ : Steady-State Roll Rate Due to Rudder  $(p/\delta_R)_{ss}$  -- Conditions on rudder-induced-rolling authority are motivated by paragraph 3.3.4.5 of Ref. 1 which specifies a minimum of 3 deg/sec of roll rate for 50-lb pedal forces.

## Numerical Values for the F4C Lateral Axes

Using these 11 parameters, four handling-quality models were developed for the F4C aircraft. The models are ordered monotonically in terms of predicted handling qualities "goodness" -- ranging from poor, model 1, to excellent, model 4. This predicted ranking was later verified in the validation experiments.

The process of developing models consists simply of choosing numerical values for the 11 parameters and solving the resulting nonlinear algebraic equations (Table II) for the model coefficients.<sup>2</sup> The values chosen for the F4C are given in Table III and the resulting model coefficients in Table IV. Transient responses for models 1 through 4 are given in Figures 1 through 4. Some of the detailed considerations concerning the numerical values are discussed below.

Parameters  $s_1$  and  $s_2$  -- Numerical values  $s_1$  and  $s_2$  for all four handling-quality models were taken from the data of Figures 5 through 10 (3.3.1.1) of Ref. 2 (pages 191 to 196) and from the data of Figure 6 of Ref. 6 (pages 43 and 44). Two of these figures -- 5 (3.3.1.1) of Ref. 2 and 6 of Ref. 6 -- are reproduced in Appendix I as Figures 99 and 100, showing the chosen numerical values. The logic governing these choices is essentially this -- we started for model 4 with the parameter values which achieved the best pilot rating and chose parameters for the remaining models such that each successive model was about one-half to one rating unit worse than the previous one. This was repeated for all conditions of Table II.

It must be acknowledged that this procedure is far from formal. Trends in pilot rating data are often much too broad to permit accurate identification of a unit pilot rating degradation increment. Moreover, where simultaneous degradation in more than one parameter is required (such as in the present case,  $\omega_d$  and  $\zeta_d$ ), there are numerous paths (in parameter space) along which the investigator may travel. The choice is left largely to his intuition. Finally, the net effect of independently degrading each of the conditions of Table II, singly or in groups of two or three, is quite unknown. We certainly cannot claim to predict the pilot ratings of the resulting models. It is reasonable, however, to expect that their monotonic ordering will stay intact.

---

<sup>2</sup>While much can be said about the details of these solutions, it is sufficient here to state that a solution exists if the chosen conditions are reasonable and that it is readily found with a few trial-and-error iterations.

Table III. Numerical Values for Parameters 1 through 11

Parameter	Handling-Quality Model			
	4 Excellent	3 Good	2 Fair	1 Poor
$s_1 = (\omega_d)^2$	6.25	5.29	3.61	2.25
$s_2 = 2\zeta_d \omega_d$	1.25	0.805	0.494	0.300
$s_3 = 1/T_R$	4.0	1.0	0.57	0.33
$s_4 = 1/T_S$	0	0	0	0
$s_5 = L_\beta$	-10.0	-10.0	-10.0	-10.0
$s_6 = (\omega_\phi / \omega_d)^2$	1.0	0.790	0.543	0.270
$s_7 = 2(\zeta_\phi \omega_\phi - \zeta_d \omega_d)$	0	0	0	0
$s_8 = \Delta\beta_{\max}$	0.017	0.087	0.240	0.210
$s_9 = (p/\delta_{AS}) _{ss}$	5.0	5.0	5.0	5.0
$s_{10} = (\beta/\delta_R) _{ss}$	-0.5	-0.5	-0.5	-0.5
$s_{11} = (p/\delta_R) _{ss}$	-0.5	-0.5	-0.5	-0.5

Table IV. Model Coefficients

Coefficient	Handling-Quality Model			
	4	3	2	1
$L_p$	-4.0	-0.981	-0.516	-0.402
$L_r$	0.865	0.177	0.391	-0.448
$L_\beta$	-10.0	-10.0	-10.0	-10.0
$L_{\delta R}$	3.30	4.58	4.79	5.035
$L_{\delta AS}$	20.0	6.34	5.25	6.11
$N_p$	0.040	0.030	0.017	0.056
$N_r$	-0.507	-0.092	-0.139	0.099
$N_\beta$	5.87	5.23	3.55	2.22
$N_{\delta R}$	-3.13	-2.65	-1.81	-1.13
$N_{\delta AS}$	0	-0.690	-0.855	-0.984
$Y_\beta$	-0.743	-0.732	-0.418	-0.327



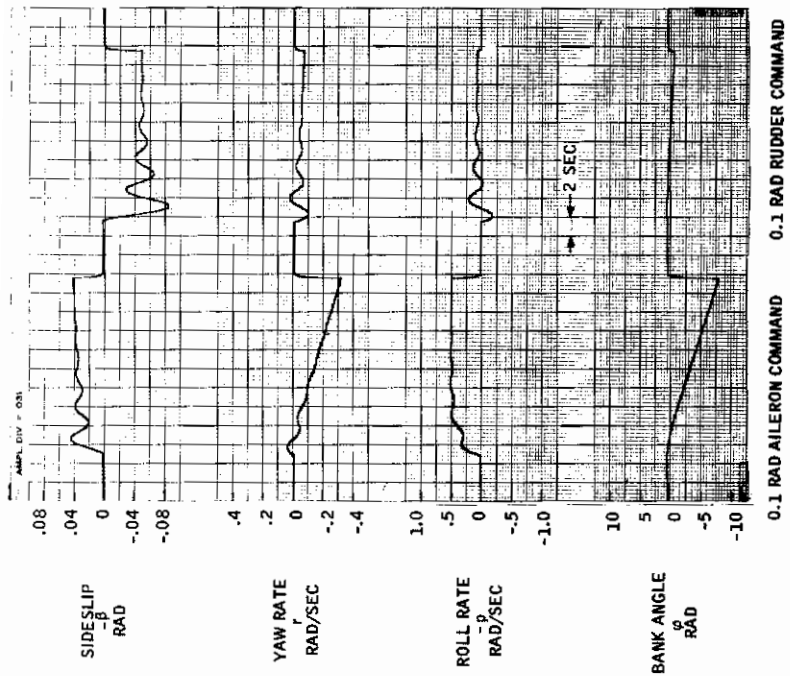


Figure 2. Step Responses -- Model 2

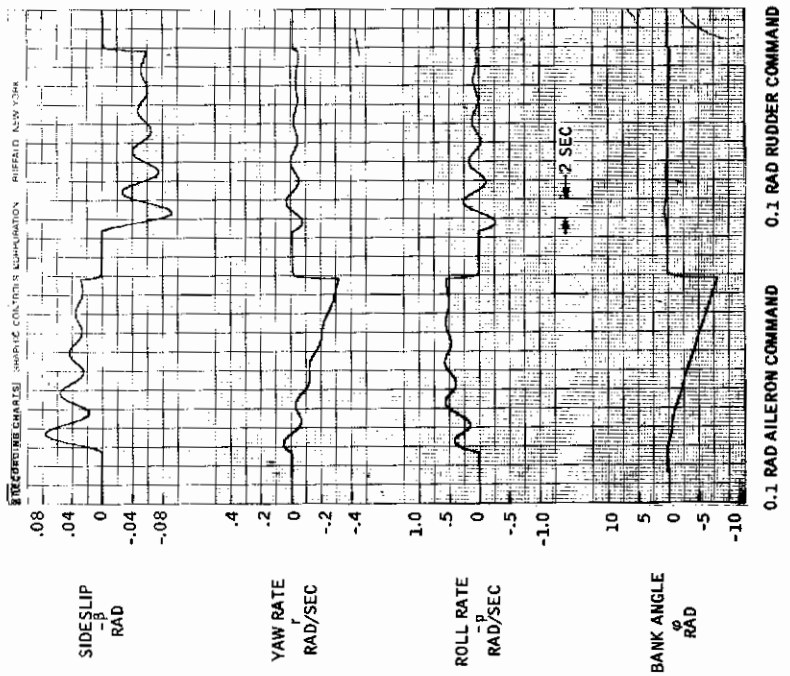


Figure 1. Step Responses -- Model 1

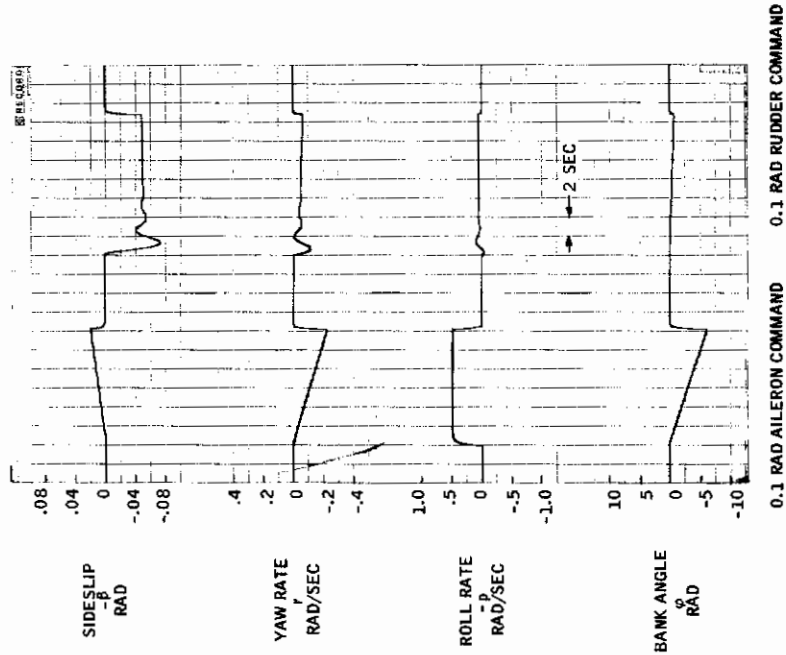


Figure 3. Step Responses -- Model 3

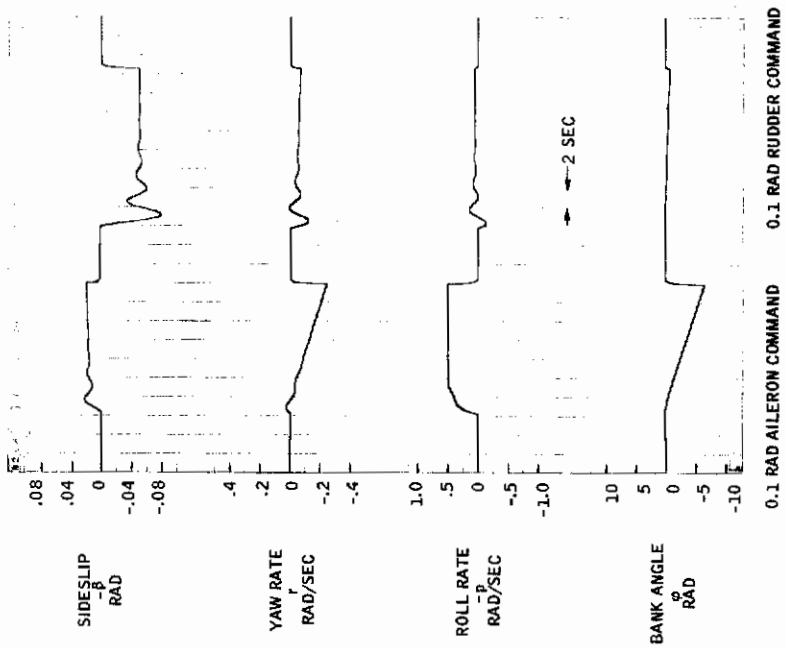


Figure 4. Step Responses -- Model 4



# Contrails

Parameter  $s_3$  -- Values for the roll time constant were taken from Figure 1 (3.3.1.2) and 16 (3.3.1.2) of Ref. 2 (pages 210 and 219). These are reproduced in Appendix I as Figures 101 and 102, which show our chosen values. It should be noted that several other handling-quality parameters have been experimentally related to  $T_R$ , notably  $L_\beta$  and  $L_\delta$ . These relationships are taken into account below.

Parameter  $s_4$  -- Because the spiral time constant ( $1/T_S$ ) is an insensitive handling-quality parameter, its values were fixed at  $1/T_S = 0$  for all models.

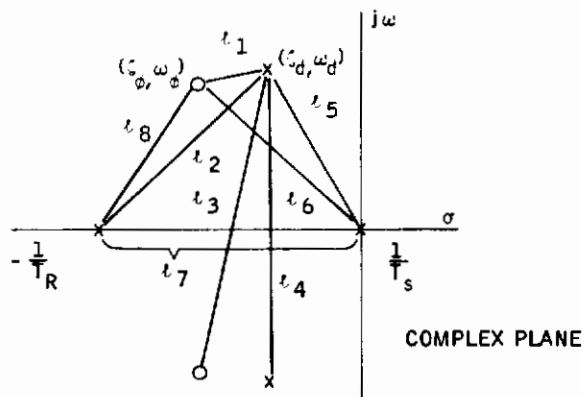
Parameter  $s_5$  -- The dihedral effect ( $L_\beta$ ) was specified according to the  $L_\beta$  versus  $T_R$  curves mentioned above. Numerical values are as shown in Figure 103, which is a reproduction of Figure 1 (3.3.6.3) of Ref. 2.

Parameters  $s_6$  and  $s_7$  -- Relevant data for the choice of zero locations are provided in Figures 17 (3.3.2.2) through 26 (3.3.2.2) of Ref. 2, the first four of which are reproduced in Appendix I as Figure 104. Note that the contours in this figure do not fully cover the four sets of  $\omega_d$ ,  $\zeta_d$ , and  $T_R$  values which have already been selected. Since each point on the contours represents a specified  $p_{osc}/p_{avg}$  roll rate response, however, the contours can be readily scaled. The required scaling parameter is obtained as follows.

By Laplace inversion of the roll-rate-due-to-aileron transfer function of Table I, the roll rate response to a unit step aileron command is given by

$$p(t) = L_{\delta AS} \left[ \frac{l_6^2}{l_5^2 l_7} - \frac{l_8^2}{l_2^2 l_7} e^{-t/T_R} + 2 \frac{l_1 l_3}{l_2 l_4 l_5} e^{-\zeta_d \omega_d t} \cos \left( \omega_d \sqrt{1 - \zeta_d^2} t + \psi_\beta \right) \right] \quad (6)$$

where  $1/T_S = 0$  and  $l_1, \dots, l_8$  are distances on the pole-zero constellation of the roll-rate-due-to-aileron transfer function.



# Contrails

The ratio of the oscillatory component (dutch roll) to the average component of roll rate is therefore proportional to

$$\frac{l_1 l_3 / l_2 l_4 l_5}{l_6^2 / l_5^2 l_7} \doteq 1/2 \frac{l_1 l_3 l_7}{l_2 l_6^2} \quad (7)^3$$

Using this scaling parameter, the contours of Figure 91 were scaled to correspond to the  $\omega_d$ ,  $\zeta_d$ , and  $T_R$  selected above. This was done for zero positions which are located at +270 deg (with respect to the dutch roll pole) only. While this particular direction is somewhat arbitrary, it does represent a compromise between desirable locations (Figure 104) and actual locations of the F4 airframe (see Figure 5). The resulting scaled contour points and choice of zero locations are shown in Figure 6.

Parameter  $s_8$  -- Numerical values for  $s_8 = \Delta\beta_{\max}$  were taken directly from the specifications given in Ref. 1 (see Figure 105).

Parameters  $s_9$  and  $s_{10}$  -- Steady-state roll rate and sideslip characteristics were set at

$$\left. \frac{p}{\delta_{AS}} \right|_{ss} = 5.0 \quad \text{and} \quad \left. \frac{\beta}{\delta_R} \right|_{ss} = -0.5$$

for all models. These reflect the F4's own characteristics, as tabulated in Table V.

Parameter  $s_{11}$  -- Rudder-induced rolling authority was restricted to 10 percent of aileron-induced rolling for all models. There are several arguments for and against such specifications. For example, if decoupled lateral/roll control is the main objective, then the 10-percent condition can be considered too high. On the other hand, if we require that wings-level flight be possible with a "one-half hardover aileron failure," then 10 percent is too low. We elected here to provide enough authority to satisfy paragraph 3.3.4.5 of Ref. 1 for appropriate force-feel characteristics.

<sup>3</sup>R. J. Woodcock of AFFDL has pointed out that this ratio does not quite correspond to the  $p_{osc}/p_{avg}$  ratio of the military specification. The latter uses oscillatory and average components after approximately one dutch roll cycle, rather than the dutch roll envelope at  $t = 0$  and the average value at  $t = \infty$ , as done above.

Table V. Steady-State Roll Rates and Sideslip for Free Airframe

Flight Condition †	$\frac{p}{\delta AS} \Big _{ss}$	$\frac{\beta}{\delta R} \Big _{ss}$
1	1.43	-0.224
2	3.97	-0.564
3	3.82	-0.163
4	6.68	-0.436
5	3.13	-0.462
6	4.77	-0.155
7	6.95	-0.240
8	6.00	-0.407
9	4.82	-0.187
10	5.92	-0.512
11	6.05	-0.516

† These flight conditions are defined in Section IV.

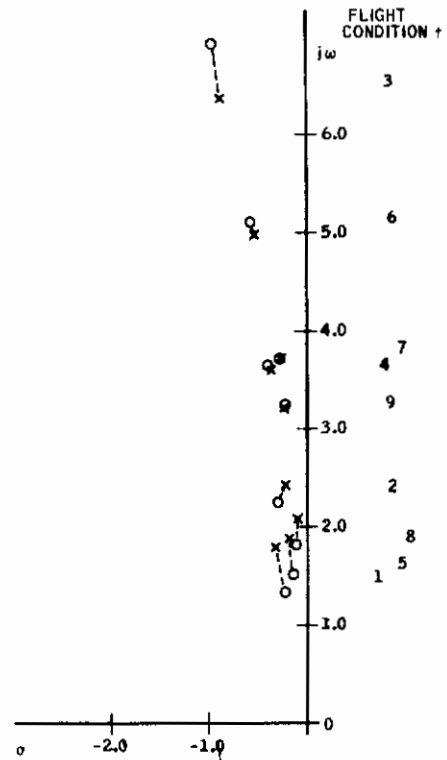


Figure 5. Zero-Pole Relationships Free Airframe

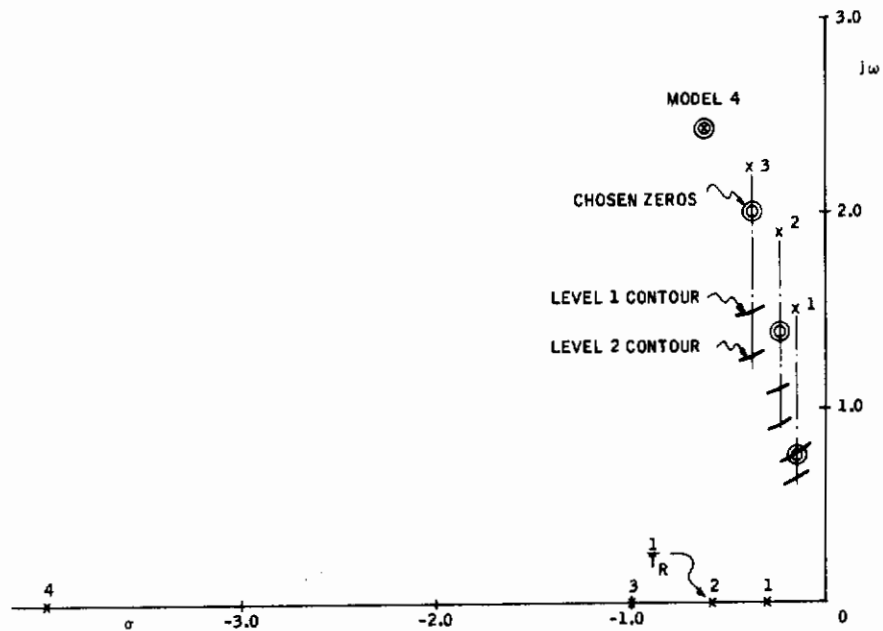


Figure 6. Zero-Pole Relationships Models

## SECTION III DESIGN MECHANICS

As indicated in Section I, the design procedure developed in this program uses model-following control techniques in a multiplant optimization formulation and newly-developed computational algorithms to compute practical aircraft control systems. These topics are discussed below.

### OPTIMAL MODEL-FOLLOWING CONTROL

The notion of controlling a dynamic system in such a way that its responses match those of a model has received much attention in the engineering literature (Refs. 7, 8, 9, 10). The controller is typically formulated as the solution of an optimization problem which, for stationary linear stochastic systems with quadratic performance indices, takes the following form.

Given the plant (aircraft),

$$\dot{x}_p = F_p x_p + G_p u_p + \Gamma_p \eta_p \quad E[\eta_p(t)\eta_p^T(\tau)] = I \delta(t-\tau) \quad (8)$$

and a dynamic model for its responses and commands,

$$\dot{x}_m = F_m x_m + G_m u_m \quad (9)$$

$$\dot{u}_m = F_u u_m + \Gamma_u \eta_u \quad E[\eta_u(t)\eta_u^T(\tau)] = I \delta(t-\tau) \quad (10)$$

find the feedback control law,  $u_p = u_p(x_p, x_m, u_m)$ , which minimizes the performance index

$$J(u_p) = E \left\{ \| H_p x_p - H_m x_m \|_Q^2 + \| u_p \|_R^2 \right\} \quad (11)^4$$

As usual, the symbol  $x_p$  denotes an  $n_p$ -dimensional state vector of the plant,  $u_p$  is an  $m_p$ -vector of control inputs, and  $\eta_p$  is an  $r_p$ -dimensional white-noise disturbance vector. The quantities  $F_p$ ,  $G_p$ , and  $\Gamma_p$  are known constant matrices of appropriate size, with the pair  $\{F_p, G_p\}$  assumed to be completely controllable.

---

<sup>4</sup>The symbolism  $\|x\|_A^2$  denotes the quadratic form  $x^T A x$ . For later reference, this expression can also be written as  $\text{Trace} \{A x x^T\}$ .

Similarly,  $x_m$  and  $u_m$  are  $n_m$ - and  $m_m$ -dimensional model states and commands, respectively. Quantities  $F_m$  and  $G_m$  are again constant known matrices, with  $F_m$  assumed to be stable.

To eliminate command-dependence of the optimal controller, the commands themselves are taken to be sample functions of the random process [Equation (10)]. This consists, again, of a stable linear system driven by a white-noise process,  $\eta_u$ . Magnitudes and spectral content of  $u_m$  are determined by matrices  $F_u$  and  $\Gamma_u$ . Optimization is then carried out over the ensemble of command functions, as well as over the ensemble of disturbances. (Other ways of dealing with command-dependence, particularly for deterministic problem formulations, can be found in Refs. 7 and 10.)

The performance measure [Equation (11)] is an expected value of selected model-following errors, compromised against total control effort exerted on the plant. The choice of errors in the performance index (as opposed to error rates) has more than surface significance. As shown below, it means that the optimal controller must include an active simulation of the model dynamics [Equation (9)]. Had error rates been chosen, no such model would be required (Ref. 8). This advantage of an error rate index, however, is outweighed by increased sensitivity of the resulting controller to plant parameter variations (Ref. 7). Low sensitivity, of course, is one of the key objectives of our design procedure.

As usual, the matrix,  $Q$ , in Equation (11) is positive semidefinite and symmetric, and  $R$  is positive definite symmetric. These conditions guarantee the existence of a unique optimal feedback control of the form

$$u_p = K_p^* x_p + K_m^* x_m + K_u^* u_m \quad (12)$$

This is a linear controller comprised of three distinct sets of signals:

- 1) State feedback from the plant with feedback gain matrix  $K_p^*$ .
- 2) Model feedforwards with gain  $K_m^*$  (these signals require simulation of model dynamics).
- 3) Command feedforwards through gain  $K_u^*$ .

A diagram of the controller is shown in Figure 7.

As shown in various references (see for example Refs. 11, 36), the gain matrices  $K_p^*$ ,  $K_m^*$ , and  $K_u^*$  are defined by the solution of a matrix Riccati equation. In particular, let:

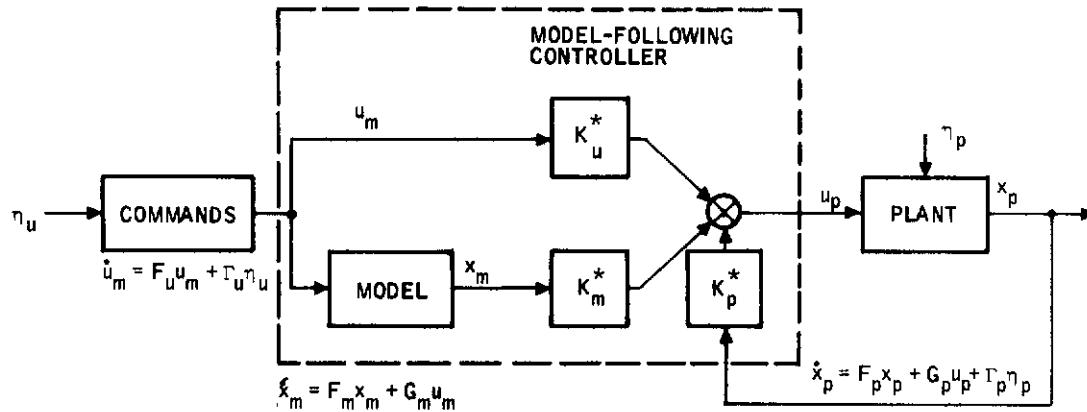


Figure 7. Model-Following Structure

$$\mathbf{x} = \begin{bmatrix} x_p \\ x_m \\ u_m \end{bmatrix}, \quad \boldsymbol{\eta} = \begin{bmatrix} \eta_p \\ \eta_u \end{bmatrix}$$

$$\mathbf{F} = \begin{bmatrix} F_p & 0 & 0 \\ 0 & F_m & G_m \\ 0 & 0 & F_u \end{bmatrix}, \quad \mathbf{G} = \begin{bmatrix} G_p \\ 0 \\ 0 \end{bmatrix}, \quad \boldsymbol{\Gamma} = \begin{bmatrix} \Gamma_p & 0 \\ 0 & 0 \\ 0 & \Gamma_u \end{bmatrix} \quad (13)$$

$$\mathbf{W} = \begin{bmatrix} H_p^T Q H_p & -H_p^T Q H_m & 0 \\ -H_m^T Q H_p & H_m^T Q H_m & 0 \\ 0 & 0 & 0 \end{bmatrix}, \quad \mathbf{P} = \begin{bmatrix} P_{11} & P_{12} & P_{13} \\ P_{21} & P_{22} & P_{23} \\ P_{31} & P_{32} & P_{33} \end{bmatrix}$$

Then

$$\begin{aligned}
 u_p &= -R^{-1} G^T P \mathbf{x} \\
 &= \left( -R^{-1} G_p^T P_{11} \right) x_p + \left( -R^{-1} G_p^T P_{12} \right) x_m + \left( -R^{-1} G_p^T P_{13} \right) u_m \\
 &= K_p^* x_p + K_m^* x_m + K_u^* u_m \quad (14)
 \end{aligned}$$



where P is given by

$$PF + F^T P + W - PGR^{-1}G^T P = 0 \quad (15)$$

This is a purely algebraic equation and very efficient algorithms exist for its numerical solution, even for high-order dynamic systems (Ref. 12).

Some of the properties of the controller [Equation (12)] are summarized below:

- 1) The feedback gains,  $K_p^*$ , depend only on plant dynamics (and W and R), not on model or command dynamics.
- 2) The model feedforwards,  $K_m^*$ , depend on plant and model dynamics (and W and R), but not on commands.
- 3) The command feedforwards,  $K_u^*$ , depend on all factors -- plant, model, commands, and W and R.

The first two of these properties were originally reported in Ref. 10, and the third one is implied there. They can be readily verified by writing out Equation (15) in partitioned form. For the  $P_{11}$ ,  $P_{12}$ , and  $P_{13}$  matrices needed in Equation (14), we get

$$P_{11}F_p + F_p^T P_{11} + W_{11} - P_{11}G_p R^{-1}G_p^T P_{11} = 0 \quad (16)$$

$$P_{12}F_m + F_p^T P_{12} + W_{12} - P_{11}G_p R^{-1}G_p^T P_{12} = 0 \quad (17)$$

$$P_{12}G_m + P_{13}F_u + F_p^T P_{13} - P_{11}G_p R^{-1}G_p^T P_{13} = 0 \quad (18)$$

Note that these equations also suggest a simpler way of computing the gain matrices. Instead of solving one  $(n_p + n_m + n_u)$ -dimensional Riccati equation as in Equation (15), we only need to solve an  $n_p$ -dimensional one, plus two linear matrix equations of order  $(n_p \times n_m)$  and  $(n_p \times n_u)$ .

## PRACTICAL MODEL-FOLLOWING CONTROL

As formulated above, the optimal model-following controller has two serious disadvantages: 1) it uses the full plant state vector,  $x_p$ , for feedback, and 2) all three sets of gains vary with the plant parameters,  $F_p$  and  $G_p$ . It thus requires complex measurement instrumentation and gain scheduling for multiplant applications. In our definition of practicality (Section I), of course, these are the very conditions to be avoided.

Traditionally, these difficulties of optimal control have been overcome by extensive simulation programs (Ref. 13). After an optimal controller was initially designed, its many signal paths were individually investigated. They were deleted if their contribution to total cost or to the total control signal was small, or were replaced by blended signals from available sensors if their contribution was significant. Gains were adjusted to work well over a range of flight conditions. In this way, the original optimal controller was eventually reduced to a practical one.

In the design procedure developed here, we attempt to avoid such after-the-fact manipulations by reformulating the original optimization problem such that the requirements of practicality are directly included.

## Problem Reformulation

The aircraft will be represented at various points of the flight envelope and for various configurations and mass distributions by a collection of frozen-point linear plants:

$$\begin{aligned} \dot{x}_p(i) &= F_p(i) x_p(i) + G_p(i) u_p + \Gamma_p(i) \eta_p & (19) \\ i &= 1, 2, \dots, p \end{aligned}$$

where  $x_p(i)$  is again the plant state vector,  $u_p$  is the vector of actuator inputs,  $\eta_p$  is white noise. The state,  $x_p$ , and the system matrices,  $F_p$ ,  $G_p$ ,  $\Gamma_p$ , are indexed by the integer  $i$ , denoting a particular frozen-point plant. The index ranges from  $i = 1$  to  $i = p$ , meaning that  $p$  distinct plants will be handled simultaneously.

We now look for a time invariant controller of the form

$$u_p(i) = K(i) \begin{bmatrix} x_p(i) \\ x_m \\ u_m \end{bmatrix}, \quad i = 1, 2, \dots, p \quad (20)$$

such that the following composite performance index is minimized:

$$J = \sum_{i=1}^p \alpha_i J(i) \quad (21)$$

where

$$J(i) = E \{ \| H_p(i) x_p(i) - H_m x_m \|_{Q(i)}^2 + \| u_p(i) \|_{R(i)}^2 \} \quad (22)$$

This cost functional is a generalization of Equation (11), representing weighted average performance over the flight envelope.

To achieve practicality, the form of the gain matrices  $[K(1), K(2), \dots, K(i), \dots, K(p)]$  cannot remain entirely arbitrary. Measurement realizability implies that certain elements of all gain matrices must vanish, and elimination of gain scheduling requires that other elements of all matrices be identical.<sup>5</sup> These conditions are imposed on the form of  $K(i)$  at the outset, thus incorporating the controller simplification requirement directly into the optimization problem. In particular, let  $y$  denote an  $\mu$ -vector of readily-observable signals, i. e.,

$$y = M(i) \begin{bmatrix} x_p(i) \\ x_m \\ u_m \end{bmatrix}, \quad i = 1, 2, \dots, p \quad (23)$$

where the matrices,  $M(i)$ , select sensed signals and account for such things as sensor position, orientation, and sensitivity as they vary with flight condition. Then the gains,  $K(i)$ , must satisfy

$$[K(1), \dots, K(i), \dots, K(p)] = [KM(1), \dots, KM(i), \dots, KM(p)] \quad (24)$$

for some constant  $(m_p \times r)$ -matrix  $K$ .

Unfortunately, this new optimization problem does not yield a unique closed-form solution. Instead, several local minima are possible, each satisfying the necessary conditions of optimality. To solve for even one requires considerable computational effort. This is the price of practicality.

### Necessary Conditions of Optimality

Optimality conditions for the gains,  $K(i)$ , can be expressed directly in terms of the performance index,  $J$  [Equation (21)], or they can be obtained from the Maximum Principle (Ref. 11).

Using the first method, we think of  $J$  as an explicit function of the gain matrices. Then optimality requires that the first partial derivatives of  $J$  with respect to  $K$  vanish; i. e.,

---

<sup>5</sup>The latter constraint may well mean that adequate performance is impossible. While this is not the case in the F4 designs considered here, the possibility is certainly real and warrants research to remove the no-gain-schedule constraint.

$$\frac{\partial}{\partial K} J[KM(1), KM(2), \dots, KM(p)] = 0 \quad (25)$$

Using the Maximum Principle, we first write the plant-model-command combination as a single system via Equations (13). This gives

$$\dot{x}(i) = F(i)x(i) + G(i)u_p + \Gamma(i)\eta \quad E[\eta(t)\eta^T(\tau)] = I\delta(t-\tau) \quad (26)$$

$$u_p = KM(i)x(i), \quad i = 1, 2, \dots, p \quad (27)$$

$$J(u_p) = E \sum_{i=1}^p \alpha_i \left[ \|x\|_{W(i)}^2 + \|u_p\|_{R(i)}^2 \right] \quad (28)$$

We then note that the composite performance index [Equation (28)] can be written as

$$J = \sum_{i=1}^p \alpha_i \text{Trace} [W(i) + M^T(i) K^T R(i) KM(i)] X(i) \quad (29)$$

where  $X(i)$ ,  $i = 1, 2, \dots, p$ , are covariance matrices defined by (Ref. 36)

$$0 = [F(i) + G(i) KM(i)] X(i) + X(i) [F(i) + G(i) KM(i)]^T + \Gamma(i) \Gamma^T(i) \quad i = 1, 2, \dots, p \quad (30)$$

These equations are used to define a Hamiltonian:

$$H = \sum_{i=1}^p \alpha_i \text{Trace} [W(i) + MKRK M(i)] X(i) + \text{Trace} S^T(i) [FGKM(i)X(i) + X(i)FGKM^T(i) + \Gamma(i) \Gamma^T(i)] \quad (31)$$

where the shorthand notation  $MKRKM(i)$  and  $FGKM(i)$  denotes  $M^T(i)K^T R(i) KM(i)$  and  $F(i) + G(i)KM(i)$ , respectively. The  $H$  is now differentiated with respect to the covariance matrices,  $X(i)$ , and the adjoint matrices,  $S(i)$ , and with respect to all of the free gains permitted by the constraint [Equation (24)]. This gives the following necessary conditions:

$$\frac{\partial H}{\partial S(i)} = FGKM(i)X(i) + X(i)FGKM^T(i) + \Gamma(i)\Gamma^T(i) = 0 \quad (32a)$$

$$i = 1, 2, \dots, p$$

$$\frac{\partial H}{\partial X(i)} = S(i)FGKM(i) + FGKM^T(i)S(i) + \alpha_i [W(i) + MKRKM(i)] = 0$$

$$i = 1, 2, \dots, p \quad (32b)$$

$$\frac{\partial H}{\partial K} = \sum_{i=1}^p [\alpha_i R(i)KM(i) + G^T(i)S(i)]X(i)M^T(i) = 0 \quad (32c)$$

These conditions were derived for single plants (i. e.,  $p = 1$ ) by Axsäter (Ref. 14) (time-varying problems) and by Levine (Ref. 15) (deterministic problems). For  $p > 1$ , they were first derived by Skelton (Ref. 16).

## Computational Solutions

As noted above, the necessary conditions may have several solutions, none of which are given analytically. They must be found by numerical solution of either Equations (25) or (32). Several iterative algorithms have been proposed for the latter equations. These include Axsäter's algorithms (Ref. 14), a modified gradient algorithm (Ref. 17), and others (Ref. 15). All require large computer budgets (for high-order system), and all suffer from initialization problems, i. e., choosing initial values for  $K$ . (Initial values determine which local minimum will finally be found.)

The design procedure described in this report uses a newly-developed algorithm for Equation (25) which exhibits comparable computational speeds but avoids the initialization problem. The algorithm proceeds by dividing the gain matrices,  $K(i)$  (for the moment these are assumed to be arbitrary), into two components:

$$K(i) = (K^1 + K^3)M(i) + \lambda K^2(i), \quad i = 1, 2, \dots, p \quad (33)$$

The first component,  $(K^1 + K^3)M(i)$ , satisfies the constraint conditions [Equation (24)] and will be called "gains to be retained". The second component,  $\lambda K^2(i)$ , with scalar multiplier  $\lambda$  does not satisfy Equation (24) and will be called "gains to be discarded". For generality, the first component is further subdivided into parts  $K^1$  and  $K^3$ , where  $K^1$  represents free gains to be optimized and  $K^3$  is fixed.

In terms of these subdivisions, the necessary conditions [Equation (25)] become



$$\frac{\partial}{\partial K^1} J [(K^1 + K^3)M(1) + \lambda K^2(1), \dots, (K^1 + K^3)M(p) + \lambda K^2(p)] = 0$$

or more simply

$$\frac{\partial}{\partial K^1} J(K^1, \lambda) = 0 \tag{34}$$

for fixed  $K^2(i)$ ,  $M(i)$ , and  $K^3$ . This last equation implies that the optimal gains are functions of  $\lambda$ ; i. e.,

$$K^1 = K^1(\lambda)$$

where, according to the Implicit Function Theorem (Ref. 18),  $K^1(\cdot)$  is defined by the following differential equation:

$$\frac{dK^1(\lambda)}{d\lambda} = - \left[ \frac{\partial^2 J(K^1, \lambda)}{\partial K^1 \partial K^1 T} \right]^{-1} \frac{\partial^2 J(K^1, \lambda)}{\partial K^1 \partial \lambda} \tag{35}^6$$

From Equation (33), however, it follows that the desired constrained gains correspond to  $\lambda = 0$ . That is,

$$K(i) = [K^1(0) + K^3] M(i), \quad i = 1, 2, \dots, p \tag{36}$$

So it is possible to obtain solutions of Equation (25) by solving Equation (35), starting with any known terminal condition [satisfying Equation (34)] at  $\lambda = 1$ , and integrating backwards toward  $\lambda = 0$ . The choice of terminal condition and method of numerical integration are discussed below. The idea of parameterizing solutions of optimization problems and solving the resulting ordinary differential equations was developed by D. K. Scharmack (Ref. 19).

Terminal Conditions -- The most appealing terminal condition is the global optimum of the performance index,  $J$ . This corresponds to the gains  $[K^*(1), K^*(2), \dots, K^*(p)]$  which are obtained by optimizing the  $i^{\text{th}}$  plant with respect to the  $i^{\text{th}}$  criterion  $J(i)$  without gain constraints, for all  $i$ . (As discussed earlier in this section, these gains are readily computed.) The resulting  $K^1, K^2, K^3$  values for  $\lambda = 1$  are:

$$K^3 = \text{given}$$

---

<sup>6</sup>Equations (34) and (35) make sense in vector matrix notation only if the matrix  $K^1$  is written out as a column vector. This is assumed.



$$K^1 = \left[ \sum_i K^*(i) M^T(i) \right] \left[ \sum_i M(i) M^T(i) \right]^{-1} - K^3 \quad (37)^7$$

$$K^2(i) = K^*(i) - (K^1 + K^3) M(i), \quad i = 1, 2, \dots, p \quad (38)$$

Starting with these terminal conditions amounts to starting in the "deepest valley of  $J$ " and forcing  $K^2$  to zero along the trajectory  $[K^1(\lambda), \lambda K^2; 1 \geq \lambda \geq 0]$ . As long as the matrix of second partials in Equation (35) remains nonsingular, the resulting solution,  $K^1(0)$ , is unique and represents a stable linear controller. Moreover, we have the reassurance that it is a point "on the walls of the deepest valley". Together with the knowledge of  $J(K^*)$  and  $J[K^1(0)]$ , this information could well suffice to terminate the search.

Numerical Integration -- The full gamut of integration techniques is available for this problem. In Ref. 19, a predictor-corrector scheme was found to be particularly useful. It consists of the following equations:

- Adams-Moulton Predictor

$$K^P = K^1(\lambda_k) + \frac{\Delta\lambda}{24} \left[ 55 \frac{dK^1}{d\lambda}(\lambda_k) - 59 \frac{dK^1}{d\lambda}(\lambda_{k-1}) + 37 \frac{dK^1}{d\lambda}(\lambda_{k-2}) - 9 \frac{dK^1}{d\lambda}(\lambda_{k-3}) \right] \quad (39)$$

- Newton-Raphson Corrector

$$K^C = K^P - \left[ \frac{\partial^2 J(K^P, \lambda_{k+1})}{\partial K^1 \partial K^{1T}} \right]^{-1} \frac{\partial J(K^P, \lambda_{k+1})}{\partial K^1} \quad (40)$$

The corrector is cycled repeatedly, each time replacing the old value  $K^P$  with the new value  $K^C$ , until a convergence criterion of the form  $|\partial J / \partial K^1| < \epsilon$  is satisfied. The final value of  $K^C$  becomes  $K^1(\lambda_{k+1})$ .

---

<sup>7</sup>As long as Equation (38) is observed, the choice of  $K^1$  is arbitrary. Here we have chosen  $K^1$  such that the gains to be discarded have minimal magnitude. This is achieved by pseudo inversion of  $[M(1) \dots M(p)]$ , a process which minimizes  $\| (K^1 + K^3) [M(1) \dots M(p)] - [K^*(1) \dots K^*(p)] \|^2 = \| K^2(1) \dots K^2(p) \|^2$ . For a discussion of the pseudo inverse, see Ref. 37.

where

$$\lambda_{k+1} = \lambda_k + \Delta\lambda, \quad \Delta\lambda < 0$$

$$k = 0, 1, 2, \dots, \frac{1}{|\Delta\lambda|}$$

The integration is initiated at  $\lambda_0 = 1$ , with  $K^1(1)$  given by Equation (37).

The utility of these equations depends, of course, on the computer time and memory required to evaluate first- and second-partial derivatives. Equations for this purpose are developed in Appendix II. It turns out that all necessary derivatives for a single predictor or corrector step can be obtained by solving  $(l+3)$  n-dimensional covariance equations [of the type of Equation (30)], where  $l$  is the number of gain components in  $K^1$ . These equations can be solved very quickly even for large systems (Refs. 20, 21). So it becomes possible, with the algorithm discussed above, to solve some fairly complex control problems. This is shown in the next section with an F4C design application. A flow diagram of the complete algorithm is shown in Figure 8.

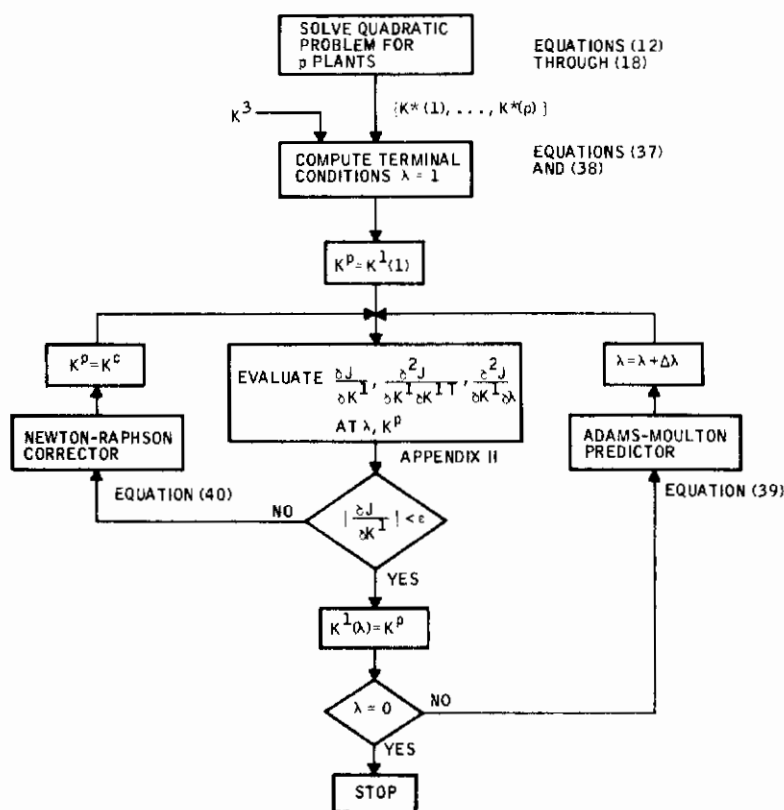


Figure 8. Flow Diagram for Computational Algorithm

## SECTION IV LATERAL-AXIS DESIGNS FOR THE F4C

The optimal control formulation and computational procedure discussed in Section III were used to design control systems for the lateral-directional axes of the F4C aircraft. Details of these designs are discussed here. We begin by describing the mathematical models used. This is followed by a discussion of individual optimal controllers at each flight condition, and finally, by a description of practical control system designs for the entire flight envelope.

### MATHEMATICAL MODELS

As required by the problem formulation, the aircraft was represented by linear differential equations at selected flight conditions. These include rigid-body dynamics, an approximation of the first asymmetric flexure mode, actuator and servo dynamics, and sensor dynamics. A handling-qualities model, a command model, and a gust model were appended, and a set of measurable signals was defined to complete the mathematical representation.

The resulting equation is 20th-order, with the following general structure:

$$\dot{x} = \begin{bmatrix} F_{rb} & G_1 & G_2 & 0 & G_3 \\ H_1 & F_f & G_4 & 0 & G_5 \\ 0 & 0 & F_{as} & 0 & 0 \\ H_2 & H_3 & H_4 & F_{se} & H_5 \\ 0 & 0 & 0 & 0 & F_w \\ \hline & & & \tilde{F}_m & \tilde{G}_m \\ & & & 0 & F_u \end{bmatrix} x + \begin{bmatrix} 0 \\ 0 \\ G_{as} \\ 0 \\ 0 \\ 0 \\ 0 \end{bmatrix} u_p + \begin{bmatrix} 0 & 0 \\ 0 & 0 \\ 0 & 0 \\ 0 & 0 \\ \Gamma_w & 0 \\ \hline 0 & 0 \\ 0 & \Gamma_u \end{bmatrix} \eta \quad (41)^8$$

$$y = [M_1 \quad 0 \quad 0 \quad M_2 \quad 0 \quad M_3 \quad M_4] x \quad (42)$$

where

$$x^T = \left( x_{rb}^T \quad x_f^T \quad x_{as}^T \quad x_{se}^T \quad x_w^T \quad \left| \quad \tilde{x}_m^T \quad u_m^T \right. \right)$$

<sup>8</sup>Blank partitions of matrices are assumed to be filled with zeros.

and

$x_{rb}$  = Rigid-body states ( $p, r, \beta, \phi$ )

$x_f$  = Flexure states ( $\xi, \dot{\xi}$ )

$x_{as}$  = Actuator/servo states ( $\delta_R, \delta_{AS}, \gamma_1, \gamma_2, \gamma_3, \gamma_4$ )

$x_{se}$  = Sensor states ( $a, \dot{a}$ )

$x_w$  = Gust-model states ( $v_g$ )

$\tilde{x}_m$  = Handling-quality-model states ( $\tilde{p}_m, \tilde{r}_m, \tilde{\beta}_m$ )

$u_m$  = Command-model states ( $u_{mR}, u_{mAS}$ )

$u_p$  = Servo inputs ( $u_{pR}, u_{pAS}$ )

$\eta$  = Gaussian white-noise components ( $\eta_w, \eta_R, \eta_{AS}$ )

$$E(\eta) = 0, E[\eta(t) \eta^T(\tau)] = I \delta(t-\tau)^9$$

For notational convenience, the flight condition dependence of the model (integer  $i, i=1, 2, \dots, p$ ) has been suppressed. Individual elements of the model are defined and discussed below.

## Rigid Body

Linearized lateral-directional aircraft equations in stability coordinates take the following general form:

$$\frac{d}{dt} \begin{bmatrix} p \\ r \\ \beta \\ \phi \end{bmatrix} = \begin{bmatrix} L_p & L_r & L_\beta & 0 \\ N_p & N_r & N_\beta & 0 \\ Y_p & Y_r & Y_\beta & g/U_o \\ 1 & 0 & 0 & 0 \end{bmatrix} \begin{bmatrix} p \\ r \\ \beta \\ \phi \end{bmatrix} - \begin{bmatrix} 0 & 0.0033 \\ 0 & 0 \\ 0.0027 & 0 \\ 0 & 0 \end{bmatrix} \begin{bmatrix} \xi \\ \dot{\xi} \end{bmatrix} \quad (43)^{10}$$

$$+ \begin{bmatrix} K_f L_{\delta R} & L_{\delta AS} \\ K_f N_{\delta R} & N_{\delta AS} \\ K_f Y_{\delta R} & Y_{\delta AS} \\ 0 \end{bmatrix} \begin{bmatrix} \delta_R \\ \delta_{AS} \end{bmatrix} - \begin{bmatrix} L_\beta/U_o \\ N_\beta/U_o \\ Y_\beta/U_o \\ 0 \end{bmatrix} v_g$$

<sup>9</sup>  $\delta(t)$  is the Dirac delta function.

<sup>10</sup> The coefficient  $K_f$  accounts for rudder flexibility. The second term of the equation represents bending mode coupling into the rigid body.

This corresponds to the first row of Equation (41):

$$\dot{x}_{rb} = F_{rb}x_{rb} + G_1x_f + G_2x_{as} + G_3x_w$$

The variables  $(p, r, \beta, \phi)$  denote roll rate, yaw rate, sideslip, and bank angle, respectively;  $\xi$  and  $\dot{\xi}$  are deflection and rate of the first bending mode;  $\delta_R$  and  $\delta_{AS}$  are rudder and aileron/spoiler actuator positions; and  $v_g$  is the lateral gust component.

Coefficients for Equation (43) are given in McDonnell Report F935 (Ref. 22) as functions of Mach, altitude, and aircraft configuration. These data were used to select 11 flight conditions [FC(i),  $i=1, 2, \dots, 11$ ] which provide broad coverage of the flight envelope and which include the various extremes of dynamic behavior. The chosen flight conditions are listed in Table VI. Their corresponding coefficients are listed in Table VII.

The major handling-quality characteristics of the F4C at these flight conditions are examined in Table VIII, which displays several lateral-directional handling-quality parameters for the unaugmented aircraft. The parameters were computed according to the approximate literal expressions tabulated in Ref. 5.<sup>11</sup> Additional qualitative assessments are provided in Figures 9 through 19, which show free-aircraft responses to step aileron and rudder commands at each flight condition. [These were taken on an analog simulation of Equation (43), neglecting flexure.] The following characteristics are evident.

Dutch Roll Damping -- Very low dutch roll damping exists over most of the flight envelope. This is true both for the damping ratio parameter ( $\zeta_d$ ) and the damping parameter ( $\zeta_d\omega_d$ ). The only exception is found at the high-q flight condition, FC(3). This condition exhibits adequate damping in terms of  $\zeta_d\omega_d$  (i. e., it exceeds MIL-F-8785's basic requirement of  $0.35$  plus the additional  $0.014(\omega_d^2|\phi/\beta|_d-20)$  required for high values of  $\omega_d^2|\phi/\beta|_d$ ), but its damping ratio of  $\zeta_d = 0.132$  is still somewhat low. Augmentation of dutch roll damping will therefore be a very necessary function of the control system.

Dutch Roll Frequency -- Although the dutch roll frequency is not really objectionable at any flight condition, it could be somewhat higher at the low dynamic pressure conditions, FC(1), FC(5), FC(8), and FC(10), for increased directional stiffness.

Roll Time Constant -- The same low-q flight conditions also exhibit sluggish roll responses.

<sup>11</sup>The literal expression for  $\zeta_\phi\omega_\phi - \zeta_d\omega_d$  was altered to include the term  $N_{\delta AS}L_r/L_{\delta AS}$ , which is significant for some flight conditions.

This change is consistent with other references, for example, Ref. 6.

Table VI. Flight Conditions

Flight Condition	Mach No.	Altitude, h (x 1000 ft)	Weight (lb)	Center of Gravity (% c)	Configuration
1	0.1998	SL	31,629	30.7	Power approach at $\alpha_{wL} = 12^\circ$
2	0.5	5	38,924	28.9	60% internal fuel 4 Sparrows, gear up
3	1.2	5	38,924	28.9	60% internal fuel 4 Sparrows, gear up
4	0.9	15	38,924	28.9	60% internal fuel 4 Sparrows, gear up
5	0.5	25	38,924	28.9	60% internal fuel 4 Sparrows, gear up
6	1.5	25	38,924	28.9	60% internal fuel 4 Sparrows, gear up
7	1.2	35	38,924	28.9	60% internal fuel 4 Sparrows, gear up
8	0.9	45	38,924	28.9	60% internal fuel 4 Sparrows, gear up
9	2.15	45	38,924	28.9	60% internal fuel 4 Sparrows, gear up
10	0.9	35	53,741	33.5	Fully loaded, 100% internal fuel, 3 external tanks, 4 Sparrows, gear up
11	0.85	5	53,741	33.5	Fully loaded, 100% internal fuel, 3 external tanks, 4 Sparrows, gear up



Table VII. Coefficients for Rigid-Body Equations

Parameter	Flight Condition										
	1	2	3	4	5	6	7	8	9	10	11
$U_o$	224.0	548.0	1317.0	950.0	508.0	1520.0	1170.0	871.0	2080.0	875.0	932.0
M	0.1998	0.5	1.2	0.9	0.5	1.5	1.2	0.9	2.15	0.9	0.85
h (ft)	SL	5000	5000	15,000	25,000	25,000	35,000	45,000	45,000	35,000	5000
$L_p$	-1.146	-1.768	-2.735	-2.216	-0.9185	-1.816	-1.346	-0.7462	-1.028	-0.5453	-1.313
$L_r$	1.073	0.4125	0.7927	0.5931	0.3036	0.6740	0.3531	0.3865	0.2624	0.2418	0.3614
$L_\beta$	-9.160	-14.52	-38.84	-23.39	-10.32	-22.52	-14.58	-12.86	-5.748	-7.620	-10.59
$L_{\delta R}$	0.4143	2.031	6.988	5.146	0.6788	4.478	2.720	0.9524	2.591	0.6874	3.010
$L_{\delta AS}$	2.802	8.952	8.845	15.25	4.345	8.225	9.774	6.045	4.933	4.228	8.447
$N_p$	0.1682	-0.0007	0.0372	-0.0110	0.0717	0.0240	-0.0056	0.0240	0.0290	-0.0026	-0.0119
$N_r$	-0.4199	-0.3831	-1.234	-0.5281	-0.2108	-0.7563	-0.3999	-0.1735	-0.2733	-0.1928	-0.5261
$N_\beta$	3.308	6.038	41.22	13.11	3.557	25.09	13.75	4.308	10.42	4.034	10.89
$N_{\delta R}$	-0.7408	-3.398	-6.732	-5.715	-1.643	-3.884	-3.298	-1.756	-1.945	-2.069	-5.619
$N_{\delta AS}$	-0.4760	-0.3075	1.564	0.3382	-0.5408	0.4994	0.2278	-0.4155	-0.0548	-0.1948	0.2353
$Y_p$	0.0156	0.0016	-0.0002	0.0002	0.0016	-0.00003	0.0002	0.0006	-0.00005	0.0005	0.0003
$Y_r$	-0.9912	-0.9975	-0.9965	0.9980	-0.9987	-0.9981	-0.9986	-0.9994	-0.9994	-0.9993	-0.9980
$Y_\beta$	-0.0930	-0.1551	-0.4534	-0.2144	-0.0713	-0.2769	-0.1510	-0.0578	-0.1321	-0.0773	-0.2257
$Y_{\delta R}$	0.0178	0.0283	0.0282	0.0283	0.0141	0.0174	0.0134	0.0092	0.0090	0.0105	0.0282
$Y_{\delta AS}$	-0.0050	-0.0036	-0.0086	-0.0046	-0.0017	-0.0036	-0.0028	-0.0012	-0.0007	-0.0015	-0.0044
$g/U_o$	0.1442	0.0586	0.0244	0.0338	0.0633	0.0211	0.0276	0.0369	0.0154	0.0367	0.0345
$\alpha_w L(\text{deg})$	12.00	3.100	-0.1000	0.5000	8.000	0.7000	1.500	5.200	1.500	4.300	0.8000
$K_f$	0.968	0.860	0.2721	0.7367	0.9323	0.3802	0.5692	0.916	0.6105	0.870	0.680

Table VIII. Handling-Quality Characteristics for the Unaugmented Aircraft

Flight Condition	$\omega_d$ (rad/sec)	$\zeta_d$	$\zeta_d \omega_d$ (sec <sup>-1</sup> )	$\omega_\phi^2 / \omega_d^2$	$\zeta_\phi \omega_\phi - \zeta_d \omega_d$ (sec <sup>-1</sup> )	$ \phi/\beta _d$	$ \dot{\beta}/\beta _d$ (sec <sup>-2</sup> )	$1/T_R$ (sec <sup>-1</sup> )	$p_{max}^\dagger$ (rad/sec)
1	1.82	0.159	0.279	0.554	-0.124	2.99	9.1	1.08	0.75
2	2.46	0.080	0.218	0.858	0.065	3.34	20.2	1.91	2.08
3	6.42	0.132	0.850	1.18	0.064	0.97	40.1	2.72	1.73
4	3.62	0.097	0.351	1.02	0.027	2.10	27.6	2.30	3.50
5	1.89	0.081	0.153	0.647	-0.031	3.13	11.1	0.89	1.64
6	5.01	0.103	0.518	1.06	0.019	0.93	23.1	1.81	2.50
7	3.71	0.070	0.258	0.992	0.022	1.10	15.1	1.38	3.64
8	2.07	0.047	0.096	0.782	0.006	3.00	12.9	0.78	3.14
9	3.23	0.064	0.207	1.01	-0.005	0.52	5.9	1.02	2.53
10	2.01	0.049	0.098	0.874	0.032	1.96	7.9	0.62	3.10
11	3.30	0.107	0.353	0.981	0.028	1.01	11.0	1.36	3.17

<sup>†</sup>Based on maximum aileron/spoiler deflections, including airload effects. Maximum surface deflections are given in Table IX.

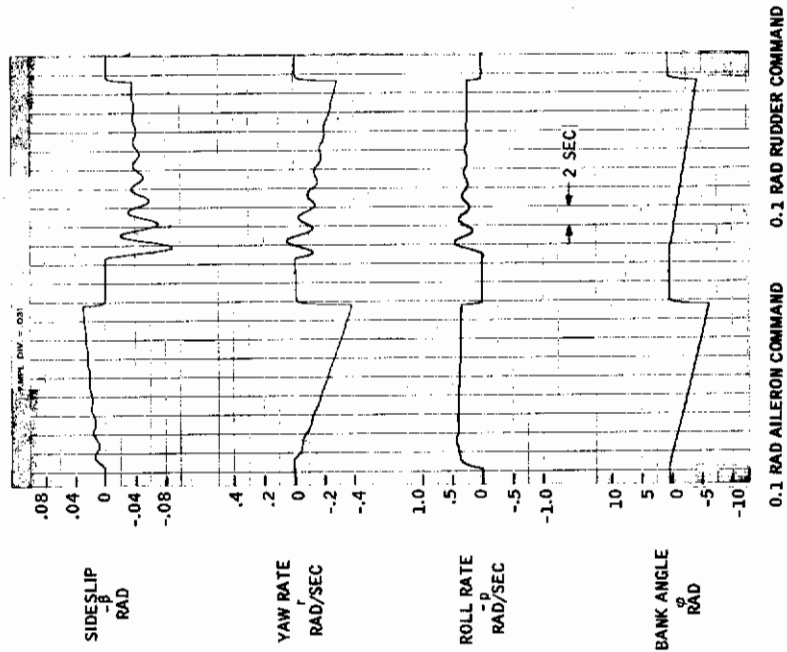


Figure 10. Step Responses -- Free Aircraft  
(Flight Condition 2, Mach 0.5,  
h = 5000 Feet)

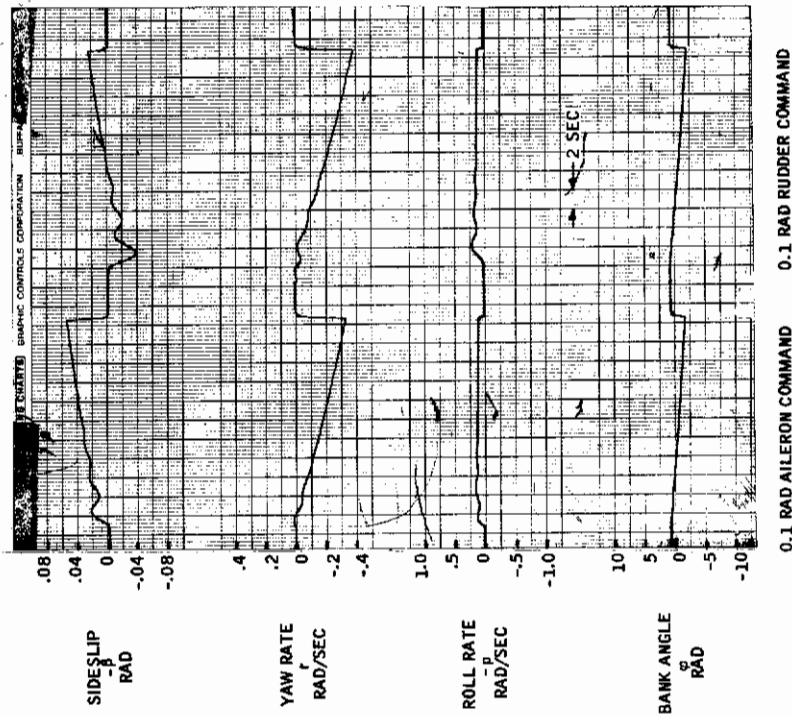


Figure 9. Step Responses -- Free Aircraft (Flight  
Condition 1, Mach 0.2, Sea Level,  
Power Approach)

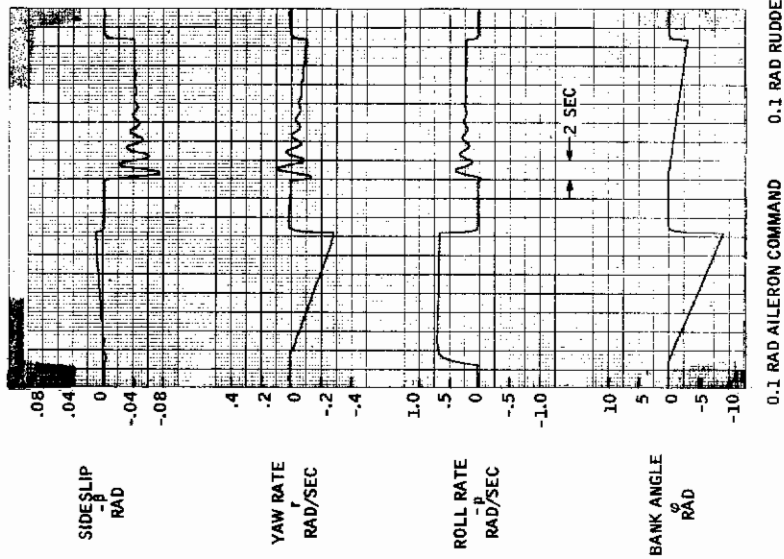


Figure 12. Step Responses -- Free Aircraft  
(Flight Condition 4, Mach 0.9,  
h = 15,000 Feet)

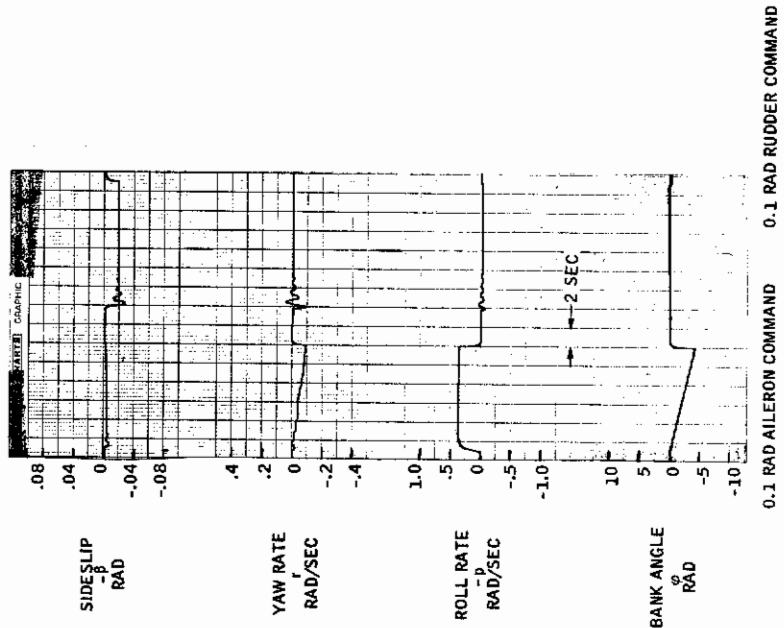


Figure 11. Step Responses -- Free Aircraft  
(Flight Condition 3, Mach 1.2,  
h = 5000 Feet)

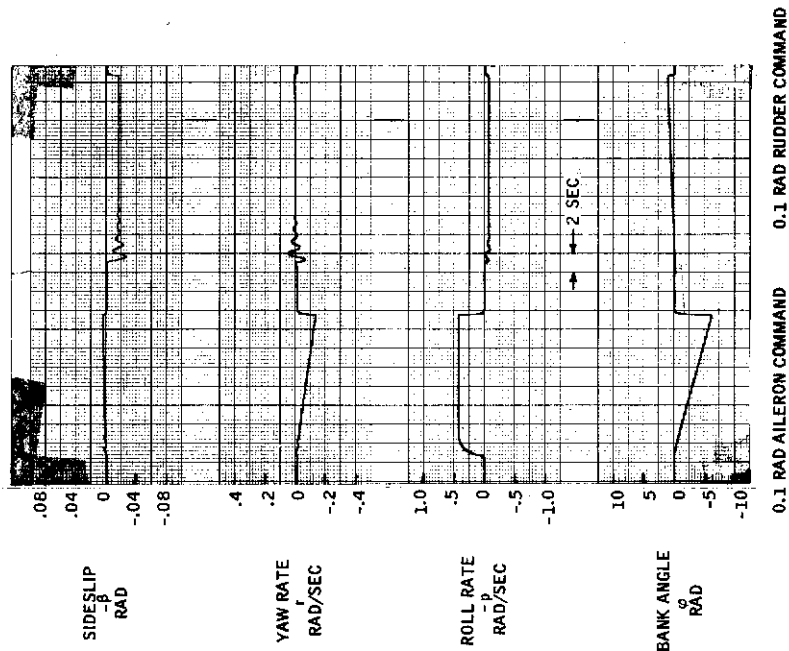


Figure 14. Step Responses -- Free Aircraft (Flight Condition 6, Mach 1.5, h = 25,000 Feet)

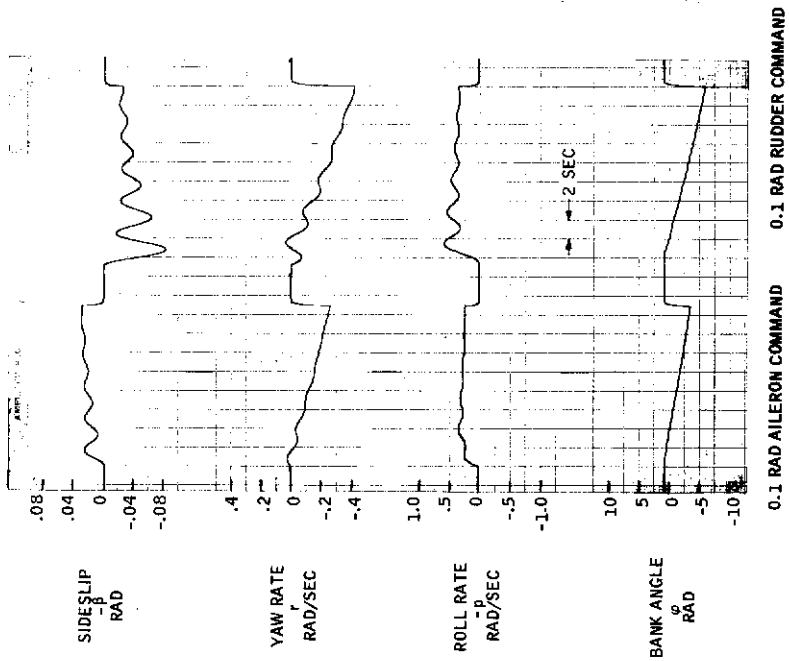


Figure 13. Step Responses -- Free Aircraft (Flight Condition 5, Mach 0.5, h = 25,000 Feet)

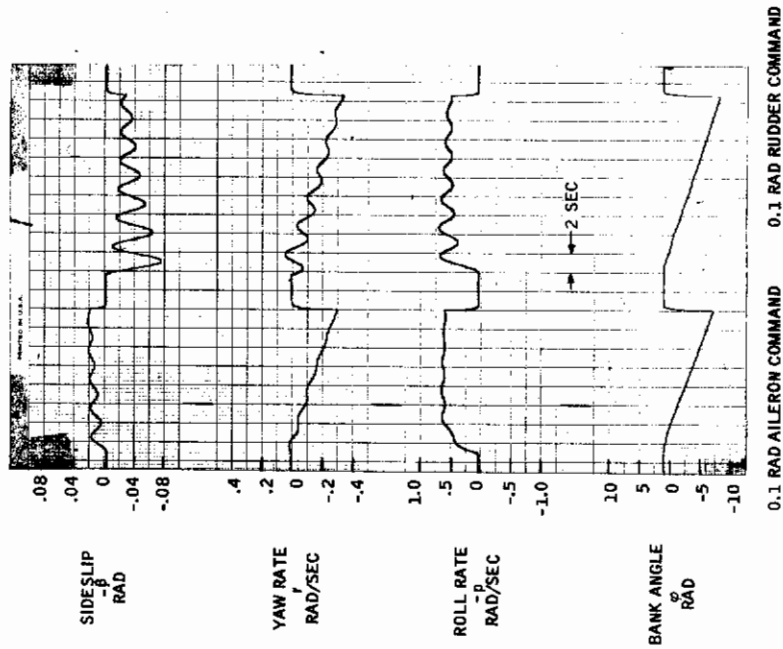


Figure 15. Step Responses -- Free Aircraft  
(Flight Condition 7, Mach 1.2,  
h = 35,000 Feet)

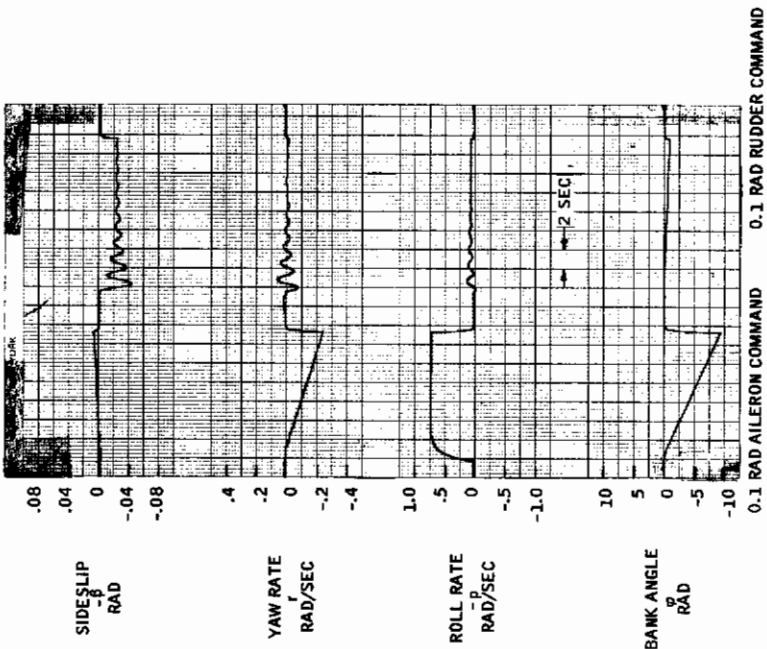


Figure 16. Step Responses -- Free Aircraft  
(Flight Condition 8, Mach 0.9,  
h = 45,000 Feet)



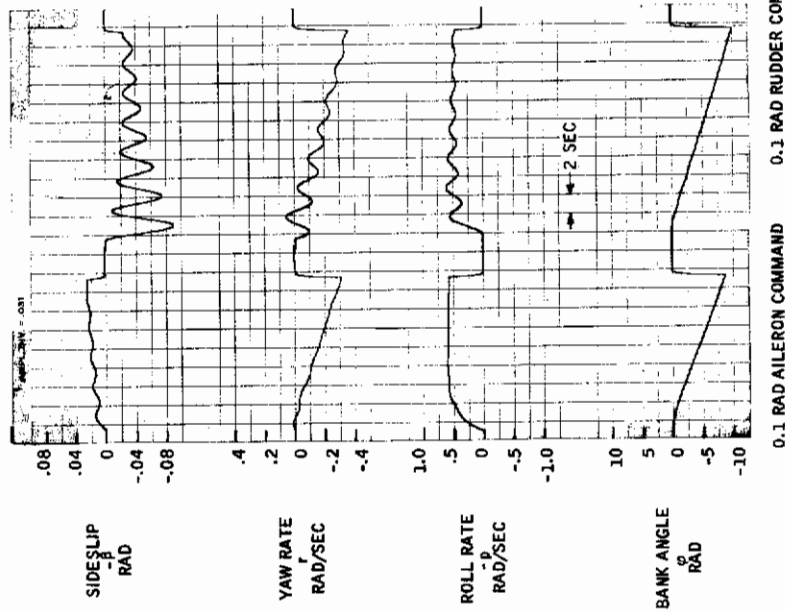


Figure 18. Step Responses -- Free Aircraft (Flight Condition 10, Mach 0.9, h = 35,000 Feet, Weight = 53,741 Pounds)

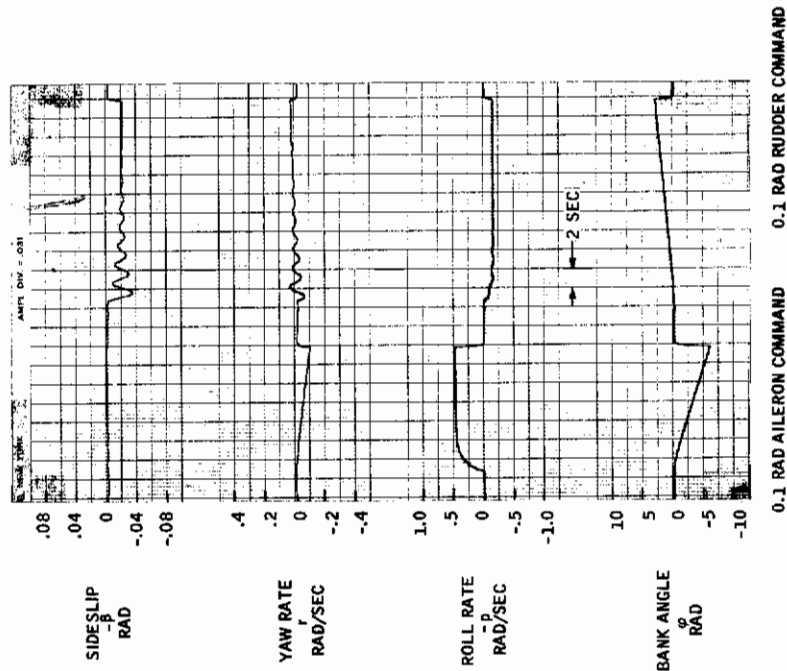


Figure 17. Step Responses -- Free Aircraft (Flight Condition 9, Mach 2.15, h = 45,000 Feet)

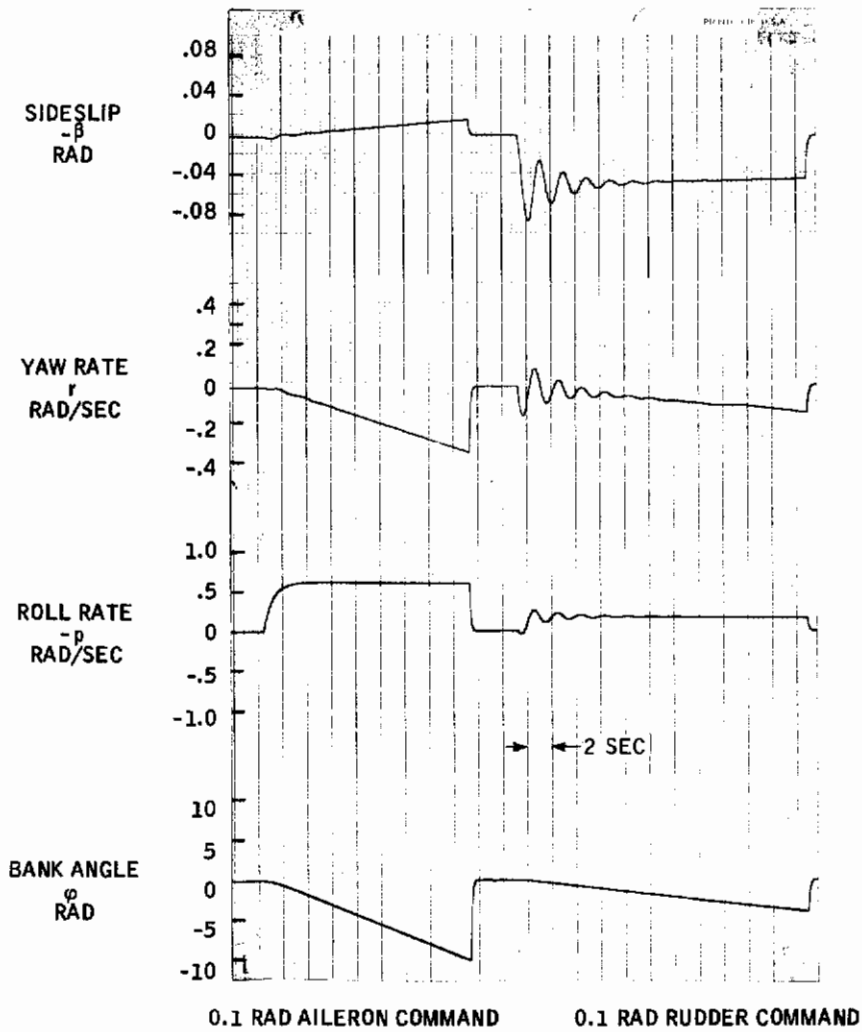


Figure 19. Step Responses -- Free Aircraft (Flight Condition 11, Mach 0.85, h = 5,000 Feet, Weight = 53,741 Pounds)

Roll/Sideslip Coupling -- The coupling parameter,  $|\phi/\beta|_d$ , ranges from low values ( $|\phi/\beta|_d \leq 1.5$ ), at which a pilot's concern for sideslip itself can degrade flying qualities, to moderate values, where  $\beta$ -p coupling is strong enough to cause oscillatory roll responses. No really high values of  $|\phi/\beta|_d$  are encountered. However, the roll rate oscillations are sufficiently severe at some flight conditions that reduction of  $|\phi/\beta|_d$  may be desirable to improve the precision of roll attitude control. This is best shown by looking at the responses in Figures 9 through 19. [See, for example, FC(1), FC(5), and FC(8).]

Zero Positions of the  $p/\delta_{AS}$  Transfer Function -- The parameters  $(\omega_\phi/\omega_d)^2$  and  $(\zeta_\phi\omega_\phi - \zeta_d\omega_d)$  determine the geometrical relationship between the  $p/\delta_{AS}$  zeros and the dutch roll poles. This relationship is connected directly with the magnitude and phasing of aileron-induced sideslip (through the coefficients  $N_{\delta_{AS}}$  and  $N_p$ ) and with the magnitude and phasing of the dutch roll component of roll rate. These, in turn, determine adverse or proverse yaw and difficulty of turn coordination.

The ideal geometric relationship of  $(\omega_\phi/\omega_d)^2 = 1$  and  $(\zeta_\phi\omega_\phi - \zeta_d\omega_d) = 0$  (corresponding to  $N_{\delta_{AS}} = 0$ ,  $N_p = g/U_0$ ) is clearly violated by the unaugmented F4. Moreover, the zeros do not consistently fall into the lower-left-quadrant position (relative to the dutch roll pole) for which turn coordination is natural (i. e., right aileron with right rudder (Ref. 2)). Consequently, it seems desirable to modify the pole-zero relationship, at least at the flight conditions exhibiting large sideslip buildups and adverse yaw. These conditions can again be found most easily by scanning the responses in Figure 9 through 19 [for example, FC(1), FC(2), FC(5), FC(8) and FC(10)]. Note that the F4 does not have major adverse yaw problems at the selected flight conditions. This is a result of the mechanical aileron/spoiler interconnection in the lateral control channel. A recent report by P. D. O'Brien (Ref. 35) indicates some adverse yaw problems at other flight conditions.

## Approximated Flexure

The first two asymmetric bending modes for the F4 with empty wing tanks occur at frequencies of 10.7 and 20.5 Hz, so the aircraft is very stiff and flexure is a secondary consideration in control system design. Nevertheless, it was decided to include the first mode in the mathematical model in order to constrain any tendency of model-following controllers to excite and/or destabilize flexure degrees of freedom. Approximate equations for this mode are derived in Appendix III and are reproduced below:

# Contrails

$$\frac{d}{dt} \begin{bmatrix} \xi \\ \dot{\xi} \end{bmatrix} = \begin{bmatrix} 0 & 1 \\ -4350 & -10.6 \end{bmatrix} \begin{bmatrix} \xi \\ \dot{\xi} \end{bmatrix} + \begin{bmatrix} 0 & 0 & 0 & 0 \\ -27 & 3 & 1800 & 0 \end{bmatrix} \begin{bmatrix} p \\ r \\ \beta \\ \phi \end{bmatrix} + \begin{bmatrix} 0 & 0 \\ 0 & 580 \end{bmatrix} \begin{bmatrix} \delta_R \\ \delta_{AS} \end{bmatrix} + \begin{bmatrix} 0 \\ \frac{1800}{U_0} \end{bmatrix} v_g \quad (44)$$

This corresponds to the second row of Equation (41):

$$\dot{x}_f = F_f x_f + H_1 x_{rb} + G_4 x_{as} + G_5 x_w$$

It must be emphasized that these equations are very crude representations of the aircraft's actual flexure characteristics. While they should be adequate for our purposes, it is unlikely that they are useful for other applications (e.g., flexure control). The numbers in the equations correspond to the Mach 0.9, h = 45,000 feet flight condition where, due to low aerodynamic mode damping, flexure problems can be expected to be most severe. Although the numbers vary somewhat over the rest of the flight envelope, we used the ones given above for all other flight conditions. The very approximate nature of the equations does not warrant the added complexity of variations with flight conditions.

## Actuators and Servos

Equations for these dynamics were taken directly from Ref. 2. They have the following form for all flight conditions:

$$\frac{d}{dt} \begin{bmatrix} \delta_R \\ \delta_{AS} \\ \gamma_1 \\ \gamma_2 \\ \gamma_3 \\ \gamma_4 \end{bmatrix} = \begin{bmatrix} -20 & 0 & 20 & 0 & 0 & 0 \\ 0 & -10 & 0 & 0 & 10 & 0 \\ \hline & & 0 & 1 & & \\ & & -10^4 & -10^2 & & \\ \hline & & & & 0 & 1 \\ & & & & -10^4 & -10^2 \end{bmatrix} \begin{bmatrix} \delta_R \\ \delta_{AS} \\ \gamma_1 \\ \gamma_2 \\ \gamma_3 \\ \gamma_4 \end{bmatrix} + \begin{bmatrix} 0 & 0 \\ 0 & 0 \\ \hline 0 & 0 \\ 10^4 & 0 \\ \hline 0 & 0 \\ 0 & 10^4 \end{bmatrix} \begin{bmatrix} u_{pR} \\ u_{pAS} \end{bmatrix} \quad (45)$$

This corresponds to row 3 of Equation (41):

$$\dot{x}_{as} = F_{as} x_{as} + G_{as} u_p$$

and represents a 10-rad lateral power actuator and a 20-rad rudder actuator, both driven by identical 100-rad,  $\zeta = 0.5$  servos. The servo states are denoted by  $\gamma_1, \gamma_2, \gamma_3,$  and  $\gamma_4,$  and  $u_{pR}, u_{pAS}$  are rudder and lateral servo inputs, respectively.

The lateral power actuator and its servo are actually mathematical equivalents of two separate but mechanically-linked actuator/servo combinations -- one for the aircraft's ailerons and the other for its spoilers. The actuator position,  $\delta_{AS}$ , is a composite representation of aileron deflection on one wing and opposite spoiler deflection on the other. (Sign convention has  $\delta_{AS}$  positive for positive rolling moments, i. e., right wing spoiler up, left wing aileron down.) The composition of  $\delta_{AS}$  is important for determining deflection limitations of the equivalent lateral actuator.

The basic mechanical limitations on all actuators are  $\pm 30$  deg rudder,  $[-30$  deg,  $0$  deg] aileron, and  $[0$  deg,  $45$  deg] spoiler. They are modified by aerodynamic loading as shown in Table IX (these data were taken from Ref. 23). The table also shows equivalent limitations for the hypothetical lateral actuator. These were obtained as follows.

We have earlier used  $u_{pAS}$  to denote the total control input to the lateral axis (i. e., the sum of stick and control system commands). By mechanical interconnections, this input is distributed to the individual aileron and spoiler actuator/servos in the following manner:

$$\text{Right aileron command} = u_{pAS}$$

$$\text{Left aileron command} = -u_{pAS}$$

$$\text{Right spoiler command} = \left(\frac{45}{30}\right) u_{pAS}$$

$$\text{Left spoiler command} = -\left(\frac{45}{30}\right) u_{pAS}$$

Each surface responds to these commands with its own actuator/servo dynamics and subject to its own mechanical limitations. For example, if we look at steady-state deflections for  $u_{pAS} > 0$ , we get zero deflection of right aileron and left spoiler (these surfaces are against their upper and lower stops, respectively), and we get the left aileron and right spoiler deflections shown in Figures 20a and 20b for FC(3). The rolling moments and yawing moments resulting from these deflections are shown in Figure 20c.<sup>12</sup>

<sup>12</sup>The ordinate of Figure 20c represents normalized yawing or rolling moments, defined, for the case of yawing, by

$$(N_{\delta SP} \delta_{SP} - N_{\delta A} \delta_A) / (45N_{\delta SP} - 30N_{\delta A})$$

Similarly for rolling.

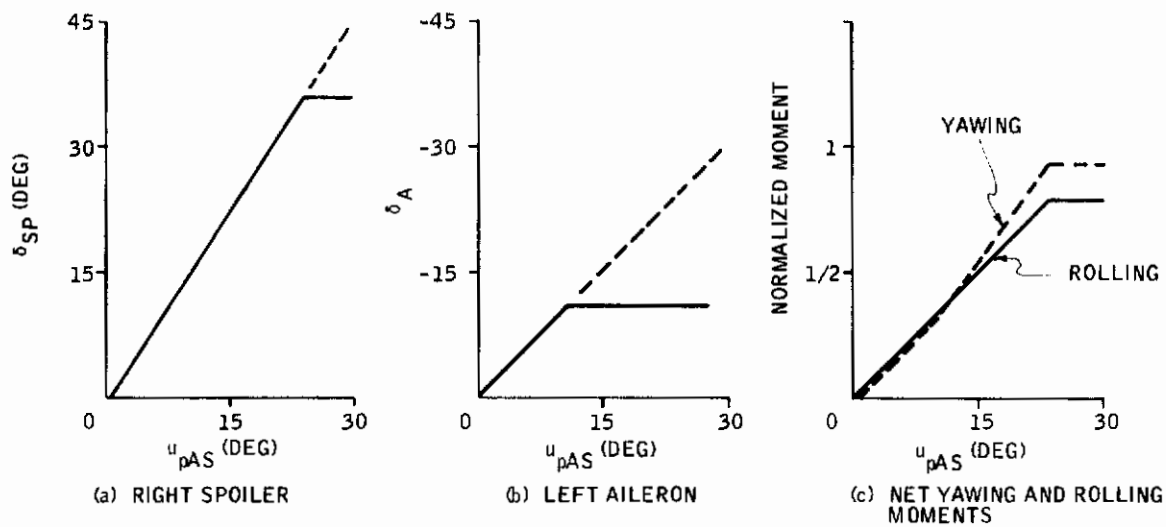


Figure 20. Lateral Surface Deflections at FC(3)

Table IX. Maximum Surface Deflections

Flight Condition	$\delta_R$		$\delta_A$ (deg)	$\delta_{SP}$ (deg)	$\delta_{AS}$	
	( $\pm$ deg)	( $\pm$ rad)			( $\pm$ deg)	( $\pm$ rad)
1	30.0	(0.524)	- 30, 0	0, 45	30	(0.524)
2	15.0	(0.262)	- 30, 0	0, 45	30	(0.524)
3	1.0	(0.0175)	- 11, 0	0, 35	26	(0.454)
4	7.0	(0.122)	- 30, 0	0, 45	30	(0.524)
5	29.0	(0.471)	- 30, 0	0, 45	30	(0.524)
6	1.5	(0.0262)	- 19, 0	0, 45	30	(0.524)
7	3.0	(0.0524)	- 30, 0	0, 45	30	(0.524)
8	23.0	(0.401)	- 30, 0	0, 45	30	(0.524)
9	4.0	(0.0700)	- 30, 0	0, 45	30	(0.524)
10	15.0	(0.262)	- 30, 0	0, 45	30	(0.524)
11	5.0	(0.0873)	- 30, 0	0, 45	30	(0.524)



# Contrails

It is clear from this latter figure that the equivalent lateral actuator/servo, which according to Equation (45) deflects in direct proportion to  $u_{pAS}$  (plus dynamics, of course), should saturate at 26 degrees or so.

The same argument was used to establish effective lateral saturation levels for the remaining flight conditions of Table IX.

Limitations have also been placed on the maximum surface rates of the rudder and effective lateral actuators. For the rudder, the constraint is 25 deg/sec (0.437 rad/sec), and for the lateral channel it is 64 deg/sec (1.12 rad/sec). The latter number approximates aileron actuators under full aerodynamic loading.

No limitations were placed on the servos. Rather, it is assumed that in fly-by-wire (FBW) applications, servo position and rate capabilities will exceed those required to drive the given actuators.

## Sensors

Feedback signals for practical control systems were confined to those already available to the existing F4 lateral-directional control system. For stability augmentation system (SAS) functions, this means roll rate and yaw rate gyro outputs, lateral accelerometer outputs, and possibly roll attitude gyro outputs. So the observations are

$$y = \begin{bmatrix} p_{se} \\ r_{se} \\ a \\ \phi \\ \tilde{x}_m \\ u_m \end{bmatrix} = \begin{bmatrix} \cos \alpha_{wL} & -\sin \alpha_{wL} & 0 & 0 \\ \sin \alpha_{wL} & \cos \alpha_{wL} & 0 & 0 \\ 0 & 0 & 0 & 0 \\ 0 & 0 & 0 & 1 \\ \hline & & & \end{bmatrix} x_{rb} + \begin{bmatrix} 0 & 0 \\ 0 & 0 \\ 1 & 0 \\ 0 & 0 \\ \hline & \end{bmatrix} \begin{bmatrix} a \\ \dot{a} \end{bmatrix} + \begin{bmatrix} & \\ & \\ & \\ I & 0 \\ \hline 0 & I \end{bmatrix} \begin{bmatrix} \tilde{x}_m \\ u_m \end{bmatrix} \quad (47)$$

This equation corresponds to Equation (42).

In Equation (47), the second-order dynamics of both rate gyros (150-rad,  $\zeta = 0.5$ ) (Ref. 22) have been neglected, so their measured outputs ( $p_{se}, r_{se}$ ) are algebraic transformations of true roll rate and true yaw rate. The transformation was derived by assuming that both instruments are aligned with a body-referenced coordinate system whose x-axis passes through the center of gravity of the aircraft and runs parallel to the water line and whose positive y-axis extends along the right wing. The angle  $\alpha_{wL}$  is the angle of attack of the water line, which is tabulated as a function of flight condition in Table VII.

The roll attitude gyro is assumed to have unity dynamics and to measure  $\phi$  without extraneous transformations.

The only sensor dynamics which are included in the mathematical model are accelerometer dynamics. These are second-order with 50-radian bandwidth and 0.5 damping (Ref. 22) and are described by the following differential equations:

$$\frac{d}{dt} \begin{bmatrix} a \\ \dot{a} \end{bmatrix} = \begin{bmatrix} 0 & 1 \\ -50^2 & -50 \end{bmatrix} \begin{bmatrix} a \\ \dot{a} \end{bmatrix} + \begin{bmatrix} 0 \\ 50^2 \end{bmatrix} a_{se} \quad (48)$$

Here  $a$  and  $\dot{a}$  denote accelerometer states and  $a_{se}$  is the total lateral acceleration at the accelerometer station.

The instrument is located at fuselage station 198.0 and water line 23.0, which is forward and below the center of gravity by the distances  $x_o$  and  $z_o$ , respectively. In stability coordinates,  $x_o$  and  $z_o$  are given by

$$\begin{pmatrix} x_o \\ z_o \end{pmatrix} = \begin{pmatrix} \cos \alpha_{wL} & \sin \alpha_{wL} \\ -\sin \alpha_{wL} & \cos \alpha_{wL} \end{pmatrix} \begin{pmatrix} c_1 \\ c_2 \end{pmatrix} \quad (49)$$

where  $(c_1)$  and  $(c_2)$  are tabulated below (Ref. 22):

FC	1	2-9	10-11
$c_1$ (ft)	10.2	9.90	10.6
$c_2$ (ft)	-0.0192	+0.388	-0.268

Due to these offsets from the center of gravity, the accelerometer will pick up yaw and roll acceleration as well as lateral acceleration. Its total input is

$$a_{se} = U_o \frac{d}{dt} \beta + U_o r + x_o \frac{d}{dt} r - z_o \frac{d}{dt} p - g\phi \quad (50)$$

This equation, together with Equation (48), corresponds to the fourth row of Equation (41), i. e.,

$$\dot{x}_{se} = F_{se} x_{se} + H_2 x_{rb} + H_3 x_f + H_4 x_{as} + H_5 x_w$$

where the matrices  $H_2, \dots, H_5$  are given by

$$\begin{aligned} H_2 &= 50^2 \begin{bmatrix} 0 \\ 1 \end{bmatrix} \{ [-z_o \ x_o \ U_o \ 0] F_{rb} + [0 \ U_o \ 0 \ -g] \} \\ H_3 &= 50^2 \begin{bmatrix} 0 \\ 1 \end{bmatrix} [-z_o \ x_o \ U_o \ 0] G_1 \\ H_4 &= 50^2 \begin{bmatrix} 0 \\ 1 \end{bmatrix} [-z_o \ x_o \ U_o \ 0] G_2 \\ H_5 &= 50^2 \begin{bmatrix} 0 \\ 1 \end{bmatrix} [-z_o \ x_o \ U_o \ 0] G_3 \end{aligned} \quad (51)$$

Note that  $x_o$  is a sizeable quantity (approximately 10 feet), so the yaw acceleration component represents a significant fraction of the signal.

### Gust Model

Lateral wind gust disturbances ( $v_g$ ) were modeled by a white noise process passed through an appropriate linear filter. The filter is first-order [corresponding to a simplified Dryden spectral form (Ref. 1)] and its magnitude and bandwidth are 6 ft/sec rms and  $U_o/1750$  rad/sec, respectively. This gives

$$\frac{d}{dt} v_g = -\left(\frac{U_o}{1750}\right) v_g + 6.0 \sqrt{\frac{U_o}{875}} \eta_w \quad (52)$$

which corresponds to row 5 of Equation (41). The variable  $\eta_w$  is scalar white noise.

## Handling-Quality Models

The four handling-quality models developed in Section II were used as criteria for the controller designs discussed here. However, to avoid model-matching of the spiral mode, the models were reduced to third-order form involving dutch roll and roll subsidence only.

The transformations necessary to reduce the models are discussed below.

Reasons for not matching the spiral motions are given later (pg. 60). At this point it is only necessary to assure the reader that the spiral mode will not be removed entirely from the design procedure. The aircraft will still have a spiral mode, which will be stable but close to the nominal  $1/T_s = 0$  condition. Only the models will not have a spiral mode.

The four rigid-body responses of the models are defined by

$$\dot{x}_m = F_m x_m + G_m u_m \quad (53)$$

where  $x_m^T = (p_m \ r_m \ \beta_m \ \phi_m)$ . Then the spiral mode, call it  $z_m$ , is given by

$$z_m = \lambda^T x_m \quad (54)$$

where  $\lambda$  is the left spiral eigenvector of matrix  $F_m$ . That is,  $\lambda$  is a four-vector defined by

$$\lambda^T F_m = -\frac{1}{T_s} \lambda^T$$

Furthermore, the dutch roll plus roll subsidence components in the responses  $x_m$  are given by

$$\begin{bmatrix} \tilde{p}_m \\ \tilde{r}_m \\ \tilde{\beta}_m \\ \tilde{\phi}_m \end{bmatrix} \triangleq x_m - \nu z_m = (I - \nu \lambda^T) x_m \quad (55)$$

where  $\nu$  is the right spiral eigenvector of  $F_m$ , which is defined by

$$\begin{aligned} F_m v &= -\frac{1}{T_s} v \\ \lambda^T v &= 1 \end{aligned} \tag{56}$$

Now let  $T_m(\lambda, v)$  be a transformation matrix defined as follows:

$$T_m(\lambda, v) = \begin{bmatrix} 1 & 0 & 0 & 0 \\ 0 & 1 & 0 & 0 \\ 0 & 0 & 1 & 0 \\ 0 & 0 & 0 & 0 \end{bmatrix} - \begin{bmatrix} v_1 \\ v_2 \\ v_3 \\ -1 \end{bmatrix} \lambda^T \tag{57}$$

Then

$$\begin{bmatrix} \tilde{p}_m \\ \tilde{r}_m \\ \tilde{\beta}_m \\ z_m \end{bmatrix} = T_m(\lambda, v) x_m \tag{58}$$

$$\frac{d}{dt} \begin{bmatrix} \tilde{p}_m \\ \tilde{r}_m \\ \tilde{\beta}_m \\ z_m \end{bmatrix} = \begin{bmatrix} & & & 0 \\ & \tilde{F}_m & & 0 \\ & & & 0 \\ 0 & 0 & 0 & -\frac{1}{T_s} \end{bmatrix} \begin{bmatrix} \tilde{p}_m \\ \tilde{r}_m \\ \tilde{\beta}_m \\ z_m \end{bmatrix} + \begin{bmatrix} \tilde{G}_m \\ \lambda^T G_m \end{bmatrix} u_m \tag{59}$$

where the  $(3 \times 3)$  and  $(3 \times 2)$  matrices  $\tilde{F}_m$  and  $\tilde{G}_m$  are obtained by partitioning  $T_m F_m T_m^{-1}$  and  $T_m G_m$ . In this last equation, the spiral mode is completely uncoupled, so we can simply ignore it to get the short-period motions:

$$\frac{d}{dt} \begin{bmatrix} \tilde{p}_m \\ \tilde{r}_m \\ \tilde{\beta}_m \end{bmatrix} = \tilde{F}_m \begin{bmatrix} \tilde{p}_m \\ \tilde{r}_m \\ \tilde{\beta}_m \end{bmatrix} + \tilde{G}_m u_m \tag{60}$$

This equation corresponds to row 6 of Equation (41). The matrices  $\tilde{F}_m$  and  $\tilde{G}_m$  for our four models of Section II are summarized in Table X.

Table X. Reduced-Order Models

$\tilde{F}_m$	$\tilde{G}_m$
<p><b>Model 1</b></p> $\begin{bmatrix} -0.402 & -0.448 & -10.0 \\ 0.0560 & 0.0993 & 2.22 \\ -0.287 & -2.20 & -0.327 \end{bmatrix}$	$\begin{bmatrix} 5.04 & 6.11 \\ -1.12 & -1.19 \\ 0.0003 & 0.0092 \end{bmatrix}$
<p><b>Model 2</b></p> $\begin{bmatrix} -0.516 & 0.391 & -10.0 \\ 0.0170 & -0.139 & 3.55 \\ -0.0854 & -1.24 & -0.418 \end{bmatrix}$	$\begin{bmatrix} 4.79 & 5.25 \\ -1.79 & -1.05 \\ 0.0008 & -0.0075 \end{bmatrix}$
<p><b>Model 3</b></p> $\begin{bmatrix} -0.981 & 0.177 & -10.0 \\ 0.0300 & -0.0920 & 5.23 \\ -0.0433 & -1.08 & -0.732 \end{bmatrix}$	$\begin{bmatrix} 4.58 & 6.34 \\ -2.63 & -0.888 \\ 0.0003 & -0.0035 \end{bmatrix}$
<p><b>Model 4</b></p> $\begin{bmatrix} -4.00 & 0.865 & -10.0 \\ 0.040 & -0.507 & 5.87 \\ -0.0102 & 1.02 & -0.743 \end{bmatrix}$	$\begin{bmatrix} 3.30 & 20.0 \\ -3.11 & -0.188 \\ 0.0017 & -0.0163 \end{bmatrix}$



## Command Models

The commands ( $u_m$ ) were assumed to consist of filtered white noise for both lateral and rudder channels. First-order lag filters were used with bandwidths ( $\omega_o$ ) to be determined during the design phase. Thus

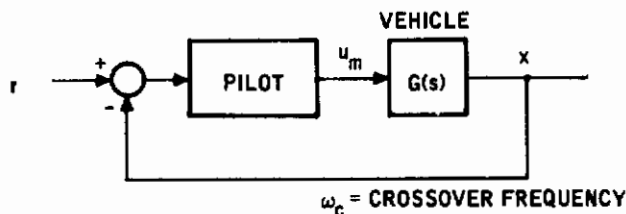
$$\frac{d}{dt} \begin{bmatrix} u_{mR} \\ u_{mAS} \end{bmatrix} = -\omega_o \begin{bmatrix} u_{mR} \\ u_{mAS} \end{bmatrix} + \sqrt{2\omega_o} \begin{bmatrix} \sigma_R & 0 \\ 0 & \sigma_{AS} \end{bmatrix} \begin{bmatrix} \eta_R \\ \eta_{AS} \end{bmatrix} \quad (61)$$

where  $u_{mR}$  is the rudder command,  $u_{mAS}$  is the lateral command,  $\eta_R$ ,  $\eta_{AS}$  are scalar white-noise components, and  $\sigma_R$ ,  $\sigma_{AS}$  are rms command magnitudes. Equation (61) corresponds to the last row of Equation (41).

The choice of these command models is largely functional. We desire a reasonable representation of the frequency content of pilot commands, yet we want to avoid the complexity of many state variables. One way to substantiate the simple models used is based on some of the notions of pilot/vehicle analysis for simple compensatory tracking tasks. This was suggested by Mr. R.O. Anderson of the Air Force Flight Dynamics Laboratory. In particular, if we assume that the "crossover model" (Ref. 3) is valid over the entire frequency range of interest, then the commands generated by the pilot will be of the form

$$u_m(s) = \frac{\omega_c}{s + \omega_c} \frac{1}{G(s)} r(s) \quad (62)$$

where the relevant quantities are defined on the standard tracking loop shown below:



For the case of bank angle tracking,  $G(s)$  is nearly a pure integration, so we would get

$$u_m(s) = \frac{sK}{s + \omega_c} r(s) \quad (63)$$

# Contrails

Starting with this expression, the problem of choosing the command model directly has been replaced by the problem of choosing a model for the input  $r(s)$ . For example, letting  $r(s)$  be white noise ( $\eta$ ) gives

$$\dot{x} = -\omega_c x + \omega_c \eta$$

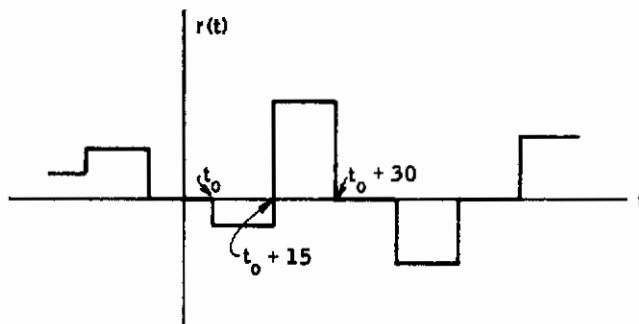
$$u_m = K(\eta - x)$$

This corresponds to a high-pass filter (low-frequency cutoff at  $\omega_c$ ) driven by white noise. Similarly, letting  $r(s)$  be Brownian motion gives

$$\dot{u}_m = -\omega_c u_m + K\eta$$

which is a low-pass filter driven by white noise. Another alternative is to let  $r(s)$  itself be low-pass filtered white noise with cutoff frequency  $\omega_i$ . Then the  $u_m(s)$  model corresponds to a bandpass filter with lower cutoff at  $\min[\omega_i, \omega_c]$  and upper cutoff at  $\max[\omega_i, \omega_c]$ . Clearly, some rationale must be established for choosing among these various possibilities.

A rationale appropriate to the present case is provided by the flight profiles which were flown in the validation phase of the program (Section V). These profiles consist of consecutive 15-second segments of flight, each characterized by a constant bank angle. This means that the input to the bank angle tracking loop (aside from atmospheric disturbances) are sample functions like the one shown below:

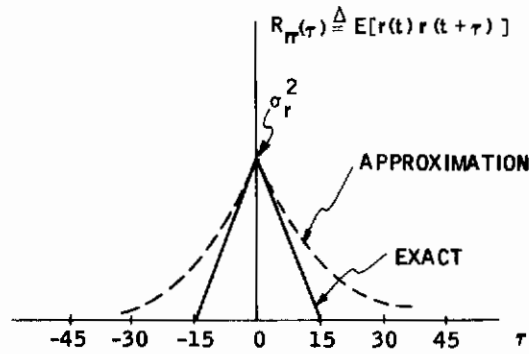


On each 15-second segment, the bank angle is an independent random variable distributed according to the discrete distribution

$$\text{Prob}[r = \phi] = \begin{cases} 0.5 & \phi = 0 \\ 0.05 & \phi = \pm 5, \pm 7.5, \pm 10, \pm 12.5, \pm 15 \end{cases}$$

so the corresponding autocorrelation function is given by Figure 21 (Ref. 38).<sup>13</sup>

<sup>13</sup>This assumes that  $t_0$  is uniformly distributed on  $[0, 15]$ , which assures statistical stationarity.



$$\text{VARIANCE} = \sigma_r^2 = 0.10 (25 + 56 + 100 + 156 + 225) = 56 (\text{DEG})^2$$

Figure 21. Autocorrelation of  $r(t)$

A continuous random process which approximates these second-order statistics is given by the equation

$$\dot{r} = -\frac{1}{15} r + \left[ \frac{\sigma_r}{\sqrt{7.5}} \right] \eta$$

It has the autocorrelation function shown in dashed lines on Figure 21 and evokes pilot commands of the bandpass variety with lower cutoff at  $\omega_l = 0.067$  and upper cutoff at  $\omega_c$ . But certainly, with such low lower cutoffs, it is entirely adequate to model the pilot's commands by simple low-pass filters, as done in Equation (61).

The above arguments establish the frequency content of the lateral command model. An identical model was also used for the rudder channel. This leaves two additional free parameters which must be specified -- the rms magnitudes of rudder and lateral commands. These were selected to evoke response levels of 60 percent of the maximum capability of the airplane, both for aileron/spoiler-induced roll rate and rudder-induced sideslip. The resulting flight-condition-dependent magnitudes are summarized in Table XI.

## OPTIMAL MODEL-FOLLOWING DESIGNS

As indicated in Section I, individual optimal model-following controllers (based upon measurement of the full state vector,  $x$ ) are required for each of the 11 flight conditions. These provide a starting point for the computational algorithm described in Section III and also generate

Table XI. Command Magnitudes

Flight Condition	Lateral Command, $\sigma_{AS}$ (rad)	Rudder Command, $\sigma_R$ (rad)
1	0.090	0.140
2	0.250	0.177
3	0.208	0.00342
4	0.420	0.0640
5	0.197	0.262
6	0.300	0.00486
7	0.436	0.0151
8	0.376	0.196
9	0.304	0.0156
10	0.372	0.161
11	0.380	0.0540

$$\sigma_{AS} = 0.6 \frac{(p/\delta_{AS})_{ss} \delta_{AS \max}}{(p_m/\delta_{AS})_{ss}}$$

$$\sigma_R = 0.6 \frac{(\beta/\delta_R)_{ss} \delta_R \max}{(\beta_m/\delta_R)_{ss}}$$

much problem insight regarding performance criteria, gain and performance sensitivities, and critical flight conditions.

Optimal model-following controllers for the F4C were developed by starting with a baseline flight condition [FC(2)] for which an adequate quadratic performance index and its resulting baseline control system were determined.

This was done for handling-quality model 4 with an assumed command bandwidth of  $\omega_0 = 4$  rad/sec. A parametric study was then performed, still at FC(2), to determine performance sensitivities with respect to  $\omega_0$  and to choose a better value. With the new  $\omega_0$ , optimal controllers were computed for each of the remaining 10 flight conditions and for handling-quality models 1 through 3, each at FC(2) and FC(3). (The latter controllers were needed for the validation experiments.) These steps are discussed below.

### Baseline Designs at FC(2)

A quadratic performance index of the following form was assumed:

$$\begin{aligned}
 J = E [ & Q_{11} (\tilde{p} - \tilde{p}_m)^2 + Q_{22} (\tilde{r} - \tilde{r}_m)^2 + Q_{33} (\tilde{\beta} - \tilde{\beta}_m)^2 \\
 & + Q_{44} z^2 + Q_{55} \xi^2 + Q_{66} \dot{\xi}^2 + R_{11} u_{pR}^2 + R_{22} u_{pAS}^2 ]
 \end{aligned}
 \tag{64}$$

As indicated by the ( $\sim$ ) notation, this index penalizes model-following errors in the dutch roll plus roll subsidence components of roll rate, yaw rate, and sideslip. In addition, small penalties are assigned to the spiral mode of the aircraft ( $z$ ) and to bending mode displacement and rate to ensure stability. The control inputs, of course, are also weighted. The structure of Equation (64) was suggested by results reported in Ref. 10.

As discussed earlier, dutch roll plus roll subsidence motions of the model are given directly by Equation (60). For the aircraft, they can be obtained with a transformation,  $T_{rb}$  [analogous to Equation (57)], applied to the rigid-body states, i. e.,

$$\begin{bmatrix} \tilde{p} \\ \tilde{r} \\ \tilde{\beta} \\ z \end{bmatrix} = T_{rb} x_{rb}
 \tag{65}$$

where

$$T_{rb} = \begin{bmatrix} 1 & 0 & 0 & 0 \\ 0 & 1 & 0 & 0 \\ 0 & 0 & 1 & 0 \\ 0 & 0 & 0 & 0 \end{bmatrix} - \begin{bmatrix} v_1 \\ v_2 \\ v_3 \\ -1 \end{bmatrix} \lambda^T$$

and where  $v$  and  $\lambda$  are right and left spiral eigenvectors of matrix  $F_{rb}$ , respectively. The transformation,  $T_{rb}$ , is tabulated in Appendix V for each flight condition.<sup>14</sup>

Dutch roll and roll subsidence components are penalized most heavily in the performance index because these are the primary contributors to handling-quality goodness. Handling qualities depend only mildly on the spiral component (Ref. 2). Moreover, it is physically undesirable to model-match the spiral mode. To illustrate this, consider the special case of an aircraft with spiral mode time constant equal to zero. Let this aircraft enter a shallow steady turn. During initial transients, all modes -- dutch roll, roll subsidence, and spiral -- will be active. Dutch roll and roll subsidence will decay, however, leaving only spiral components in the steady turn. These will be governed by the following equation:

$$0 = -r_s + Y_{\beta} \beta_s + Y_{\phi} \phi_s \quad (66)^{15}$$

where subscripts  $( )_s$  denote spiral components. A similar expression holds for the spiral mode of a model, i. e.,

$$0 = -r_{ms} + Y_{\beta m} \beta_{ms} + Y_{\phi m} \phi_{ms} \quad (67)$$

Clearly, a turn with zero model-following errors can be flown only if  $Y_{\phi} = Y_{\phi m}$  and  $Y_{\beta} = Y_{\beta m}$ . For unequal values, zero errors in one variable must be purchased at the expense of nonzero errors in one or both of the others. In particular, the conditions  $(r_s - r_{ms}) = 0$  and  $(\phi_s - \phi_{ms}) = 0$  will be accompanied by nonzero sideslip errors and by degraded turn coordination. The issue is one of basic physics: The aircraft must yaw, as decreed by Newton, at the rate

<sup>14</sup>Using  $T_{rb}$ , the correspondence between the performance index [Equation (64)] and the general index [Equation (11)] can be readily visualized. The matrix  $H_p$  is  $(6 \times 6)$  and equals  $\begin{bmatrix} T_{rb} & | \\ \hline & | I \end{bmatrix}$ ,  $H_m$  is  $(6 \times 3)$  and equals  $\begin{bmatrix} I \\ 0 \end{bmatrix}$ , and  $Q$  and  $R$  are diagonal.

<sup>15</sup> $Y_r \doteq -1$ ,  $Y_{\delta AS} \doteq Y_{\delta R} \doteq 0$



# Contrails

$r_s = Y_\phi \phi_s + Y_\beta \beta_s = (g/U_0) \phi_s + Y_\beta \beta_s$ . Either the model satisfies this same relationship (i. e., it is flight-condition-dependent) or we live with poor coordination. Both are avoided with the performance index [Equation (64)] which penalizes dutch roll plus roll subsidence errors most heavily and adds just enough weight (Q44) on the spiral to keep it stable. As has been pointed out in Section II, spiral stability is not required from a handling-qualities viewpoint. It is, however, needed for our computational procedures. Q44 will be selected to make  $1/T_s$  (closed loop) positive but small.

Honeywell's doubly-iterative algorithm, DIAK (Ref. 12), for the solution of the matrix Riccati equation, was used to minimize Equation (64) for several choices of quadratic weights:  $\{Q_{ij}, i = 1, 2, \dots, 6; R_{ij}, i = 1, 2\}$ . The controllers for each set of weights were compared both on the basis of rms responses (using command levels of Table XI and lateral gust levels of 6 ft/sec rms) and on the basis of rudder and lateral step responses (using step magnitudes equal to the rms levels in Table XI). The rms responses are direct outputs of the DIAK program, and step responses were obtained by appending a numerical integration routine. After only a few iterations (seven) on the weights, a suitable controller was obtained. Results for all weights considered are summarized in Table XII, which shows various rms levels generated when the controlled aircraft is subjected to random commands and disturbances. The corresponding rigid-body feedback gains are given in Table XIII.<sup>16</sup>

The first few runs in Table XII indicate that any desired level of model-following performance can be achieved by lowering the weights on control ( $R_{11}$ ,  $R_{22}$ ) sufficiently. This is accompanied by higher bending mode deflections and rates, higher actuator deflections and rates, and higher control gains. The bending mode positions and rates developed during any of the runs are hardly significant --  $\sigma_z = 0.079$  yields an rms deflection at the wing tip of 0.54 inch.<sup>17</sup> Actuator rates, on the other hand, are very significant when compared with the actuator limits specified earlier in Section IV. Consequently, lower limits on control weights are determined by the capabilities of the F4's actuators.

The rms actuator rates shown in Table XII do not themselves serve to constrain  $R_{11}$  and  $R_{22}$  because they exceed actuator rate limits for all runs (even run 1, which exhibits poor model-following performance). This is due to the wideband command model ( $\omega_0 = 4$ ) used for the baseline design. As shown later, lower bandwidths produce lower rates. Instead of rms actuator rates, therefore, step responses were used to constrain the weights. Responses were computed for step magnitudes equal to the 60 percent max levels of Table XI, with position and rate

<sup>16</sup> There are a total of 40 gains for each controller, i. e., 20th-order dynamics with two control inputs. For brevity, only the rigid-body feedbacks are shown in Table XIII.

<sup>17</sup> This is based on the flexure model of Appendix III and is subject to all assumptions used there.

Table XII. Iterations for Baseline Design Quadratic Weights and RMS Responses

Run No.	P (rad/sec)	$\tilde{p} - \tilde{p}_m$ (rad/sec)	r (rad/sec)	$\tilde{r} - \tilde{r}_m$ (rad/sec)	$\beta$ (rad)	$\tilde{\beta} - \tilde{\beta}_m$ (rad)	z	$\xi$	Deflection Limits					
									$\delta R$ (rad)	$\delta AS$ (rad)	$\delta R$ (rad/sec)	$\delta AS$ (rad/sec)		
1 Q, R RMS response	---	Q11 10.0 0.327	---	Q22 1.0 0.145	---	Q33 10.0 0.062	Q44 0.001 3.64	Q55 0.1 0.0401	Q66 0.01 0.433	R11 10.0 0.055	R22 10.0 0.267	0.262 $\delta R$ (rad)	0.437 $\delta AS$ (rad/sec)	1.12 $\delta AS$ (rad/sec)
2 Q, R RMS response	---	10.0 0.148	---	1.0 0.091	---	10.0 0.072	0.001 4.36	0.1 0.065	0.01 0.967	1.0 0.130	1.0 0.388	---	---	---
3 Q, R RMS response	---	10.0 0.083	---	1.0 0.061	---	100.0 0.0035	0.001 4.5	0.1 0.079	0.01 1.4	0.1 0.21	0.1 0.45	---	---	6.8
4 Q, R RMS response	---	10.0 0.084	---	1.0 0.059	---	1000.0 0.0011	0.001 4.56	0.1 0.079	0.01 1.44	0.1 0.20	0.1 0.45	---	---	6.898
5 Q, R RMS response	---	10.0 0.122	---	1.0 0.052	---	1000.0 0.00174	0.001 4.45	0.1 0.074	0.01 1.15	0.5 0.187	0.5 0.417	---	---	5.28
6 Q, R RMS response	---	10.0 0.121	---	1.0 0.0616	---	100.0 0.00645	0.001 4.46	0.1 0.0738	0.01 1.14	0.5 0.178	0.5 0.416	---	---	5.22
7 Q, R RMS response	---	10.0 0.149	---	1.0 0.0633	---	100.0 0.00911	0.001 4.36	0.1 0.0701	0.01 0.981	1.0 0.164	1.0 0.394	---	---	4.46

Table XIII. Rigid-Body Feedback Gains for Baseline Design Iterations

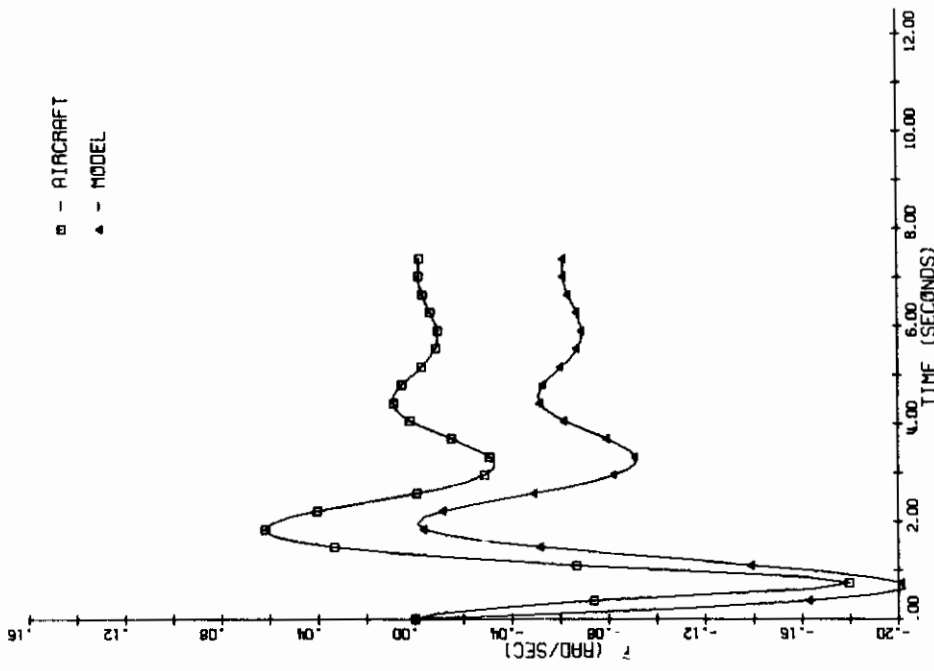
Run No.	To Rudder				To Lateral			
	$K_{11}$	$K_{12}$	$K_{13}$	$K_{14}$	$K_{21}$	$K_{22}$	$K_{23}$	$K_{24}$
	(p)	(r)	( $\beta$ )	( $\phi$ )	(p)	(r)	( $\beta$ )	( $\phi$ )
1	-0.0841	0.629	-0.217	-0.0371	-0.709	-0.367	1.18	-0.000129
2	-0.575	1.38	-0.862	-0.0878	-2.60	-0.687	3.32	-0.0263
3	-2.37	6.08	-24.9	-0.310	-8.63	-2.50	9.83	-0.0776
4	-1.78	12.0	-90.7	-0.407	-8.76	-3.70	21.70	-0.053
5	-0.534	7.06	-39.4	-0.280	-3.81	-1.67	8.54	-0.014
6	-0.773	3.45	-10.2	-0.178	-3.77	-1.19	5.19	-0.0294
7	-0.474	2.69	-6.72	-0.142	-2.61	-0.894	4.10	-0.0174

limits of actuators included. Qualitatively, these responses behave essentially linearly for large control weights and exhibit steady-state rate-limit oscillations when the weights are too small. In the transition, they hit the limits for a cycle or two and then decay quickly toward a stable solution.

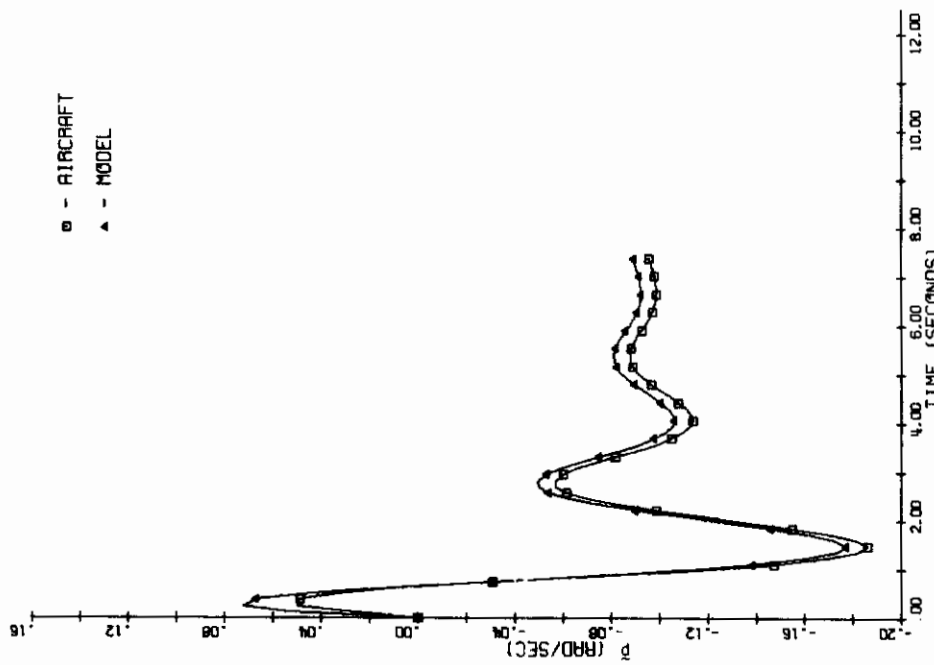
Normally,  $R_{11}$  and  $R_{22}$  would be adjusted somewhere below the transition range to ensure against oscillations, and we would live with the required performance sacrifices at lower command levels. In this program, however, the criteria validation objective makes good model-following performance imperative, particularly at low commands. For this reason, baseline values for  $R_{11}$  and  $R_{22}$  (run 7) were advanced somewhat into the transition range.<sup>18</sup> The resulting transient responses are shown in Figures 22 and 23 for 60 percent max commands and in Figures 24 and 25 for low-level 6 percent max commands. Some observations about these responses are given below:

- 1) For small commands, the controller has excellent modal characteristics (frequency, damping, time constants) when compared with the model's modes.
- 2) DC model-following errors are significant but tolerable. Sideslip errors to the 60 percent max lateral commands, for example, are large percentagewise but amount to only 0.4 deg.

<sup>18</sup>This runs the risk of rate-limit oscillations during the validation experiments. These did in fact occur on a few trials both in Minneapolis and at WPAFB after large sharp pilot rudder commands. The problem can be "fixed" by magnitude and rate-limiting the sum of all feedforward commands. It can be solved by readjustments of R.

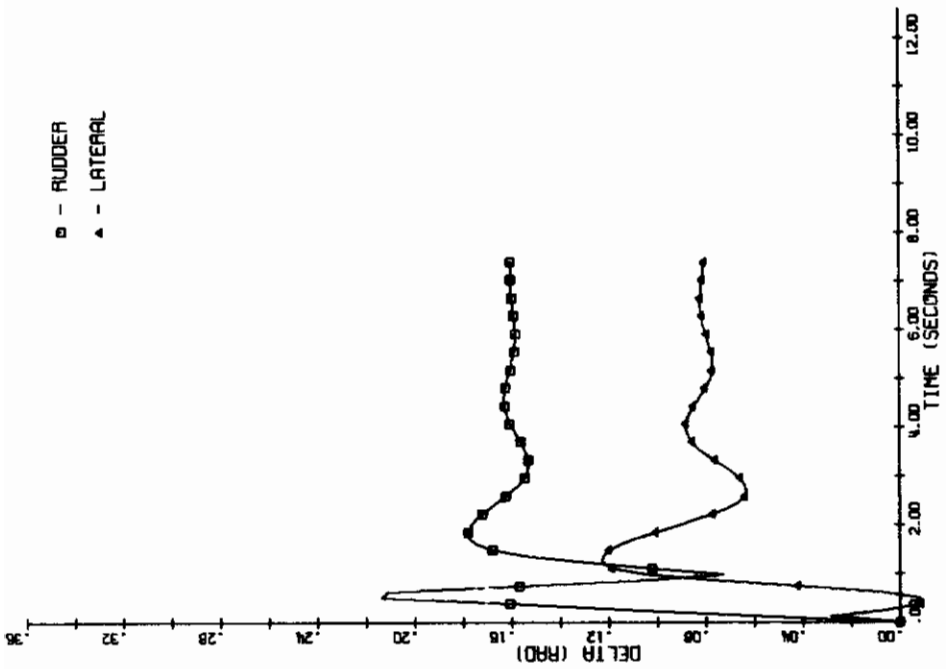


a) Roll Rate ( $\dot{p}$ ,  $\dot{p}_m$ )

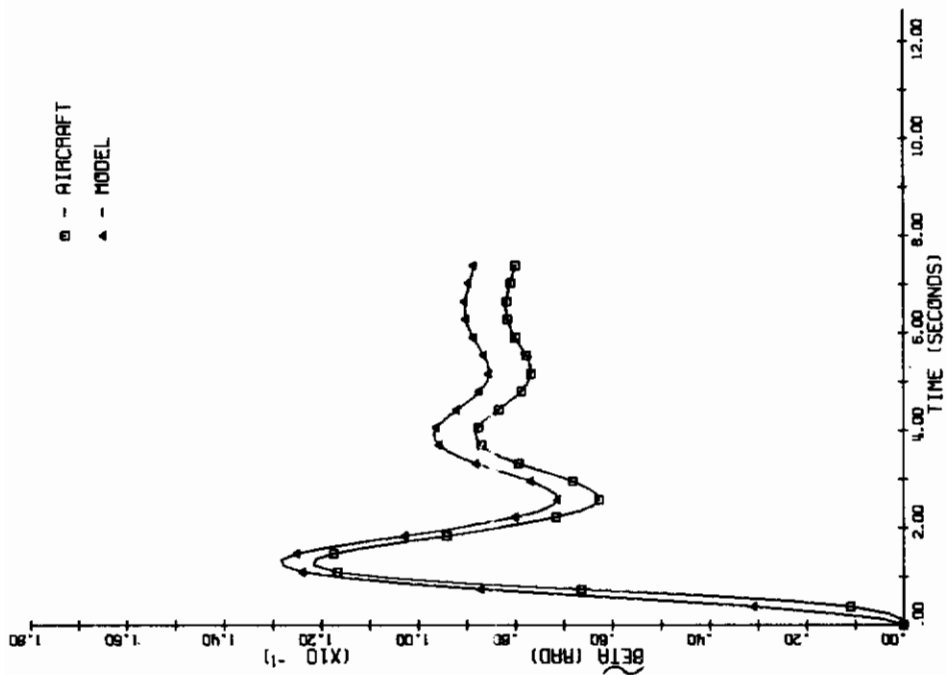


b) Yaw Rate ( $\dot{r}$ ,  $\dot{r}_m$ )

Figure 22. Step Responses -- Run 7 -- 0.177-Rad Rudder Command

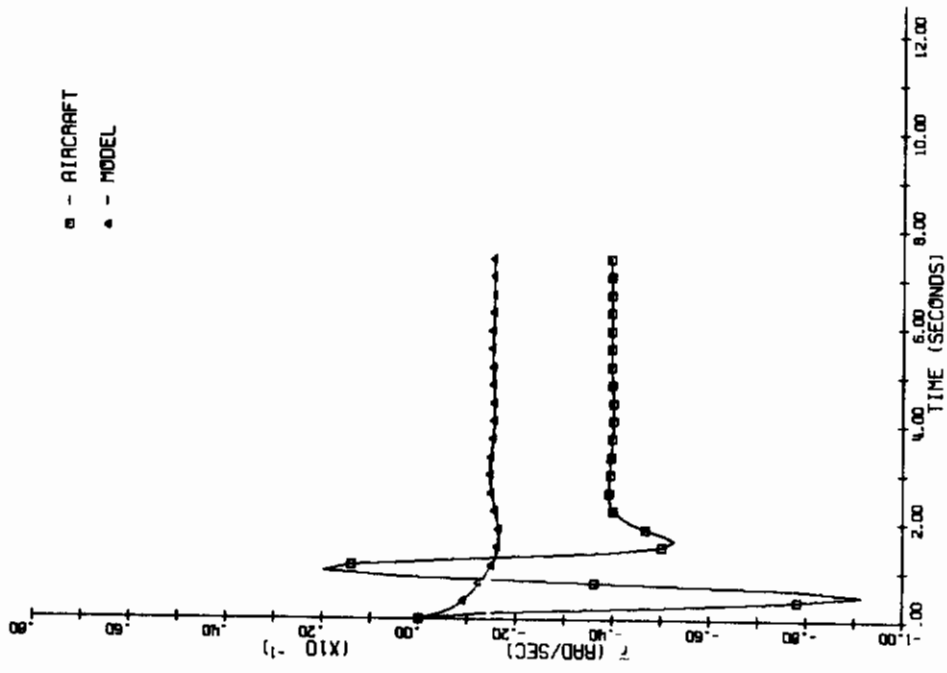


d) Actuator Position ( $\delta_R, \delta_{AS}$ )

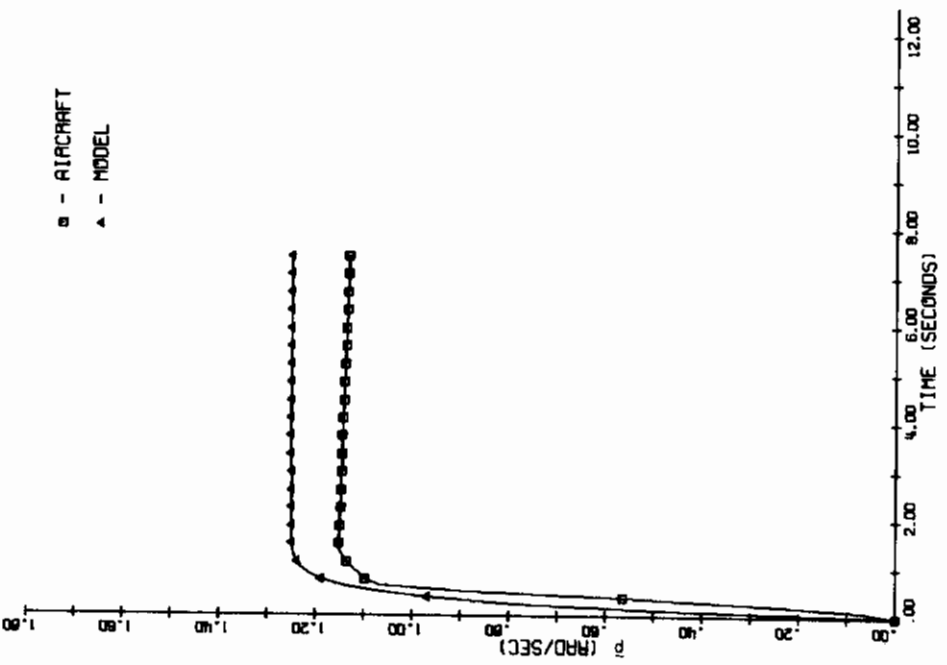


c) Sideslip ( $\tilde{\beta}, \tilde{\beta}_m$ )

Figure 22. Step Responses -- Run 7 -- 0.177-Rad Rudder Command (Concluded)



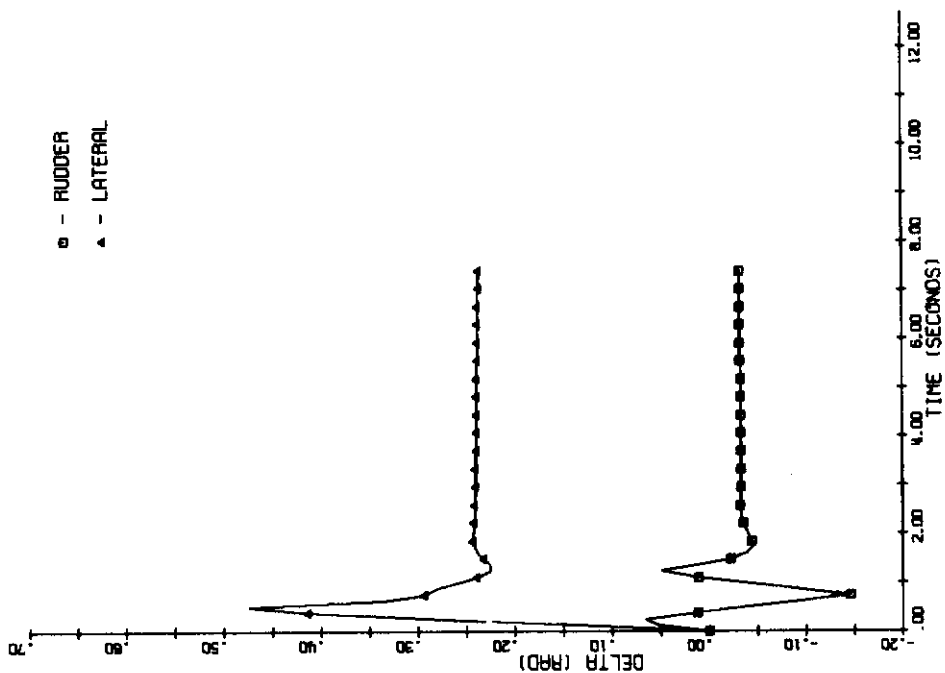
a) Roll Rate ( $\tilde{p}$ ,  $\tilde{p}_m$ )



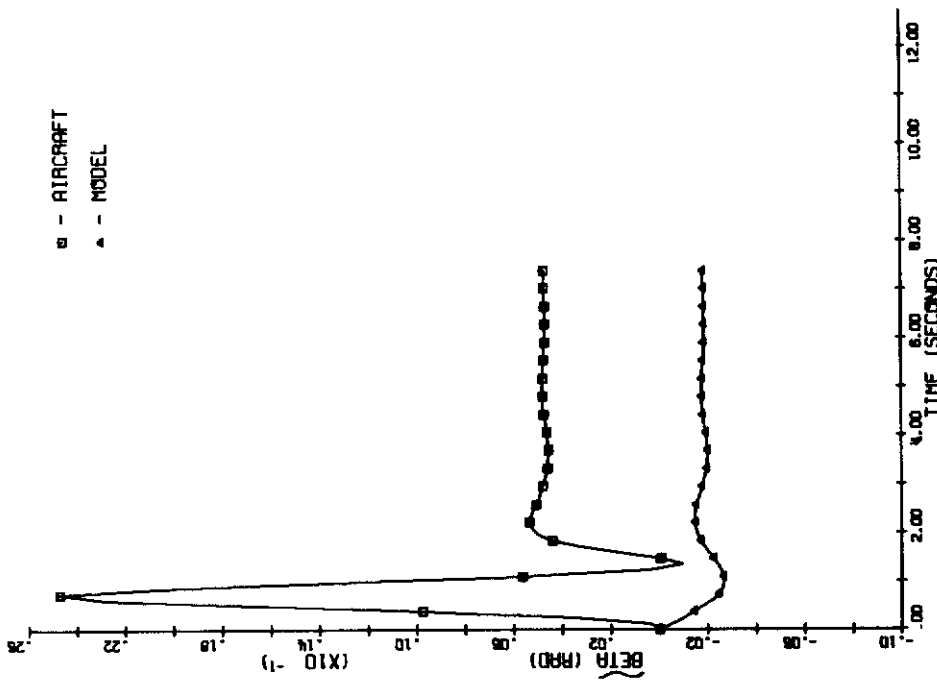
b) Yaw Rate ( $\tilde{r}$ ,  $\tilde{r}_m$ )

Figure 23. Step Responses -- Run 7 -- 0.250-Rad Lateral Command



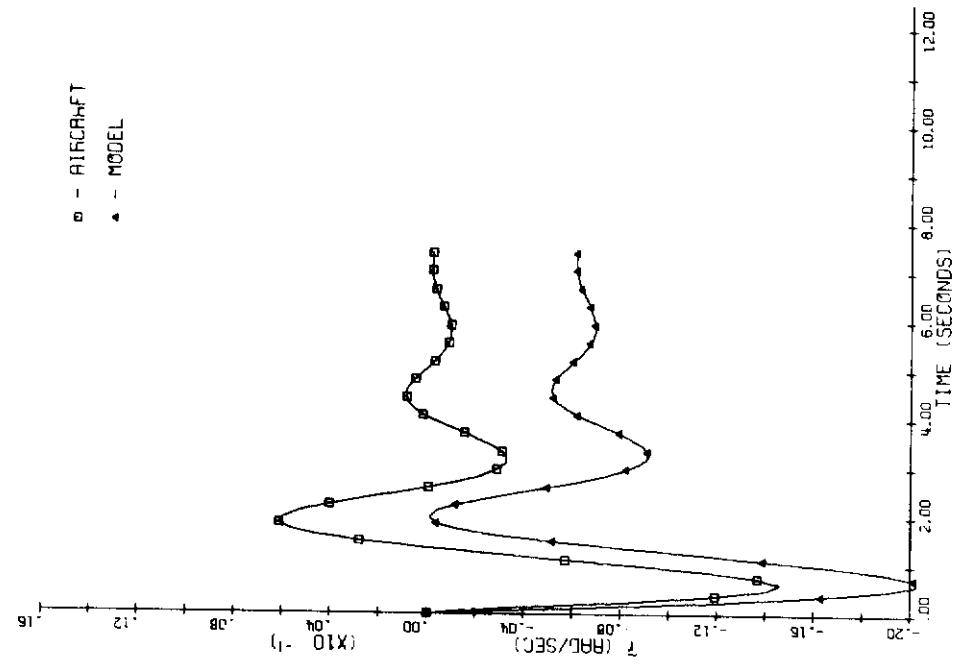


d) Actuator Position ( $\delta_R, \delta_{AS}$ )

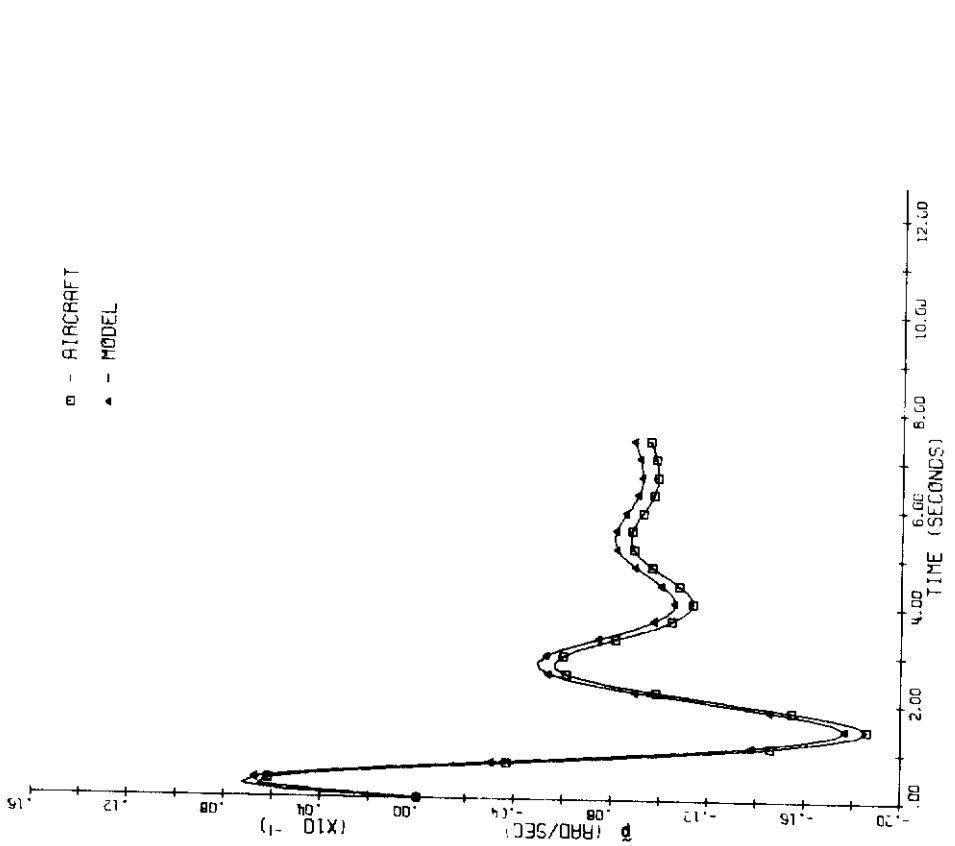


c) Sideslip ( $\tilde{\beta}, \tilde{\beta}_m$ )

Figure 23. Step Responses -- Run 7 -- 0.250-Rad Lateral Command (Concluded)

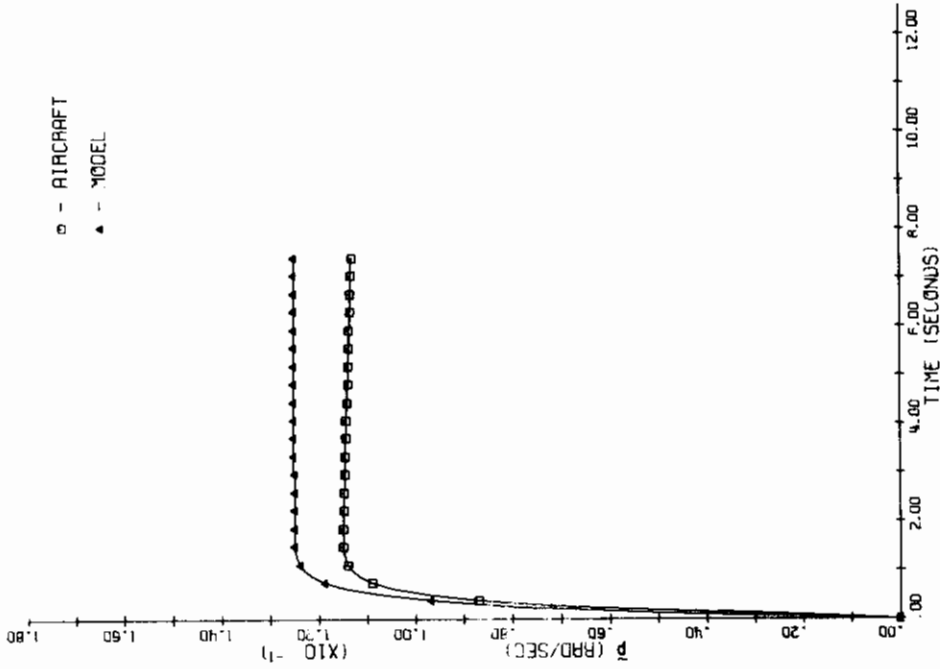


a) Roll Rate ( $\tilde{p}, \tilde{p}_m$ )



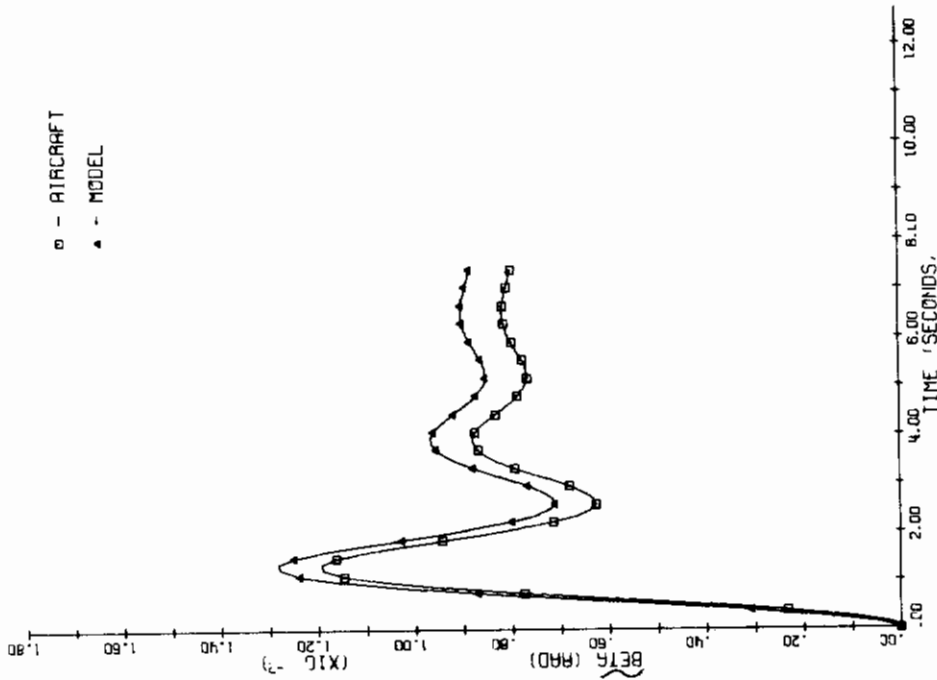
b) Yaw Rate ( $\tilde{r}, \tilde{r}_m$ )

Figure 24. Step Responses -- Run 7 -- 0.0177-Rad Rudder Command



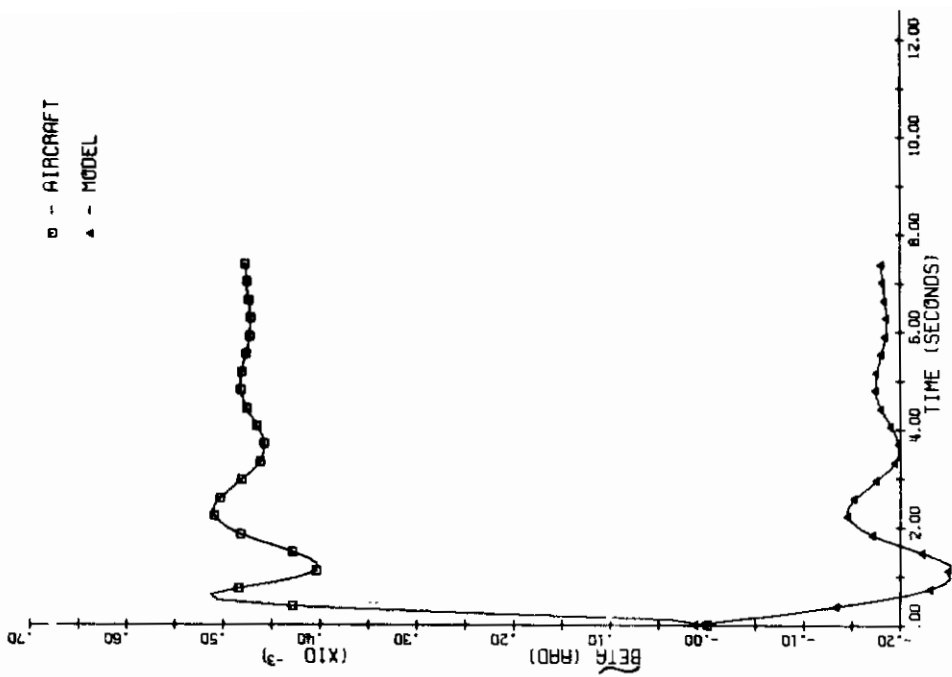
a) Roll Rate ( $\tilde{p}, \tilde{p}_m$ )

Figure 25. Step Responses -- Run 7 --  
0.025-Rad Lateral Com-  
mand

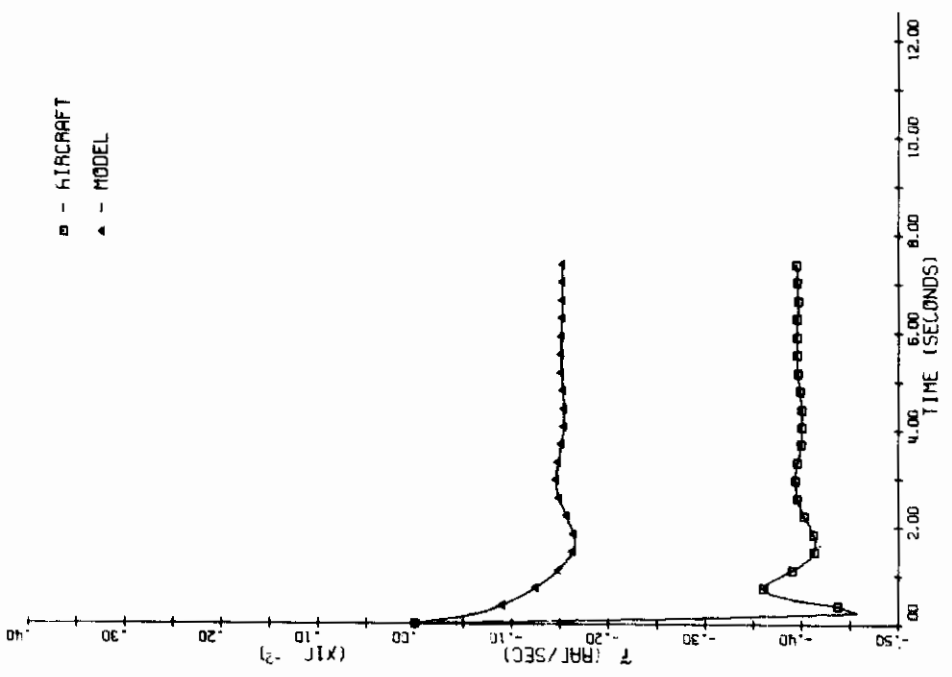


c) Sideslip ( $\tilde{\beta}, \tilde{\beta}_m$ )

Figure 24. Step Responses -- Run 7 --  
0.0177-Rad Rudder Com-  
mand (Concluded)



c) Sideslip ( $\tilde{\beta}, \tilde{\beta}_m$ )



b) Yaw Rate ( $\tilde{r}, \tilde{r}_m$ )

Figure 25. Step Responses -- Run 7 -- 0.025-Rad Lateral Command (Concluded)

- 3) The F4 can barely follow model roll rate responses for large lateral commands. Heavy saturation of the lateral rate limit is required. At the same time, rate limiting of the rudder actuator prevents proper coordination of sideslip, so a large momentary sideslip spike (1.4 deg peak) occurs.

## Command Bandwidth Study

Using the quadratic weights from run 7 at FC(2), several additional runs were made with different command bandwidths but identical rms command levels. Results of these runs are recorded in Figures 26, 27, and 28 and in Table XIV. Recall from Section III that the command model affects only the command feedforward gains of the controller, so each data point on these curves represents a controller with different command feedforwards but with identical feedback gains and feedforward gains from the model.

The curves depict two kinds of performance variables -- normalized rms responses to random commands, and steady-state errors to step commands. The rms responses are shown in Figures 26 and 27. These say, in effect, that the aircraft performs well when forced at low frequencies and poorly when forced at high frequencies, with one notable exception -- roll rate performance, which also deteriorates at very low frequencies due to the response decay (in p) produced by a slightly stable spiral mode. The same effect is evident in the steady-state error curves of Figure 28 [except for yaw rate error, which is not very critical (Ref. 10)].

The command feedforward gains which correspond to Figures 26, 27, and 28 are given in Table XIV. These gains show a marked decrease at high frequencies, with some peaking of the lateral feedforwards in the frequency range of best roll rate performance.

The dividing line between low frequencies (good performance) and high frequencies (poor performance) falls somewhere around 1 to 2 rad/sec, which is, not surprisingly, very close to the bandwidth of the uncontrolled airframe ( $\omega_d = 2.46$ ,  $1/T_R = 1.91$  from Table VIII). From an error standpoint, then, the free-aircraft bandwidth forms a reasonable candidate for  $\omega_0$ .

Following these results and using  $\omega_d$  and  $1/T_R$  data for the F4C (Table VIII), a command bandwidth of 1 rad/sec was selected and used in all subsequent controller designs.

## Other Optimal Controllers

Optimal model-following controllers were computed for all of the remaining flight conditions and for handling-quality models 1, 2, and 3 at FC(2) and FC(3). Initially, these computations were based on the

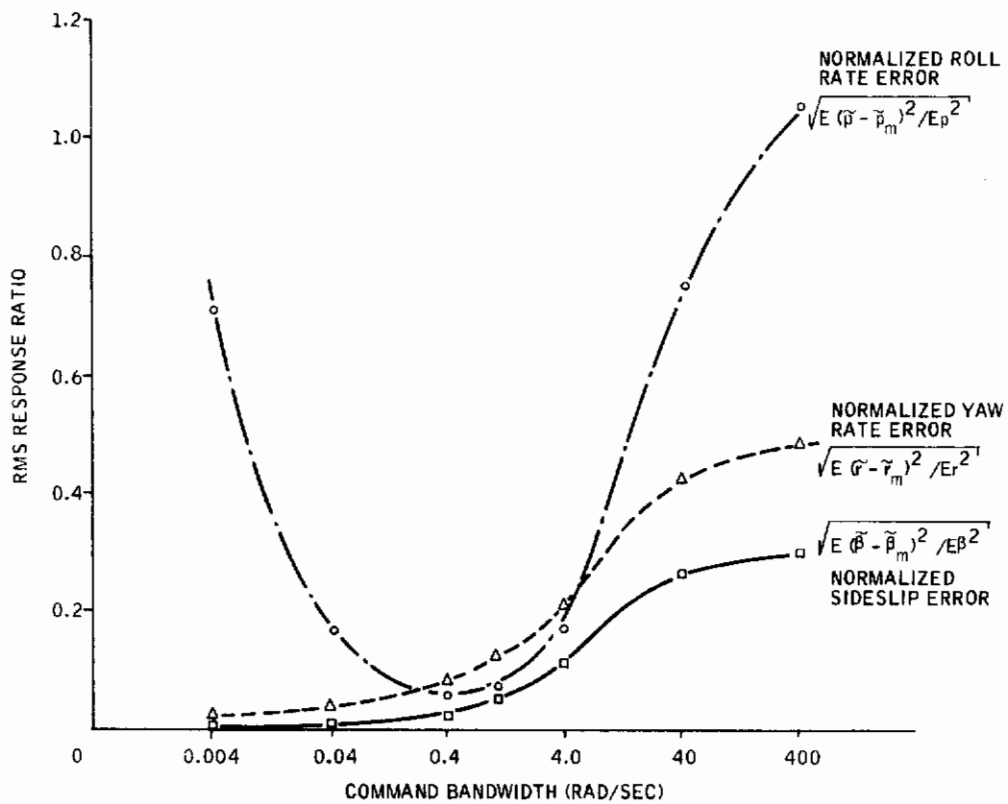


Figure 26. RMS Response Ratios versus Command Bandwidth

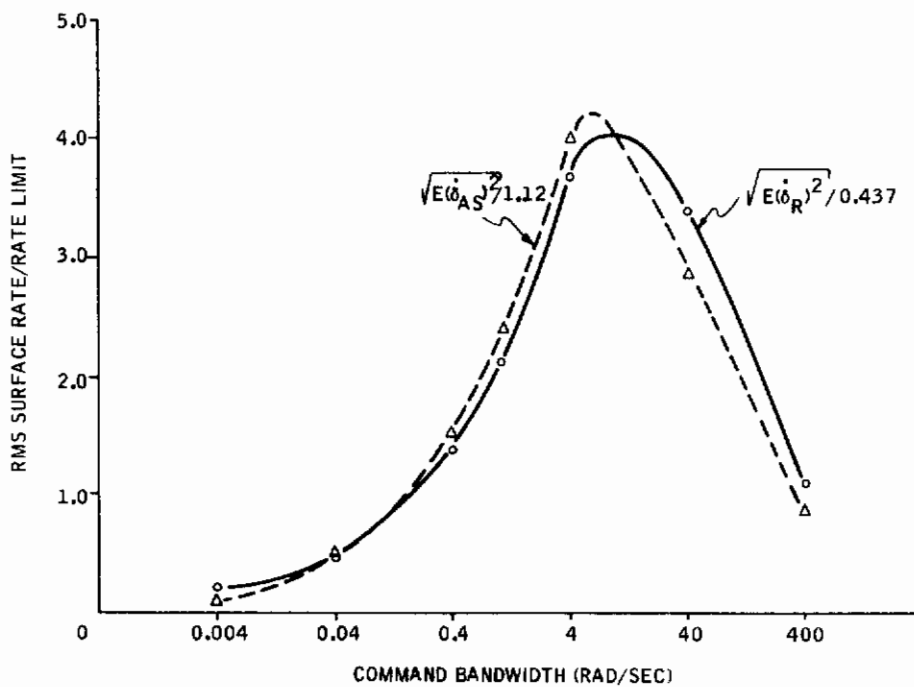


Figure 27. Surface Rate versus Command Bandwidth



# Contrails

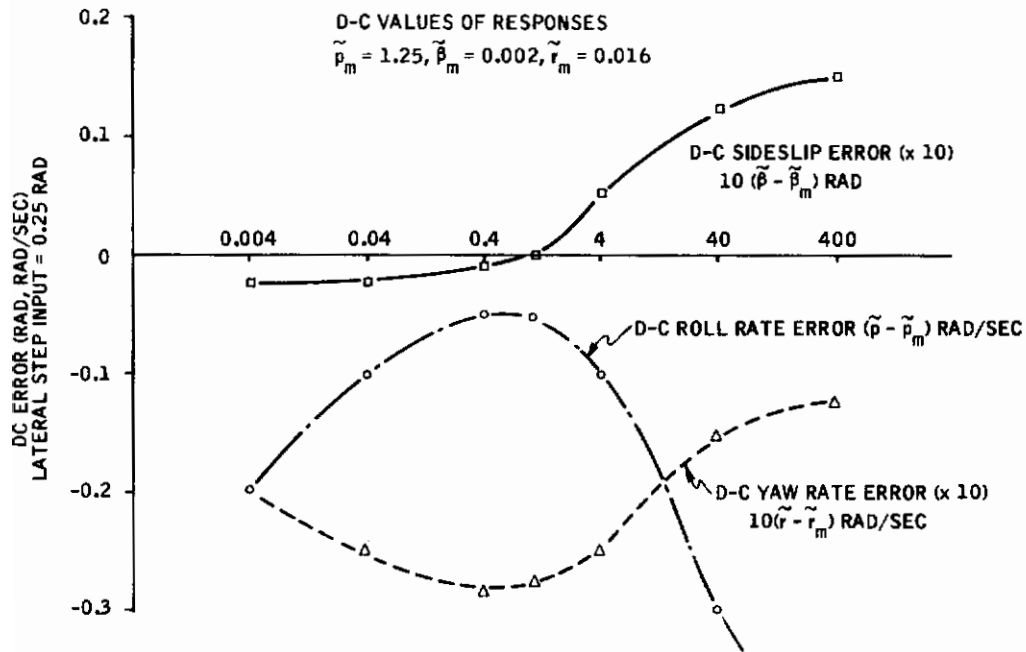


Figure 28. Steady-State Errors for Lateral Step versus Command Bandwidth

Table XIV. Command Feedforward Gains as a Function of  $\omega_0$  [FC(2), Q, R from Run 7]

$\omega_0$	$K_u^a$
0.004	$\begin{bmatrix} 1.22 & -0.170 \\ 0.739 & 3.11 \end{bmatrix}$
0.04	$\begin{bmatrix} 1.20 & 0.0228 \\ 0.611 & 4.35 \end{bmatrix}$
0.4	$\begin{bmatrix} 1.18 & 1.45 \\ 0.531 & 4.92 \end{bmatrix}$
1.0	$\begin{bmatrix} 1.15 & 0.187 \\ 0.507 & 4.80 \end{bmatrix}$
4.0	$\begin{bmatrix} 0.926 & 0.321 \\ 0.439 & 4.00 \end{bmatrix}$
40.0	$\begin{bmatrix} 0.207 & 0.200 \\ 0.124 & 1.05 \end{bmatrix}$
400.0	$\begin{bmatrix} 0.0218 & 0.0214 \\ 0.0117 & 0.105 \end{bmatrix}$

- ${}^a(K_u)_{11}$  = Rudder command ( $u_{mR}$ ) to rudder servo ( $u_{pR}$ )
- $(K_u)_{22}$  = Lateral command ( $u_{mAS}$ ) to lateral servo ( $u_{pAS}$ )
- $(K_u)_{12}$  =  $u_{mAS}$  to  $u_{pR}$
- $(K_u)_{21}$  =  $u_{mR}$  to  $u_{pAS}$

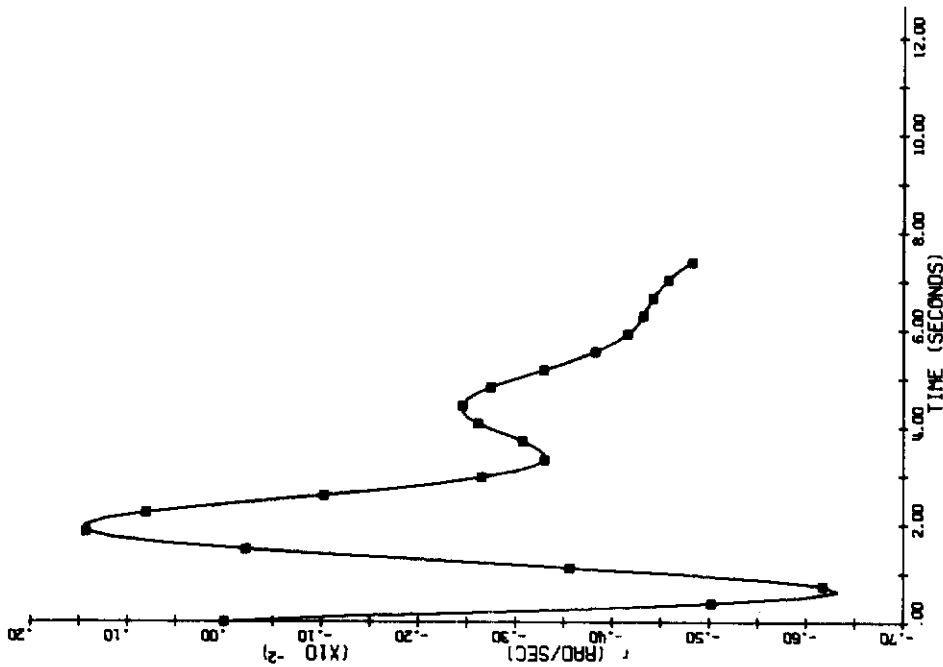
same quadratic weights used for the baseline design. The weights proved unacceptable, however, at some flight conditions. At low dynamic pressure (flight conditions 5, 8, and 10), the optimal controllers exhibited rate-limit oscillations upon application of 60 percent max magnitude stick and/or pedal step commands. As discussed earlier, this problem can be eliminated by increasing the control weights  $R_{11}$  and  $R_{22}$ . In supersonic flight (flight conditions 3, 6, 7, and 9), the baseline weights produced excessive model-following errors in sideslip. Performance was improved by decreasing  $R_{11}$  and  $R_{22}$ . Note, however, that the aircraft has very little rudder authority in supersonic flight (Table IX), so model-following errors in sideslip-due-to-rudder can really be improved only for very low level commands. For larger commands, the sideslip response saturates, with no other ill-effects (see figures below).<sup>19</sup>

The final quadratic weights used for each flight condition are summarized in Table XV, and step responses for the resulting optimal controllers (model 4) are shown in Figures 29 to 39. The traces for models 1, 2, and 3 are given in Figures 40 to 45. For flight conditions 2 through 11, these responses were obtained on the six-degree-of-freedom Minneapolis simulation described in Section V. This simulation lacked flaps, however, so the power approach responses (flight condition 1) were obtained by numerical integration. Qualitatively, Figures 29 through 45 indicate excellent model-following performance throughout the flight envelope. A more detailed look at performance and particularly at the variations of performance and controller gains over the flight envelope is given below:

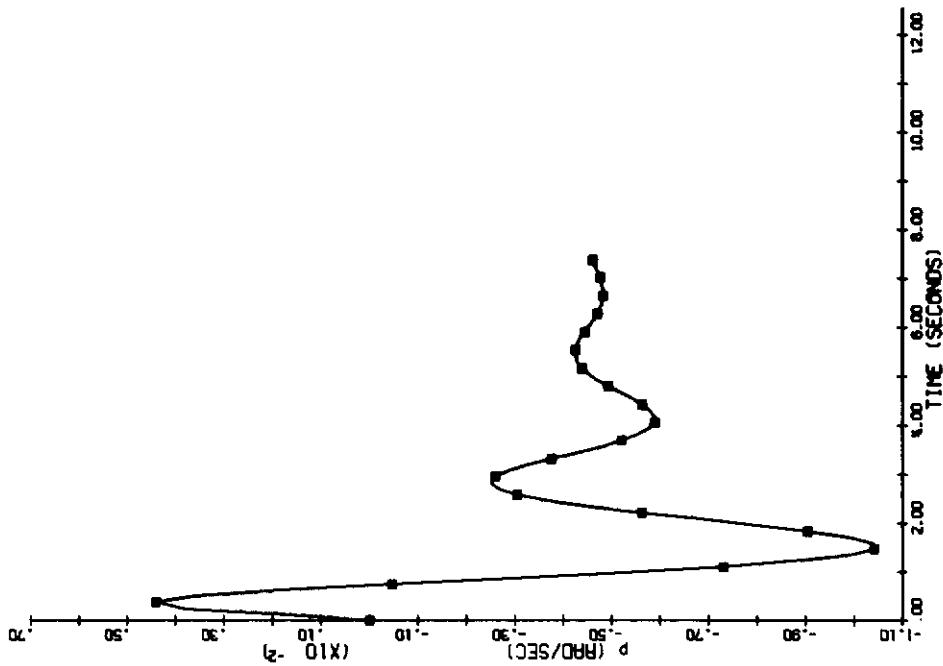
Table XV. Quadratic Weights for All Flight Conditions

Flight Condition	Quadratic Weights						Control Weights	
	$Q_{11}$	$Q_{22}$	$Q_{33}$	$Q_{44}$	$Q_{55}$	$Q_{66}$	$R_{11}$	$R_{22}$
1	10	1	100	0.001	0.1	0.01	1.0	1
2	10	1	100	0.001	0.1	0.01	1.0	1
3	10	1	100	0.001	0.1	0.01	0.1	1
4	10	1	100	0.001	0.1	0.01	2.0	1
5	10	1	100	0.001	0.1	0.01	5.0	2
6	10	1	100	0.001	0.1	0.01	0.1	1
7	10	1	100	0.001	0.1	0.01	0.5	1
8	10	1	100	0.001	0.1	0.01	2.0	1
9	10	1	100	0.001	0.1	0.01	0.2	1
10	10	1	100	0.001	0.1	0.01	5.0	2
11	10	1	100	0.001	0.1	0.01	2.0	1

<sup>19</sup> This suggests that the lateral acceleration response may be more appropriate for model-following at these speeds.

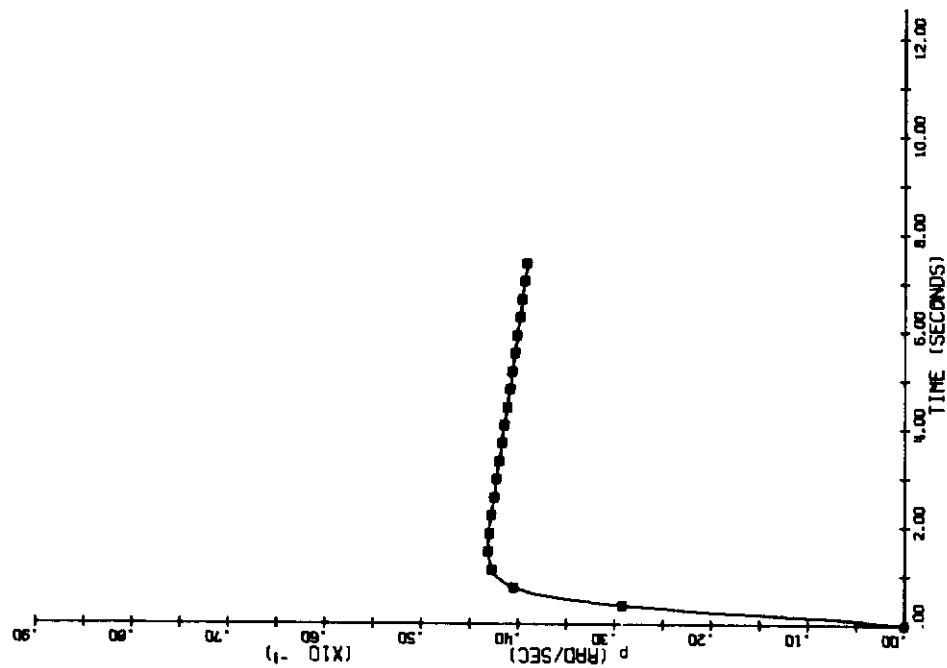


a) Roll Rate (0.01-Rad Rudder Command)

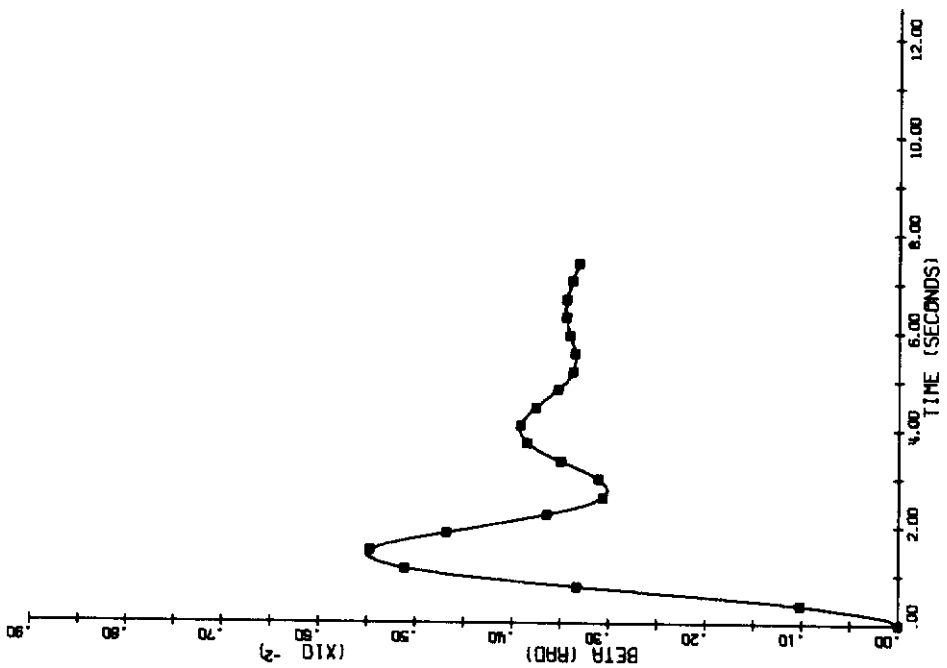


b) Yaw Rate (0.01-Rad Rudder Command)

Figure 29. Step Responses -- Optimal Quadratic Controller (Flight Condition 1, Model 4)

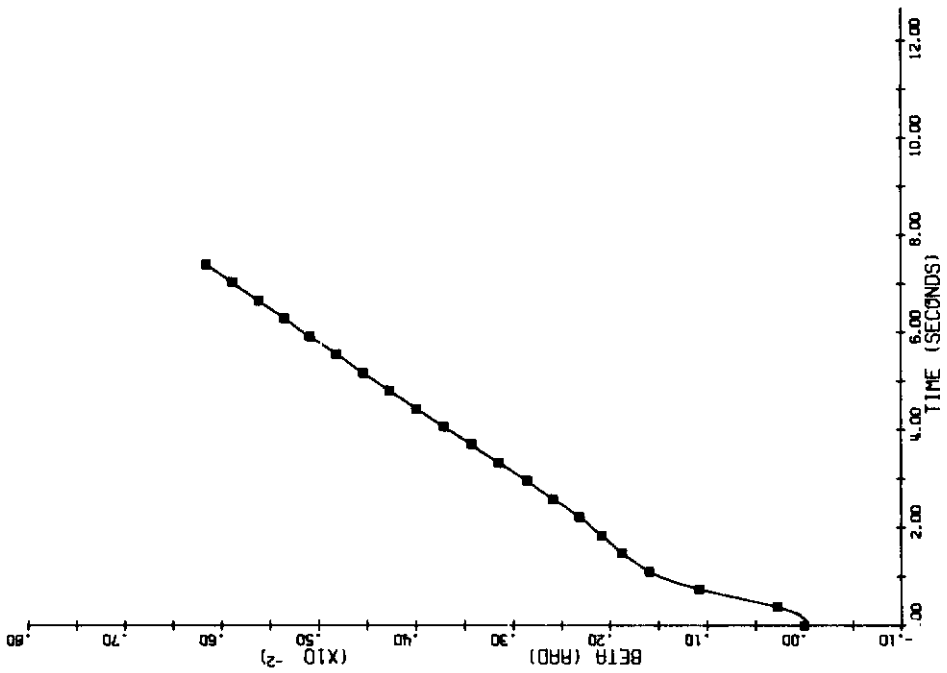


d) Roll Rate (0.01-Rad Lateral Command)

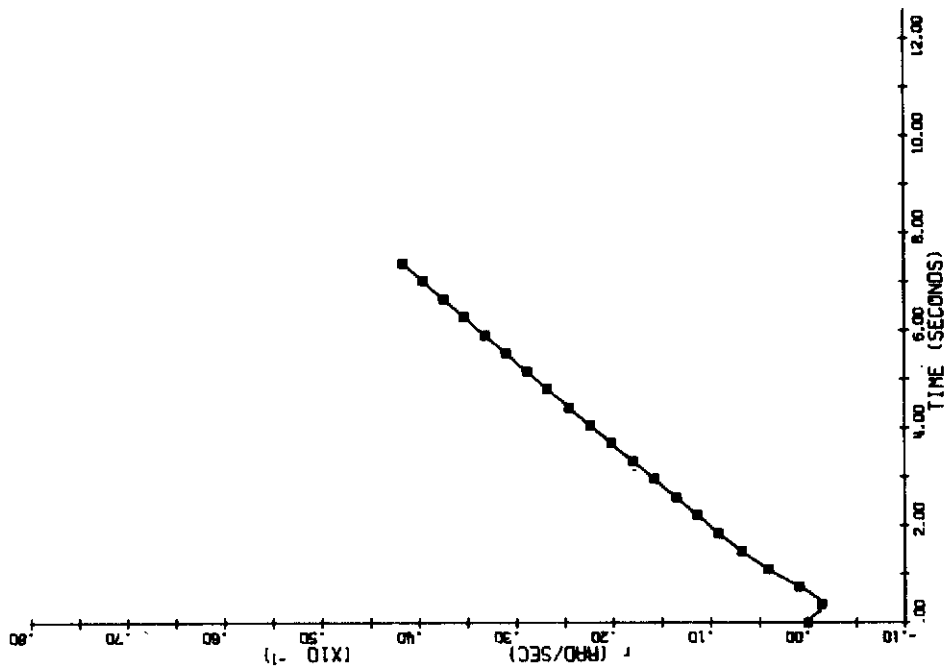


c) Sideslip (0.01-Rad Rudder Command)

Figure 29. Step Responses -- Optimal Quadratic Controller (Flight Condition 1, Model 4) (Continued)



f) Sideslip (0.01-Rad Lateral Command)



e) Yaw Rate (0.01-Rad Lateral Command)

Figure 29. Step Responses -- Optimal Quadratic Controller (Flight Condition 1, Model 4) (Concluded)

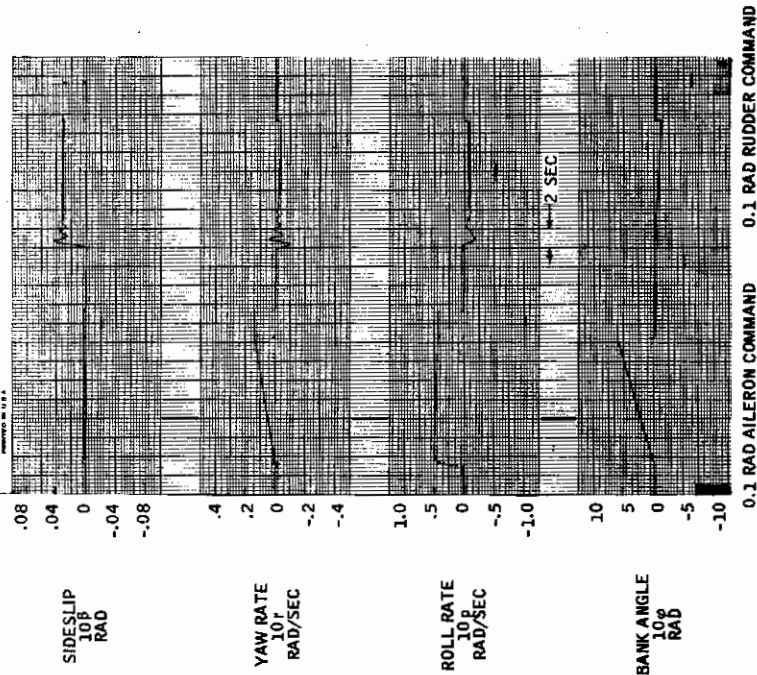


Figure 30. Step Responses -- Optimal Quadratic Controller (Flight Condition 2, Model 4, Minneapolis Simulation)

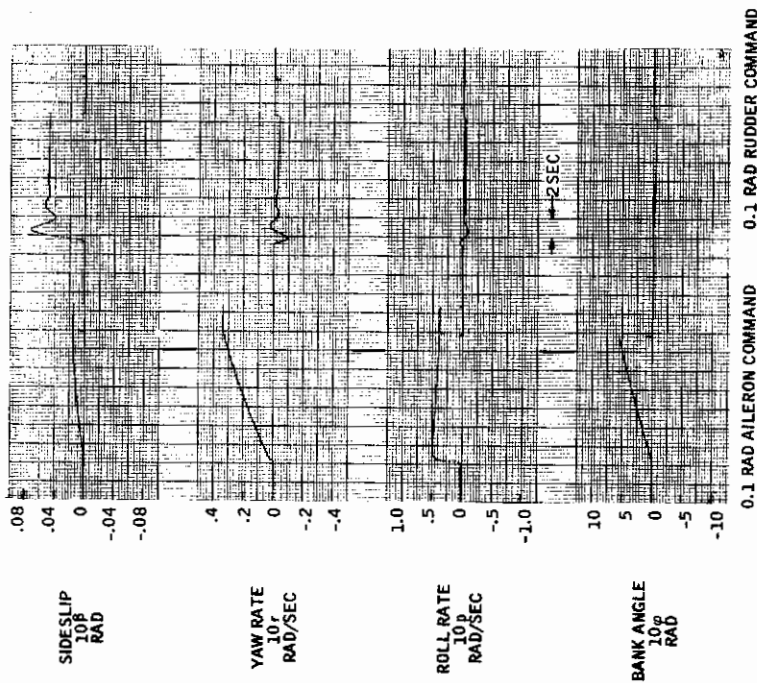


Figure 31. Step Responses -- Optimal Quadratic Controller (Flight Condition 3, Model 4, Minneapolis Simulation)



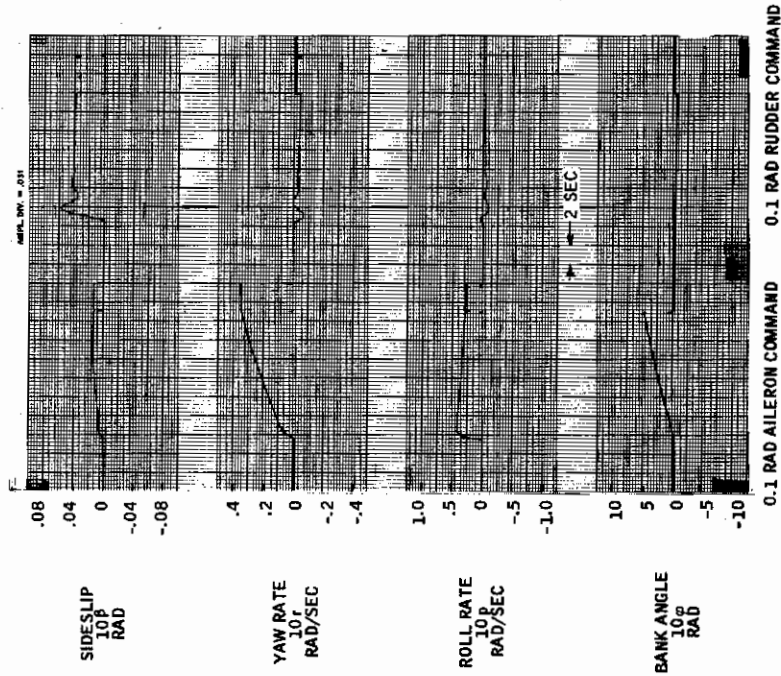


Figure 33. Step Responses -- Optimal Quadratic Controller (Flight Condition 5, Model 4, Minneapolis Simulation)

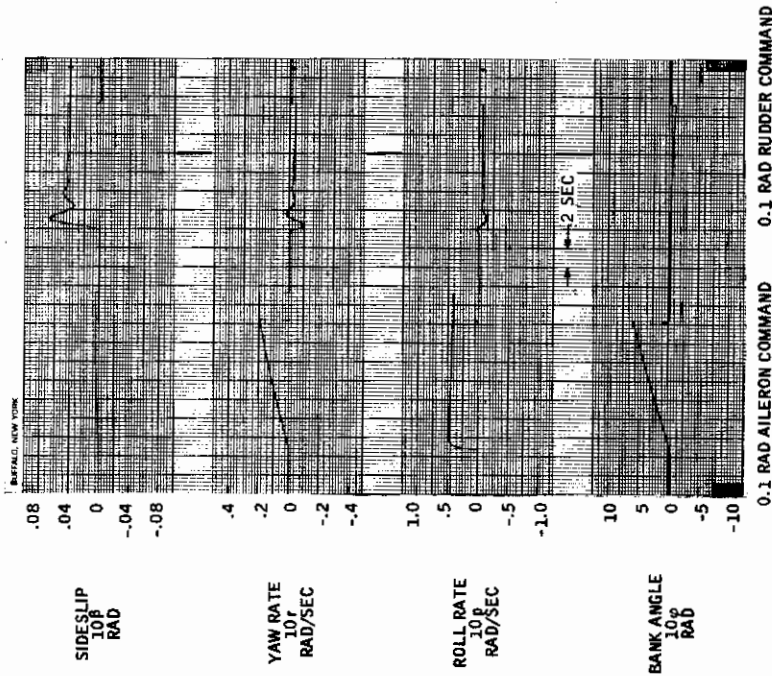


Figure 32. Step Responses -- Optimal Quadratic Controller (Flight Condition 4, Model 4, Minneapolis Simulation)

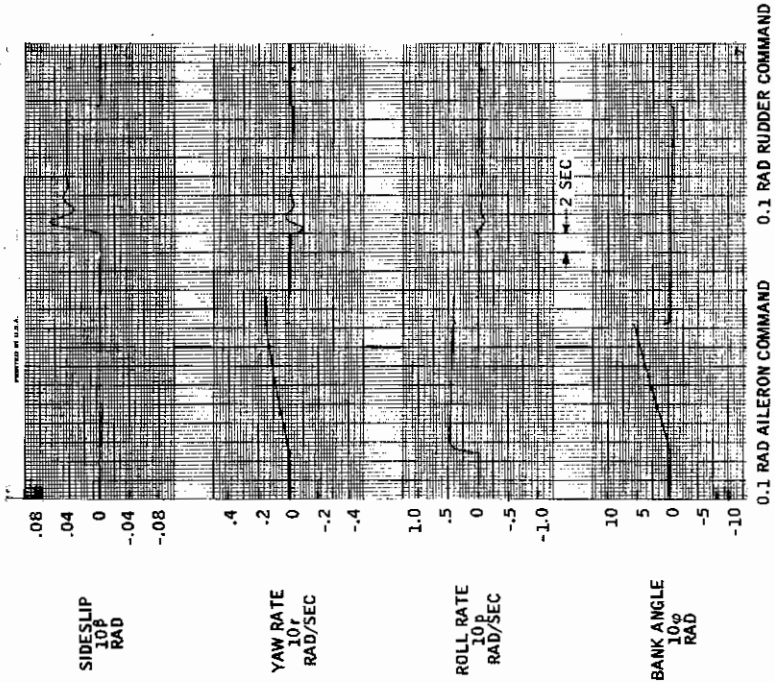


Figure 35. Step Responses -- Optimal Quadratic Controller (Flight Condition 7, Model 4, Minneapolis Simulation)

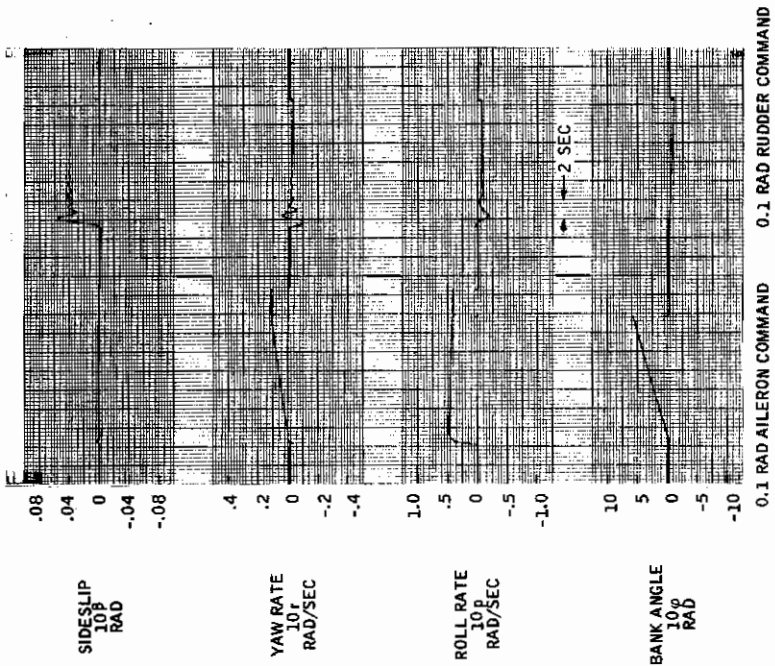


Figure 34. Step Responses -- Optimal Quadratic Controller (Flight Condition 6, Model 4, Minneapolis Simulation)



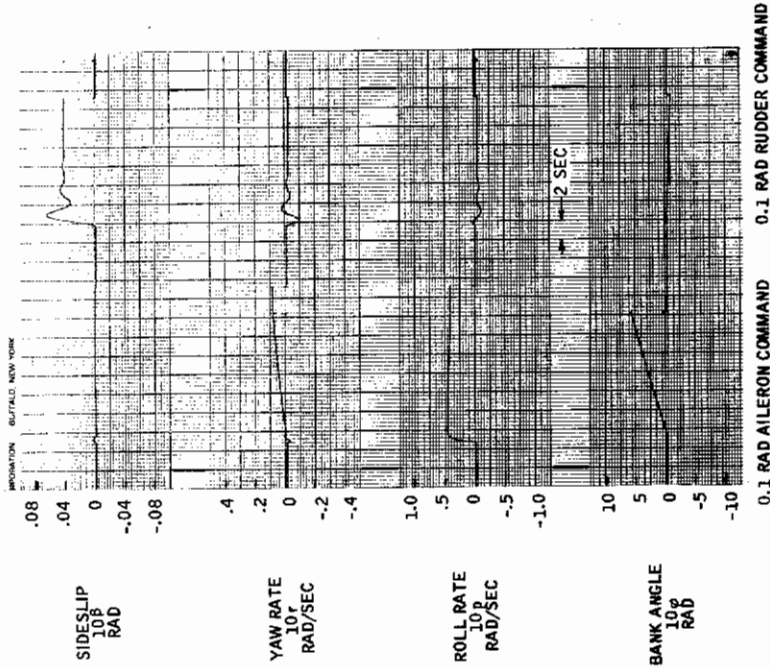


Figure 36. Step Responses -- Optimal Quadratic Controller (Flight Condition 8, Model 4, Minneapolis Simulation)

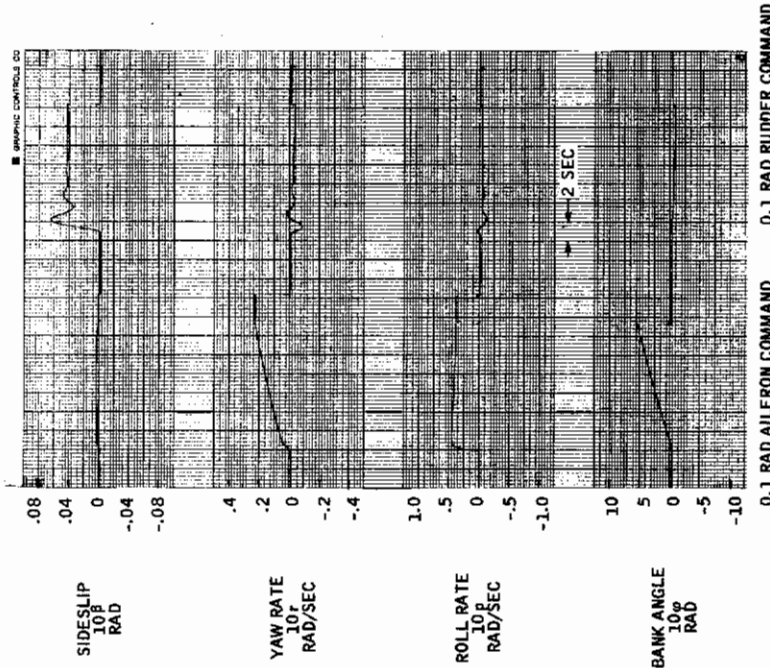


Figure 37. Step Responses -- Optimal Quadratic Controller (Flight Condition 9, Model 4, Minneapolis Simulation)

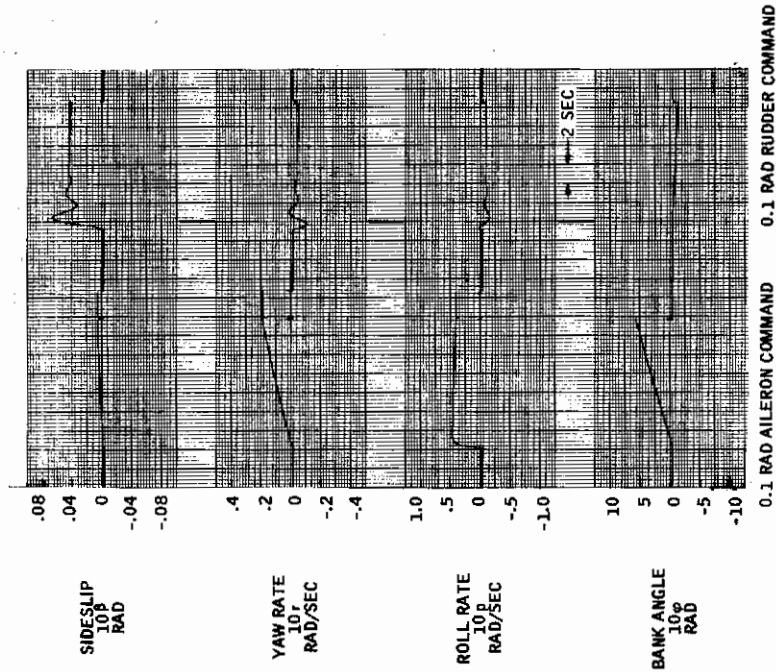


Figure 38. Step Responses -- Optimal Quadratic Controller (Flight Condition 10, Model 4, Minneapolis Simulation)

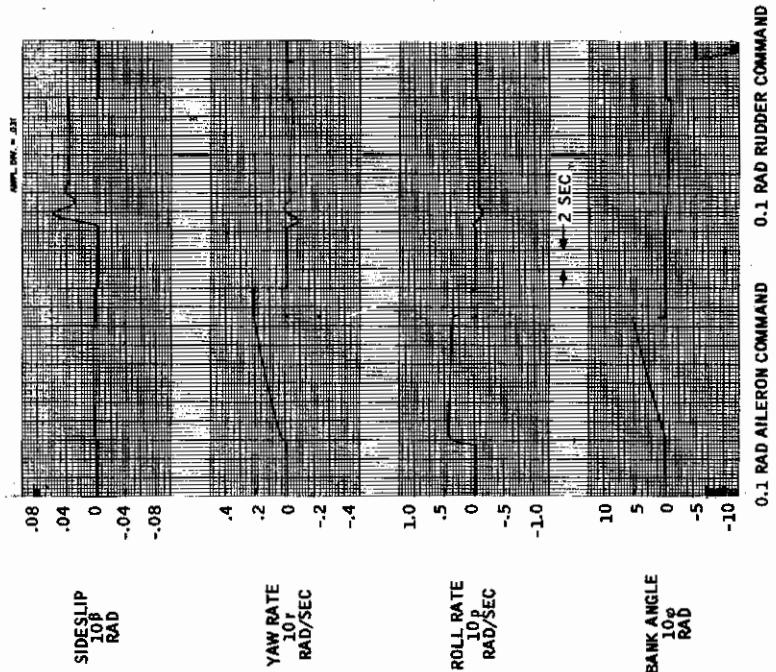


Figure 39. Step Responses -- Optimal Quadratic Controller (Flight Condition 11, Model 4, Minneapolis Simulation)



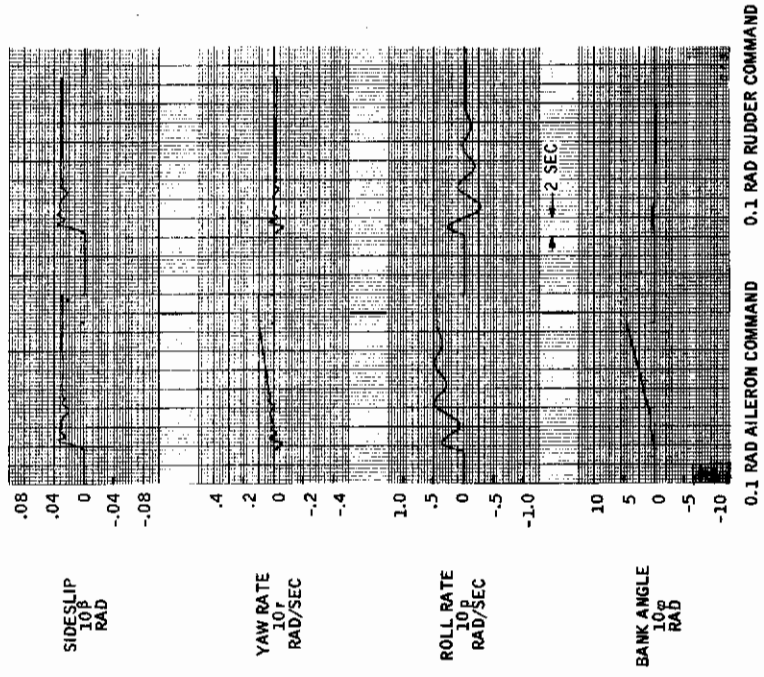


Figure 41. Step Responses -- Optimal Quadratic Controller (Flight Condition 3, Model 1, Minneapolis Simulation)

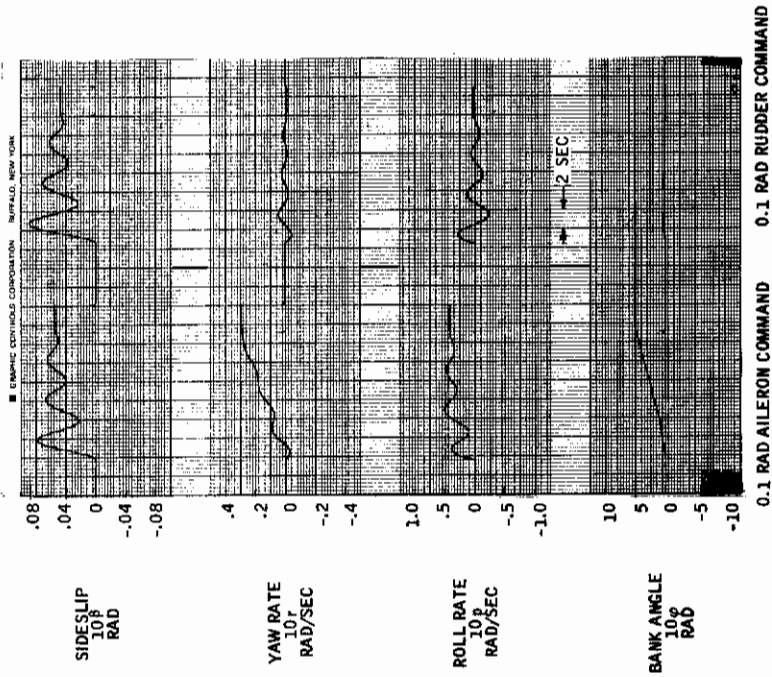


Figure 40. Step Responses -- Optimal Quadratic Controller (Flight Condition 2, Model 1, Minneapolis Simulation)

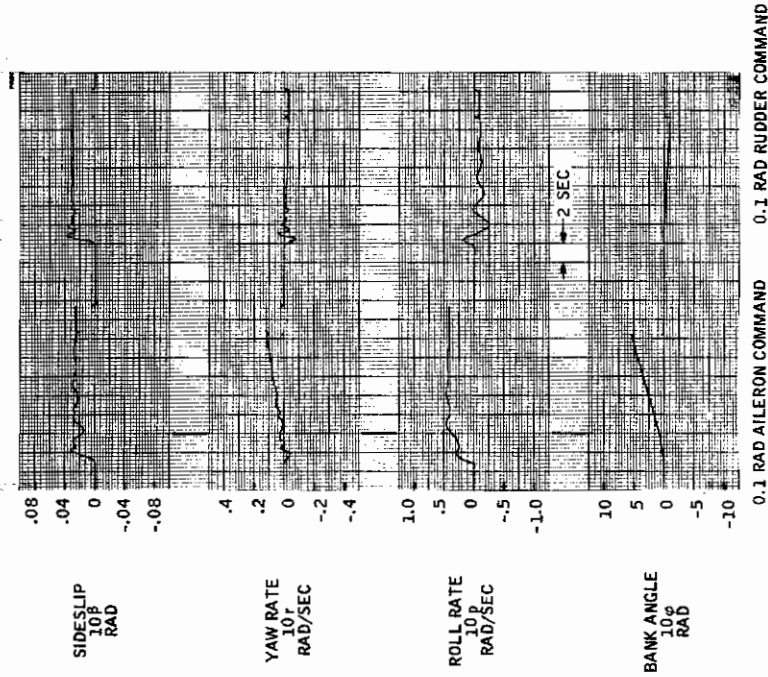


Figure 42. Step Responses -- Optimal Quadratic Controller (Flight Condition 2, Model 2, Minneapolis Simulation)

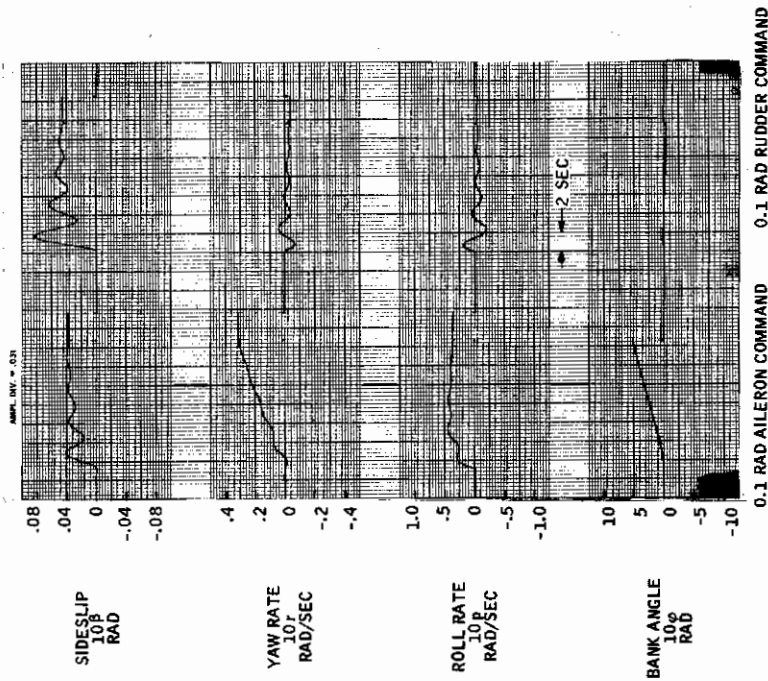


Figure 43. Step Responses -- Optimal Quadratic Controller (Flight Condition 3, Model 2, Minneapolis Simulation)



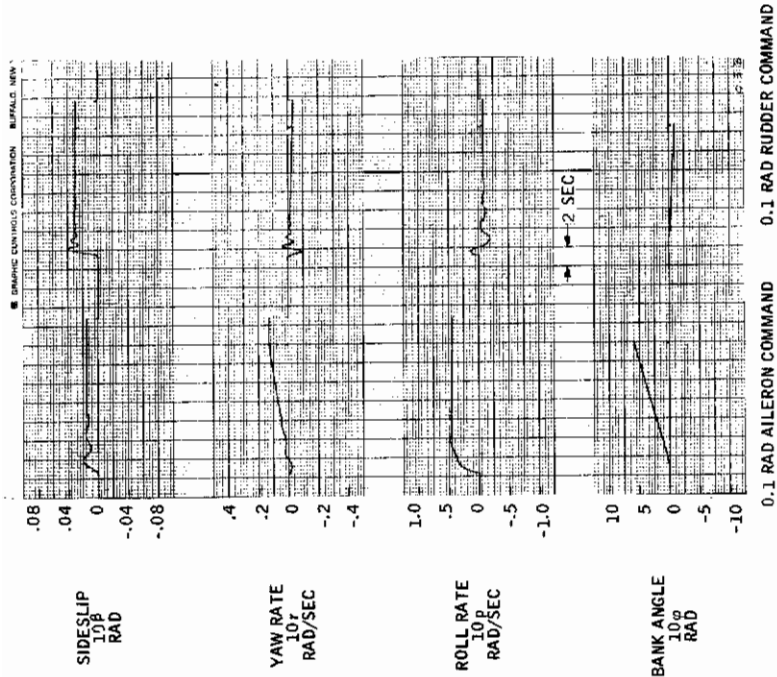


Figure 45. Step Responses -- Optimal Quadratic Controller (Flight Condition 3, Model 3, Minneapolis Simulation)

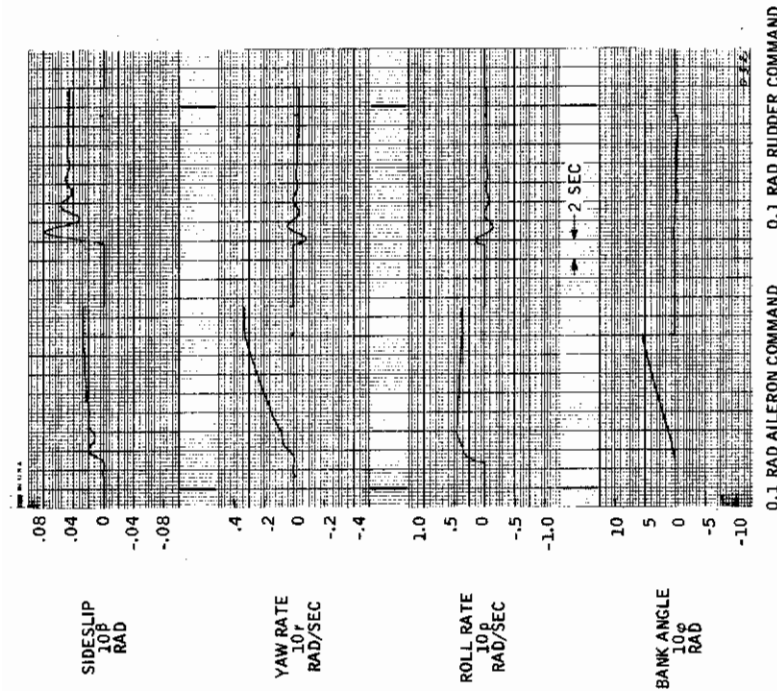


Figure 44. Step Responses -- Optimal Quadratic Controller (Flight Condition 2, Model 3, Minneapolis Simulation)

## Performance Sensitivity

By performance sensitivity we mean variations (or differences) in rms performance achieved by optimal model-following controllers at their respective flight conditions. These variations are shown in Figures 46, 47, and 48, which plot various performance variables of the model 4 controllers (Figures 29 through 39) on the Mach-altitude plane.

Figure 46 shows rms model-following errors for 0.1-rad rms rudder commands applied identically to each flight condition (no gusts and no lateral commands). Three normalized error variables are shown:

- 1) Normalized rms roll rate error (Figure 46a)

$$\sqrt{E(\tilde{p} - \tilde{p}_m)^2 / E\tilde{p}_m^2} \quad (68)$$

- 2) Normalized rms yaw rate error (Figure 46b)

$$\sqrt{E(\tilde{r} - \tilde{r}_m)^2 / E\tilde{r}_m^2} \quad (69)$$

- 3) Normalized rms sideslip error (Figure 46c)

$$\sqrt{E(\tilde{\beta} - \tilde{\beta}_m)^2 / E\tilde{\beta}_m^2} \quad (70)$$

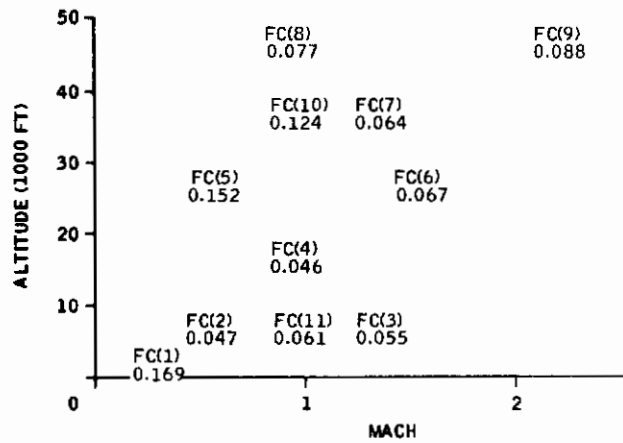
The same measures are shown for 0.1-rad rms lateral commands in Figure 47 and for 6-ft/sec rms gust inputs only in Figure 48. (The gust responses are not normalized, since  $E\tilde{\beta}_m^2 = E\tilde{r}_m^2 = E\tilde{p}_m^2 = 0$ .)

Performance is seen to be quite uniform over the flight envelope, with a little degradation in roll rate response to rudder at the low- $q$  flight conditions 1 and 5, and in yaw rate and sideslip response to lateral, flight conditions 1, 5, and 9. Note that the normalized error values in these latter responses are quite high because of the very low model responses [ $\sqrt{E\tilde{r}_m^2} = 0.0053$  rad/sec and  $\sqrt{E\tilde{\beta}_m^2} = 0.00086$  rad] to a 0.1-rad rms lateral command. So, while the errors are large percentage-wise, they are quite tolerable.

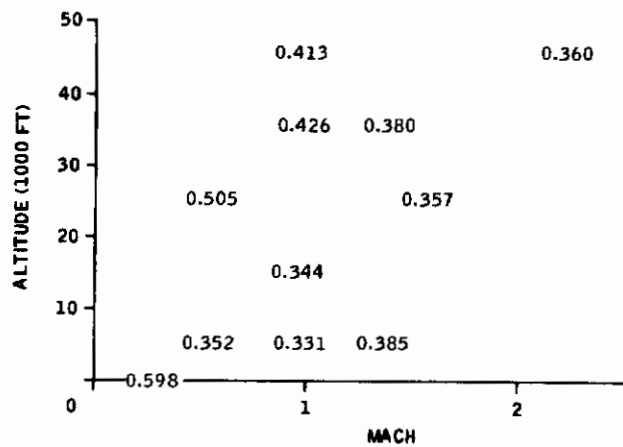
## Gain Sensitivity

Similar Mach-altitude plots can be constructed for all of the feedback and feedforward gains of the optimal controllers. This amounts to 40 separate plots, however, which would be too much data for easy assimilation. Instead, Table XVI was constructed which gives average values and maximum/minimum values for each gain. With this table,

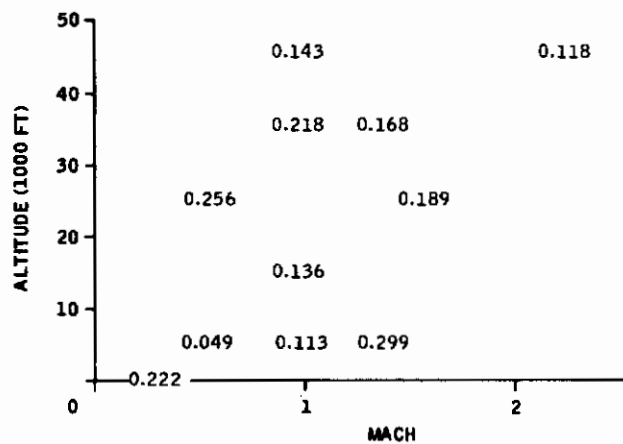
# Contrails



(a) NORMALIZED RMS ROLL RATE ERROR



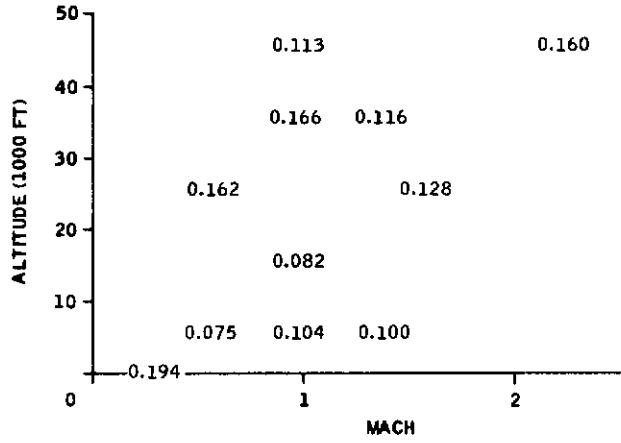
(b) NORMALIZED RMS YAW RATE ERROR



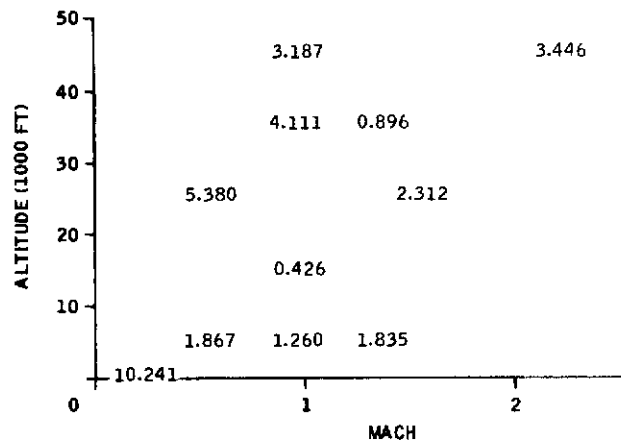
(c) NORMALIZED RMS SIDESLIP ERROR

Figure 46. Performance Sensitivity of Optimal Controller (0.1-Rad RMS Rudder Command)

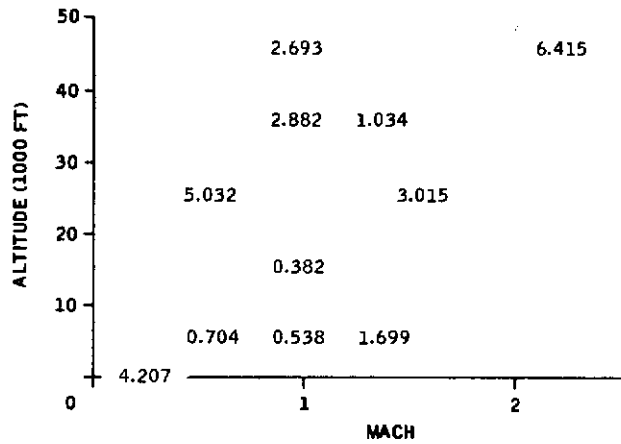
# Contrails



(a) NORMALIZED RMS ROLL RATE ERROR



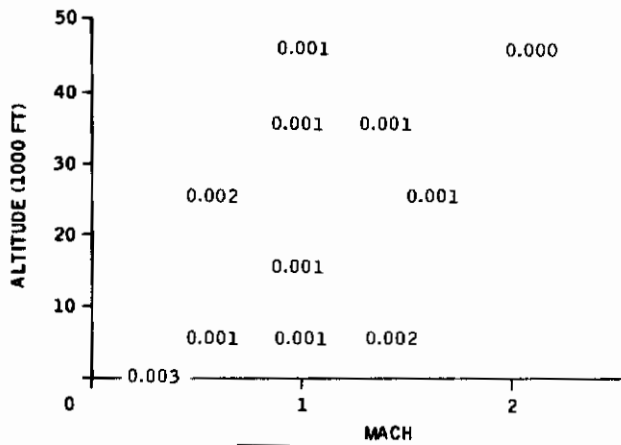
(b) NORMALIZED RMS YAW RATE ERROR



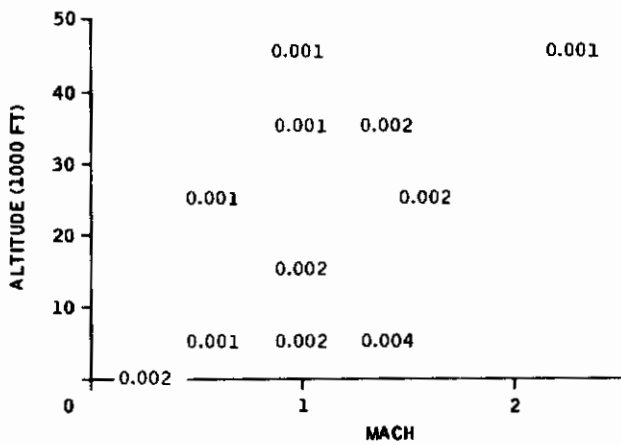
(c) NORMALIZED RMS SIDESLIP ERROR

Figure 47. Performance Sensitivity of Optimal Controllers (0.1-Rad RMS Lateral Command)

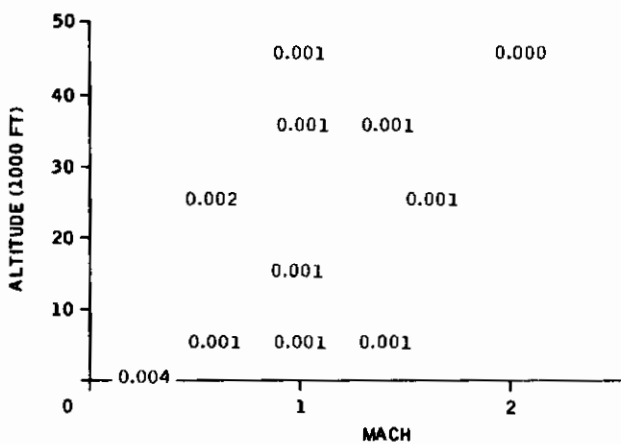
# Contrails



(a) ROLL RATE  $\sqrt{E(\rho)^2}$  (RAD/SEC)



(b) YAW RATE  $\sqrt{E(\gamma)^2}$  (RAD/SEC)



(c) SIDESLIP  $\sqrt{E(\beta)^2}$  (RAD)

Figure 48. Performance Sensitivity of Optimal Controller (6-Ft/Sec RMS Lateral Gust)

Table XVI. Gain Summary

Gain	Average Value Over All Flight Controllers	Minimum Value	Maximum Value	Negligible	Constant	Variable
p to $\begin{cases} u_{pR} \\ u_{pAS} \end{cases}$	-1.325 -2.404	-4.674 -2.887	0.319 -1.916		X	X
r to $\begin{cases} u_{pR} \\ u_{pAS} \end{cases}$	3.086 -0.948	1.550 -1.668	5.090 -0.399		X X	
$\beta$ to $\begin{cases} u_{pR} \\ u_{pAS} \end{cases}$	-3.415 3.508	-8.445 1.877	6.717 5.892		X	X
$\phi$ to $\begin{cases} u_{pR} \\ u_{pAS} \end{cases}$	-0.144 -0.010	-0.546 -0.034	-0.054 0.003	X	X	
$\xi$ to $\begin{cases} u_{pR} \\ u_{pAS} \end{cases}$	0.012 1.924	-0.004 1.089	0.056 2.180	X	X	
$\zeta$ to $\begin{cases} u_{pR} \\ u_{pAS} \end{cases}$	-0.002 0.015	-0.008 0.010	-0.000 0.020	X X		
$\delta_R$ to $\begin{cases} u_{pR} \\ u_{pAS} \end{cases}$	-0.342 -0.082	-0.625 -0.243	-0.152 -0.021	X	X	
$\delta_{AS}$ to $\begin{cases} u_{pR} \\ u_{pAS} \end{cases}$	-0.477 -1.445	-1.619 -2.507	-0.021 -0.777		X	X
$\gamma_1$ to $\begin{cases} u_{pR} \\ u_{pAS} \end{cases}$	-0.069 -0.016	-0.127 -0.050	-0.030 -0.004	X X		
$\gamma_2$ to $\begin{cases} u_{pR} \\ u_{pAS} \end{cases}$	-0.000 -0.000	-0.001 -0.000	-0.000 -0.000	X X		
$\gamma_3$ to $\begin{cases} u_{pR} \\ u_{pAS} \end{cases}$	-0.048 -0.159	-0.163 -0.268	-0.002 -0.086	X X		
$\gamma_4$ to $\begin{cases} u_{pR} \\ u_{pAS} \end{cases}$	-0.000 -0.001	-0.001 -0.002	-0.000 -0.000	X X		
a to $\begin{cases} u_{pR} \\ u_{pAS} \end{cases}$	0.000 0.000	-0.000 -0.000	0.000 0.000	X X		
$\dot{a}$ to $\begin{cases} u_{pR} \\ u_{pAS} \end{cases}$	0.000 -0.000	-0.000 -0.000	0.000 0.000	X X		
$\tilde{P}_m$ to $\begin{cases} u_{pR} \\ u_{pAS} \end{cases}$	1.193 1.764	-0.002 1.136	4.254 2.252		X	X
$\tilde{r}_m$ to $\begin{cases} u_{pR} \\ u_{pAS} \end{cases}$	-2.617 0.852	-4.862 0.222	-1.217 1.803		X X	
$\tilde{\beta}_m$ to $\begin{cases} u_{pR} \\ u_{pAS} \end{cases}$	5.984 -3.314	0.629 -5.231	15.466 -1.747		X	X
$u_{mR}$ to $\begin{cases} u_{pR} \\ u_{pAS} \end{cases}$	1.461 0.517	0.619 -0.034	2.512 1.094		X	X
$u_{mAS}$ to $\begin{cases} u_{pR} \\ u_{pAS} \end{cases}$	1.079 4.800	-1.830 3.861	4.664 6.612		X	X
v g to $\begin{cases} u_{pR} \\ u_{pAS} \end{cases}$	-0.006 -0.003	-0.021 -0.015	-0.001 0.001	X X		



it is relatively easy to locate negligible gains, gains which are (more or less) constant over the flight envelope, and gains which vary significantly. These assessments are indicated in the table. Some of the assessments made in the table are quite bold. Gains are thrown out if they are much below 0.25 and are called constant if  $K_{\max}/K_{\min} < 10$ . Our goal is a first-cut look at sensitivity.

From Table XVI, there remain only a few gains with significant variations over the flight envelope:

- Roll rate-to-rudder servo
- Sideslip-to-rudder servo
- Lateral actuator position-to-rudder servo
- Model roll rate-to-rudder servo
- Model sideslip-to-rudder servo
- Rudder command-to-lateral servo
- Lateral command-to-rudder servo

From this we draw the obvious conclusion that the rudder channel shows the greatest gain sensitivity over the flight envelope and that, if gain scheduling were to be required, it would be here. It is important to note, however, that the gain variations are not so severe as to preclude a practical fixed-gain design.

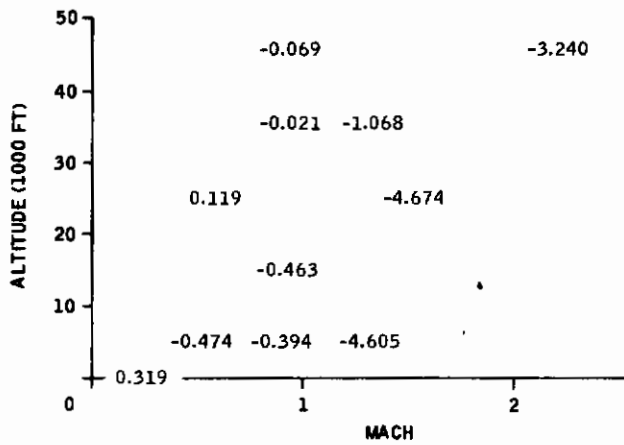
Mach-altitude plots of the remaining variable gains are given in Figure 49. The trend emerging from these curves is simple -- the gains are high in absolute value for high- $q$  flight conditions and low for low- $q$  flight conditions. This corresponds closely to the inverse trend exhibited by the rudder flexibility factor,  $K_f$ , and by the rudder sensitivity coefficients,  $N_{\delta R}$  and  $L_{\delta AS}$  (see Table VII).

## PRACTICAL CONTROLLER DESIGNS

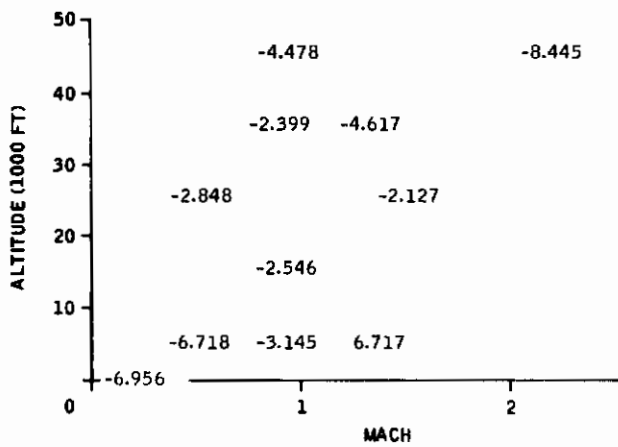
Using the optimal model-following controllers described above as a starting point, a practical fixed-gain control system was designed to follow model 4 over all flight conditions. The computational algorithm of Section III was used to carry out the design calculation. The algorithm was programmed and first debugged and tested on several single flight condition cases ( $p = 1$ ). Five critical flight conditions were then selected. The practical controller was designed for these ( $p = 5$ ) and checked against the remaining conditions.

The computational algorithm proved fully successful for all single-flight-condition cases, generating a practical controller in approximately 20 minutes of H-1800 computing time. (On current machines,

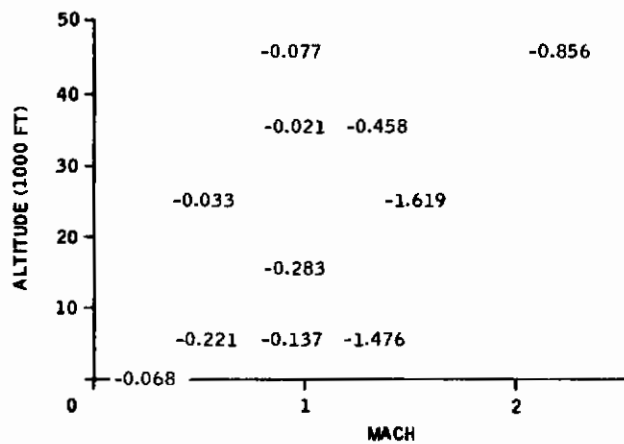
# Contrails



(a) ROLL RATE TO RUDDER



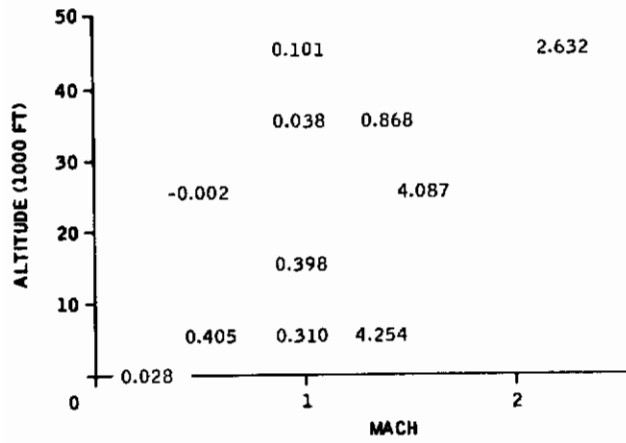
(b) SIDESLIP TO RUDDER



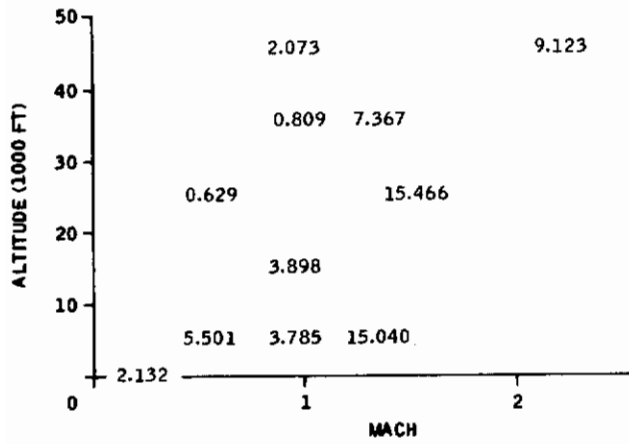
(c) LATERAL ACTUATOR POSITION TO RUDDER

Figure 49. Gain Sensitivity

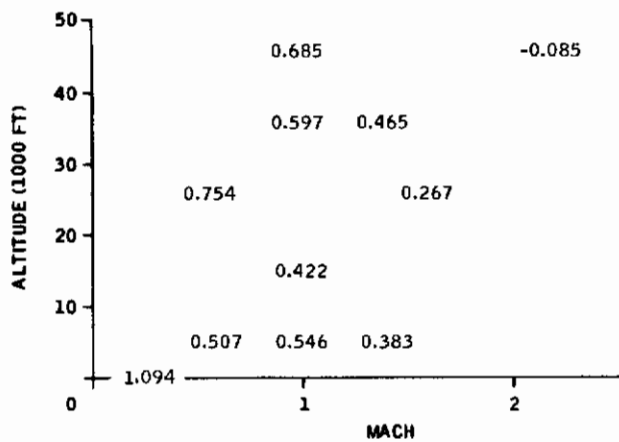
# Contrails



(d) MODEL ROLL RATE TO RUDDER



(e) MODEL SIDESLIP TO RUDDER



(f) RUDDER COMMAND TO LATERAL

Figure 49. Gain Sensitivity (Continued)

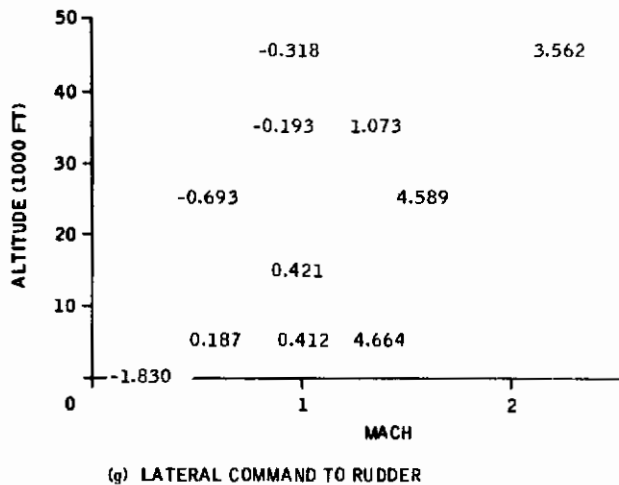


Figure 49. Gain Sensitivity (Concluded)

this means two minutes). For the five-flight-conditions case, more computer time (160 H-1800 minutes) and some human assistance were required to obtain a successful design. The details are discussed below.

### Single-Flight-Condition Cases

Five different combinations of sensed signals were used to debug the algorithm and to investigate practical control at the baseline flight condition, FC(2). Signals were selected by constraining the structure of the controller gain matrix, as shown in Figures 50 and 51. Figure 50 shows the total permitted gain structure of practical controllers for the assumed complement of measured signals given by Equation (47). {In terms of Section III notation, this equals  $[K^1(\lambda) + K^3] M + \lambda K^2$ ,  $\lambda = 0$ .} Each (x) denotes a possible gain feeding some sensed signal to one of the two servo inputs. In contrast, Figure 51 shows five constrained versions of the same matrix. Each (x) here denotes a gain to be retained ( $K^1$ ), with all blanks indicating prespecified zeros ( $K^3$ ) in the final practical gain matrix.

As an example, consider the structure for controller PC1. This feeds measured yaw rate, lateral accelerometer, and rudder command to the rudder servo and measured roll rate, bank angle, and lateral command to the lateral servo. No flexure, actuator, servo, or model states are used. The optimum performance achieved with this constrained gain

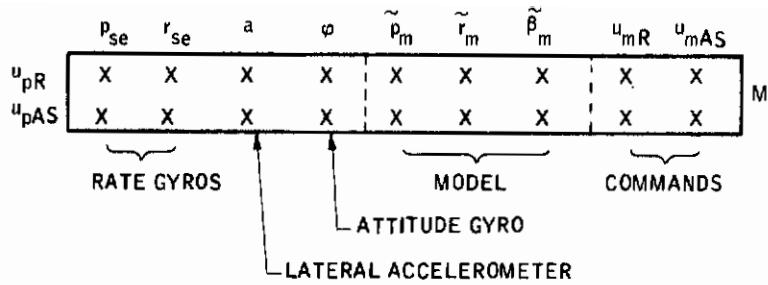


Figure 50. Structure of the Practical Gain Matrix,  $[K^1(\lambda) + K^3] M + \lambda K^2, \lambda = 0$

CONTROLLER	$[K^1(\lambda) + K^3] M + \lambda K^2, \lambda = 0$																						
PC1	<table border="1" style="margin: auto;"> <tr> <td style="width: 10%;"></td> <td style="width: 10%; text-align: center;">X</td> <td style="width: 10%; text-align: center;">X</td> <td style="width: 10%;"></td> <td style="width: 10%;"></td> <td style="width: 10%;"></td> <td style="width: 10%;"></td> <td style="width: 10%;"></td> <td style="width: 10%;"></td> <td style="width: 10%; text-align: center;">X</td> <td style="width: 10%;"></td> </tr> <tr> <td style="width: 10%;"></td> <td style="width: 10%; text-align: center;">X</td> <td style="width: 10%;"></td> <td style="width: 10%; text-align: center;">X</td> <td style="width: 10%;"></td> <td style="width: 10%;"></td> <td style="width: 10%;"></td> <td style="width: 10%;"></td> <td style="width: 10%;"></td> <td style="width: 10%;"></td> <td style="width: 10%; text-align: center;">X</td> </tr> </table>		X	X							X			X		X							X
	X	X							X														
	X		X							X													
PC2	<table border="1" style="margin: auto;"> <tr> <td style="width: 10%;"></td> <td style="width: 10%; text-align: center;">X</td> <td style="width: 10%; text-align: center;">X</td> <td style="width: 10%;"></td> <td style="width: 10%; text-align: center;">X</td> <td style="width: 10%; text-align: center;">X</td> <td style="width: 10%; text-align: center;">X</td> <td style="width: 10%; text-align: center;">X</td> <td style="width: 10%;"></td> <td style="width: 10%; text-align: center;">X</td> <td style="width: 10%;"></td> </tr> <tr> <td style="width: 10%;"></td> <td style="width: 10%; text-align: center;">X</td> <td style="width: 10%;"></td> <td style="width: 10%; text-align: center;">X</td> <td style="width: 10%; text-align: center;">X</td> <td style="width: 10%; text-align: center;">X</td> <td style="width: 10%; text-align: center;">X</td> <td style="width: 10%; text-align: center;">X</td> <td style="width: 10%;"></td> <td style="width: 10%; text-align: center;">X</td> <td style="width: 10%;"></td> </tr> </table>		X	X		X	X	X	X		X			X		X	X	X	X	X		X	
	X	X		X	X	X	X		X														
	X		X	X	X	X	X		X														
PC3	<table border="1" style="margin: auto;"> <tr> <td style="width: 10%;"></td> <td style="width: 10%; text-align: center;">X</td> <td style="width: 10%; text-align: center;">X</td> <td style="width: 10%; text-align: center;">X</td> <td style="width: 10%;"></td> <td style="width: 10%; text-align: center;">X</td> <td style="width: 10%; text-align: center;">X</td> <td style="width: 10%; text-align: center;">X</td> <td style="width: 10%; text-align: center;">X</td> <td style="width: 10%;"></td> <td style="width: 10%; text-align: center;">X</td> </tr> <tr> <td style="width: 10%;"></td> <td style="width: 10%; text-align: center;">X</td> <td style="width: 10%;"></td> <td style="width: 10%;"></td> <td style="width: 10%; text-align: center;">X</td> <td style="width: 10%; text-align: center;">X</td> <td style="width: 10%; text-align: center;">X</td> <td style="width: 10%; text-align: center;">X</td> <td style="width: 10%;"></td> <td style="width: 10%; text-align: center;">X</td> <td style="width: 10%;"></td> </tr> </table>		X	X	X		X	X	X	X		X		X			X	X	X	X		X	
	X	X	X		X	X	X	X		X													
	X			X	X	X	X		X														
PC4	<table border="1" style="margin: auto;"> <tr> <td style="width: 10%;"></td> <td style="width: 10%; text-align: center;">X</td> <td style="width: 10%; text-align: center;">X</td> <td style="width: 10%; text-align: center;">X</td> <td style="width: 10%; text-align: center;">X</td> <td style="width: 10%;"></td> <td style="width: 10%; text-align: center;">X</td> <td style="width: 10%; text-align: center;">X</td> <td style="width: 10%; text-align: center;">X</td> <td style="width: 10%; text-align: center;">X</td> <td style="width: 10%;"></td> </tr> <tr> <td style="width: 10%;"></td> <td style="width: 10%; text-align: center;">X</td> <td style="width: 10%;"></td> <td style="width: 10%;"></td> <td style="width: 10%; text-align: center;">X</td> <td style="width: 10%; text-align: center;">X</td> <td style="width: 10%; text-align: center;">X</td> <td style="width: 10%; text-align: center;">X</td> <td style="width: 10%;"></td> <td style="width: 10%; text-align: center;">X</td> <td style="width: 10%;"></td> </tr> </table>		X	X	X	X		X	X	X	X			X			X	X	X	X		X	
	X	X	X	X		X	X	X	X														
	X			X	X	X	X		X														
PC5	<table border="1" style="margin: auto;"> <tr> <td style="width: 10%;"></td> <td style="width: 10%; text-align: center;">X</td> <td style="width: 10%; text-align: center;">X</td> <td style="width: 10%; text-align: center;">X</td> <td style="width: 10%; text-align: center;">X</td> <td style="width: 10%;"></td> <td style="width: 10%; text-align: center;">X</td> <td style="width: 10%; text-align: center;">X</td> <td style="width: 10%; text-align: center;">X</td> <td style="width: 10%; text-align: center;">X</td> <td style="width: 10%;"></td> </tr> <tr> <td style="width: 10%;"></td> <td style="width: 10%; text-align: center;">X</td> <td style="width: 10%; text-align: center;">X</td> <td style="width: 10%; text-align: center;">X</td> <td style="width: 10%; text-align: center;">X</td> <td style="width: 10%;"></td> <td style="width: 10%; text-align: center;">X</td> <td style="width: 10%; text-align: center;">X</td> <td style="width: 10%; text-align: center;">X</td> <td style="width: 10%; text-align: center;">X</td> <td style="width: 10%;"></td> </tr> </table>		X	X	X	X		X	X	X	X			X	X	X	X		X	X	X	X	
	X	X	X	X		X	X	X	X														
	X	X	X	X		X	X	X	X														

Figure 51. Gain Structure of Single-Flight-Condition Practical Controllers

configuration is summarized in Table XVII, which compares several performance variables with the optimal baseline design. The degree of deterioration is self-evident -- 63 percent for the quadratic cost, 73 percent for rms roll rate error, 48 percent for yaw rate error, and 280 percent for sideslip error.

Additional gain configurations were generated by adding other signals to the PC1 complement. First, model feedforwards were added (PC2) which yielded large improvements. Quadratic cost deterioration was reduced to 29 percent, roll rate error to 44 percent, yaw rate error to zero, and sideslip error to 73 percent. More rigid-body feedbacks were then added -- measured roll rate-to-rudder (PC3), bank angle-to-rudder (PC4), and measured yaw rate plus lateral accelerometer-to-lateral (PC5). Each addition provides some improvement in the total quadratic cost but trades improvements in one model-following error against small deteriorations of another. For this reason, the PC2 configuration was selected as the first candidate for multiple-flight-condition practical controller designs.

A typical lambda-history of the quadratic cost for the computation of a practical controller is shown in Figure 52. This shows the computational algorithm starting at  $\lambda = 1$  with the optimal control ( $J^* = 0.656$ ) and integrating backwards toward  $\lambda = 0$ . The integration uses a step size of  $\Delta\lambda = -0.2$  which is successful down to  $\lambda = 0.2$ , where the step size is halved by an automatic provision in the algorithm. This provision reduces the step size whenever two corrector steps are required

Table XVII. RMS Performance of Single-Flight-Condition Practical Controllers for Flight Condition 2<sup>†</sup>

Controller	Quadratic Cost (J)	RMS Performance								
		p	$\tilde{p} - \tilde{p}_m$	r	$\tilde{r} - \tilde{r}_m$	$\beta$	$\tilde{\beta} - \tilde{\beta}_m$	z	$\xi$	$\tilde{\xi}$
Baseline	0.656	0.837	0.149	0.304	0.0633	0.0844	0.00911	4.36	0.0701	0.981
PC1	1.07		0.257		0.0930		0.0350	3.56	0.0639	0.680
PC2	0.847		0.213		0.0621		0.0158	4.26	0.0707	0.714
PC3	0.836		0.206		0.0713		0.0181	4.34	0.0706	0.731
PC4	0.788		0.198		0.0749		0.0148	4.31	0.0707	0.720
PC5	0.680		0.155		0.0643		0.0156	4.38	0.0700	0.959

<sup>†</sup>Computed for  $\omega_0 = 4.0$ , to provide direct comparison with the baseline design. The commands were simultaneous rudder and lateral, with rms levels given in Table XI.



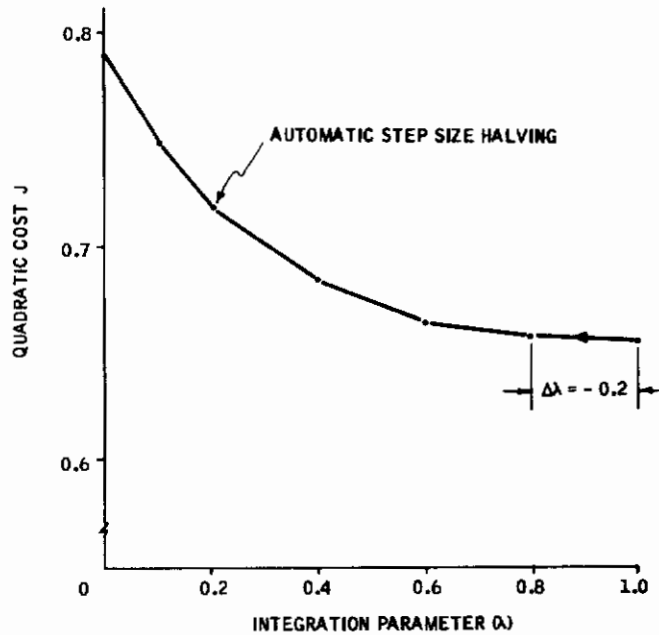


Figure 52. Typical Cost History for Computation of Practical Controller (PC4)

to satisfy the corrector convergence test,  $\left| \frac{\partial J}{\partial K^I} \right| < \epsilon$ , shown in the flow diagram, Figure 8. Various other kinds of deescalation/escalation schemes could, of course, also be used. The value,  $\epsilon$ , for the corrector convergence test was set at  $0.1 J(\lambda)$ .

### Multiple-Flight-Condition Cases

Round One -- Following these single-flight-condition designs, a fixed-gain controller, PC6, was computed for five flight conditions considered simultaneously. The chosen flight conditions were 1, 3, 4, 5, and 9, which span the range of dynamic pressure, Mach, and altitude. The constrained gain structure was that of PC2, Figure 51, the command bandwidth was  $\omega_0 = 1.0$ , and the quadratic performance index was

$$J = \sum_{i=1, 3, 4, 5, 9} \frac{1}{J^*(i)} J(i) \quad (70)$$

where  $J^*(i)$  denotes the optimal quadratic cost at the  $i^{\text{th}}$  flight condition. The values of  $J^*(i)$  are shown in Figure 53 at  $\lambda = 1$ . [Note that we are now reintroducing the flight condition dependence ( $i$ ) of the mathematical model and of all performance variables. This was dropped earlier in Section IV for notational convenience.]

# Contrails

The computations associated with this multiple-flight-condition design consumed 160 minutes of H-1800 time. The optimal cost surface  $J(K)$  proved to be exceedingly complex, forcing the predictor-corrector algorithm to snake its way through narrow "trenches" leading away from the global optimum. The cost surface had to be scaled and the integration step size reduced twice before the final answer was obtained. A summary of the solution process is given by the lambda-histories of the  $J(i)$ 's shown in Figure 53. The initial integration step size was again  $\Delta\lambda = -0.2$  which worked well down to  $\lambda = 0.4$ . Here it was halved, and halved again at  $\lambda = 0.2$  by the automatic step size adjustment provision. We stopped computations at two points to study the matrix of second partial derivatives  $(\partial^2 J)/(\partial K^1 \partial K^1 T)$ . At the first point,  $\lambda = 1$ , this matrix exhibited an eigenvalue spread of 2090 to 0.011. Intuitively this means that the performance surface in  $K^1$ -space consists of very narrow hyper-dimensional "trenches." The eigenvalue spread was reduced to about  $10^3$  to 1 by reducing the accelerometer sensitivity by the factor 1/100. This requires a larger accelerometer feedback gain and thus effectively scales the cost surface. The matrix of second partials was also checked at  $\lambda = 0.2$ . Here its eigenvalues ranged from -2.2 to 278. The negative value indicates that we are no longer at a unique minimum but have passed an inflection point somewhere along the way. It also means that the cost surface is not likely to be locally quadratic (in  $K^1$ ), so the use of Newton-Raphson corrector steps is no longer justified. The computations were therefore continued with predictor steps only. Because of the behavior of  $(\partial^2 J)/(\partial K^1 \partial K^1 T)$ , however, the global optimality (in  $K^1$  space) of our final answer is suspect.

The gains obtained at  $\lambda = 0$  are given below:

	$p_{se}$	$r_{se}$	$a$	$\phi$	$x_m$			$u_m$	
$u_{pR}$	0	0.170	0.00872	0	-0.0603	0.202	-1.50	1.61	0
$u_{pAS}$	-1.50	0	0	-0.0236	1.15	-0.310	0.507	0	1.89

Performance over all 11 flight conditions is summarized in Figures 54 and 55. These figures show the same Mach-altitude plots used previously and can be directly compared with the optimal controller performance plots of Figures 46 and 47.

Such comparisons show, first of all, more performance variation over the flight envelope. But this is to be expected. What is more important is that we see some very significant performance deteriorations. Looking at maximum deteriorations over all flight conditions, for example, the ratios

$$\text{Max.}_{FC(i) \ i = 1, \dots, 11} \left\{ \frac{\text{rms error of PC6}}{\text{rms error of optimal controller}} \right\}$$

come out as indicated in Table XVIII.

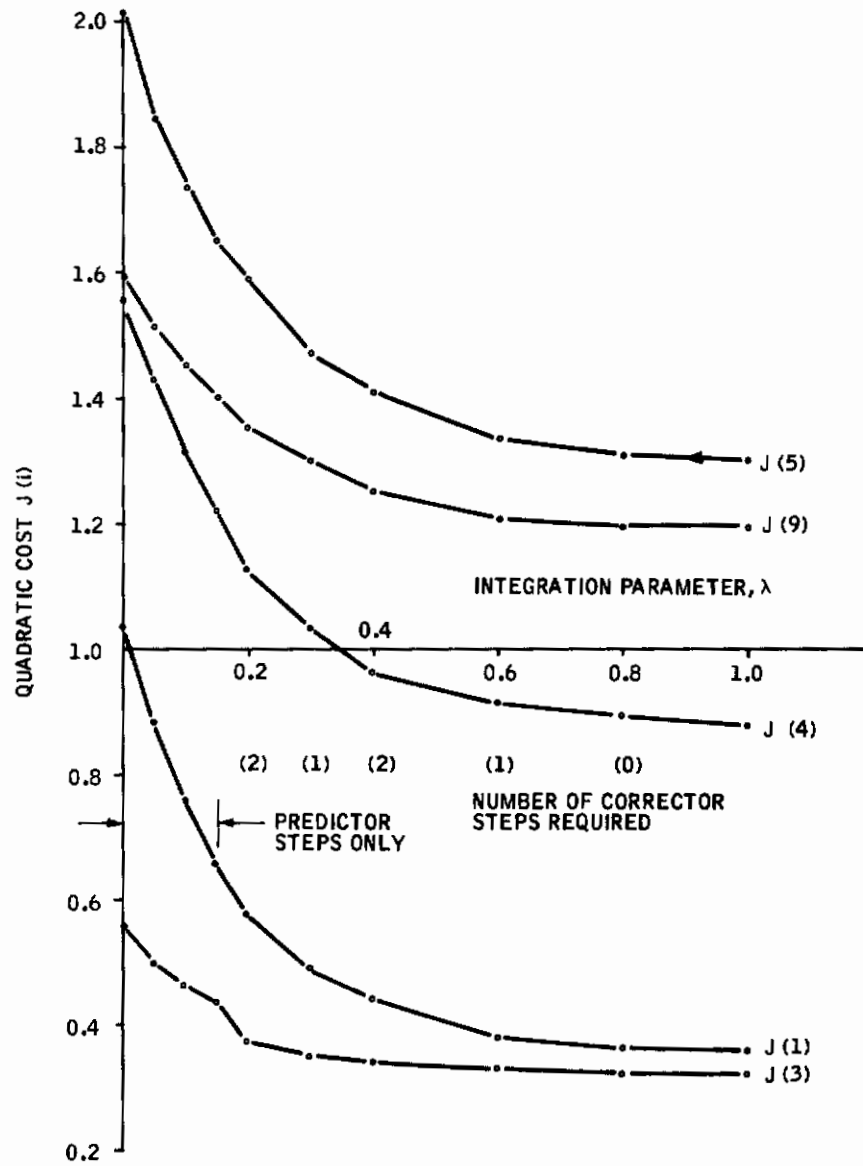
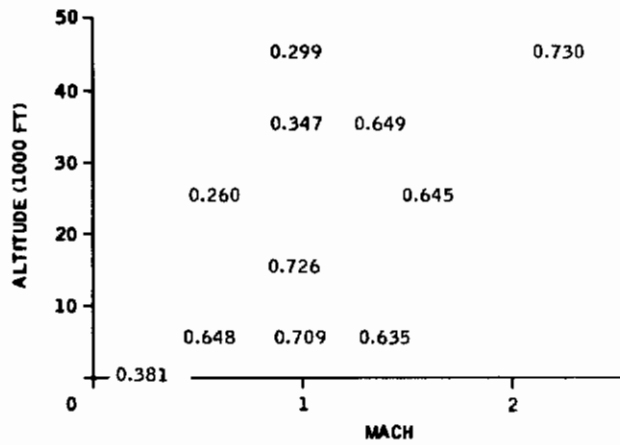
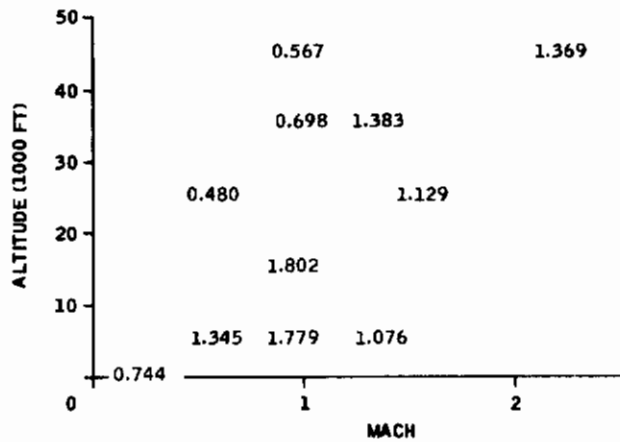


Figure 53. Lambda-Histories of Costs for Practical Controller Computation (PC6)

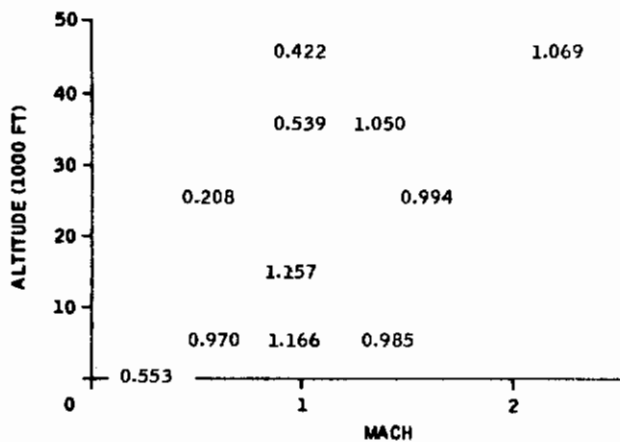
# Contrails



(a) NORMALIZED RMS ROLL RATE ERROR



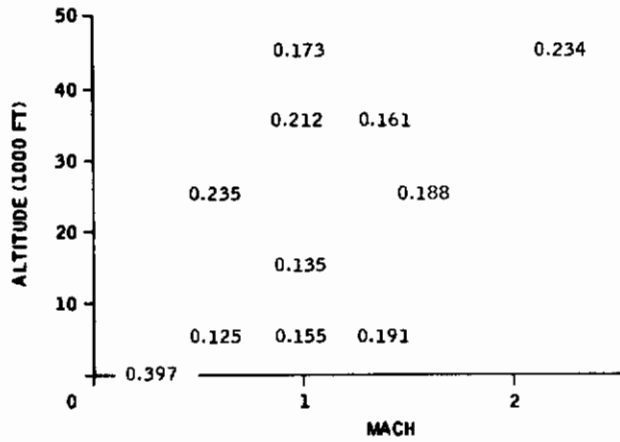
(b) NORMALIZED RMS YAW RATE ERROR



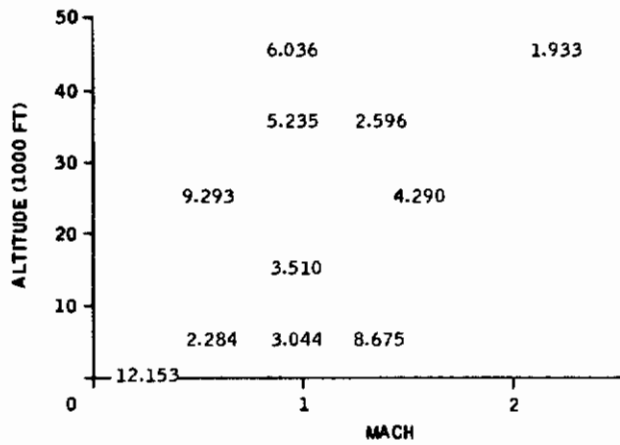
(c) NORMALIZED RMS SIDESLIP ERROR

Figure 54. Performance Sensitivity of PC6 (0.1-Rad RMS Rudder Command)

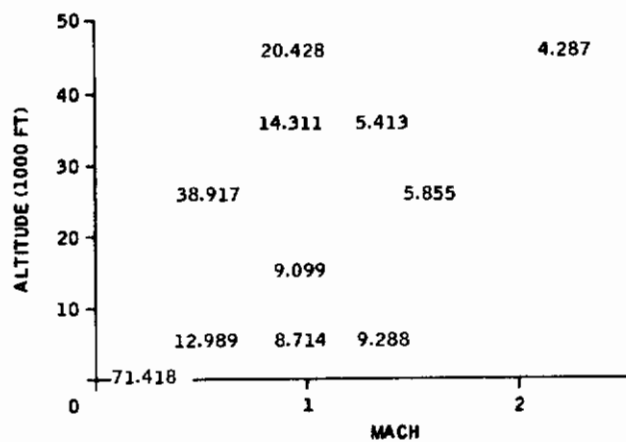
# Contrails



(a) NORMALIZED RMS ROLL RATE ERROR



(b) NORMALIZED RMS YAW RATE ERROR



(c) NORMALIZED RMS SIDESLIP ERROR

Figure 55. Performance Sensitivity of PC6 (0.1-Rad RMS Lateral Command)

Table XVIII. Maximum Deterioration Ratios, PC6

Command	Roll Rate Error	Yaw Rate Error	Sideslip Error
Rudder	15	5	20
Lateral	2	8	24

This table must be interpreted in the light of the kinds of responses being commanded. For rudder responses, we are commanding sideslip, so an error deterioration of 20-to-1 looks bad. For lateral responses, on the other hand, we are commanding roll rate for which the 2-to-1 deterioration looks reasonably good. Roll and yaw rate response to rudder and sideslip and yaw rate response to lateral are extraneous<sup>20</sup> responses which are small for the optimal controllers and so could still be tolerable even at a 15-to-1 or 24-to-1 error increase over the optimal. These interpretations are examined on some selected PC6 step responses in Figures 56, 57, and 58, which show that roll rate responses to lateral are indeed good, sideslip responses to rudder are not acceptable, and sideslip responses due to lateral would be acceptable if their oscillations were better damped. The step responses also show something which rms performance numbers cannot -- performance is poor (particularly in responses to rudder) because of inadequate damping of the aircraft's own dutch roll mode (also evident from the low yaw rate-to-rudder gain). This makes the controller unacceptable.

At the time of design, reasons for the failure of PC6 to damp dutch roll were not self-evident. Moreover, a practical controller was needed in short order to begin the validation experiments. Therefore, all further investigations of PC6 were temporarily set aside and an interim practical controller (PC7) was developed according to the rationale discussed below.

Round Two -- By studying the characteristics of the quadratic optimal controllers and the various practical designs, it became evident that good model-following performance was associated, in all cases, with closed-loop aircraft roots which are far removed from the origin of the complex plane (relative to the model roots) and which are well damped. This fact is illustrated in Figure 59, which shows roots of the optimally-controlled aircraft for the entire flight envelope.<sup>21</sup> The

<sup>20</sup> Recall that the rms errors involve dutch roll plus roll subsidence components only, no spiral.

<sup>21</sup> Not shown are servo, accelerometer, and bending mode roots.



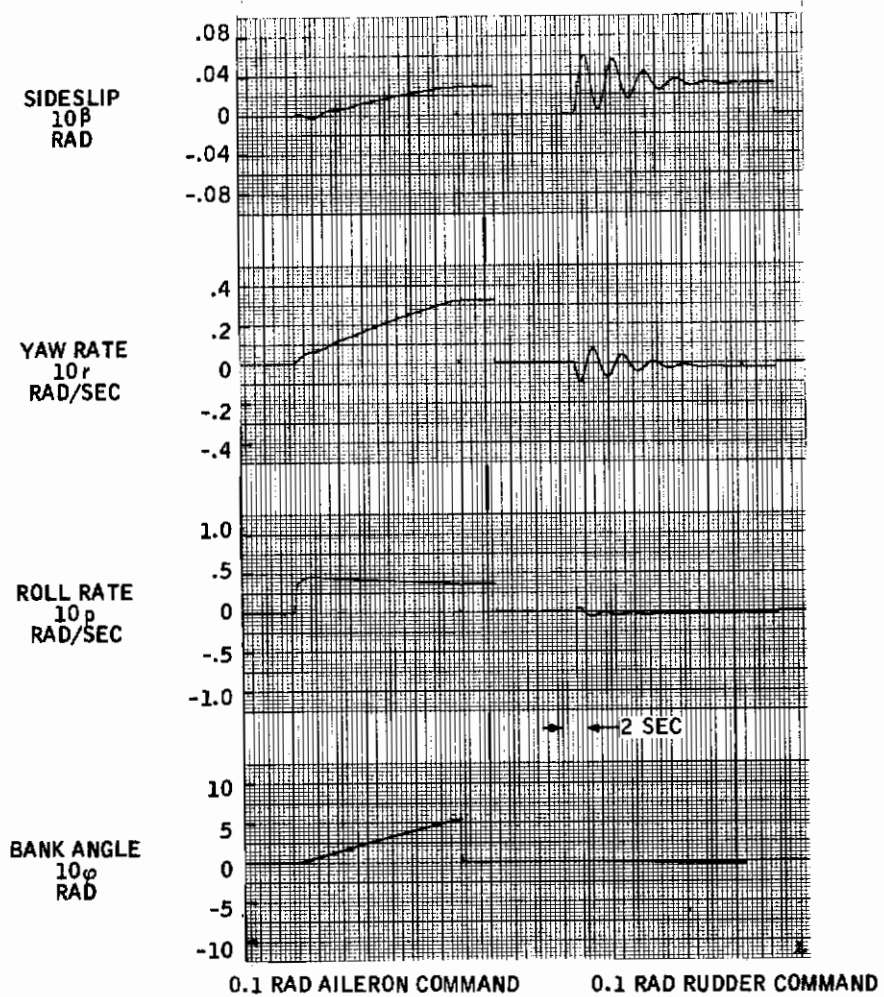


Figure 56. Step Responses -- PC6 at Flight Condition 2, Minneapolis Simulation

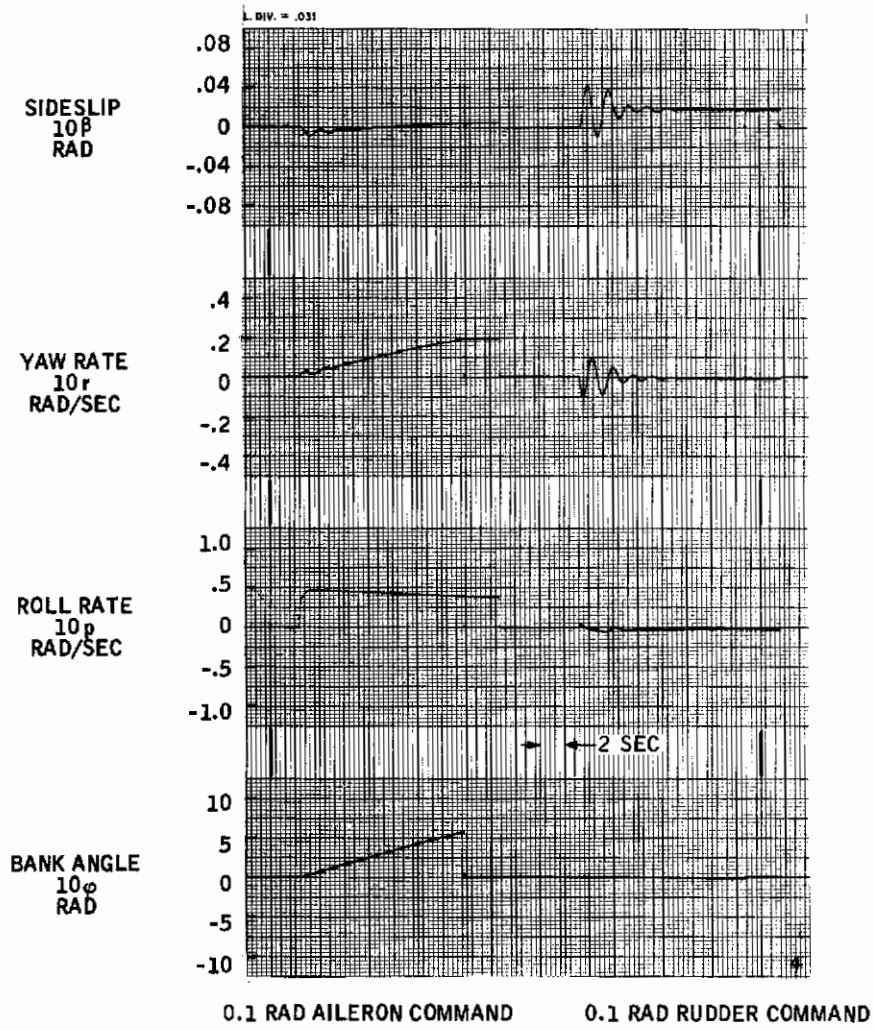


Figure 57. Step Responses -- PC6 at Flight Condition 4, Minneapolis Simulation

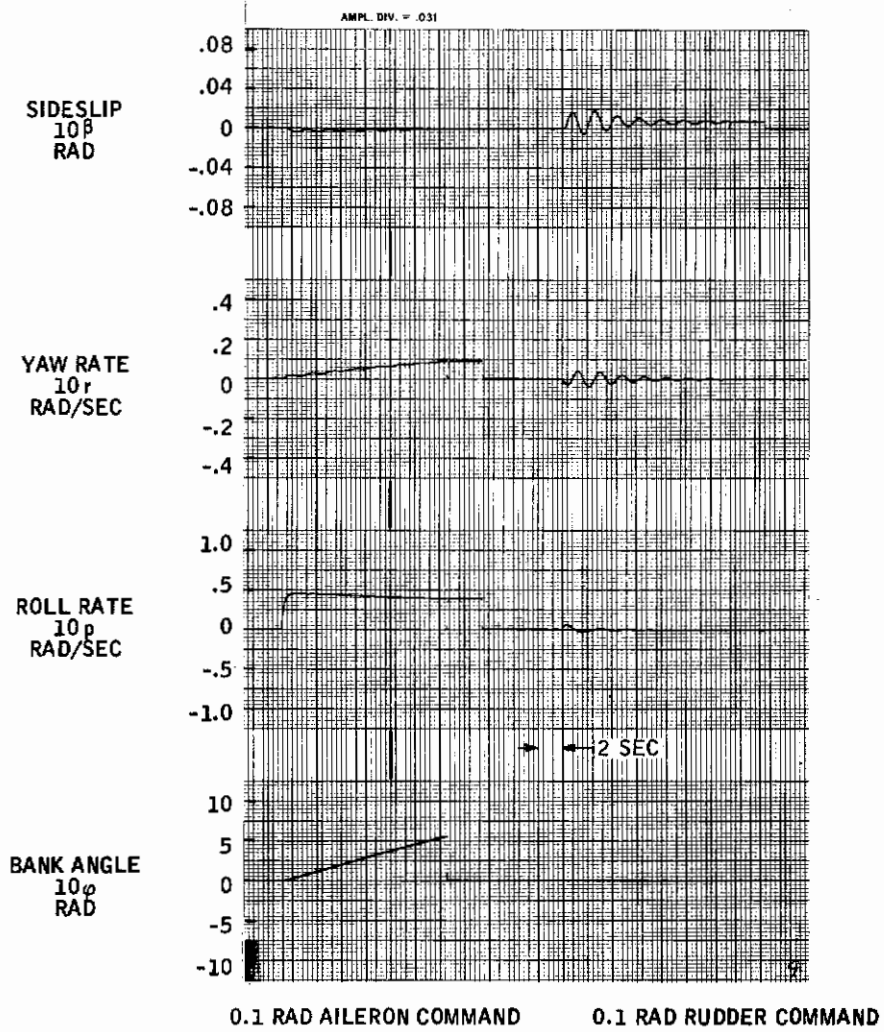


Figure 58. Step Responses -- PC6 at Flight Condition 9, Minneapolis Simulation

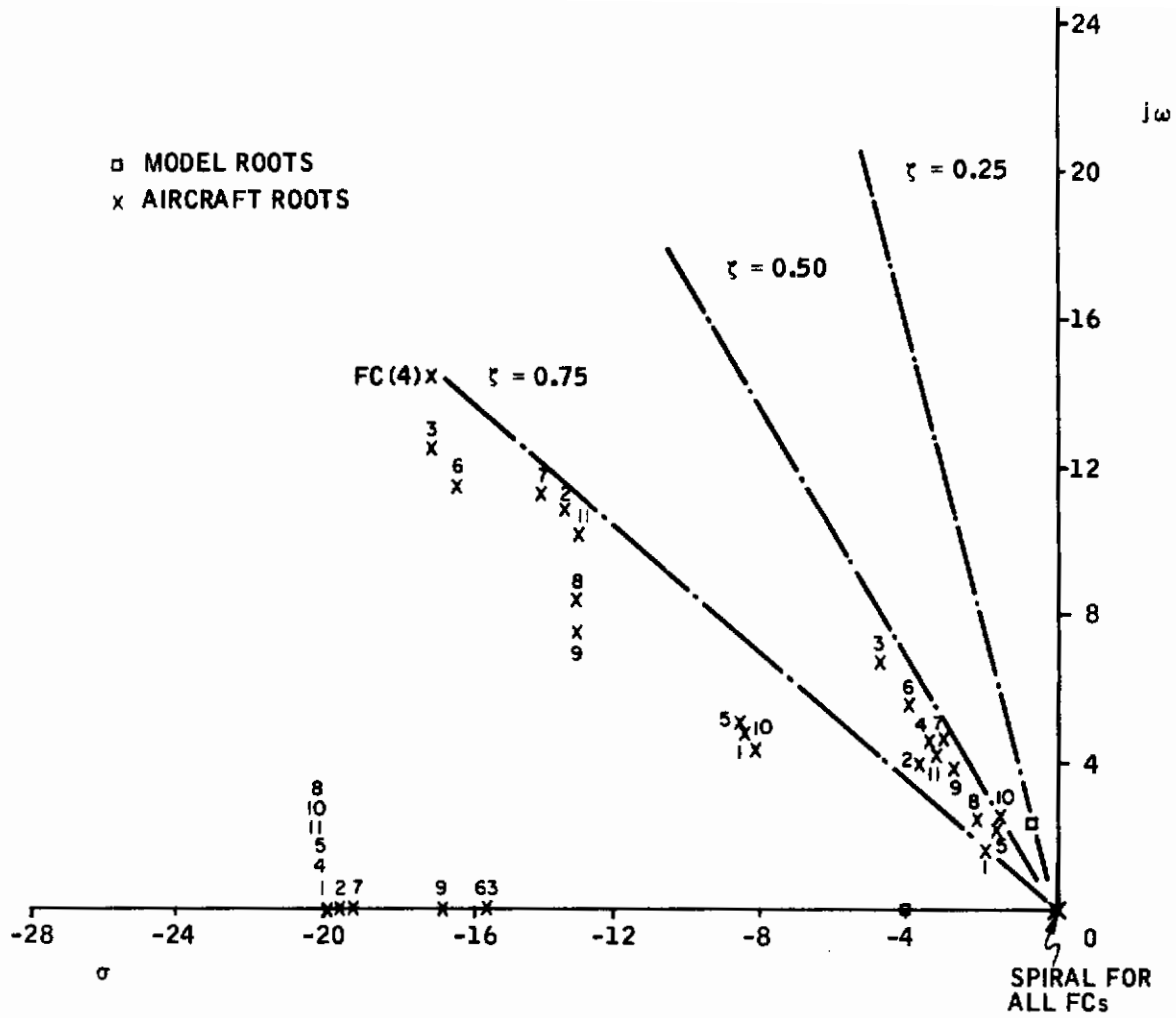


Figure 59. Roots of Optimally-Controlled Aircraft



implication is that exact root locations are not at all critical to model-following performance. Only relative distance is important.

Proceeding on this premise, a set of fixed-feedback gains was determined (using the flight-condition-dependent optimal gains and some trial-and-error) which moves all poles at all flight conditions relatively far into the left-hand plane. The results are shown in Figure 60. They fall short of the quadratic controllers (particularly at low dynamic pressure), but the overall effect is good. These feedback gains were then assigned to the prespecified gain matrix,  $K^3$ , in the computational algorithm, leaving only command and model feed forwards for  $K^1$ . The resulting gain structure is shown in Figure 61a. The algorithm was used as usual to compute the remaining feedforwards  $K^1$ . The same five flight conditions and the same performance index was used. Compared with the previous design, the computations were trivial -- one hour of H-1800 time on a smooth cost surface.

The final gains of PC7 are given in Figure 61b. Its rms performance for all 11 flight conditions is shown on the Mach-altitude plots of Figures 62 and 63, and step response traces are provided in Figures 64 through 74.

The rms performance of PC7 can again be summarized by looking at maximum values of the ratio (rms error with PC7)/(rms error with optimal controllers) over the flight envelope. This gives the data shown in Table XIX.

Table XIX. Maximum Deterioration Ratios, PC7

Command	Roll Rate Error	Yaw Rate Error	Sideslip Error
Rudder	16	3	7
Lateral	2	6	106

Sideslip response to rudder shows clear improvement over PC6, roll rate response to lateral commands is about the same, and the remaining responses are mixed, with sideslip error due to lateral command showing another big increase. (The 106 occurs at flight condition 2. Excluding it, we would get a lesser maximum deterioration of 35-to-1 for flight condition 4.)

The transient responses verify improvements in sideslip due to rudder and show that sideslip due to lateral is reasonable even at the low- $q$  flight conditions (1, 2, and 5), where it is large but nonoscillatory and should be easy to coordinate. Regarding coordination, qualitative evaluation flights with PC7 (Appendix V) have shown that "bottom rudder" (right rudder command on a turn to the right) is required to null lateral

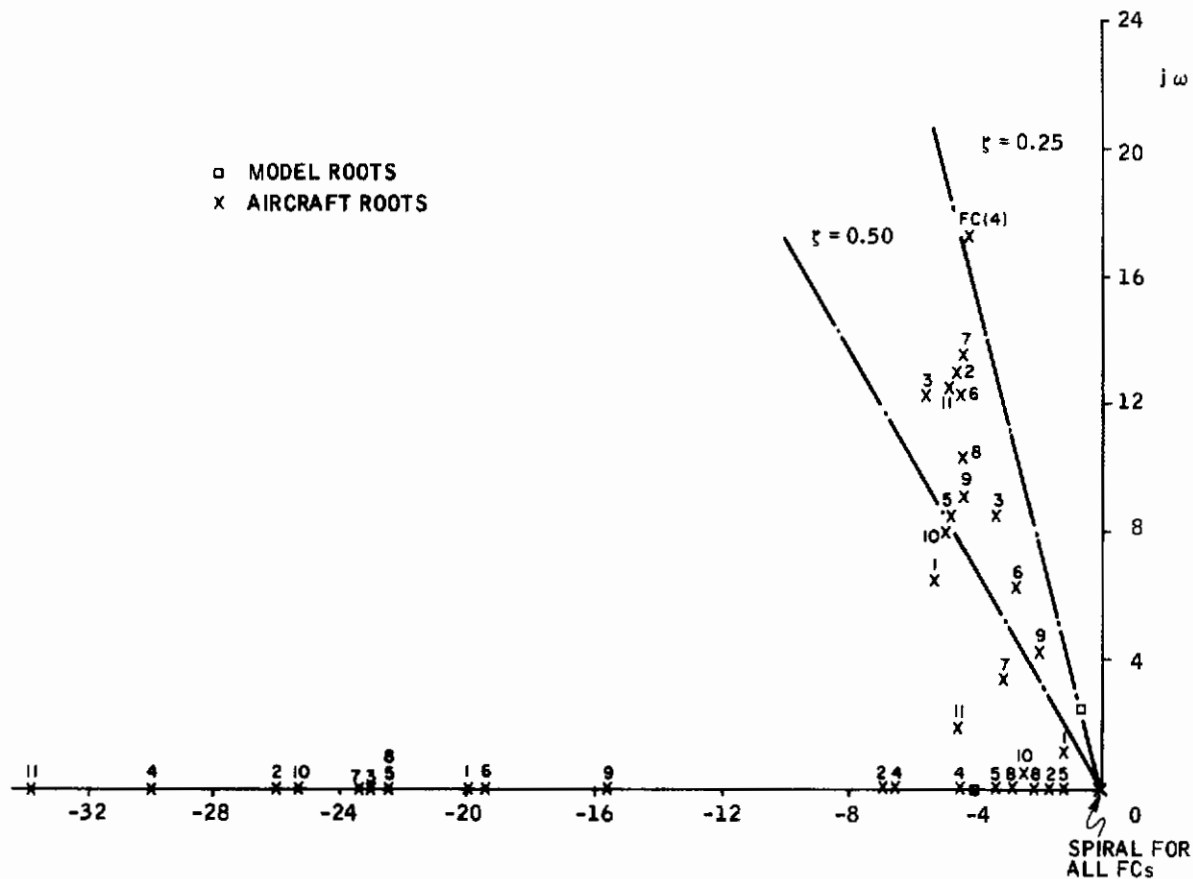


Figure 60. Roots of Practical Controller

	$p_{se}$	$r_{se}$	$a$	$\phi$	$x_m$			$u_m$		
$u_{pR}$	0	3.0	0.03	-0.10	x	x	x	x	0	M
$u_{pAS}$	-2.0	-1.0	-0.03	0.01	x	x	x	0	x	

a) STRUCTURE FOR THE ALGORITHM  
 $(x) = K^1, (\text{NUMERICAL VALUE}) = K^3$

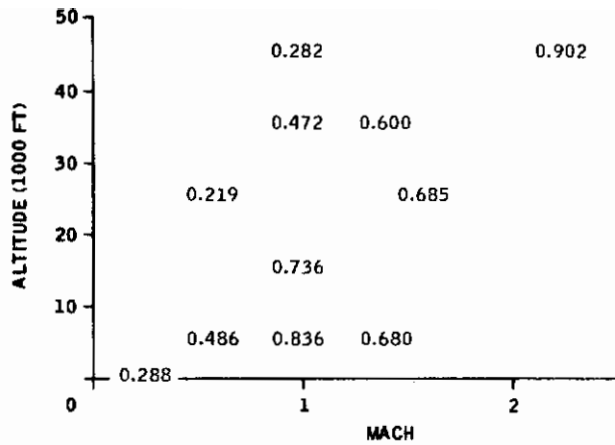
0	3.0	0.03	-0.10	-0.254	-1.80	-1.82	1.53	0	M
-2.0	-1.0	-0.03	0.01	1.75	0.275	1.14	0	1.56	

b) FINAL NUMBERS

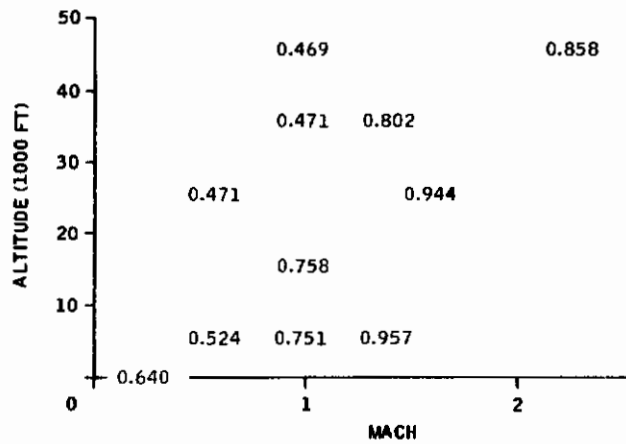
Figure 61. Gain Structure for PC7,  
 $[K^1(\lambda) + K^3] M, \lambda = 0$



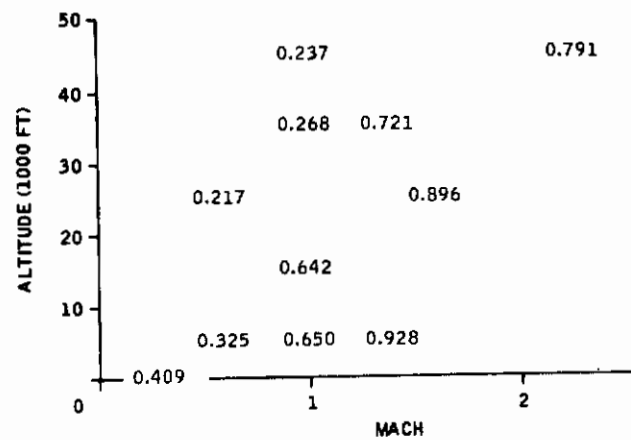
# Contrails



(a) NORMALIZED RMS ROLL RATE ERROR



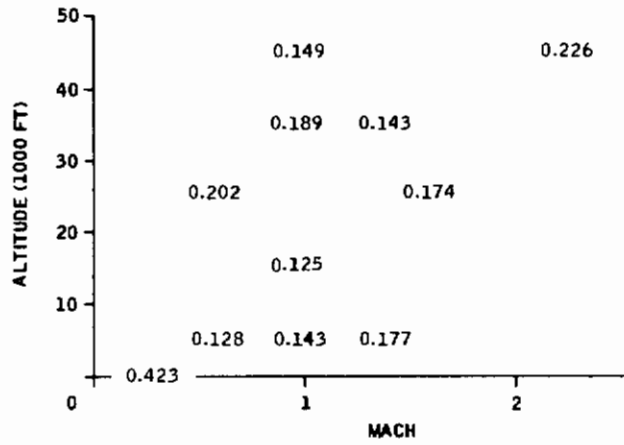
(b) NORMALIZED RMS YAW RATE ERROR



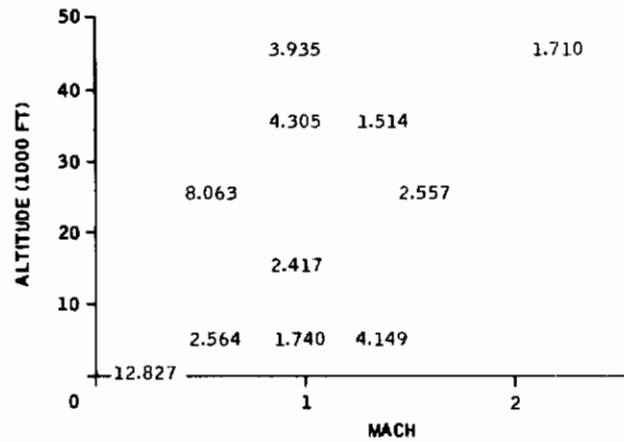
(c) NORMALIZED RMS SIDESLIP ERROR

Figure 62. Performance Sensitivity of PC7  
(0.1-Rad RMS Rudder Command)

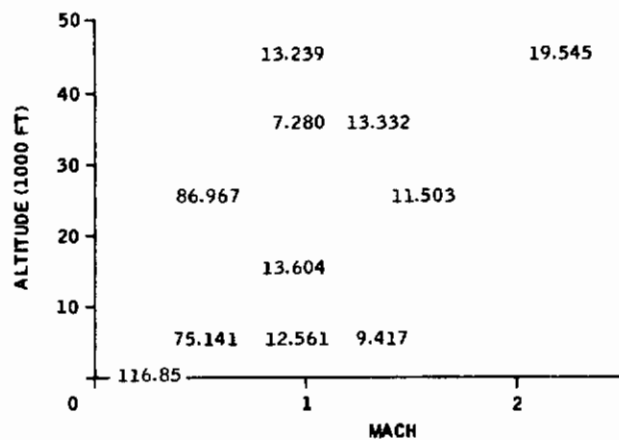
# Contrails



(a) NORMALIZED RMS ROLL RATE ERROR

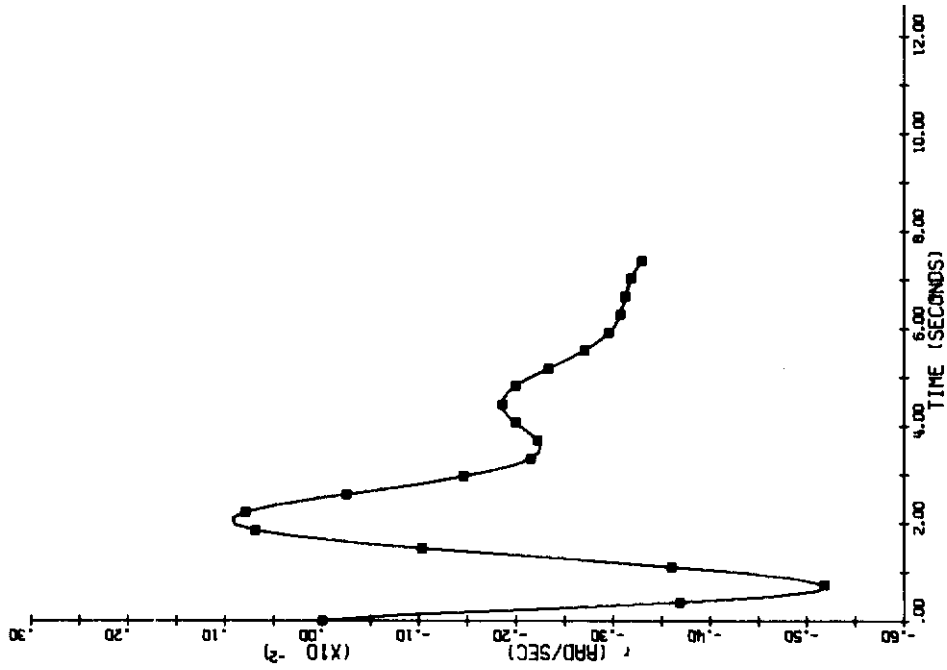


(b) NORMALIZED RMS YAW RATE ERROR

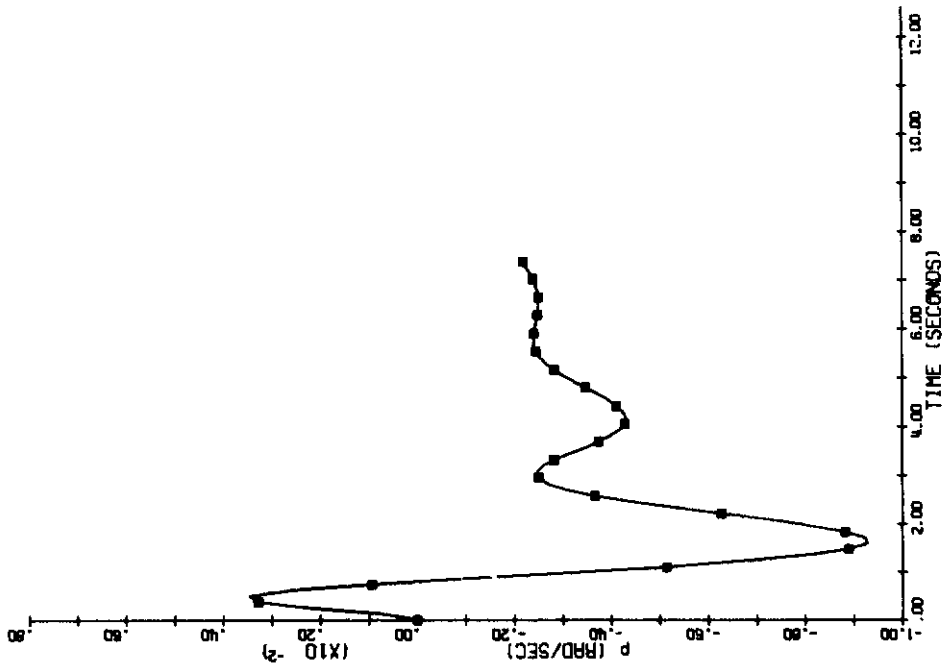


(c) NORMALIZED RMS SIDESLIP ERROR

Figure 63. Performance Sensitivity of PC7  
(0.1-Rad RMS Lateral Command)

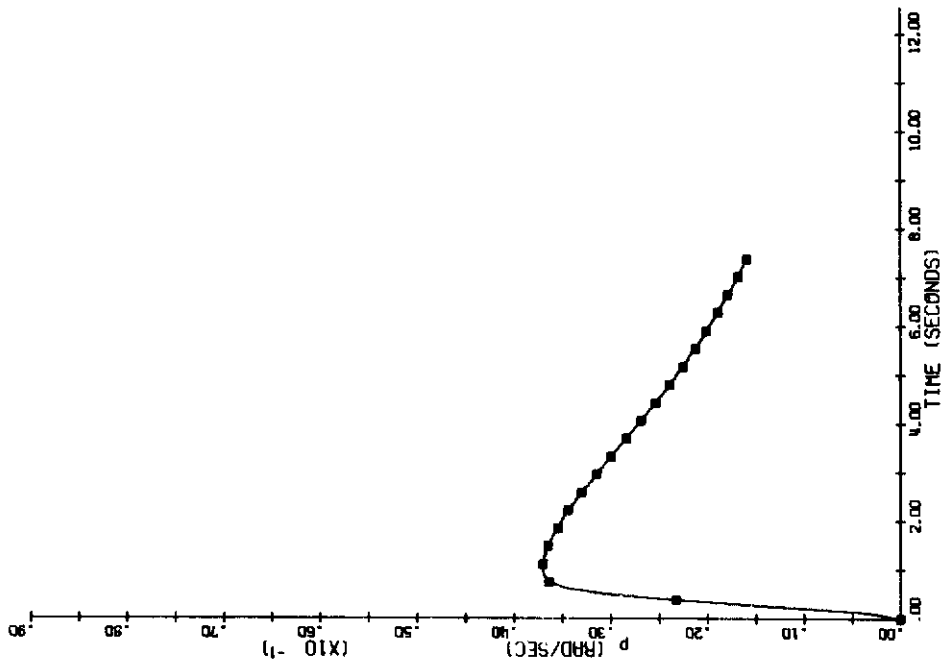


b) Yaw Rate (0.01-Rad Rudder Command)

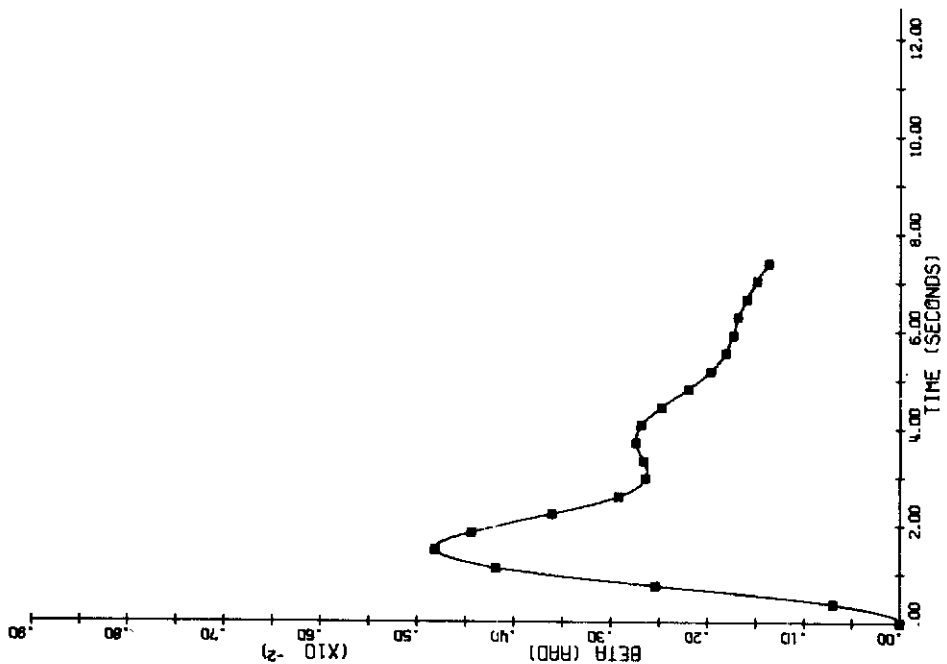


a) Roll Rate (0.01-Rad Rudder Command)

Figure 64. Step Responses -- PC7 at Flight Condition 1

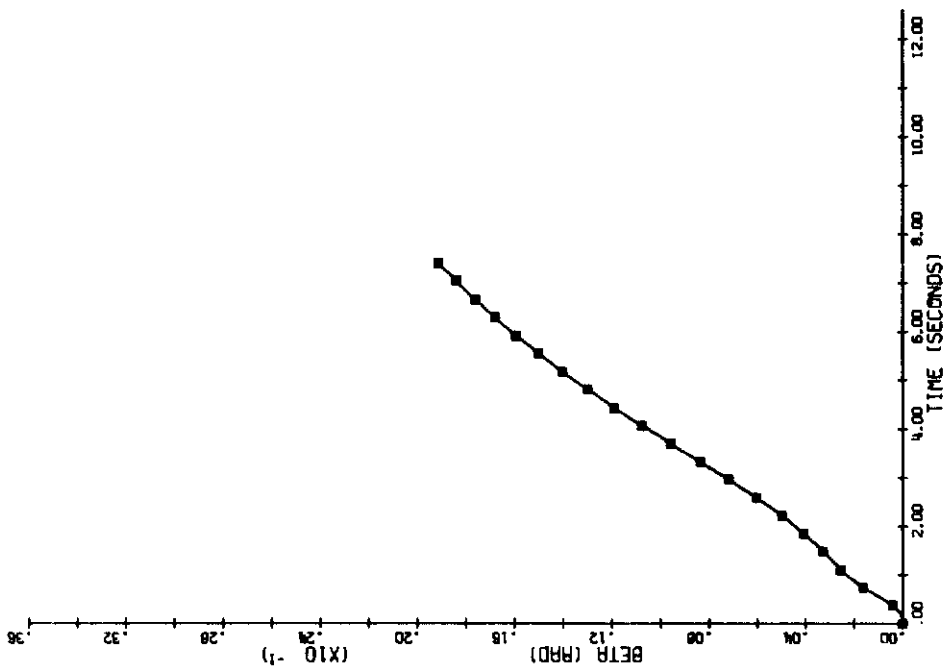


d) Roll Rate (0.01-Rad Lateral Command)

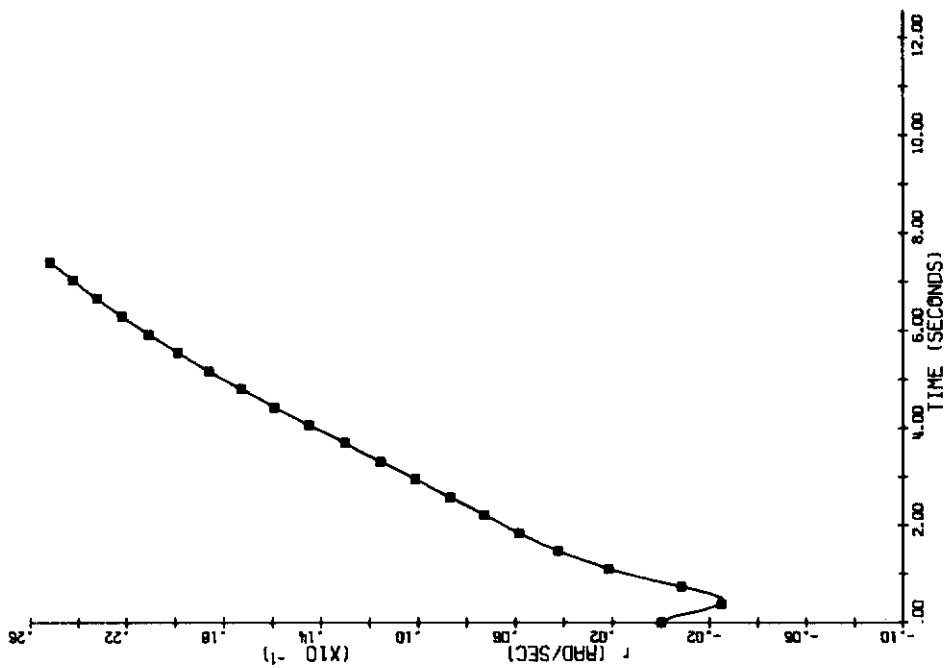


c) Sideslip (0.01-Rad Rudder Command)

Figure 64. Step Responses -- PC7 at Flight Condition 1 (Continued)

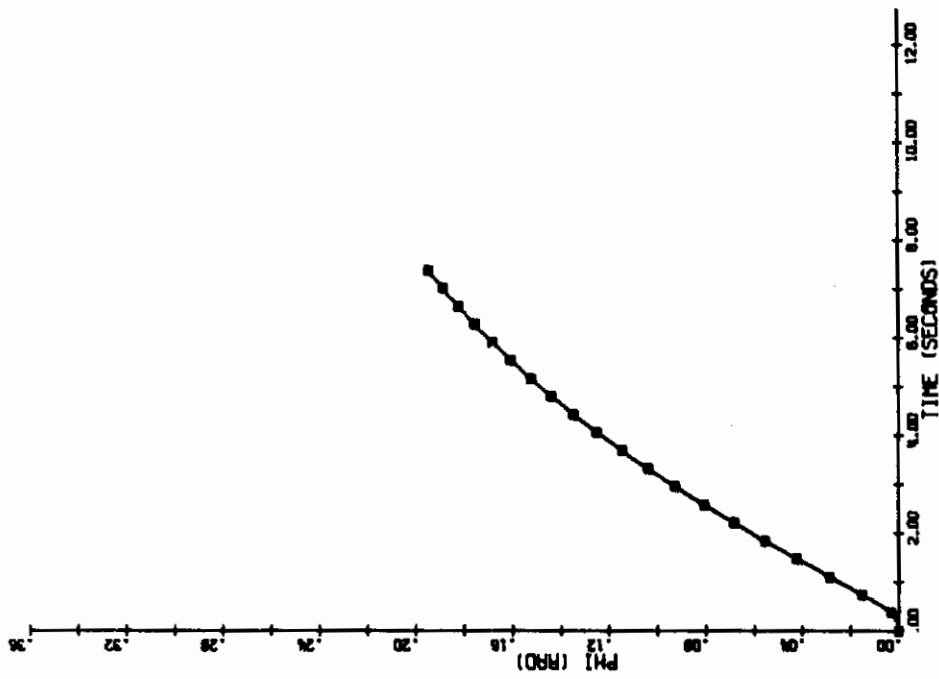


f) Sideslip (0.01-Rad Lateral Command)



e) Yaw Rate (0.01-Rad Lateral Command)

Figure 64. Step Responses -- PC7 at Flight Condition 1 (Continued)



g) Bank Angle (0.01-Rad Lateral Command)

Figure 64. Step Responses -- PC7 at Flight Condition 1 (Concluded)



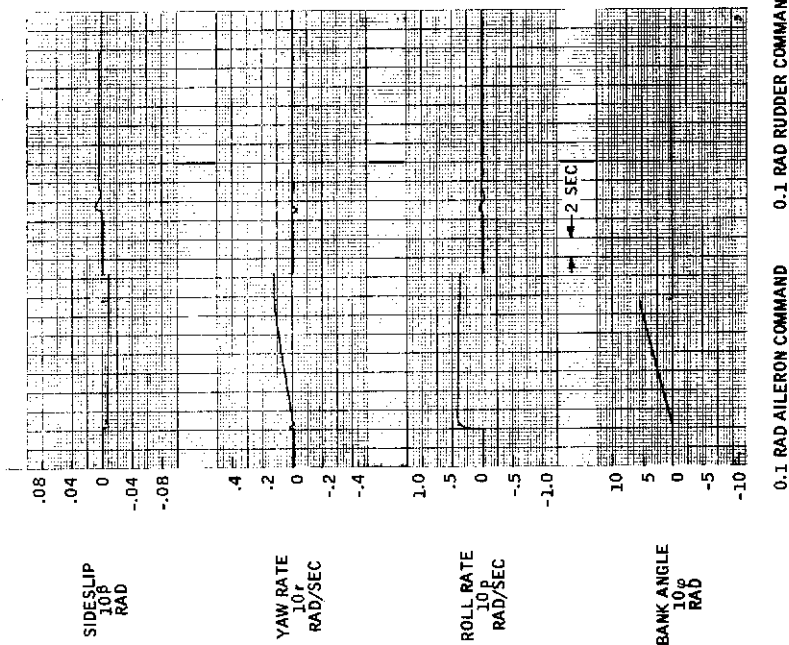


Figure 65. Step Responses -- PC7 at Flight Condition 2, Minneapolis Simulation

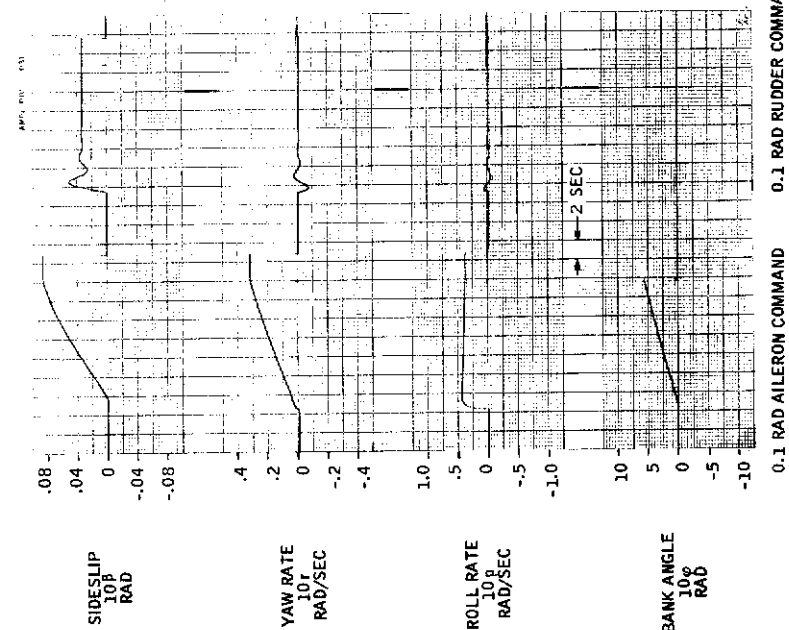


Figure 66. Step Responses -- PC7 at Flight Condition 3, Minneapolis Simulation

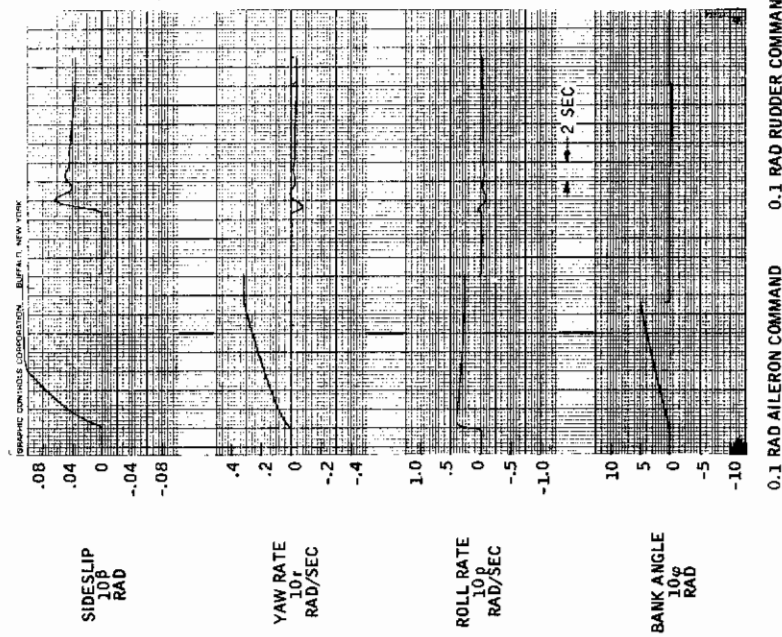


Figure 67. Step Responses -- PC7 at Flight Condition 4, Minneapolis Simulation

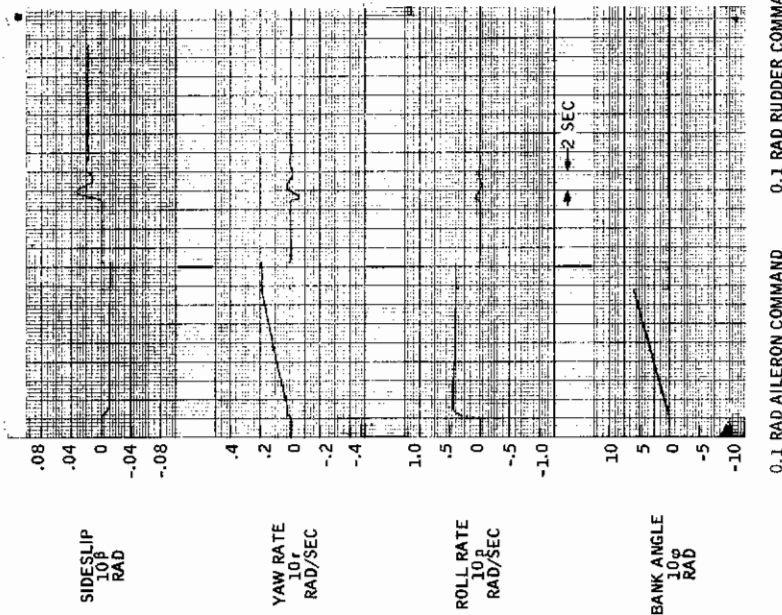


Figure 68. Step Responses -- PC7 at Flight Condition 5, Minneapolis Simulation

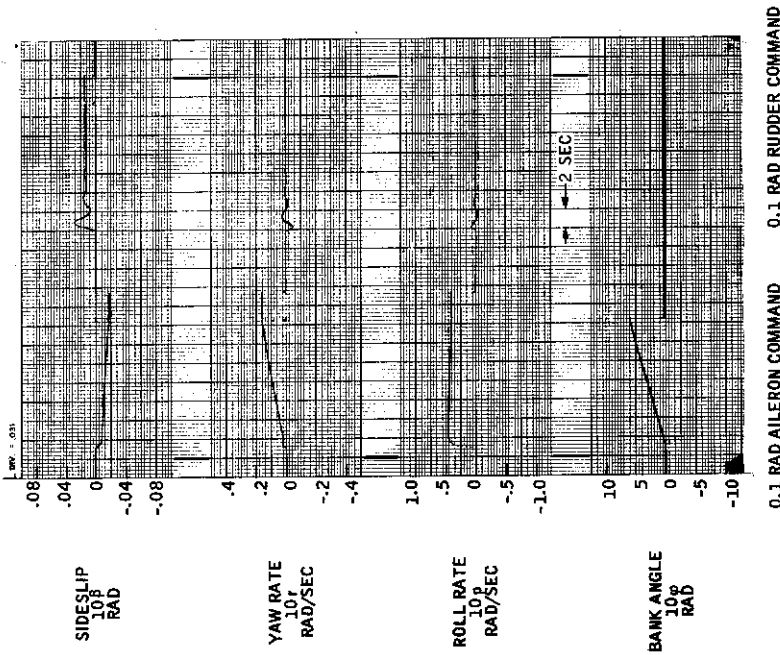


Figure 70. Step Responses -- PC7 at Flight Condition 7, Minneapolis Simulation

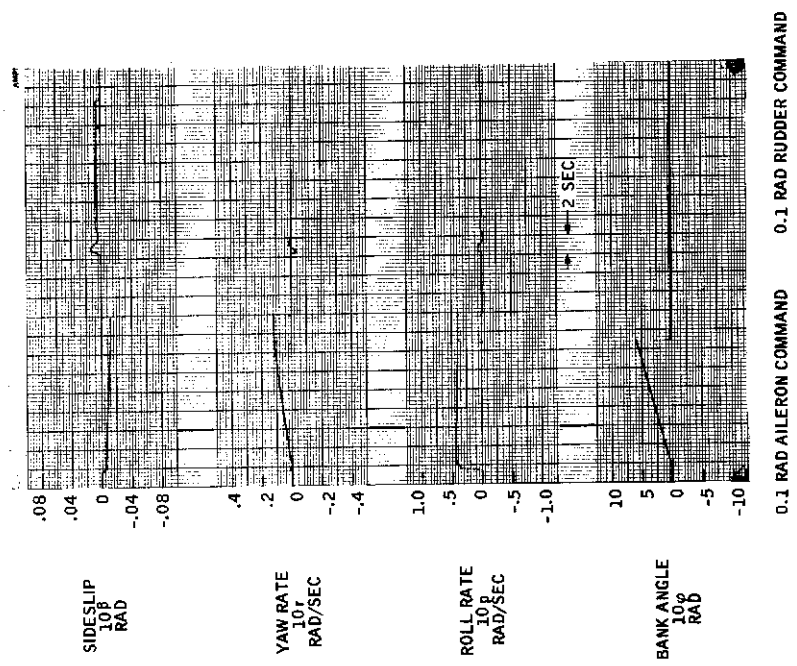


Figure 69. Step Responses -- PC7 at Flight Condition 6, Minneapolis Simulation

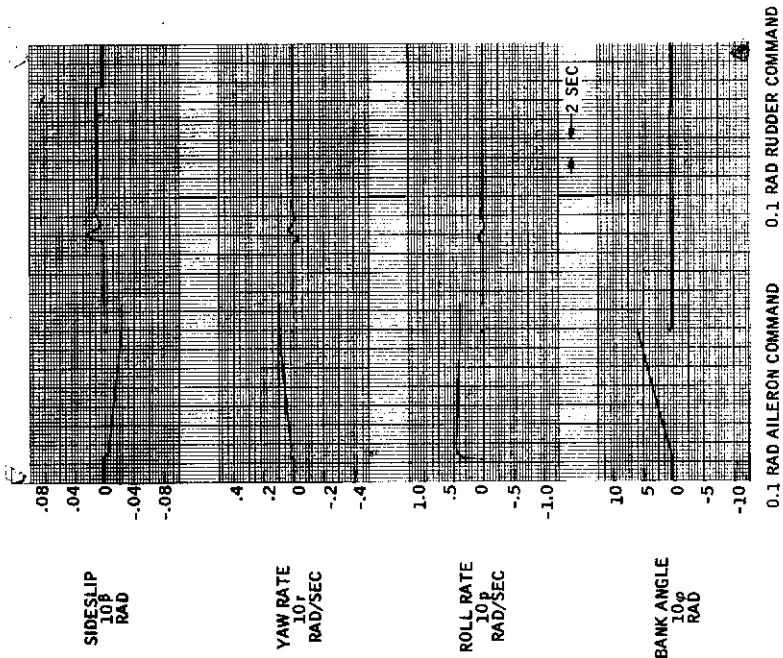


Figure 72. Step Responses -- PC7 at Flight Condition 9, Minneapolis Simulation

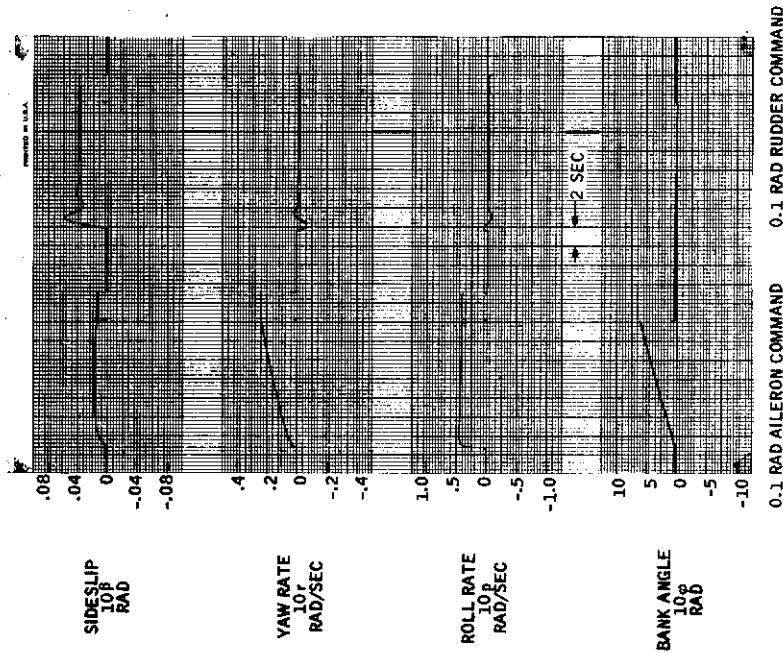


Figure 71. Step Responses -- PC7 at Flight Condition 8, Minneapolis Simulation



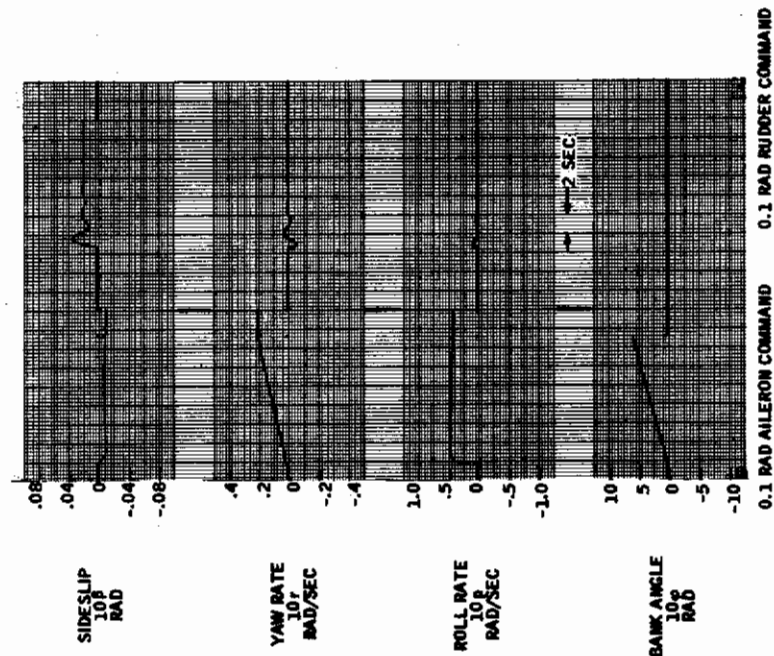


Figure 74. Step Responses -- PC7 at Flight Condition 11. Minneapolis Simulation

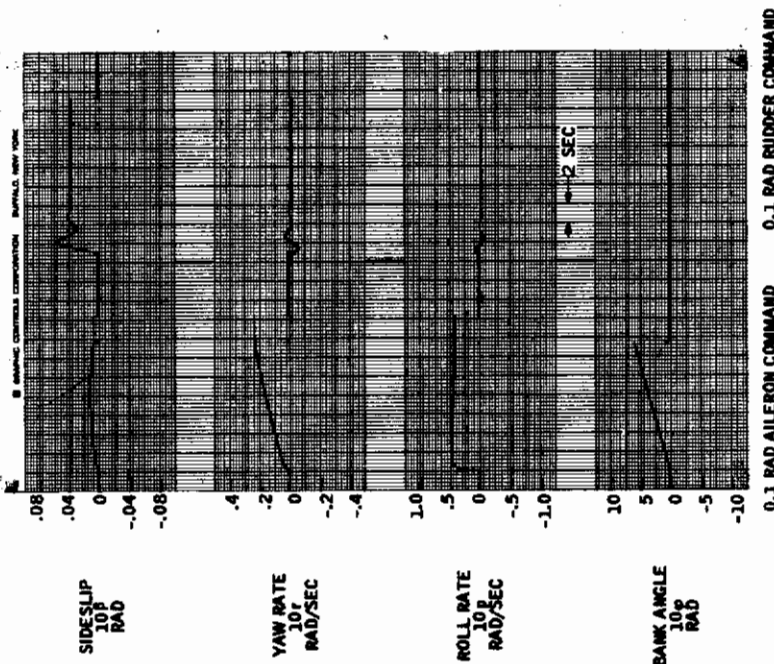


Figure 73. Step Responses -- PC7 at Flight Condition 10, Minneapolis Simulation

acceleration at low dynamic pressure, and "top rudder" (left rudder command on a right turn) is required at high dynamic pressure. This sign reversal corresponds to the sign reversal of sideslip in the step response traces of Figures 64 through 74 (i. e., compare the low-q flight conditions 1, 2, 5, 8, and 10 with the high-q conditions 3, 4, 6, 7, 9, and 11). The reversal is caused by the controller's feedforward terms. These represent a compromise between the large rudder inputs required to coordinate at low-q and small rudder inputs required at high-q. The compromise does too little at one end and too much on the other, so the pilot must compensate. This problem would not exist with a gain-scheduled controller. It has caused no difficulties, however, in our simulation experiments.

The step response traces also show that no adverse yaw problem exists except at power approach, FC(1). There are other difficulties at this flight condition. The controlled aircraft has an overly stable spiral and tends to build up large sideslip angles if not coordinated. More work should therefore be done for power approach. However, because neither the simulation in Minneapolis nor at WPAFB included power approach aerodynamics, the PC7 controller was modified no further and flown in its present form.

Qualitative evaluation flights with PC7 are given in Appendix V, which shows traces for piloted S-turns, hardover-rudder and one-engine-out conditions, and flight in a 6-ft/sec lateral gust environment. Responses of the controlled aircraft with an outer bank angle hold loop, and sample traces from the formal validation trials are also shown.

## Hindsight and Interpretations

Both PC6 and PC7 are legitimate products of the design procedure described in this report, so the fact that one is acceptable while the other is not demands some reconciliation.

On the surface the problem is simple. The optimal cost,  $J$  [Equation (71)], achieved by PC6 and PC7 are  $J_{PC6} = 9.3$  and  $J_{PC7} = 12.6$  (the optimal controllers achieve  $J = 5$ ), yet PC7 is preferred over PC6. So the performance index must not reflect our true notions of goodness. This is not very helpful, especially since it means that performance indices which are perfectly adequate for optimal (full-state feedback) controllers are not adequate for practical (limited-state feedback) controllers. A more detailed answer is needed.

One clue to the details is provided by Tables XVIII and XIX, which contrast the performance deterioration ratios of PC6 and PC7. We see that PC7 essentially trades off sideslip error to lateral commands against sideslip error to rudder commands. That this is a physically meaningful tradeoff is easy to see. In order to get low sideslip errors to rudder commands we must damp the dutch roll, i. e., sensed yaw rate-to-rudder feedback with positive sign. The yaw rate gyro, however, picks up roll rate at high angles of attack (flight conditions 1, 2,



5, 8, and 10). This means that in a rolling maneuver (i. e., response to lateral commands) the rudder will deflect trailing-edge-left for positive rolls and trailing-edge-right for negative rolls, thus building up large sideslip errors. A glance at Figure 63c and at the transient responses shows this effect.

The difficulty, then, is that the optimization problem is structured to reach an unacceptable tradeoff. The tradeoff involves sideslip against sideslip, however, so the problem is not one of improper choice of quadratic weights. Rather, it involves improper choice of command magnitudes. To illustrate this, note that for statistically independent rudder commands, lateral commands, and gusts the cost  $J(i)$  at any flight condition can be written as

$$J(i) = J_{Rud} \sigma_R^2 + J_{Lat} \sigma_{AS}^2 + J_{Gust} \sigma_{v_g}^2 \quad (72)$$

where  $J_{Rud}$ ,  $J_{Lat}$ , and  $J_{Gust}$  can be computed by evaluating  $J(i)$  using rudder only, lateral only, or gust only inputs, respectively. Such a computation is carried out in Table XX for the optimal controller, for PC6, and for PC7, all at flight condition 2. We see that  $J_{Rud}$  dominates for PC6 and  $J_{Lat}$  dominates for PC7. Moreover, in each case the dominating term does so on the strength of the sideslip error component.

Table XX. Breakdown of Quadratic Cost Components for Flight Condition 2

Cost Components	0.1-Rad RMS Lateral Command			0.1-Rad RMS Rudder Command		
	OPT	PC6	PC7	OPT	PC6	PC7
$10E(\tilde{p} - \tilde{p}_m)^2$	0.0112	0.0314	0.0327	0.0002	0.0395	0.0222
$E(\tilde{r} - \tilde{r}_m)^2$	0.0001	0.0015	0.0019	0.0013	0.0195	0.0029
$100E(\tilde{\beta} - \tilde{\beta}_m)^2$	0.0000	0.0130	<u>0.4200</u>	0.0010	<u>0.3150</u>	0.0350
$0.001E(z)^2$	0.0130	0.0144	0.0187	0.0001	0.0001	0.0000
$0.1E(\xi)^2$	0.0000	0.0000	0.0002	0.0000	0.0001	0.0000
$0.01E(\dot{\xi})^2$	0.0005	0.0002	0.0002	0.0000	0.0000	0.0000
$E(u_{pR})^2$	0.0005	0.0008	0.0162	0.0086	0.0095	0.0059
$E(u_{pAS})^2$	0.0290	0.0248	0.0349	0.0032	0.0084	0.0025
Total	0.0543	0.0861	<u>0.5249</u>	0.0144	<u>0.3921</u>	0.0685
		$J_{Lat}$			$J_{Rud}$	

# Contrails

This means that the sideslip error tradeoff can be effectively controlled by adjusting command variances during design --  $\sigma_R^2$  should be increased when  $J_{Rud}$  becomes too large and, conversely,  $\sigma_{AS}^2$  should be increased when  $J_{Lat}$  becomes too large. Unfortunately, the optimal solution provides little help in determining values for the variances. For it, the values of  $J_{Rud}$ ,  $J_{Lat}$ , and  $J_{Gust}$  are all individually minimized. (Optimal controllers are optimal for any combination of  $\sigma_R^2$ ,  $\sigma_{AS}^2$ ,  $\sigma_{v_g}^2$ .) So

the tradeoff must be controlled by carrying out several practical controller solutions iteratively, or perhaps by extending the algorithm of Section III to permit adjustments of command variances (and/or quadratic weights) as lambda integrates toward zero and the nature of the tradeoff evolves. This is a fruitful area of further research.

## SECTION V VALIDATION METHOD

The design criteria of Section II and the controllers developed in Sections III and IV were validated with a formal program of piloted experiments. The rationale for these validations, the experimental design, procedures, and equipment setup are discussed in this section. The investigation was initially conducted at Honeywell-Minneapolis and later completely replicated at WPAFB. The procedure description contains a general discussion of both simulations, and unique aspects of each are highlighted. Specific details of the experimental procedure can be found in Appendixes VI through XI.

### INTRODUCTION

The objectives of the experimental program were threefold:

- 1) To validate handling-quality design criteria used in the design phase of the program
- 2) To evaluate the resulting practical lateral-directional control system using pilot performance measurement and rating scale values
- 3) To cross-validate pilot opinion measures with performance measures.

A basic premise underlying the validation program is that neither rating data nor performance data alone can provide adequate evaluations of the "quality" of a controller/vehicle configuration. Simply stated, pilot ratings tell us how a pilot feels about flying a system, while performance data tell us how well he can satisfy mission requirements with the system. Both pieces of information are important for evaluation. It is reasonable to expect, of course, that the two measures are interrelated. It is the intent of the third objective to explore this relationship and to add to its data base. Accordingly, the validation program was designed to collect both kinds of data in a form which can be statistically analyzed and interpreted.

### THE EXPERIMENTAL DESIGN

A 2 x 5 x 3 mixed-design analysis of variance (Ref. 24) was used to combine factorially five systems and two flight conditions (see Figure 75). Three pilot subjects performed under each of the resulting 10 experimental conditions.

# Contrails

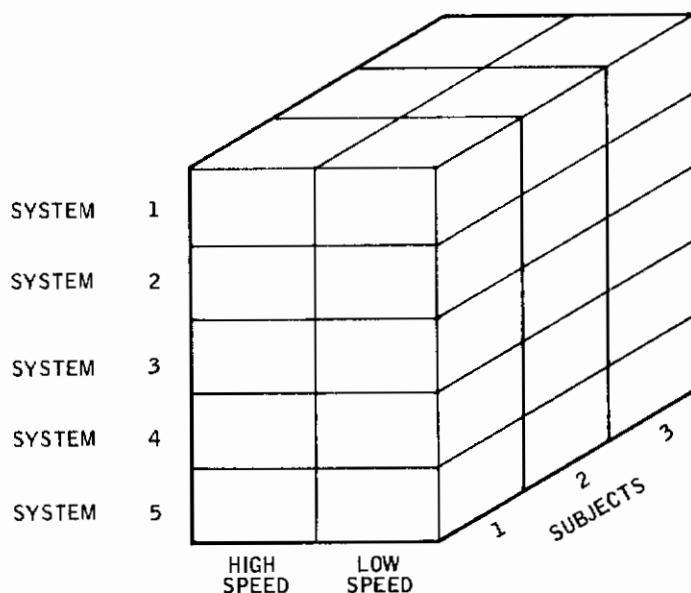


Figure 75. Experimental Design

In the case of performance data, 10 trials were flown in each cell, where a trial was defined as a single flight profile three minutes long. The order of presentation of conditions was randomized to minimize order effects across subjects. The randomization procedure for both the WPAFB and Minneapolis simulations is described in Appendix VII.

In the case of pilot rating data, only two trials were flown in each cell, and the definition of a trial was altered somewhat, as discussed under "Validation Procedure" later in this section.

## Independent Variables

The following fixed variables were of interest: (1) system type, and (2) flight condition.

Five different systems were evaluated, each consisting of an F4C aircraft with a particular lateral-directional controller. The controller for systems 1, 2, 3 and 4 was a quadratic-optimal, flight-condition-dependent, model-following controller designed to follow handling-quality models 1, 2, 3, and 4, respectively. As developed in Section II, these models are predicted to exhibit an ascending order of handling-quality "goodness." That is, model 1 has poor predicted handling qualities; model 2 is predicted to be fair; model 3 is predicted to be good; and model 4 is predicted to be excellent. It was anticipated that systems 1,

2, 3, and 4 would exhibit a consonant ranking, and, in fact, if they did, the design criteria would be validated (the first validation objective).

The controller of system 5 was a practical model-following controller (PC7 of Section IV) which was designed to follow handling-quality model 4 but involved only practical feedback signals and fixed gains. We did not predict a performance or rating measurement for this system. However, since the four optimal systems were selected along a continuum of "goodness," the data of this experiment would locate the practical system along the same continuum and thus serve to evaluate the practical controller (the second validation objective).

Identical pitch-axis controllers were used for each system.

The second independent variable was flight condition. The nature of the validation and the piloting task itself required that we sample as broad a range of flight conditions as possible. It should be noted, however, that the factorial character of the experimental design significantly increases the number of observations for any single addition of levels of independent variables. Accordingly, only two flight conditions -- low-speed (Mach 0.5; 328 kt) and high-speed (Mach 1.2; 787 kt) -- were selected as representative points of the speed range of the F4 vehicle.

This combination of five systems and two flight conditions formed the fixed-variable design of the study. The three subjects were treated as random variables.

## Dependent Variables

For each performance data trial, the following variables were recorded on magnetic tape, at the rate of three sample points per second:

- 1) Altitude error ( $E_h$ )
  - 2) Velocity error ( $E_v$ )
  - 3) Lateral error ( $E_y$ )
  - 4) Bank angle ( $\phi$ )
  - 5) Sideslip ( $\beta$ )
  - 6) Pilot aileron stick command ( $\delta_{PAS}$ )
  - 7) Pilot rudder command ( $\delta_{PR}$ )
- } See discussion on task, below.

Several summary scores were also computed on-line and displayed to the experimenter at the end of each trial. These scores were:

1) Single-axis rms errors:

$$a) \quad \bar{E}_h = \sqrt{\frac{1}{N} \sum_{i=1}^N E_h^2(t_i)}$$

$$b) \quad \bar{E}_v = \sqrt{\frac{1}{N} \sum_{i=1}^N E_v^2(t_i)}$$

$$c) \quad \bar{E}_y = \sqrt{\frac{1}{N} \sum_{i=1}^N E_y^2(t_i)}$$

where N is the total number of samples for each trial (N ≈ 540).

2) Multiaxis rms errors:

$$a) \quad \text{Three-axis error} = \sqrt{\bar{E}_h^2 + \bar{E}_v^2 + \bar{E}_y^2}$$

$$b) \quad \text{Two-axis error} = \sqrt{\bar{E}_h^2 + \bar{E}_y^2}$$

For pilot rating trials, the following measures were taken immediately after each trial:

- 1) Cooper-Harper Ratings (Reference 39)
- 2) Global Ratings (Reference 40)

Voice recordings of pilot comments were collected for all rating and performance trials.

Both performance data and rating data were formally analyzed to evaluate the independent variables. Conclusions reached and numbers obtained were compared to cross-validate the two types of data (the third validation objective).



## THE TASK

The task was selected on the basis of specific critical requirements:

- 1) New learning or interference from prior learning was kept to a minimum.
- 2) The task included the use of full cockpit instrumentation and controls.
- 3) The task provided a structure for controlling intrasubject variability; i. e., all subjects perceived, understood, and performed the task in a similar manner and were subject to the same experimental controls.

The task chosen consisted of a series of 20 flight profiles. Ten profiles were generated for each flight condition. The profiles consisted of twelve 15-second intervals during which constant bank angle turns or wings-level flight were commanded. On the average, six intervals of any profile were wings-level flight. The commanded bank angles ranged from 5 to 15 deg in 2.5-deg steps. The detailed procedure used to generate the profiles is contained in Appendix VI, along with a listing of the high-speed and low-speed profiles used during the experiment.

All profiles were initiated at 2000 feet mean sea level and required a 2000-fpm climb to approximately 8000 feet mean sea level. The atmosphere was assumed to be standard ICAO. The climb rate was chosen to ensure that all instruments and appropriate controls would be used by the pilot. The trial was initiated with a 2000-fpm climb rate.

Figure 76 is a pictorial representation of a typical flight profile. The aircraft simulation at Minneapolis was subjected to random side gusts with 6-ft/sec rms magnitudes and spectral content satisfying MIL-F-8785. A series of experimenter errors contributed to a lack of gusts in the WPAFB simulation.

The primary display of the flight path course to the pilot was the flight director. The glide slope portion of the display (pitch command bar) was used to display deviations from the commanded 2000-fpm climb, while the localizer portion of the display (lateral command bar) was used to display deviations from the commanded course centerline. The perceptual motor task for the pilot was simply to detect any deviations from pitch and lateral command bar center and to make appropriate corrections to keep the needles centered. Flight path error equations (discussed in Appendix VI) associated with the profile generator were used to drive the pitch and lateral error displays.

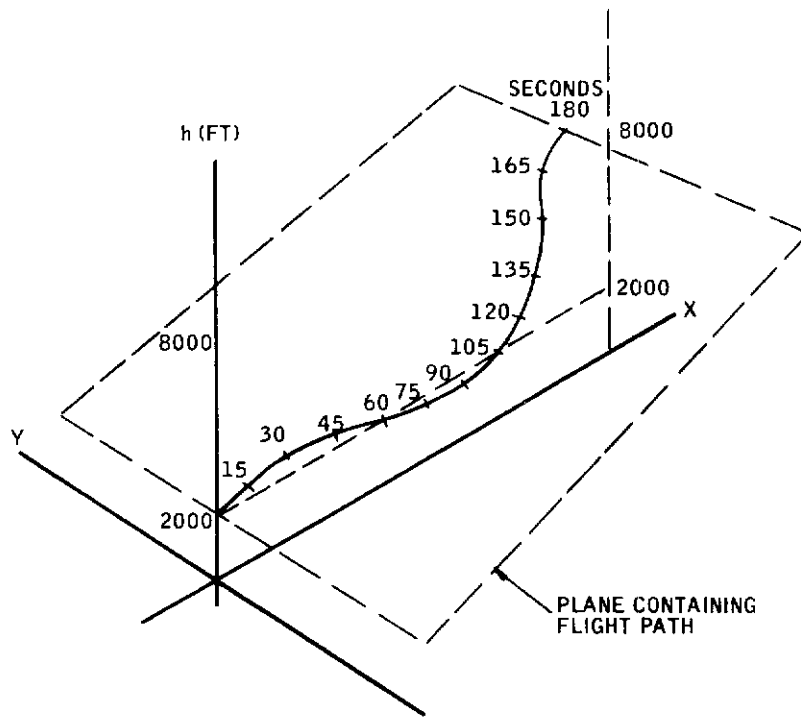


Figure 76. Typical Flight Profile

## SUBJECTS

The qualifications and experience of the subject participants are listed in Table XXI. Subject D. S. performed at both facilities.

Table XXI. Subject Data for Pilots Who Participated in Performance Data Sessions

Location	Subject Initials	Service	Age	Highest Military Rank	IFR Hours	Total Hours	Aircraft Type
Minneapolis	R. P.	Navy	29	Lt. /USN	496	1276	A4, SM3A, T34, T28, TM13M, H34, F9
	D. S.	USAF	38	Major	340	3200	RF101, F86, T33, U3
	T. H.	Navy	28	Lt. /USN	165	1407	T34, T2A, TF9J, F4B
WPAFB	W. S. <sup>a</sup>	USAF	36	Major	2080	3160	T34, F100, T38, T33, B57, F86, F102
	R. K. <sup>a</sup>	USAF	35	Major	980	2947	T37, T34, T33, F100, F105, F104, F4, T39, T38, KC135

<sup>a</sup>Graduates of Air Force Test Pilot School at Edwards AFB, California

The two Navy pilots who participated in the Minneapolis simulation were both employed by Northwest Orient Airlines based in the Twin Cities. Subject D. S. is employed by Honeywell Inc. Subjects W. S. and R. K. are current jet-rated pilots and are on active duty with the Air Force.

Four additional Air Force pilots stationed at WPAFB participated in the validations. They did not participate in Phase I of the experiment (see "Validation Procedure" later in this section), but received 20 training trials and rated the systems according to the procedure of Phase II. Their experience and qualifications are listed in Table XXII. In later analyses, these subjects will be treated as a separate group, since the experimental procedures and controls do not fully apply.

Table XXII. Subject Data for Pilots who Rated Models at WPAFB

Subject Initials	Service	Age	Highest Military Rank	IFR Hours	Total Hours	Aircraft Type
J. S.	USAF	35	Major	695	4250	T33, F4, F8, F86, F102, T39
R. E. *	USAF	34	Major	915	2705	F4, F100, F102, F104, T38, T37, T33
T. H.	USAF	40	Lt. Col.	700	4150	T39, F4, F101, F102, F86
D. Z. *	USAF	32	Captain	365	2450	F105, F100, F4, KC135, T39, F104, T33, T39, H13

\*Graduates of Air Force Test Pilot School at Edwards AFB, California.

Every attempt was made to schedule one data session per day per subject to reduce the effects of fatigue and boredom. However, scheduling difficulties and technical problems resulted in some subjects participating in two data sessions in one day. No subject flew more than two sessions in one day and on these occasions the subject was given a minimum of two hours rest between sessions.

## SIMULATION EQUIPMENT

The simulation arrangement for WPAFB and Minneapolis is described in the following paragraphs. It should be pointed out that a number of differences existed between the two simulations, most notably the old nemesis - fixed (Minneapolis) versus moving-base (WPAFB). However,

the data collection methods, experimental procedures and controls, and the experimental design were, for all practical purposes, comparable. So, although we could not pool data from the two simulations, we did not anticipate major differences in the conclusions drawn from each.

The equipment description will be covered by facility. Figures 77 and 80 should be compared for a broad overview of the differences.

## The WPAFB Simulation

For the experiments at Wright-Patterson Air Force Base, the simulation used was the Air Force Flight Dynamics Laboratory (AFFDL) moving-base simulator. The AFFDL hybrid simulation was implemented on an EAI 8400 digital computer with associated A/D, D/A link and four PACE 231-R analog computers. The analog and digital computing equipment was located in Building 192. The moving-base cockpit simulator, and motion and instrument drive equipment were located in adjacent Building 195. Communication between the two buildings was provided by means of voice intercom and closed-circuit TV directed at the instrument panel.

Figure 77 is a block diagram of the simulation. The airframe equations of motion were provided by AFFDL as part of their overall F4 simulation. Nonlinear aerodynamics were simulated with analog nonlinear equipment, and various angular relationships such as  $\alpha$  and  $\beta$  were generated by analog resolvers. Position and altitude computations were performed digitally. Honeywell supplied digital simulations of the lateral controllers, of rudder, aileron and spoiler actuator dynamics, and of the navigation error display drives. The simulator cockpit was a modified T37 arrangement with all "flying" being performed from the left seat. Figure 78 shows a photograph of the cockpit and an instrument layout.

Flight instruments consisted of an airspeed indicator, a Mach meter, an altimeter, a sideslip indicator, a rate-of-climb indicator, an angle-of-attack meter, a flight director, and a horizontal situation indicator. Engine rpm was also displayed. Navigation errors were displayed on the lateral and pitch command needles of the flight director (Lear Siegler, Model No. 4058E). Figure 79 illustrates this display. The pitch needle was driven directly by  $E_h$ , with  $\pm 4000$  feet full-scale sensitivity, while the lateral needle was driven by  $c_1 \tan^{-1}(c_2 E_y)$ . The constants  $c_1$  and  $c_2$  were selected to match the pitch needle sensitivity near  $E_y = 0$  and to saturate the lateral display when  $\tan^{-1}(-)$  reaches  $\pi/2$ . This eliminates display saturation for all finite errors. (For a 100-volt instrument,  $c_1 = 63.7$  and  $c_2 = 0.0004$ .)

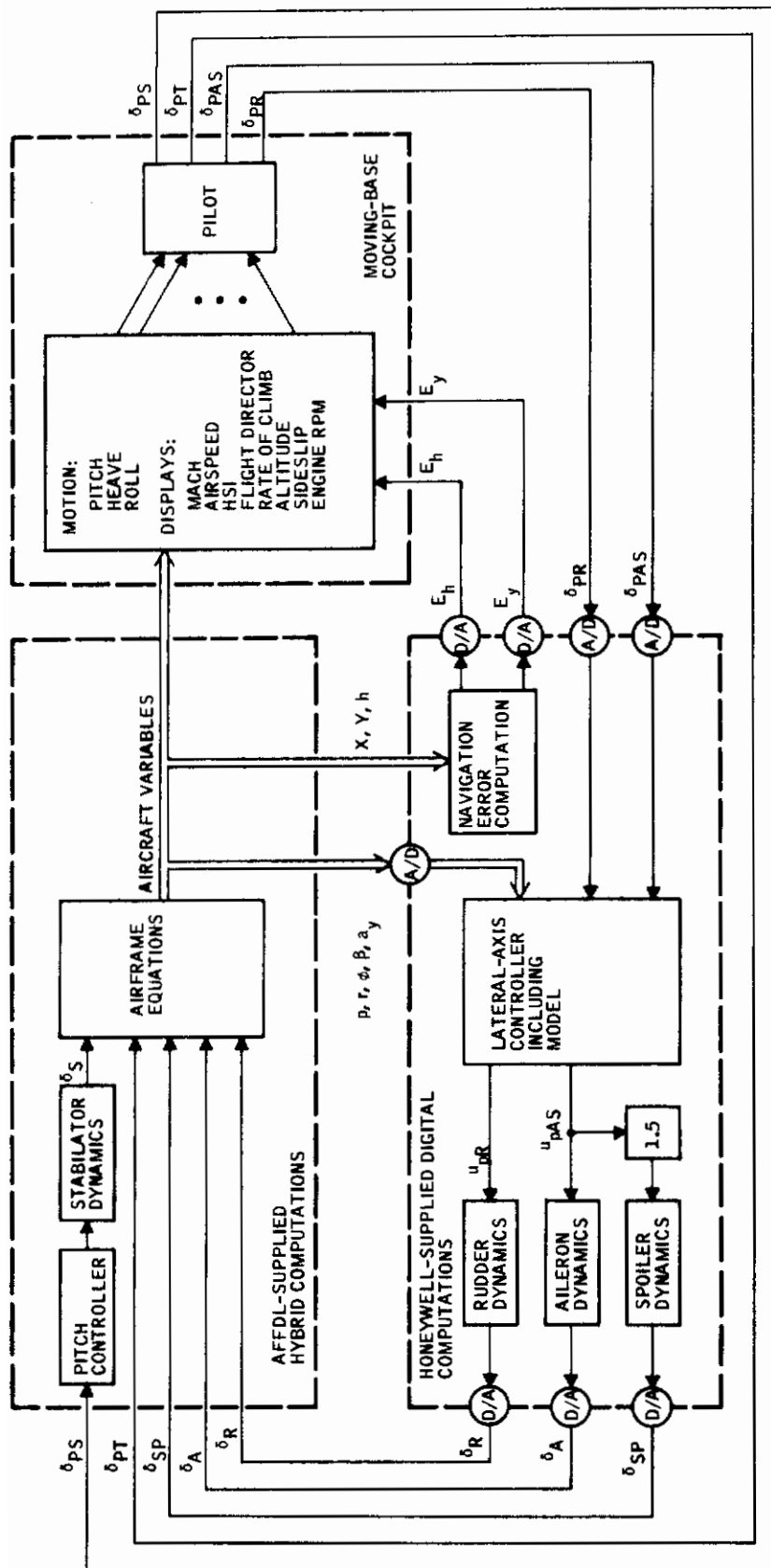


Figure 77. WPAFB Simulation Block Diagram



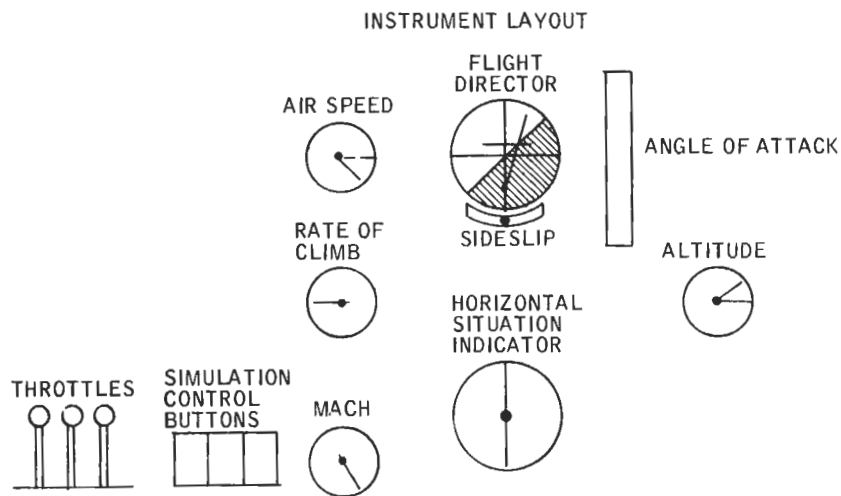


Figure 78. Cockpit of AFFDL Moving-Base Simulator



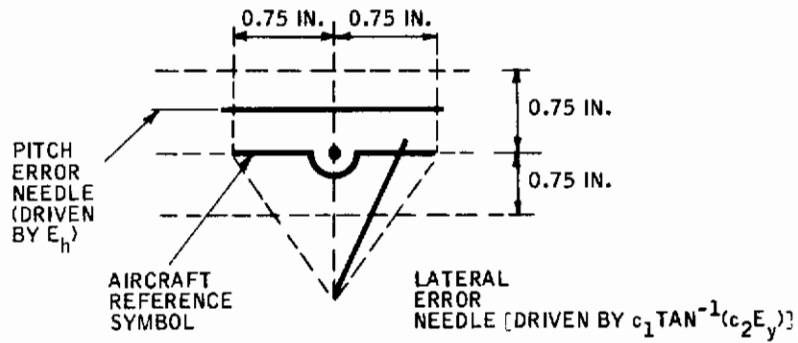


Figure 79. Navigation Error Display, WPAFB

Table XXIII. Cockpit Control Summary -- WPAFB Simulation

Cockpit Control	Max. Deflection		Sensitivity	
	Inches	Lb	Lb/Inch	Effective Gain
Pitch stick				
Fore	7.5	34	5.0 <sup>b</sup>	
Aft	7.5	37		
Roll stick				
Left	9.25 <sup>a</sup>	20	1.4 <sup>b</sup>	19 $\frac{p(\text{deg}/\text{sec})}{\text{inch}}$
Right	6.5 <sup>a</sup>	20		
Rudder	±3.5	±36	~ 10	6.2 $\frac{\beta(\text{deg})}{\text{inch}}$

<sup>a</sup>Limited by position of pilot's legs.

<sup>b</sup>Force/displacement, evaluated at 5-lb force.

Cockpit controls included stick, rudder pedals, and two throttles. No asymmetric thrust was simulated, however, so the throttles commanded a single engine. There was also a third lever on the throttle quadrant to enable the afterburners. Cockpit control force gradients and excursions are listed in Table XXIII. Effective stick and rudder gains (deg/sec roll rate per inch and deg sideslip per inch, respectively) were selected by pilot/subject D. S. and remained constant throughout the experiment. These gains were invariant with flight condition (see Section IV). Effective pitch gains were also set by pilot D. S., but varied with flight condition. The stick in the simulator had no noticeable breakout forces in either roll or pitch.

The cockpit motion system provided limited three-degree-of-freedom motion in pitch, roll, and heave. Motion limits were  $\pm 7.5$  deg pitch attitude,  $\pm 19$  deg roll attitude, and  $\pm 5$  inches in heave.

Overall pilot comment on the AFFDL simulation was complimentary. The subject who had "flown" both the AFFDL and Minneapolis simulators noted that they were similar and that both were satisfactory for the task. The Air Force subjects who "flew" the AFFDL simulator remarked that it was quite realistic for the task.

Transient response traces of the WPAFB simulation are shown in Appendix VII.

Figures 130 through 139 of Appendix VII show the lateral transient responses of the free aircraft for flight conditions 2 through 11. These responses were obtained on the WPAFB simulation using 1.5-deg lateral and rudder step forcing functions. The roll rate trace for flight condition 11 (Figure 139) is missing due to a recorder malfunction. However, the information contained in the traces of the other states in this figure is sufficient to validate the simulation for this flight condition.

Figures 140 through 149 of Appendix VII show the lateral transient response of the controlled aircraft at WPAFB for flight conditions 2 and 3 with models 1 through 4 and their optimal controllers, as well as model 4 with the practical controller.

## Minneapolis Simulation

The Honeywell simulation at Minneapolis was implemented on a 40K memory, SDS Sigma-5 digital computer with associated A/D and D/A links, and a PACE 231-R-5 analog computer. The fixed-base cockpit simulator was located in an area adjacent to, but not physically visible from, the computer control console. The test director at the computer

control console maintained communication with the pilot subject in the cockpit through a voice intercom.

Figure 80 is a block diagram of the Minneapolis simulation. All computations, including the equations of motion, were digital. The analog computer was used to buffer the D/A converted signals to the cockpit and strip recorder and also to buffer and null bias the stick, pedal, and throttle inputs from the cockpit.

The aerodynamics and the airframe equations of motion used, with certain modifications, were standard nonlinear six-degree-of-freedom equations and are described, except for the modifications, in Technical Report AFFDL-TR-70-48 (Ref. 34). The principal modifications were:

- 1) Replacement of the pitch aerodynamic moment equation by a constant-gain model which made the pitch axis appear as if it were being controlled by a  $C^*$  controller (Ref. 41).
- 2) Modification of the lift equations by deleting spoiler, aileron and stabilator terms. Since the total lift contribution of these terms is very small relative to other terms of the lift equation, and since the generation of these terms required a disproportionate amount of computer time, they were removed.

The simulation's lateral control systems, rudder, aileron and spoiler dynamics, and navigation error display drives were identical to those used in the WPAFB simulation. In addition, the Minneapolis simulation included a digital lateral wind gust generator which was operative throughout the experimental program at Minneapolis. This gust routine was inadvertently deactivated at WPAFB.

The Minneapolis cockpit simulator is shown in Figure 81 together with its instrument layout. Flight instruments consisted of tape-type air-speed indicator/Machmeter, angle-of-attack indicator, altimeter, vertical velocity indicator, and engine rpm indicators, as well as rate-of-turn indicator, lateral acceleration (needle and ball), flight director, and horizontal situation indicator. Navigation errors were again displayed on the lateral and longitudinal error needles of the flight director (Astronautics, Part No. 109931-508). This display differs somewhat from the corresponding WPAFB display, as shown in Figure 82. Sensitivities matched WPAFB values.

Cockpit controls included stick, rudder pedals, and two throttles. The throttles controlled two independent engines, each simulated by a thrust buildup time constant of 5 seconds. This provides asymmetric thrust capability which was used for one-engine-out demonstrative flights with the practical control system (Appendix V). Cockpit control force gradients and excursions are presented in Table XXIV. Effective gains were again set by pilot/subject D. S.

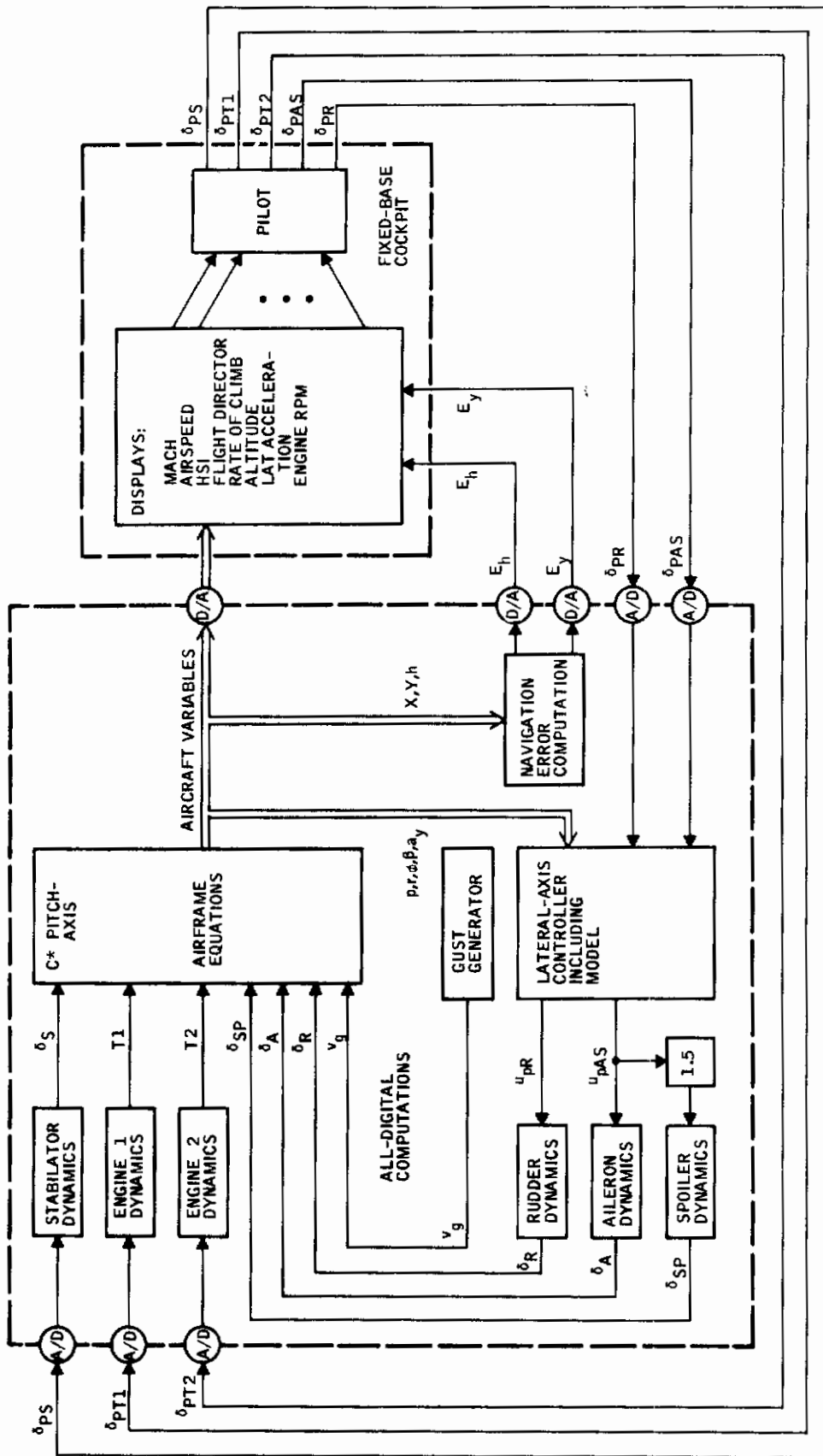


Figure 80. Minneapolis Simulation Block Diagram

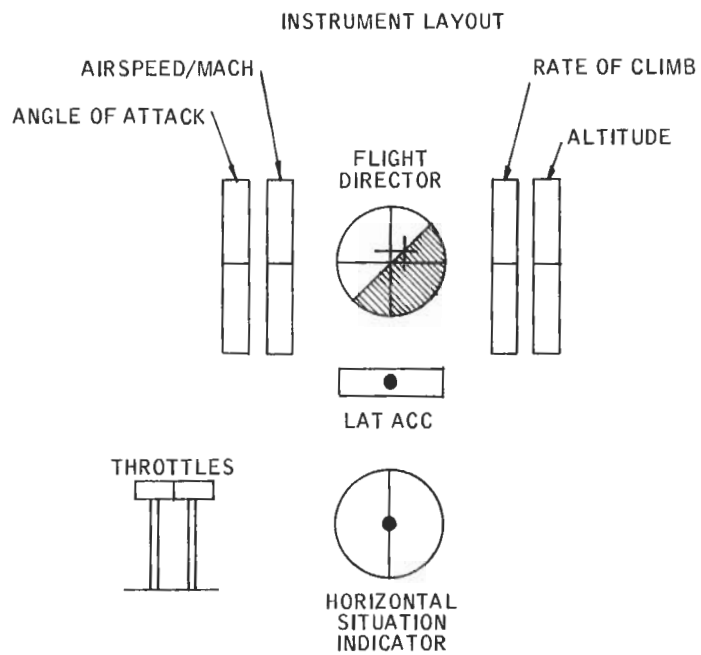
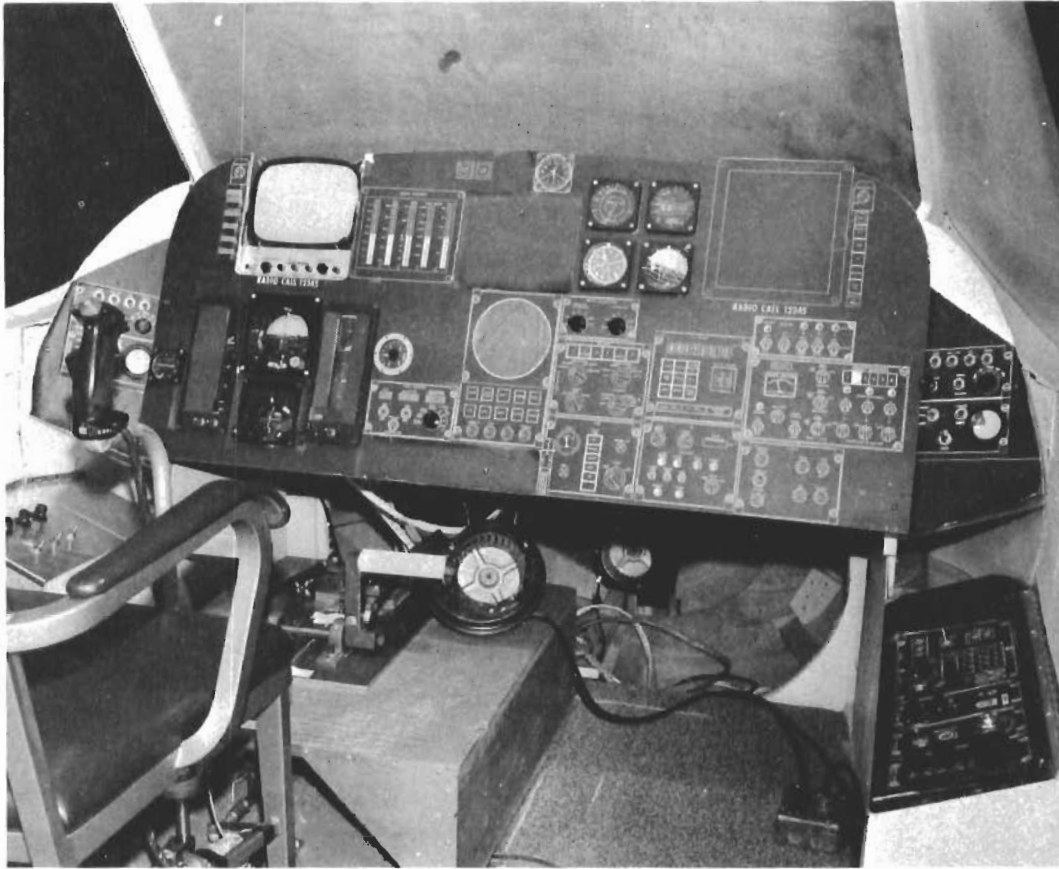


Figure 81. Cockpit of Minneapolis Simulator



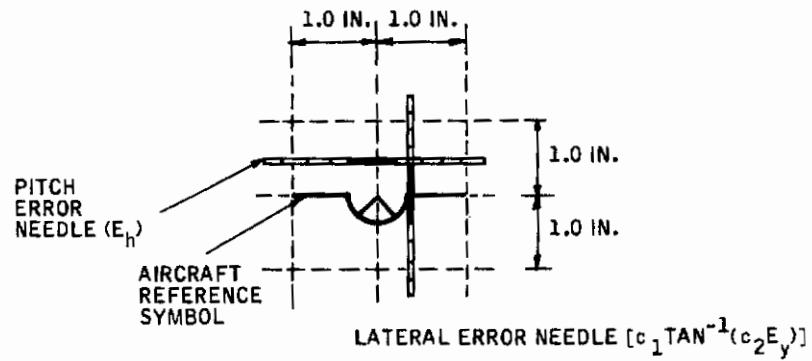


Figure 82. Navigation Error Display

Table XXIV. Cockpit Control Summary --  
Minneapolis Simulation

Cockpit Control	Max. Deflection		Sensitivity	
	Inches	Lb	Lb/Inch	Effective Gain
Pitch stick				
Fore	6.0	10	≈1.7	
Aft	5.0	9		
Roll stick				
Left	6.0	6	1.4 <sup>a</sup>	27 $\frac{p(\text{deg/sec})}{\text{inch}}$
Right	6.5	5		
Rudder pedals	±3.5	±100	≈29	2.6 $\frac{\beta(\text{deg})}{\text{inch}}$

<sup>a</sup>Force/displacement, evaluated at 3.5-lb force.



A two-pound breakout in both pitch and roll was simulated. This compares favorably with the 1.7-pound pitch, 2.33-pound roll breakout forces of the F4 (Ref. 33).

Overall pilot comment on the Minneapolis simulation was that it was "more than adequate." The subject who flew both the Minneapolis and the AFFDL simulations remarked that they were similar from a pilot's viewpoint and that both "felt all right." Another of the Minneapolis subjects stated that the simulation "flew like an A4." The third Minneapolis subject stated that the stick was too sensitive for flight condition 2 but that flight condition 3 felt right. This is based on considerable flight time in the F4 aircraft by the third Minneapolis subject.

Transient responses of the Minneapolis simulation are again given in Appendix VII. Figures 150 through 159 of Appendix VII show the lateral transient responses of the free aircraft for flight conditions 2 through 11. These traces correlate very well with the traces of the design equations described in Section IV. (In contrast to the nonlinear aerodynamic data used for the simulation, the design equations were derived from linear aerodynamic data for fixed-flight conditions.)

Figures 160 and 161 of Appendix VII are traces of the pitch transient response of the free aircraft at Minneapolis for flight conditions 2 and 3. Lateral transient responses for the controlled aircraft at each flight condition are contained in Section IV.

## VALIDATION PROCEDURE

Since experimental conditions were completely randomized by subject/condition, it was not possible to collect pilot rating data during the collection of pilot performance data without unnecessarily interrupting the performance data collection. Therefore, to maintain the integrity of the experimental design, the experiment was divided into two complete phases plus a familiarization phase. Phase I consisted of measuring pilot performance under the restrictions of the 2 x 5 x 3 experimental design, and Phase II consisted of pilot rating measurements under the same experimental design.

Phase II followed the completion of Phase I data collection.

### Familiarization

Each pilot/subject was briefed on the purpose and background of the study effort. No attempt was made to withhold any information about the experiment. The subjects were urged to ask questions at any time during the briefing or during the practice sessions which followed. The simulation system and hardware was explained in detail. Sketches were made of typical flight profiles and the navigation task was clearly defined.

The subjects were taken to the simulation cockpit and the experimenter explained the task once again. The experimenter then flew a practice trial which the subject watched. Following the demonstration, the subject was allowed to begin the practice sessions.

The practice sessions were handled in a similar manner as the formal data sessions; i. e., the trial content, sequences, and instructions were the same. Each subject was given 20 three-minute trials. The trial sequence was random, with the only restriction being that all combinations of models and flight conditions were flown twice during the 20 practice trials. The training sequences for each subject are contained in Appendix X. Throughout the practice sessions, the subjects received immediate feedback about their performance errors and were allowed to inspect their final records at the end of the session. Particularly close attention was paid to the subject's performance during the training phase to ensure that the subjects maintained a high-performance level and did not become "sloppy" on any parameter while controlling direction and altitude. All subjects were cautioned repeatedly to avoid trading altitude errors for lateral errors on the more difficult systems. They were advised that nothing had been done to the pitch axis and therefore they should be able to control the pitch axis with a high degree of accuracy.

## Phase I - Performance Data Collection

All subjects were required to participate in five formal data sessions. Each data session consisted of 20 three-minute data trials lasting approximately 1.5 hours. The total time per session included a constant 30-second intertrial interval and a five-minute break following 10 trials.

A single trial within the 20-trial sequence was identified by a unique combination of profile type, system, and gust sequence. These combinations were placed in a random sequence for a particular data session such that each system was flown twice during the data session. No data session was arranged in the same way as any other data session although all data sessions contained two trials for each system. The data sequences for each subject are contained in Appendix XI.

Communication with the subject was kept to a minimum throughout the study. However, if necessary, the subject was provided with feedback on his performance if he requested it or if his performance began to deteriorate in an unpredictable manner. For the most part, we attempted not to identify the particular system number as it was being flown. If the subject specifically asked which system he was flying at the time, we told him. However, he was never told which system he was going to fly prior to the start of the trial. In most cases he was informed by the experimenter of the trial number and whether the flight condition

was high or low speed. The subject was also provided information about the next flight conditions from the IAS display. The nominal air-speed (Mach 1.2 or 0.5) for the next trial was displayed to him as the instruments were set prior to the start of the trial.

## Phase II - Rating Scale Collection

The purpose of Phase II was to gather pilot opinion data. Two rating scales were used -- the Cooper-Harper scale and the Global scale.

Each subject was briefed on the purpose of the rating scales and the procedure for collecting these data. Briefly, the subjects were told that the procedure and task would be the same as in Phase I, except that the intertrial interval would be longer to give them time to fill out the forms. They were asked to rate the system in question immediately after they had flown it. As in Phase I, the subjects were presented with a random sequence of 20 trials containing two trials for each of the 10 experimental conditions. They rated each system/flight condition as it was flown. This allowed us to gather two observations on each combination, thus providing a measure of the scale's reliability. The two scale forms are contained in Appendix XII.

All rating trials were flown using only two flight profiles -- Profile No. 8 for high-speed trials and Profile No. 11 for low-speed (see Appendix VI).

## Minneapolis/WPAFB Procedural Differences

Minor procedural differences existed at WPAFB and Minneapolis. These primarily affected the lengths of trial sequences and the rating scale data collection.

At Minneapolis, the trial sequences were automatically cycled with a fixed intertrial interval of 30 seconds, whereas WPAFB intertrial times were variable from 1 to 5 minutes.

At Minneapolis, a "trial start" light was illuminated on the panel to indicate the start of the run and turned off on completion of the trial. These cues were given verbally at WPAFB, together with verbal instructions to adjust afterburners for the next trial (off for low speed, on for high).

All rating trials at Minneapolis closely followed the procedures outlined under Phase II. These rules were relaxed somewhat at WPAFB, allowing pilots to deviate from the defined task after the first minute of a trial.

## SECTION VI RESULTS OF THE VALIDATION PROGRAM

### METHOD OF ANALYSIS

Parametric statistical analyses were performed on the data of the validation study to account for measurement variability. This acknowledges the fact that human subjects do not perform a task consistently enough to form conclusions from a single observation of behavior. Even simple reaction-time measurements will vary from trial-to-trial, day-to-day, and subject-to-subject. In addition, the particular equipment used and subject population may contribute to increased variability. Briefly, the largest sources of behavior variability which have been classified are:

- 1) Intersubject variability (training differences, experience differences)
- 2) Intrasubject variability (motivation, attitude, fatigue, boredom)
- 3) Treatment variability (stimulus variables, task variables, response variables)

The design of an experiment using human subjects begins with an understanding of the sources of variability and some a priori knowledge of how the data are to be collected and analyzed. The techniques of statistical inference provide the structure and assumptions for dealing with this type of data. Simply stated, the data are treated as samples of population distributions. Statistical inference techniques then allow us to determine in probability terms whether or not observed differences are large enough to have come from different population distributions or whether the observed differences are products of chance.

Because of the dual nature of our evaluation approach to the problem of handling-quality validation, two distinctly different sources of data were used. On one hand, we have used performance data which theoretically can assume any value from zero to infinity (i. e., they are, without question, interval data). And, on the other hand, we have used rating scale data which have a limited range (e. g., Cooper-Harper has a range from 1 to 10) and which only approaches interval properties.

In the case of performance data, we have not hesitated to compute means and standard deviations and analysis of variance statistics. In a near classical sense, the performance data follow the assumptions which form the basis of statistical inference techniques.



By contrast, the manipulation of the rating scale data presents a problem. Mudd (Ref. 25) and others have stated that the use of analysis of variance statistics and other data summary methods are permissible with data that is "purportedly equal-interval." His statements raised some strong criticism from Ridgeway (Ref. 26) and, also, support by Barrett, et al. (Ref. 27). Ridgeway claims that the assumptions behind parametric analysis of variance techniques are violated when applied to rating scale data of the Cooper-Harper type and cannot therefore be used. Mudd and Barrett both claim that the techniques are relatively insensitive to the data produced by rating scales and yield satisfactory and accurate results.

Our approach in this study was based on strong pragmatic considerations. Rating data form a foundation of the handling-qualities area and, in fact, are the data upon which our models are based. They are therefore important to the study. To interpret the data, however, it is necessary to reduce them from raw form. We have therefore sided implicitly with Mudd and have performed analyses of variance on these data. The question of legitimacy remains to be answered. We simply caution the reader to critically review the results with this controversy in mind.

## DATA SOURCES

As described in Section V, the validation program has produced a great quantity of raw data. We have digitized time histories of key variables for each of 600 three-minute trials and Cooper-Harper and Global pilot opinion ratings for 120 trials. The list of summary scores which can be gleaned from these data is virtually endless. In order to keep the data analysis task manageable, therefore, we have chosen to deal only with the following data sources:

- Primary Performance Measures:
  - 1) Lateral rms error ( $\bar{E}_y$ ) at WPAFB
  - 2) Lateral rms error ( $\bar{E}_y$ ) at Minneapolis
  - 3) Altitude rms error ( $\bar{E}_h$ ) at WPAFB
  - 4) Altitude rms error ( $\bar{E}_h$ ) at Minneapolis
  - 5) Velocity rms error ( $\bar{E}_v$ ) at WPAFB
  - 6) Velocity rms error ( $\bar{E}_v$ ) at Minneapolis

- Pilot Rating Scores:

- 7) Cooper-Harper ratings at WPAFB
- 8) Cooper-Harper ratings at Minneapolis
- 9) Global (handling qualities) rating at WPAFB  
(3 subjects)
- 10) Global (handling qualities) rating at Minneapolis
- 11) Global (demands on pilot) rating at WPAFB  
(3 subjects)
- 12) Global (demands on pilot) rating at Minneapolis
- 13) Global (handling qualities) rating at WPAFB  
(4 subjects)
- 14) Global (demands on pilot) rating at WPAFB  
(4 subjects)

- Secondary Measures:

- 15) RMS aileron stick commands at WPAFB ( $\bar{\delta}_{PAS}$ )
- 16) RMS rudder commands at WPAFB ( $\bar{\delta}_{PR}$ )

These choices are largely dictated by the objectives and experimental design of the validation program. We wish to validate our criteria and practical controller on the basis of performance in a lateral-axis flying task and on the basis of pilot evaluations -- hence, the lateral error scores and the various pilot rating scores. The altitude and velocity error scores are introduced to provide a measure of interaction between the lateral and longitudinal axes. The secondary measures of stick and rudder activity are attempts to find other sensitive indicators of control system quality. Wright-Patterson and Minneapolis data are kept separate because of significant irreconcilable differences between the two simulations.

Following our method of analysis, each of the 16 data sources will be viewed as a random variable with an unknown probability distribution. The scores obtained for individual trials are random samples drawn from these distributions. The distributions themselves are thought to be functionally dependent on the independent variables of the experiment -- the five systems flown, the two flight conditions, and the pilot/subjects. The object of our analysis will be to determine whether the distributions are in fact different for each system, flight condition, and pilot, or whether they are identical. In addition, we seek quantitative statements about the magnitude of differences, if they exist.



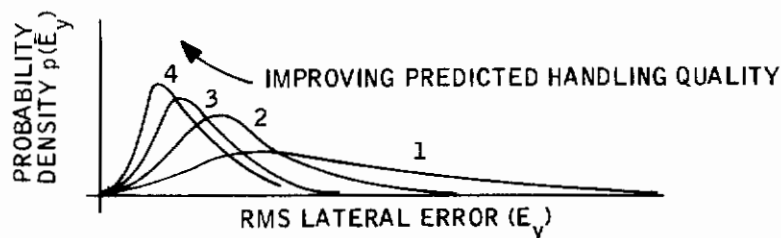
In order to present the analyses and their results in a meaningful way, we will begin with a qualitative examination of the full collection of random samples for two selected data sources -- lateral error and Cooper-Harper ratings (3 subjects) at WPAFB. This provides a general look at the distributions and at their differences for different values of the independent variables. We will then add quantitative analyses for the same two data sources -- averages, variances, analysis-of-variance statistics, and orthogonal comparisons. Finally, the same quantitative information will be presented for all of the remaining data sources, and the overall implications of the data will be summarized.

## A QUALITATIVE LOOK AT THE DATA

### Lateral Error at WPAFB

Figure 83 shows some histogram plots of the 300 lateral rms error scores obtained at WPAFB. These plots give the number of experimental outcomes which fell into 50-foot "bins," for bin locations between zero and 2000 feet.<sup>22</sup> The plots thus constitute crude experimental probability density functions of the random variable  $\bar{E}_y$  at WPAFB.

To examine the effects of each of our independent variables, the total number of samples in Figure 83 has been broken down in three different ways. First, in Figure 83, the samples are grouped according to the system with which they are obtained. This gives five histograms, 60 samples each, which show qualitatively how the probability density function of  $\bar{E}_y$  changes as a function of the independent systems variable. This is the so-called "main effect of systems." We see first of all that all of the five distributions seem to have the same characteristic shape, something approaching chi-square if we indulge our imagination a little. The average value and spread of the distributions decrease steadily from the predicted worst system (1) to the predicted best system (4), and little difference exists between systems 4 and 5. Qualitatively, then, the main effect of systems looks something like this:



<sup>22</sup>As indicated on the plots by a parenthetical number at the right extreme of the abscissa, four trials fell outside of the 2000-foot range. These are 2068, 2998, 4065, and 5632 feet in magnitude.

# Contrails

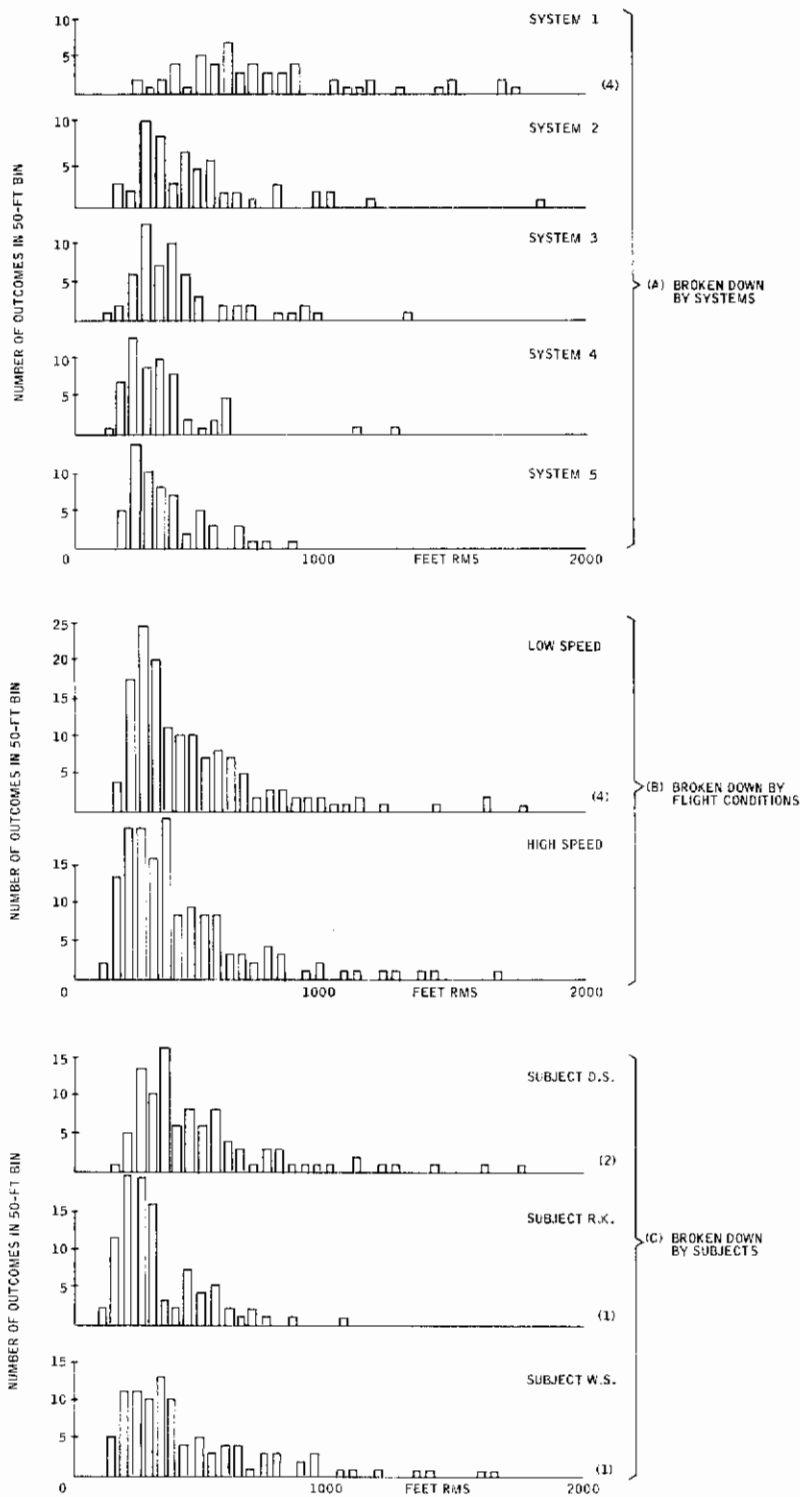


Figure 83. Histogram of Lateral RMS Errors at WPAFB

# Contrails

The second breakdown of the 300 lateral error samples is shown in Figure 83. Here the samples are grouped according to the flight condition for which they were obtained. This gives two histograms with 150 samples each whose differences constitute the "main effect of flight condition." We again see the characteristic "chi-square" shape, but the two distributions do not appear to differ much. Qualitatively, we would say that the effect of flight condition is insignificant.

The third breakdown in Figure 83 is a grouping according to pilot/subjects. This gives three histograms, 100 samples each, which again have the same shape but differ in average value, notably for subject R.K. Such differences must be expected, of course, due to the variability of the subject population.

There are several other breakdowns which could be constructed from the original 300 samples of data. For example, we can subdivide the 100 samples for each pilot/subject according to the system with which they were obtained. This would give three sets of five histograms, each with 20 samples. They would show us whether the effect of systems is the same for each subject or whether the systems influence each subject differently. Such differences are called "interaction effects," between, in this case, the independent systems variable and the subject variable. Other possible interactions are systems and flight condition, flight condition and subject, and a triple interaction of systems, flight condition and subjects. Histograms for each of these effects have too few samples, however, to give a good idea of the distributions, so we will leave their analysis to later quantitative procedures.

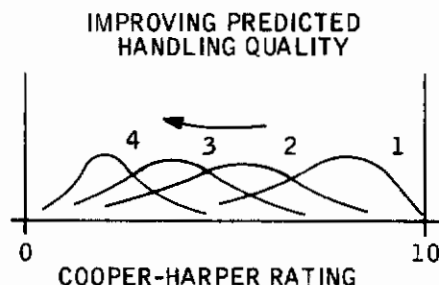
Perhaps the most significant property of all histograms in Figure 83 is the large variance. It is evident that no matter what the system and the flight condition are or who the pilot is, we can expect individual lateral error scores to range anywhere from a couple of hundred feet to a thousand feet or more. But, as we have seen, this does not mean that there are no differences between systems, flight conditions, and subjects, nor that performance measures such as rms error scores cannot detect differences. The histograms clearly show that subject R.K. flew with lower average errors and perhaps a little more consistently (less variation about the average) than the other subjects. Similarly, system 4, with good predicted handling qualities, was flown with lower average error and more consistently than systems 3, 2, and 1, each with successively poorer predicted handling qualities. Such is the qualitative relationship between handling qualities and performance capabilities of a controller/aircraft configuration.

The large variance creates some doubts, of course, whether our observations are justified. This will be remedied shortly via formal quantitative analysis.

## Cooper-Harper Ratings at WPAFB

Figure 84 shows a set of histograms for Cooper-Harper rating scores which is completely analogous to Figure 83. Here the bin size is 0.5 rating units, and bin locations range over the full Cooper-Harper scale from zero to 10. The total sample size is only 60, so the histograms look sparse when compared with Figure 83. The original rating for all scales is contained in Appendix XI.

The total collection of samples has again been broken down by systems, flight conditions, and subjects. In the first grouping, Figure 84(A), we see a definite ordering of systems on the basis of average values, and we see a variance behavior which is broad in the middle of the scale and tends to tighten at both extremes. However, there are too few samples in the histograms to make strong statements about this variance behavior or to say much about the shape of the distributions. Indeed, since rating data only approaches interval properties, we may be stretching the definition a bit to speak of shape in the usual way. Such theoretical questions aside, the main effect of systems appears to match the sketch below:



The 60 Cooper-Harper ratings are grouped by flight condition in Figure 84(B). Here we can begin to see some "shape" and some signs that the low-speed flight condition is slightly preferred.

The third breakdown [Figure 84(C)] shows a strong main effect of subjects. Subject D. S. uses both ends of the scale more liberally than both other subjects, while the constricted use of the scale by subject R. K. favors the low end and by subject W. S. favors the high end. These differences are again attributable to variability of the subject population.

Finally, the histograms of Figure 84 show that Cooper-Harper ratings as well as lateral errors exhibit large variance, so formal quantitative procedures should be used to establish the validity of conclusions based on either of these data sources.

# Contrails

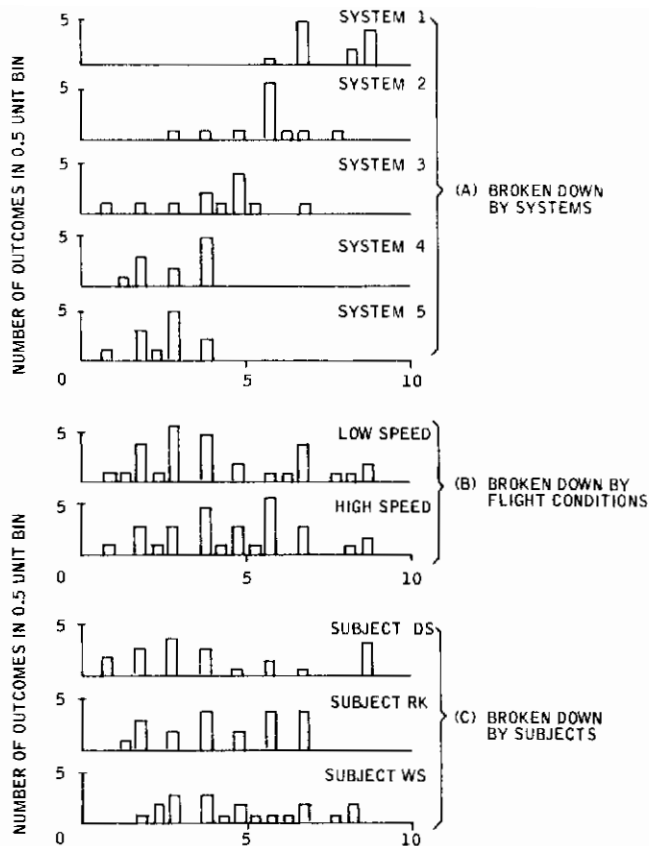


Figure 84. Histogram of Cooper-Harper Ratings at WPAFB (3 Subjects)

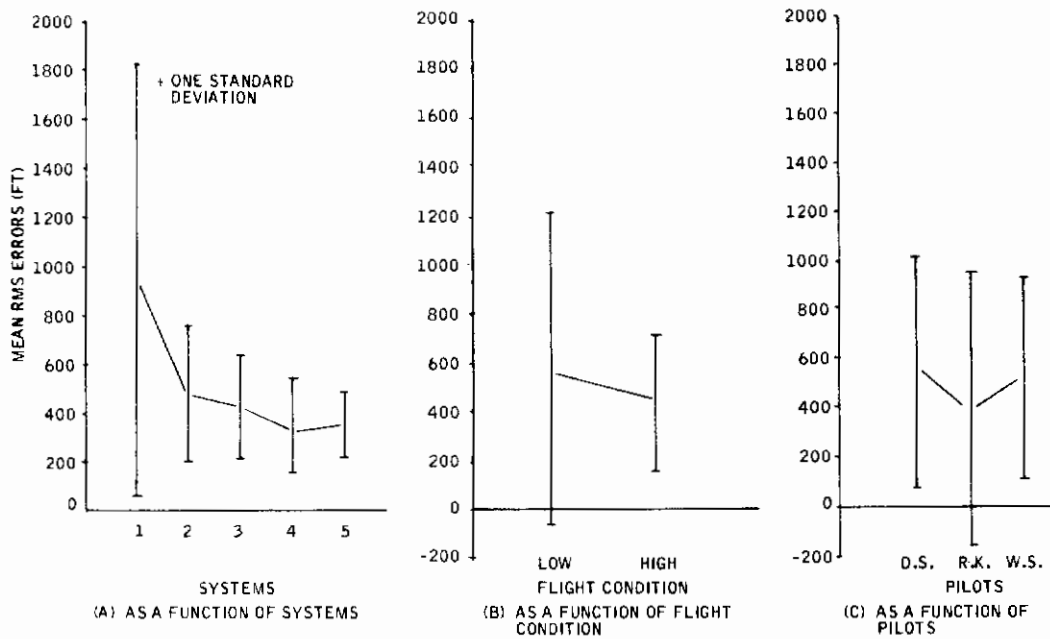


Figure 85. Mean RMS Lateral Errors at WPAFB



## QUANTITATIVE ANALYSIS

After this brief qualitative look at two of our data sources, we proceed to add quantitative interpretations. This will be done by computing means and standard deviations, by assessing significance of differences via analyses of variance and orthogonal comparisons,<sup>23</sup> and finally by rank ordering the main effect of systems. The object, of course, is to establish validity and to sharpen earlier qualitative conclusions.

We will again treat the lateral error data source at WPAFB and the Cooper-Harper data source at WPAFB separately and in some detail. Results for the other data sources will be presented in a summary fashion.

### Lateral Error at WPAFB

Mean values and standard deviations of the lateral error histograms of Figure 85 are presented graphically in Figure 85. These statistics are again broken down to show the main effects of systems, flight condition and subjects. An ordering of the main effect of systems is apparent. The average error values decrease from system 1 through system 4 with a slight increase for system 5. Note that this is precisely the predicted ordering. The range of error from system 1 to system 4 is approximately 589 feet rms. Likewise, there appears to be a consistent decrease in variability from 1 to 5. System 1 differs most noticeably from the others both in terms of mean error value and standard deviations.

The main effect of flight condition is also shown in Figure 85. The average error value for the low-speed flight condition is greater than the high-speed condition by approximately 137 feet rms. The standard deviation is also larger for the low-speed flight condition. Note, however, that these differences are not apparent from the histograms. Either our impressions from the histograms are wrong or the differences in Figure 85B will turn out to be statistically insignificant. The latter is in fact the case, as we shall see later.

The third breakdown is a presentation of errors as a function of the subjects variable. Subjects D.S. and W.S. are quite similar in both means and standard deviations. Subject R.K., on the other hand, is some 156 feet more accurate than the average error of the other two subjects. The standard deviation associated with R.K.'s performance is noticeably greater, however. This is not evident from the histograms because of a single R.K. trial which fell out at 5632 feet.

---

<sup>23</sup> Readers not familiar with these procedures are encouraged to consult either Winer (Ref. 28) or Scheffe (Ref. 29), the latter for the mathematically more sophisticated.



So far, the mean and standard deviation values of Figure 85 only add numbers to our original impressions from the histograms. We still do not know whether differences are significant or products of chance. To decide this question we use the analysis of variance and individual orthogonal comparisons.

Recall that the particular experimental design chosen was a  $2 \times 5 \times 3$  mixed-design. The main effects of interest are the fixed effects of systems and flight condition and the random effect of pilots. The analysis of variance is designed to determine the level of statistical significance of these effects as well as the significance of all possible interaction effects in the experiment. By inspection we were able to order the main effect of systems, but systems 3, 4, and 5 are very close in mean value (relative to their standard deviations) so our initial confidence in such orderings is low. Likewise, the difference between flight conditions is not large enough to justify conclusions without further evaluation. The needed confidence is provided by the analysis of variance and by orthogonal comparisons.

The output of an analysis of variance is an F-statistic ( $F \geq 0$ ), which is computed under the statistical hypothesis ( $H_0$ ) that all the means of a particular main effect are identical. Under this hypothesis, the F-statistic is distributed according to the F-distribution law (Ref. 29). We can therefore determine critical values ( $F_p$ ) such that (under  $H_0$ ) probability ( $F \geq F_p$ ) =  $p$ , say for  $p = 0.05$  and  $p = 0.01$ . Then, if the F-statistic comes out greater than  $F_p$ , we must either conclude that  $H_0$  is refuted (i.e., the means are different) or that we have observed a rare event of probability,  $p$ . This is condensed by saying that the means are different at a level of significance equal to  $p$  (or, more simply, the effect is significant at level  $p$ ). If  $F$  comes out less than  $F_p$ , the data provide insufficient support for the rejection of  $H_0$  at level  $p$ .

A similar procedure applies to orthogonal comparisons, where F-statistics are used to assess differences of individual means within a main effect.

Table XXV presents the results of the analysis of variance performed on the WPAFB lateral errors data.

In this table, the main effect of systems is significant beyond the 0.01 level (as indicated by superscript a). The F-value of 113.546 with 4 and 8 degrees of freedom is much larger than the  $F_p$  value of 7.01 required for significance at the 0.01 level. This simply shows that the pilot subjects were not able to fly the five systems with the same degree of accuracy.

Table XXV. Analysis of Variance of WPAFB  
Lateral Error Data

Source of Variance	Degrees of Freedom	Mean Square	F
Systems (A)	4	3593739.000	113.546 <sup>a</sup>
Flight condition (B)	1	1411813.750	N. S.
Subjects (C)	2	857618.000	4.647 <sup>b</sup>
A x B	4	661073.125	5.993 <sup>b</sup>
B x C	2	343191.562	N. S. <sup>c</sup>
A x C	8	31649.957	N. S.
A x B x C	8	110301.750	N. S.
Residual	270	184550.281	N. S.
Total	299	---	---

<sup>a</sup> p ≤ 0.01

<sup>b</sup> p ≤ 0.05

<sup>c</sup> N. S. = Nonsignificant

The other significant effects are subjects and the interaction of flight condition and system,<sup>24</sup> both at the 0.05 level (as indicated by superscript b). The significant effect of subjects is a random effect and has limited interpretability beyond saying that the pilots perform differently. The factors which contribute to that difference are not readily apparent.

The interaction of flight condition and systems means that the effect of systems is different at the two speeds. This will be given a graphical interpretation later in this section.

<sup>24</sup>The general model used in the analysis of variance to represent a single observation ( $x_{ijkl}$ ) for the *i*th system, *j*th flight condition, and *k*th subject is a sum of the following components:

$$x_{ijkl} = \alpha_i + \beta_j + \gamma_k + \alpha\beta_{ij} + \alpha\gamma_{ik} + \beta\gamma_{jk} + \alpha\beta\gamma_{ijk} + \epsilon_{ijkl}$$

where  $\alpha_i$ ,  $\beta_j$ ,  $\gamma_k$  represent unique main effects attributable to the system, flight condition, and subject alone;  $\alpha\beta_{ij}$ ,  $\alpha\gamma_{ik}$ , and  $\beta\gamma_{jk}$  are unique interaction effects attributable to the combined action of system plus flight condition, etc.;  $\alpha\beta\gamma_{ijk}$  is the unique triple-interaction of all three factors acting together; and  $\epsilon_{ijkl}$  is a purely random component. When we say that the main effect of systems is significant, this means  $\alpha_i \neq \alpha_j$  for some *i*, *j* at the specified level of probability, *p*.

All other effects are significant at a level  $p > 0.05$ . This means that the data do not strongly refute the  $H_0$  hypothesis (the F-value would occur purely by chance in one out of 20 or fewer repetitions of the experiment, on the average). We have therefore chosen the 0.05 level as an upper cutoff and will simply call these outcomes nonsignificant (N.S.). Note in particular that the main effect of flight condition is nonsignificant.

The analysis of variance just presented has established the level of significance of all main and interaction effects. It says little, however, about the significance of differences within a single independent variable. Consider the systems variable, for example, which takes on five values -- systems 1 - 5. Using the analysis of variance, we have established with a high degree of certainty that the mean error values for these five systems are different. However, we have not shown that the mean for system 1 differs from system 2, system 2 from 3, and so forth. In short, we have not established the significance of our rank ordering of system means. This is done in Table XXVI with individual orthogonal comparisons.

Table XXVI. Individual Comparisons (Scheffe)  
of WPAFB Lateral Error Data

System Comparison	Degrees of Freedom	F
1 vs 2	1/8	193.510 <sup>a</sup>
1 vs 3	1/8	249.413 <sup>a</sup>
1 vs 4	1/8	328.801 <sup>a</sup>
1 vs 5	1/8	317.442 <sup>a</sup>
2 vs 3	1/8	N.S.
2 vs 4	1/8	17.826 <sup>a</sup>
2 vs 5	1/8	15.258 <sup>a</sup>
3 vs 4	1/8	5.476 <sup>b</sup>
3 vs 5	1/8	N.S.
4 vs 5	1/8	N.S.

<sup>a</sup><sub>p</sub> < 0.01

<sup>b</sup><sub>p</sub> < 0.05

The comparisons of Table XXVI are computed according to Scheffe's test (Ref. 29), which is the most conservative of the commonly used individual comparison methods. They show that differences in mean lateral errors between system 1 and all other systems are highly significant. System 2 does not differ from system 3, but does differ from systems 4 and 5. Further, system 3 differs from system 4 but does not

differ from system 5. Systems 4 and 5 were not different. The F-values for system 1 versus all other systems are extremely large (for 1 and 8 degrees of freedom) and indicate a very strong effect on pilot performance accuracy relative to the other systems.

Basically, each comparison in Table XXVI can be interpreted as a comparison between the difference of two means (a statistical estimate) and the accuracy to which the difference can be estimated from all 300 lateral error samples. This is illustrated in Figure 86 which shows the values of all possible differences compared with the standard deviation of their estimation errors. The latter quantity is given by  $\sqrt{2\sigma^2(\text{AXC})/60} = 32.5$  feet (see Ref. 28), where  $\sigma^2(\text{AXC})$  is the AXC mean square shown in Analysis of Variance Table XXV. This is the standard deviation which "counts" as far as data analysis is concerned, not the standard deviations shown in Figure 85.

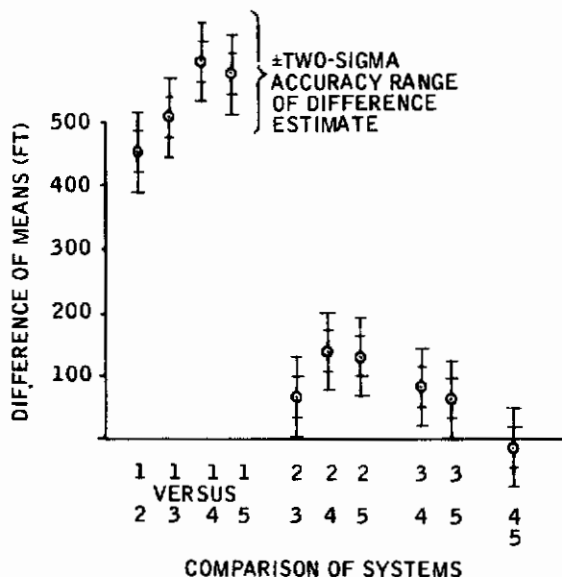


Figure 86. Graphical Interpretation of Individual Comparisons

In Figure 86, two means are different at a level 0.05 or less if their difference plus or minus two-sigma does not include the zero value. Hence, all comparisons except 2 versus 3, 3 versus 5, and 4 versus 5 are significant.

### Cooper-Harper Data at WPAFB

A similar formal analysis procedure was carried out for the Cooper-Harper rating data. This begins with Figure 87 which shows a three-way

# Contrails

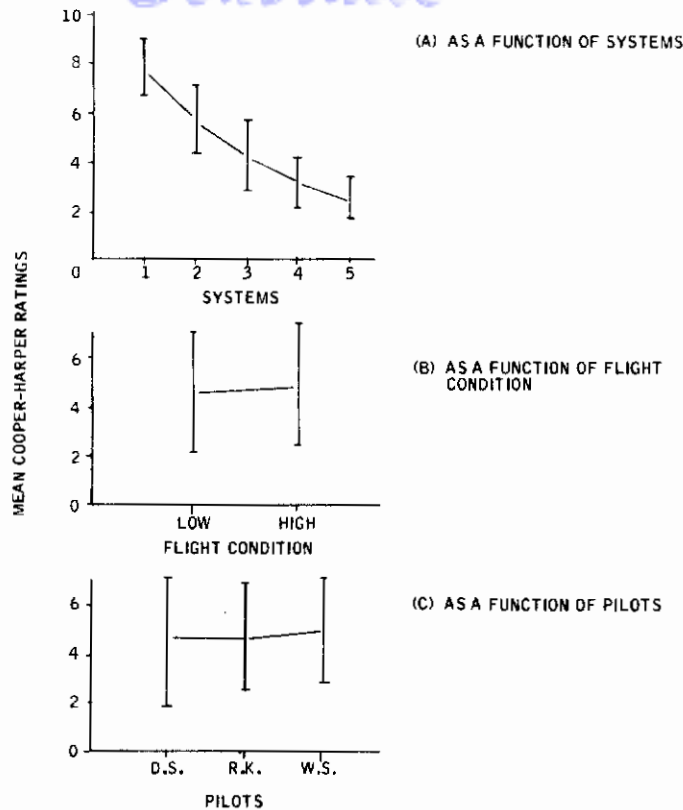


Figure 87. Mean Cooper-Harper Ratings at WPAFB (3 Subjects)

breakdown of Cooper-Harper rating data by systems, flight condition and pilots. Again, an ordering of the main effect of systems is apparent, with system 1 being the least acceptable and system 5 the most acceptable. The average Cooper-Harper value for system 1 is 7.8 with a decreasing trend across systems to an average of 2.7 for system 5. Note that system 5 obtained a better average rating than system 4. This is contrary to the performance data which showed that system 5 errors were greater than system 4 and contrary to our original predictions. Later analyses of the Cooper-Harper data will show that, in fact, no significant difference exist between 4 and 5. (We have already shown this for lateral error data.) For all systems, the standard deviations appear comparable.

By inspection, the main effect of flight condition does not appear to differ appreciably, although the low-speed flight condition is slightly preferred. The average rating values differ by only 0.4 of a rating point. Again, the standard deviations for both flight conditions appear comparable.

For the main effect of pilots, all subjects appear quite similar in both mean rating values and standard deviations, although subject D. S. appears to be more variable in his rating behavior. If you recall, the histogram plots revealed that subject D. S. used both ends of the scale more than the other two subjects. One explanation for this is that



subjects R.K. and W.S. are both graduates of the test pilot school and, therefore, are more experienced raters and can be expected to be less variable in their rating behavior.

Again, we have been able to order the Cooper-Harper data, but we lack confidence about the observed differences in mean values for each of the main effects. Therefore, an analysis of variance was also computed for these data. We have already stated that the use of this analysis technique for rating data is subject to question. So the reader is again cautioned to review the results from this standpoint.

A summary of the analysis of variance is contained in Table XXVII.

The main effect of systems is significant at  $p < 0.01$ . All other main effects are nonsignificant. In particular, the mild preference shown for the low-speed flight condition is not significant. The observed differences between subjects is also not significant. The difference in rating behavior noted earlier is apparently lost. These data also show a significant interaction between flight condition and subjects, models and subjects, and, for the first time, a significant triple interaction. The interaction effects will be dealt with later in this section.

Individual comparisons for WPAFB rating data are shown in Table XXVIII. These data detect differences between systems 2 and 3 and 3 and 5 which do not show up in the performance data. The pilots apparently were able to control system 3 as accurately as 2 and 5, but they rated 2 poorer than 3 and 3 poorer than 5.

No differences were detected between systems 4 and 5 and between systems 3 and 4. All other differences are significant. The Cooper-Harper data, therefore, are more sensitive than the lateral-axis data, in that they discriminate between more pairs of systems.

## Other Data Sources

All of our data sources were subjected to the same formal analyses as have just been described for lateral errors and Cooper-Harper ratings at WPAFB. Results of these analyses are summarized in Figures 88 through 95 and in Tables XXIX and XXX. The figures present mean values and standard deviations of the various scores, again broken down into the main effects of systems, flight condition, and subjects. The tables present summaries of the levels of significance of each effect, as given by the analysis of variance, and summaries of individual comparisons, as given by Scheffe's test.



Table XXVII. Analysis of Variance of WPAFB  
Cooper-Harper Data (3 Subjects)

Source of Variance	Degrees of Freedom	Mean Square	F
Systems (A)	4	54.116	23.249 <sup>a</sup>
Flight condition (B)	1	1.980	N.S.
Subjects (C)	2	0.990	N.S.
A x B	4	2.074	N.S.
B x C	2	3.290	5.909 <sup>a</sup>
A x C	8	2.328	4.180 <sup>a</sup>
A x B x C	8	3.115	5.594 <sup>a</sup>
Residual	30	0.557	N.S.
Total	59		

<sup>a</sup><sub>p</sub> < 0.01

Table XXVIII. Individual Comparisons of WPAFB  
Cooper-Harper Data (3 Subjects)

System Comparison	Degrees of Freedom	F
1 vs 2	1/8	10.745 <sup>b</sup>
1 vs 3	1/8	33.098 <sup>a</sup>
1 vs 4	1/8	60.010 <sup>a</sup>
1 vs 5	1/8	67.705 <sup>a</sup>
2 vs 3	1/8	6.126 <sup>b</sup>
2 vs 4	1/8	19.969 <sup>a</sup>
2 vs 5	1/8	24.506 <sup>a</sup>
3 vs 4	1/8	N.S.
3 vs 5	1/8	6.126 <sup>b</sup>
4 vs 5	1/8	N.S.

<sup>a</sup><sub>p</sub> < 0.01

<sup>b</sup><sub>1</sub> < 0.05

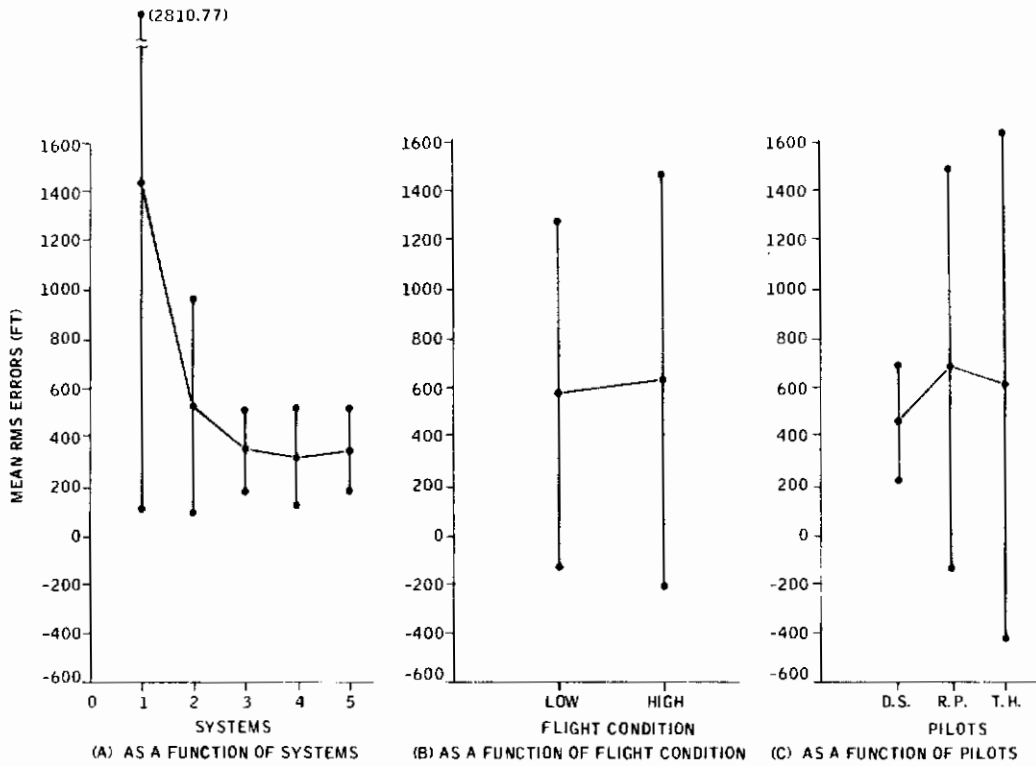


Figure 88. Mean RMS Lateral Errors at Minneapolis

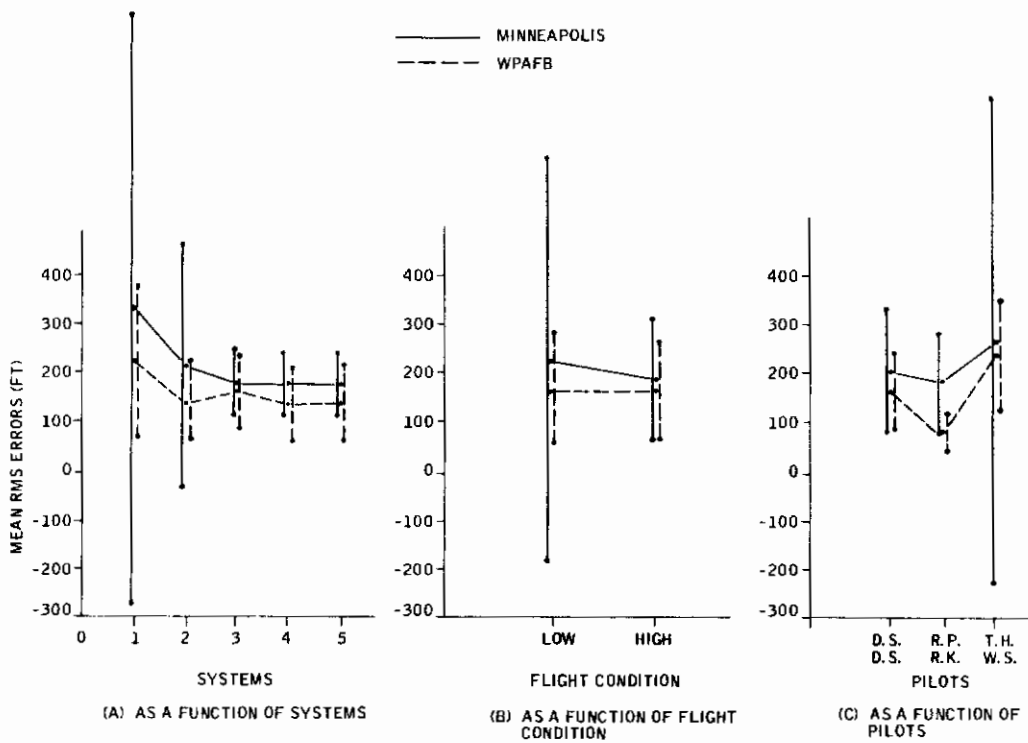


Figure 89. Mean RMS Altitude Errors at WPAFB and Minneapolis

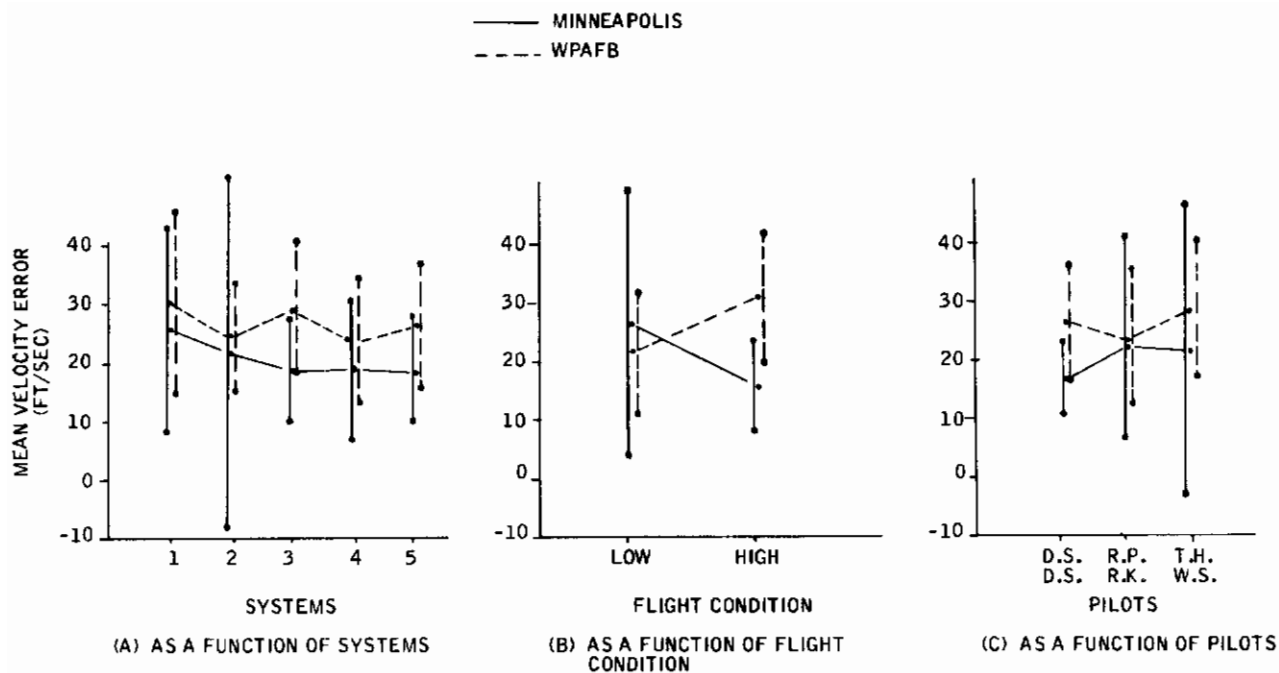


Figure 90. Mean RMS Velocity Errors at WPAFB and Minneapolis

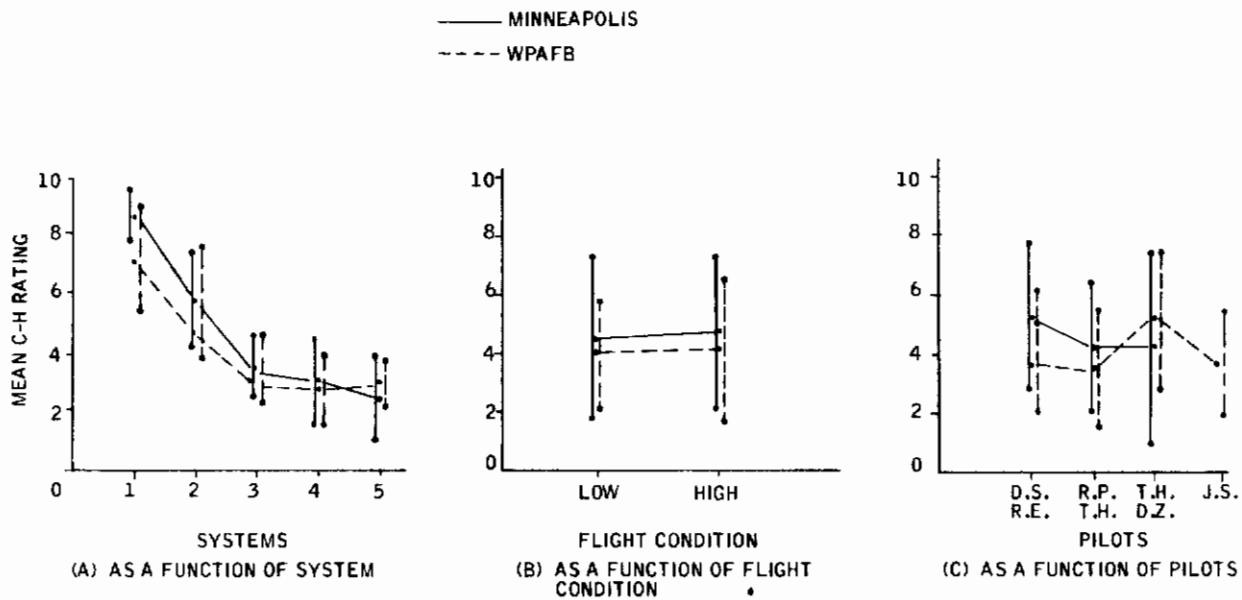


Figure 91. Mean Cooper-Harper (C-H) Ratings at WPAFB (4 Subjects) and Minneapolis

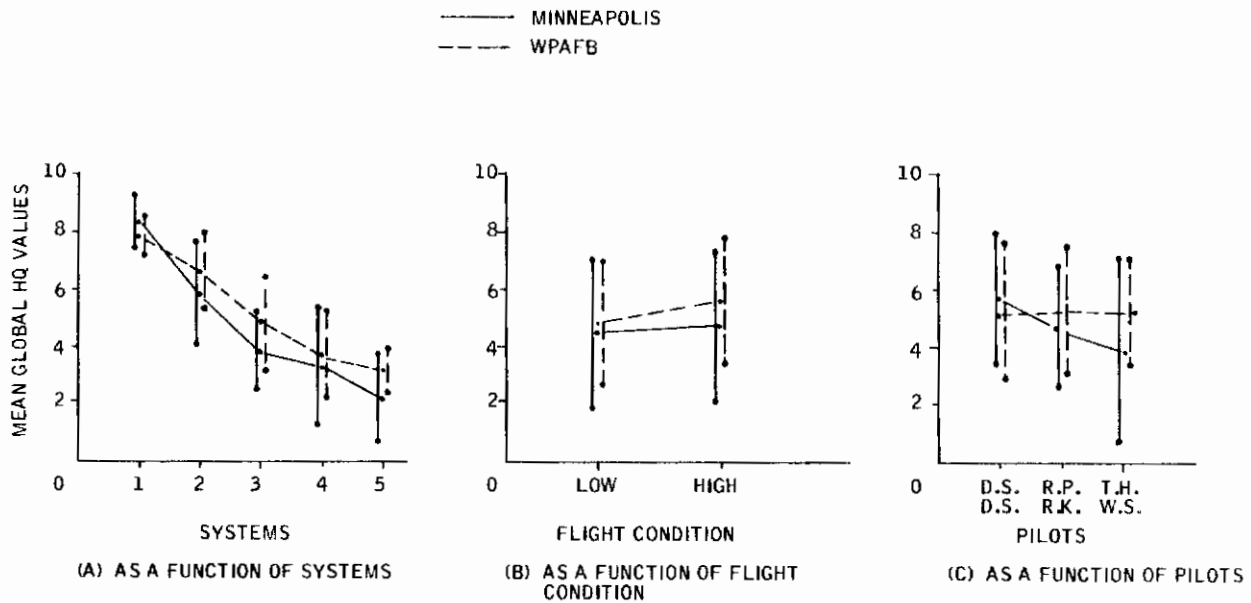


Figure 92. Mean Global "Handling-Quality (HQ)" Ratings at WPAFB (3 Subjects) and Minneapolis

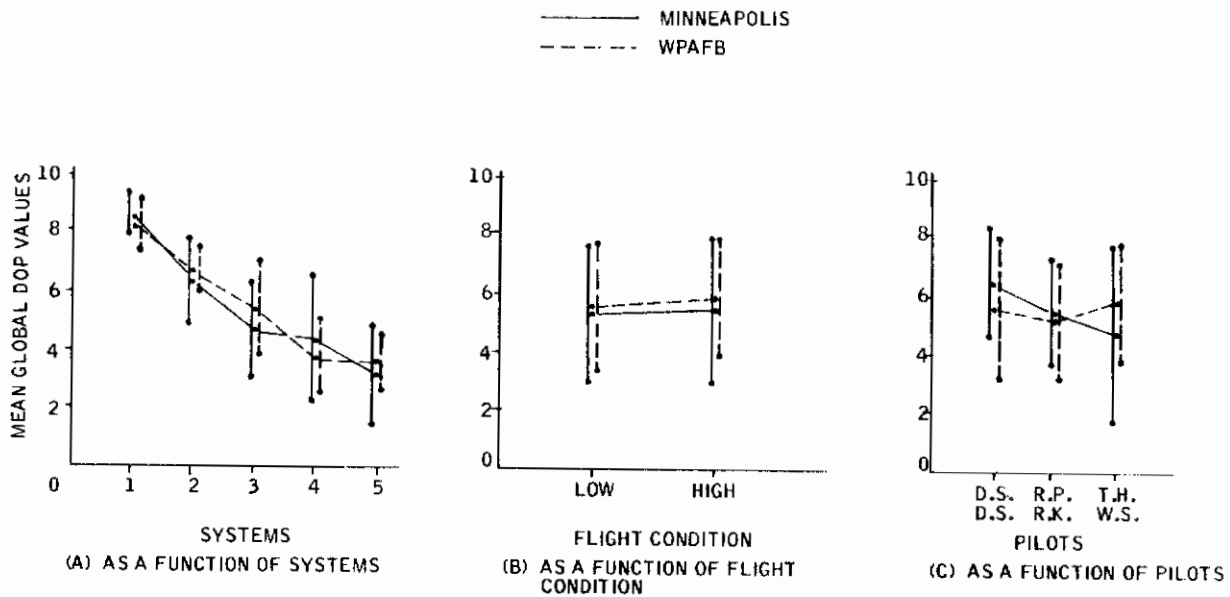


Figure 93. Mean Global "Demand-on-Pilot (DOP)" Ratings at WPAFB (3 Subjects) and Minneapolis

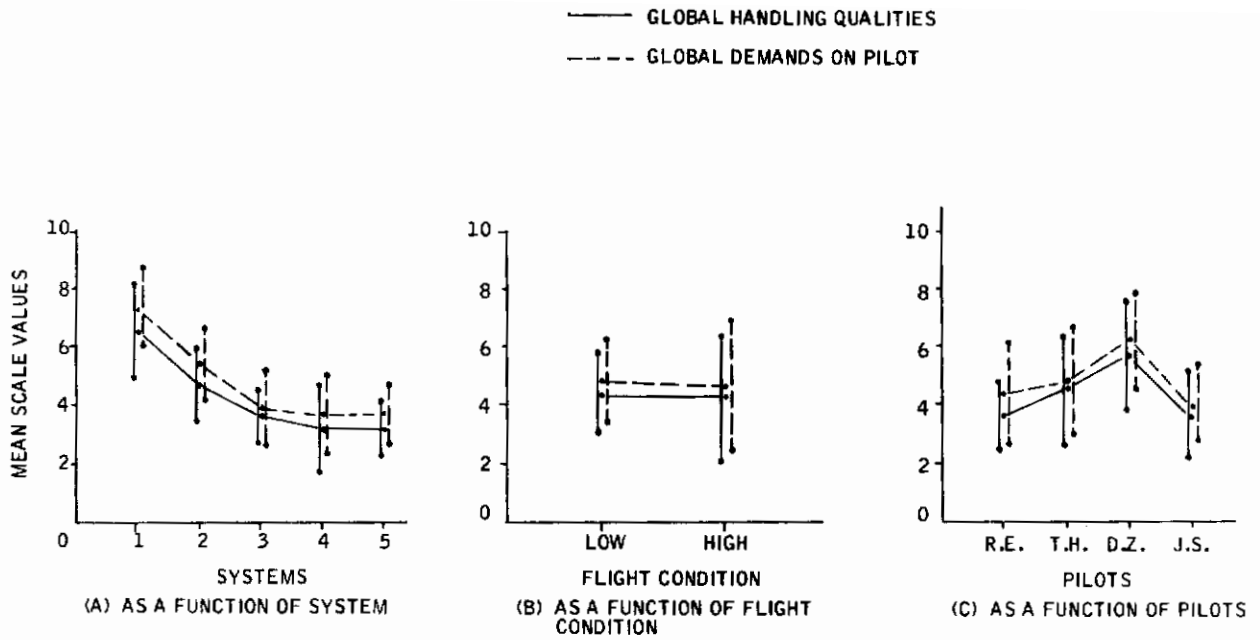


Figure 94. Mean Global DOP and HQ Ratings at WPAFB (4 Subjects)

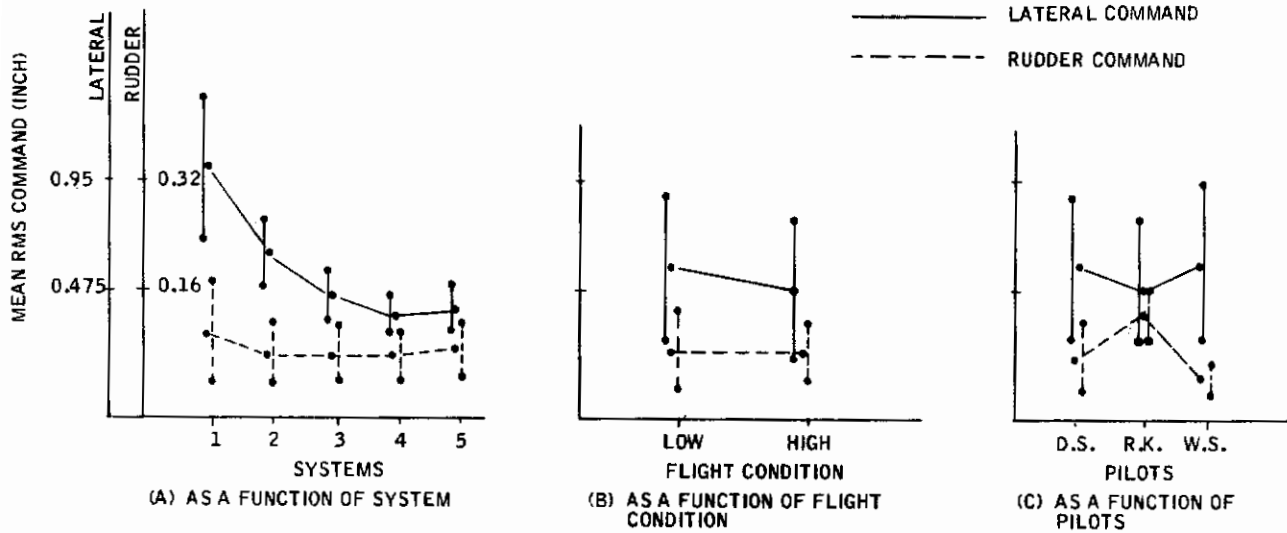


Figure 95. Mean RMS Lateral Commands and Rudder Commands at WPAFB

Table XXIX. Summary of Levels of Significance for Main Effects and Interactions of the Dependent Variable Analysis of Variance

Data Source	(A) Systems	(B) Flight Condition	(C) Subjects	A x B	A x C	B x C	A x B x C
Lateral error, WPAFB	p < 0.01	---	p < 0.05	p < 0.05	---	---	---
Lateral error, Minneapolis	p < 0.05	---	p < 0.05	p < 0.05	p < 0.01	---	---
Altitude error, WPAFB	p < 0.05	---	p < 0.01	p < 0.05	p < 0.05	---	---
Altitude error, Minneapolis	p < 0.05	---	---	---	---	---	---
Velocity error, WPAFB	p < 0.05	---	p < 0.05	---	---	p < 0.01	---
Velocity error, Minneapolis	---	---	p < 0.05	---	---	p < 0.01	---
Cooper-Harper, WPAFB	p < 0.01	---	---	---	p < 0.01	p < 0.01	p < 0.01
Cooper-Harper, Minneapolis	p < 0.01	---	---	---	---	---	---
Cooper-Harper, 4-subject group, WPAFB	p < 0.01	---	p < 0.01	---	p < 0.01	---	---
Global, handling qualities, WPAFB	p < 0.01	---	---	---	---	p < 0.05	p < 0.01
Global, handling qualities, Minneapolis	p < 0.01	---	p < 0.01	---	---	---	---
Global, demands on pilot, WPAFB	p < 0.01	---	---	---	---	p < 0.05	p < 0.01
Global, demands on pilot, Minneapolis	p < 0.01	---	p < 0.01	---	---	---	---
Global, handling qualities, 4-subject group, WPAFB	p < 0.01	---	p < 0.01	---	---	---	---
Global, demands on pilot, 4-subject group, WPAFB	p < 0.01	---	p < 0.01	---	---	---	---
Lateral commands, WPAFB	p < 0.01	p < 0.05	p < 0.01	p < 0.05	p < 0.05	---	---
Rudder commands, WPAFB	p < 0.05	---	p < 0.01	---	p < 0.05	---	---



Table XXX. Summary of Levels of Significance for Individual Orthogonal Comparisons of all Pairs of Systems

Data Source	1 vs. 2	1 vs. 3	1 vs. 4	1 vs. 5	2 vs. 3	2 vs. 4	2 vs. 5	3 vs. 4	3 vs. 5	4 vs. 5
Lateral error, WPAFB	<0.01	<0.01	<0.01	<0.01	<0.01	<0.01	<0.01	<0.05	---	---
Lateral error, Minneapolis	<0.01	<0.01	<0.01	<0.01	---	---	---	---	---	---
Altitude error, WPAFB	<0.01	<0.01	<0.01	<0.01	---	---	---	---	---	---
Altitude error, Minneapolis	<0.05	<0.01	<0.01	<0.01	---	---	---	---	---	---
Velocity error, WPAFB	<0.01	---	<0.01	---	---	---	---	<0.05	---	---
Velocity error, Minneapolis	---	---	---	---	---	---	---	---	---	---
Cooper-Harper, WPAFB	<0.05	<0.01	<0.01	<0.01	<0.01	<0.01	<0.01	---	<0.05	---
Cooper-Harper, Minneapolis	<0.01	<0.01	<0.01	<0.01	<0.01	<0.01	<0.01	---	---	---
Cooper-Harper, 4-subject group, WPAFB	<0.01	<0.01	<0.01	<0.01	---	<0.05	---	---	---	---
Global, handling qualities, WPAFB	<0.01	<0.01	<0.01	<0.01	<0.01	<0.01	<0.01	<0.01	<0.01	---
Global, handling qualities, Minneapolis	<0.01	<0.01	<0.01	<0.01	<0.05	<0.01	<0.01	---	<0.05	---
Global, demands on pilot, WPAFB	<0.01	<0.01	<0.01	<0.01	<0.01	<0.01	<0.01	<0.01	<0.01	---
Global, demands on pilot, Minneapolis	<0.05	<0.01	<0.01	<0.01	<0.05	<0.05	<0.01	---	---	---
Global, handling qualities, 4-subject group, WPAFB	<0.01	<0.01	<0.01	<0.01	---	<0.05	<0.05	---	---	---
Global, demands on pilot, 4-subject group, WPAFB	<0.01	<0.01	<0.01	<0.01	<0.01	<0.01	<0.01	---	---	---
Lateral commands, WPAFB	<0.01	<0.01	<0.01	<0.01	<0.01	<0.01	<0.01	<0.05	---	---
Rudder commands, WPAFB	<0.05	<0.05	<0.01	<0.05	---	---	---	---	---	---

# Contrails

These data summaries more or less speak for themselves. For the main effect of systems, the graphs show the predicted ordering of means (for systems 1 - 4) in all data sources except altitude and velocity errors. System 5 is slightly better than system 4 for all pilot opinion measures, and a bit poorer than system 4 for all performance measures. We could not have asked for better agreement between fact and prediction.

Statistically, the main effect of systems is significant for all data sources except velocity error. This is a highly encouraging result, since it says that the handling-quality goodness property we are trying to measure does in fact prevail through nearly all of our measured variables. It influences primary performance measures, rating measurements, performance measures in other axes, and secondary indicators.

Individual comparisons of Table XXX substantiate the ordering of means to a level of significance and resolution depending on the particular data source. In general, pilot rating data differentiates between more sets of means. However, lateral error and lateral commands at WPAFB are also sensitive indicators, while rating data from the four-subject group at WPAFB is rather insensitive. By far the most significant column in Table XXX is the 4 versus 5 comparison on the extreme right. Not a single data source detected differences between the best predicted optimal system and the practical control system -- again a highly satisfying result.

For the main effects of flight condition and pilot/subjects, Figures 88 through 95 and Table XXIX, show the expected result -- insignificant flight condition effects (except for lateral commands) and significant subjects effects. The former reflects the fact that each of our five controller/aircraft systems was designed to look the same at all flight conditions (Section IV), and the latter reflects expected variability in the subject population.

There are also a number of interesting interactions effects. The first is the A x B or systems-by-flight condition interaction for lateral errors at WPAFB which has been mentioned previously. As Table XXIX indicates, this interaction also shows up in lateral errors at Minneapolis and altitude errors and rudder commands at WPAFB. It is interpretable as a difference in the main effect of systems at each flight condition and is shown graphically for the case of lateral error at WPAFB in Figure 96. We see that the interaction arises primarily because the systems effect is more pronounced at the low-speed flight condition than at high speed. However, the ordering of systems is unaltered, so our experimental findings are unaffected.

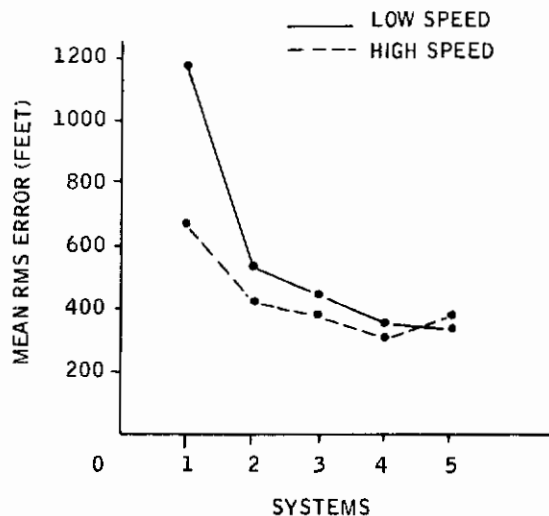


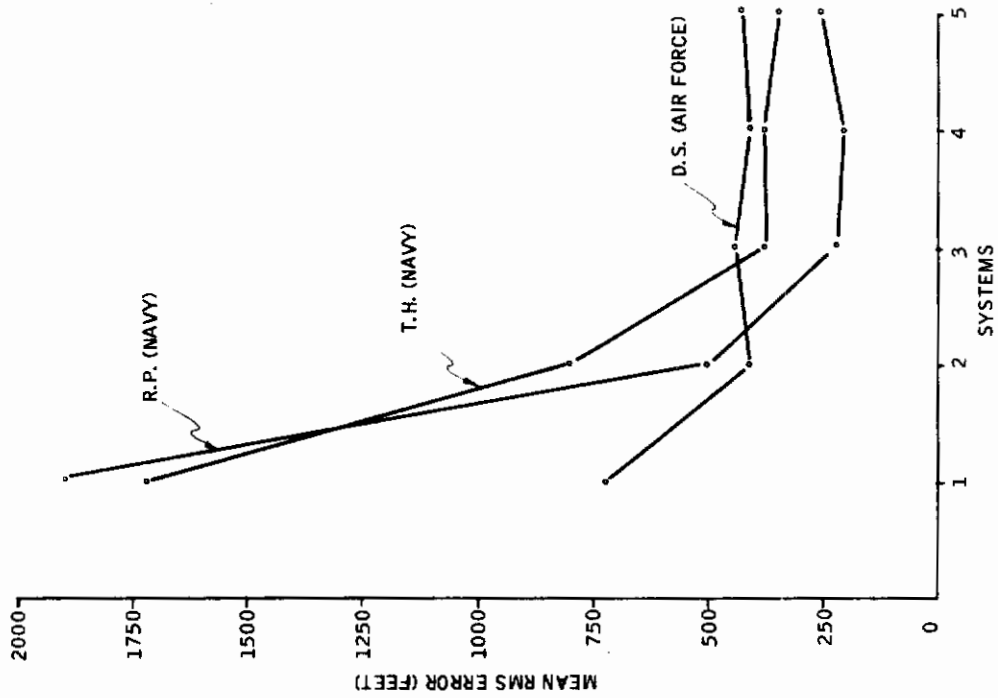
Figure 96. Illustration of A x B Interaction - Lateral Error, WPAFB

A second interaction is A x C, or systems-by-subjects, which is interpretable as a difference of the systems effect for each pilot/subject. This interaction is very prominent in the lateral error data at Minneapolis and also in the Cooper-Harper ratings at WPAFB (3 and 4 subjects). It is examined graphically in Figure 97. This figure contrasts the main effect of systems for lateral error data at Minneapolis and WPAFB when these data are further broken down by pilot/subjects.

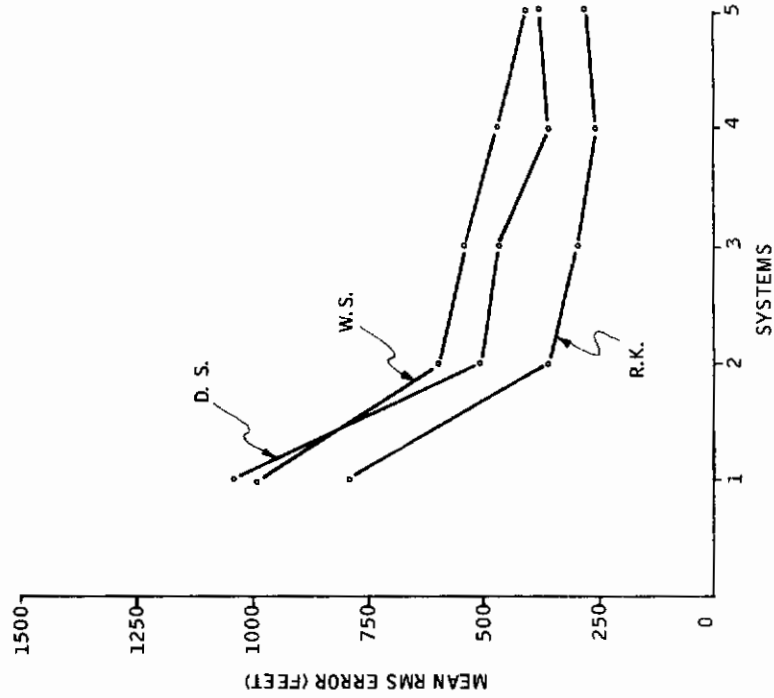
The interaction is clearly evident in the Minneapolis data. Subject D. S. was able to fly systems 1 and 2 with more accuracy than the other two pilots but did not fly systems 3, 4 and 5 as accurately as the Navy pilots. While the interaction does not change our conclusions, it is responsible for the very insensitive nature of the Minneapolis lateral error data (see Table XXX).

A series of arc-tangent transformations were attempted on these data to increase the sensitivity of the analysis. All attempts were unsuccessful. The interaction between the main effect of systems and the random effect of pilots is simply too large to overcome.

There were also occurrences of B x C, or flight condition-by-subject, interactions and of triple interactions between systems, flight condition and subjects. The latter is difficult if not impossible to explain in a meaningful manner for cases where a triple interaction is not predicted.



a) Systems Main Effect by Pilot, Minneapolis -- Lateral Errors with Interaction



b) Systems Main Effect by Pilot, WPAFB -- Lateral Errors Without Interaction

Figure 97. Illustration of A x C Interaction

The former means that the main effect of flight condition is different for different subjects. In view of the variability of the subject population, i. e., training, experience, flight time, etc., such differences can be expected.

## SUMMARY OF RESULTS

All these discussions are best summarized by reiterating the rank ordering of systems which the data provide. This is done by Table XXXI for the major lateral rms error and rating scale data sources. The ranking is consistent except for the reversal of systems 5 and 4 on the rating data. However, no significant differences were detected between systems 4 and 5 for any of the analysis performed. The brackets in each column enclose systems which were not found to be significantly different at least at the 0.05 level.

Table XXXI. Rank-Order of Systems for Main Data Sources

Lateral Error		Cooper-Harper		Global	
WPAFB	Minneapolis	WPAFB <sup>a</sup>	Minneapolis	WPAFB <sup>a</sup>	Minneapolis
1	1	1	1	1	1
[ 2 3 ]	[ 2 3 ]	2	2	2	2
		[ 4 5 ]	3	3	3
4	4		4	4	
5	5	[ 4 5 ]	[ 4 5 ]	[ 4 5 ]	[ 4 5 ]

<sup>a</sup>Three subjects

The two measures -- performance and rating -- turned out to be complementary not contradictory. The dual nature of our measurement approach to the validation of handling-quality models combined the best aspects of rating and performance measures and yielded an accurate assessment of the controlled vehicle. For instance, the mean Cooper-Harper scale value for system 3 at WPAFB was 4.3. This scale value corresponds to an error score of 414 feet from course centerline for this task and has a standard deviation of 212 feet. Likewise, system 2 at Minneapolis obtained an average rating of 5.8 which corresponds to a mean error at 526 feet rms from centerline with a standard deviation of 443 feet. Thus, we were not only able to establish differences between the systems on the basis of how the pilot felt toward them, but we were also able to measure how accurately he could use them. We have,

in effect, developed a crude "map" which relates average pilot ratings to average performance in a pilot tracking task of the type used in this experiment.

For lateral error versus Cooper-Harper rating data at WPAFB, this map has the form shown in Figure 98. This figure is not meant to imply, of course, that the variables are uniquely related, i. e., other variables such as workload play a role. The figure merely shows the relationship for five data points, corresponding to each of our five systems.

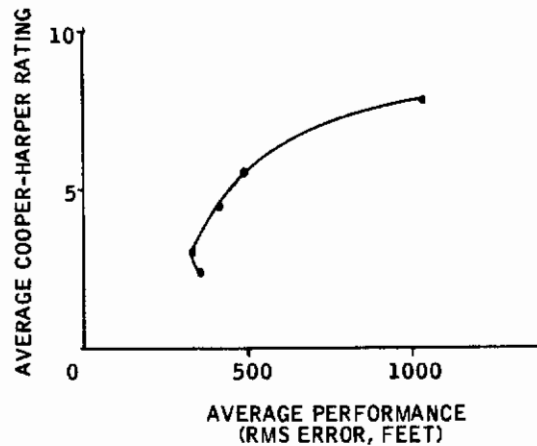


Figure 98. Rating/Performance Relationship



## SECTION VII CONCLUSIONS

In overview, the program has demonstrated that the design procedure developed here represents a powerful approach to the design of augmentation systems. The program has shown that handling-quality models for the controller/vehicle combination are a meaningful way to express design criteria, and that the F4C aircraft can be made to follow such models with a practical control system designed by the procedure. This is true at least to the resolution of pilot opinion and performance data gathered in the validation experiments. Some additional more specific items which emerged during the course of the program are restated briefly below:

- 1) Model-following performance of the F4C is constrained by rate limits of the actuators. In particular, the rapid roll rate response of model 4 cannot be matched at high command levels.
- 2) Bandwidths of the free airframe are good candidates for command model bandwidths in the design procedure.
- 3) The F4C's lateral-directional gain sensitivity over the flight envelope is low. The highest sensitivity occurs in the rudder channel, where some performance gains may be possible with a simple gain schedule.
- 4) Large deterioration ratios occur between the rms error responses of optimal controllers and those of practical controllers. This should not be discouraging, however, since the results here show that such deteriorations are still quite tolerable from the viewpoint of rating and performance data -- witness the insignificant differences between systems 4 and 5. Apparently the optimal controllers overdo the job of model-following. However, these statements must remain tentative because the deteriorations we are talking about are primarily in sideslip which could not be fully evaluated in either simulator (i. e., fixed-base and limited moving-base without lateral displacement).
- 5) Command magnitudes in the design equations are crucial to the quality of the final practical controller solution, as they influence the kinds of performance tradeoffs made by the optimization. At the moment no procedure other than design iteration is available to choose the magnitudes.

# Conclusions

Some of the items in this list naturally point to future areas of development. Certainly the question of command magnitudes should receive further study. Perhaps the computational algorithm could be extended to display the tradeoffs being made as the integration parameter,  $\lambda$ , grinds toward zero (this is straightforward) and to permit adjustment of magnitudes and/or quadratic weights in an on-line interactive fashion between designer and design algorithm (this is not so straightforward).

Other extensions of the algorithm which should be pursued are removal of fixed-gain constraints (i. e. , fixed plus variable gains) and applications to compensator design problems (other than the handling-quality model, which can be thought of as a feedforward compensator).

On a more fundamental note, the entire design procedure could be used to generate controllers for arbitrary handling-quality models -- for example, models which are not based on traditional "aircraft dynamics." It thus becomes a design tool for basic handling-quality studies in such problem areas as control-configured vehicles (CCV), space shuttle, V/STOL, and so on.

And finally, on a point of philosophy, the results of the validation program have shown that a high positive relationship exists between performance data and rating data, at least for the task used in this study. The value of collecting both kinds of data is the additional precision of measurement attained. In those situations where this precision is necessary we recommend that performance data be included along with rating data.

APPENDIX I  
HANDLING-QUALITIES DATA

The figures in this appendix are reproduced from their references without alteration. All legends, source references, and symbolism refer to the original references. We have added only the numbered double line circles which identify our choice of numerical values and the phrase "Figure 00: Taken from Reference [j]" at the bottom of each figure. These latter numbers refer to our own figure identification and our own list of references.

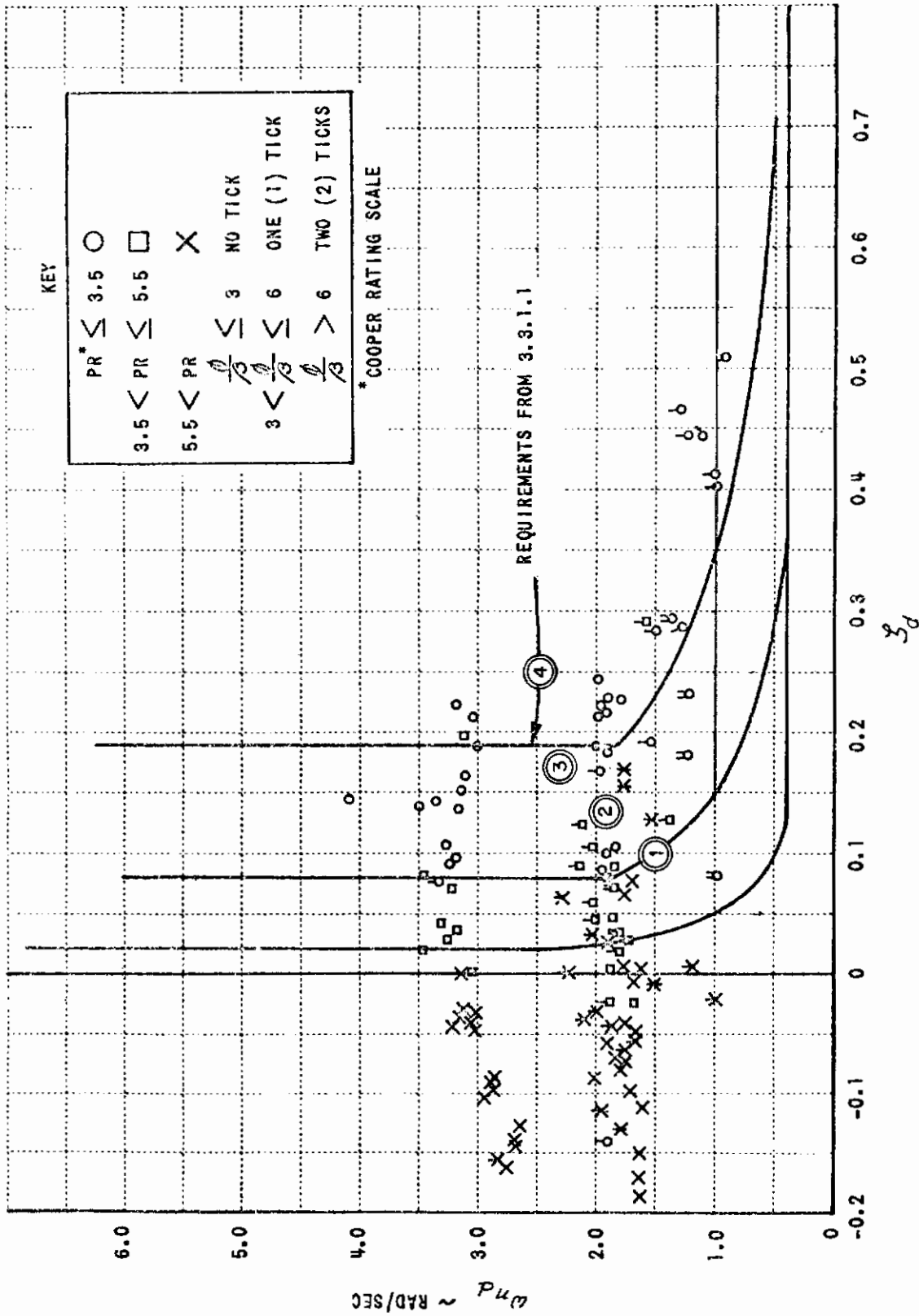


Figure 5 (3.3.1.1). DUTCH ROLL DATA (FROM REFERENCES G7 AND F21)

Figure 99. Data for Handling-Quality Parameters  $s_1$  and  $s_2$  (Taken from Ref. 2)

①	Fig. 1a	Ref. 3	$1.63 < \omega_d < 1.99$
②	Fig. 1b	Ref. 3	$2.62 < \omega_d < 3.50$
③	Fig. 1a	Ref. 8	$1.57 < \omega_d < 1.90$
④	Fig. 3a	Ref. 9	$1.44 < \omega_d < 1.57$
⑤	Fig. 3a	Ref. 7	$1.08 < \omega_d < 1.22$
⑥	Fig. 3a	Ref. 7	$1.98 < \omega_d < 2.38$
⑦	Fig. 3a	Ref. 7	$3.90 < \omega_d < 4.58$
⑧	Fig. 2a	Ref. 4	$2.27 < \omega_d < 3.13$
⑨	Fig. 2a	Ref. 4	$3.24 < \omega_d < 3.59$
⑩	Fig. 2b	Ref. 4	$4.00 < \omega_d < 4.44$
⑪	Fig. 2b	Ref. 4	$5.00 < \omega_d < 5.25$
⑫	Fig. 2b	Ref. 4	$5.85 < \omega_d < 6.46$

Raised  
one rating point  
over Fig. 4

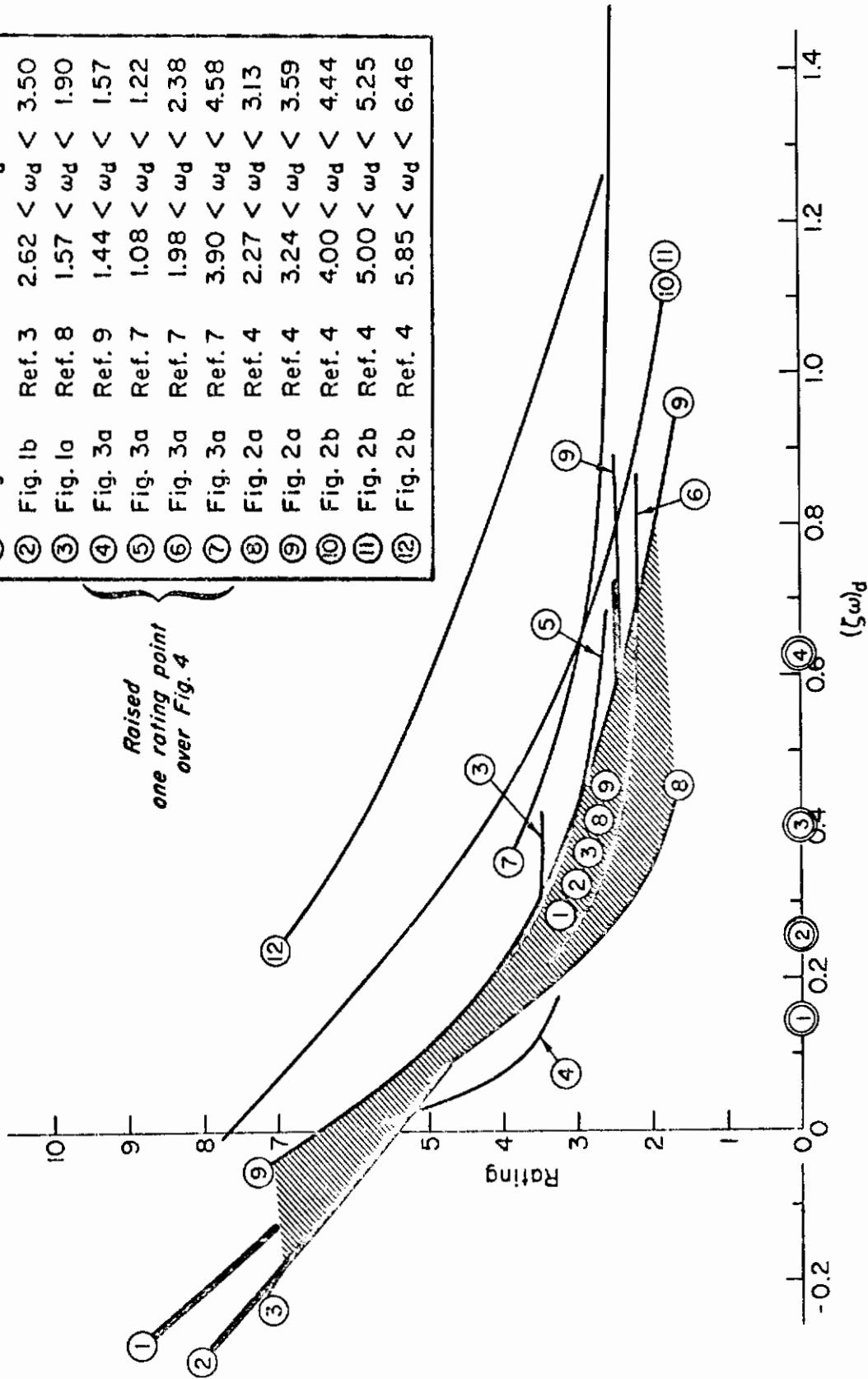


Figure 6. Superposition of "Adjusted" Faired Data  
a) Ratings vs.  $(z\omega)_d$

Figure 100. Data for Handling-Quality Parameters  $s_1$  and  $s_2$   
(Taken from Ref. 6)

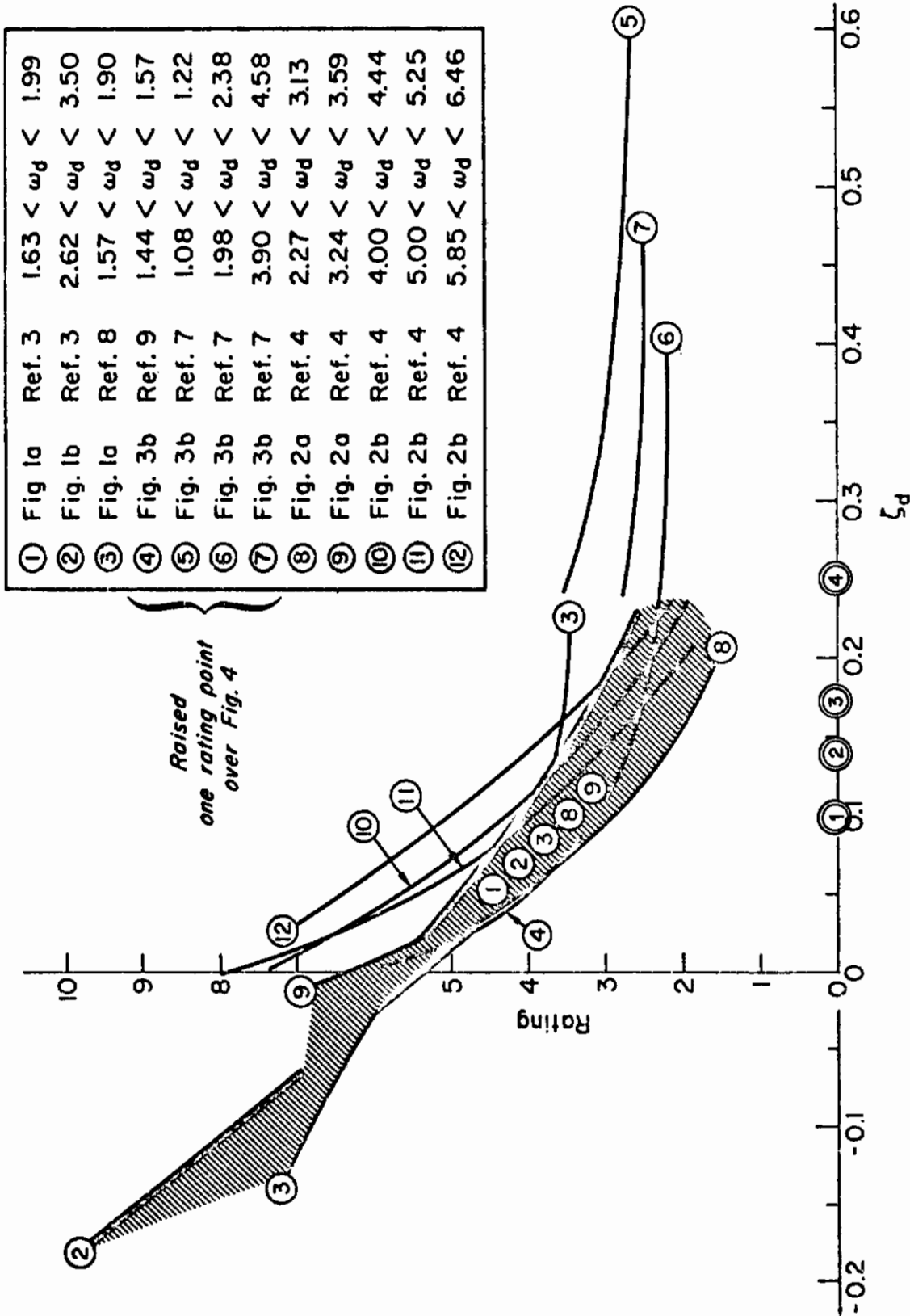


Figure 6 (concl'd). Superposition of "Adjusted" Paired Data  
 b) Ratings vs.  $s_d$

Figure 100. Data for Handling-Quality Parameters  $s_1$  and  $s_2$   
 (Taken from Ref. 6) (Concluded)



REF. 12 IS HERE REF. F30  
 REF. 13 IS HERE REF. F22  
 REF. 14 IS HERE REF. F19  
 REF. 15 IS NASA TN D-1328  
 REF. 16 IS NASA TN D-792  
 REF. 57 IS HERE REF. B48

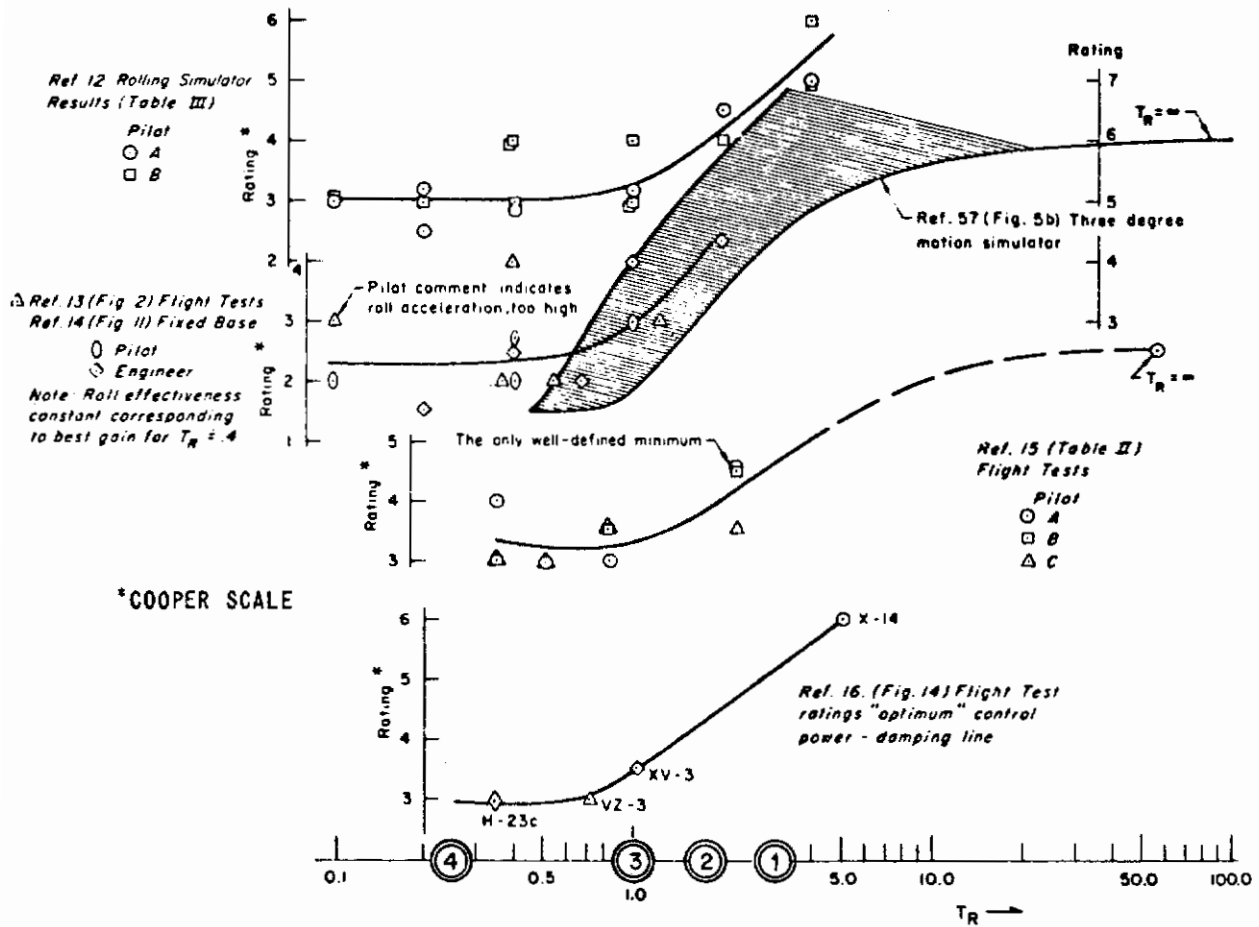


Figure 1 (3.3.1.2)

RATINGS VERSUS ROLL DAMPING - FLIGHT TEST,  
 MOVING-BASE, FIXED-BASE WITH RANDOM INPUT  
 (FROM REFERENCE F8)

Figure 101. Data for Handling-Quality Parameter  $s_3$   
 (Taken from Ref. 2)

REF. 13 IS HERE REF. F22

REF. 14 IS HERE REF. F30

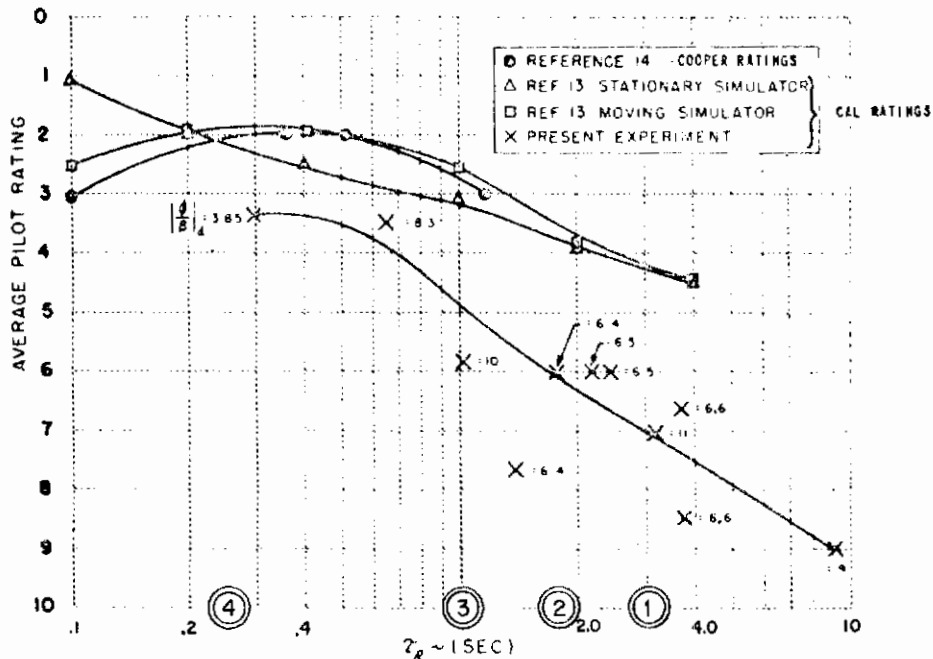


Figure 16 (3.3.1.2)

AVERAGE PILOT RATING OF ROLL MODE TIME CONSTANT  
(FROM REFERENCE F12)

Figure 102. Data for Handling-Quality Parameter  $s_3$   
(Taken from Ref. 2)

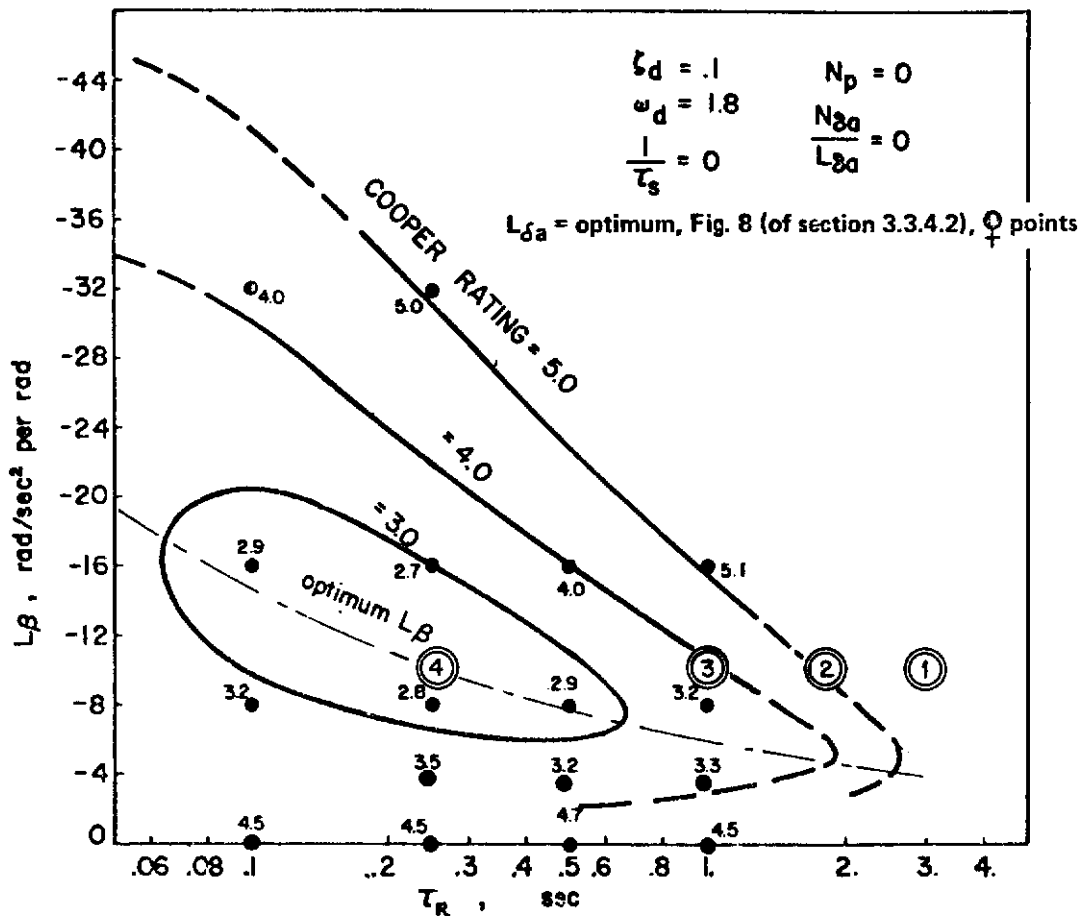


Figure 1 (3.3.6.3)

LATERAL FLYING QUALITIES BOUNDARIES  
 ( $L_{\beta}$  vs.  $\tau_R$ ,  $\zeta_d = .1$ ) (FROM REFERENCE G10)

Figure 103. Data for Handling-Quality Parameter  $s_5$   
 (Taken from Ref. 2)

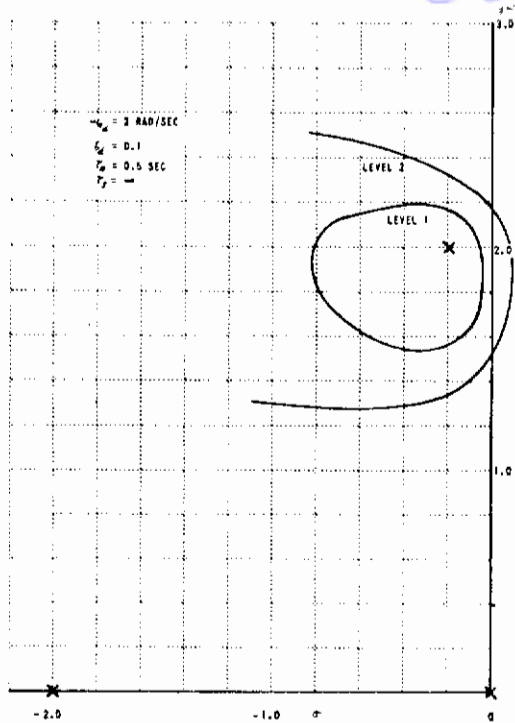


Figure 17 (3.3.2.2)  
 AREAS OF  $p/\delta_{AS}$  TRANSFER FUNCTION  
 ZERO LOCATIONS FOR FLIGHT PHASE  
 CATEGORIES A AND C

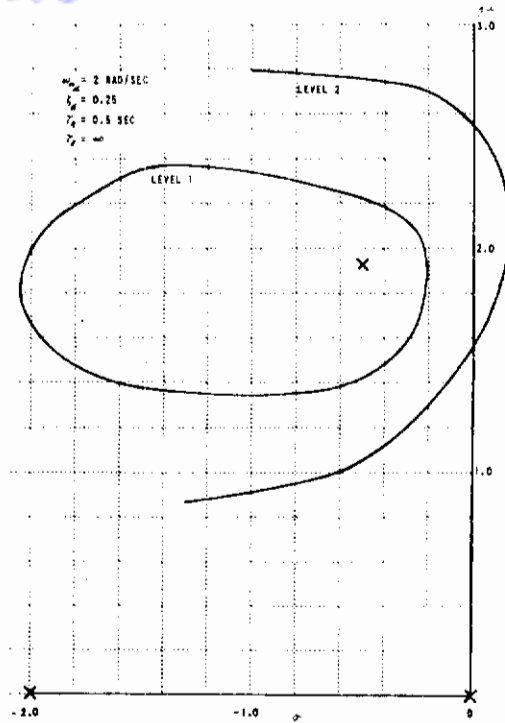


Figure 18 (3.3.2.2)  
 AREAS OF  $p/\delta_{AS}$  TRANSFER FUNCTION  
 ZERO LOCATIONS FOR FLIGHT PHASE  
 CATEGORIES A AND C

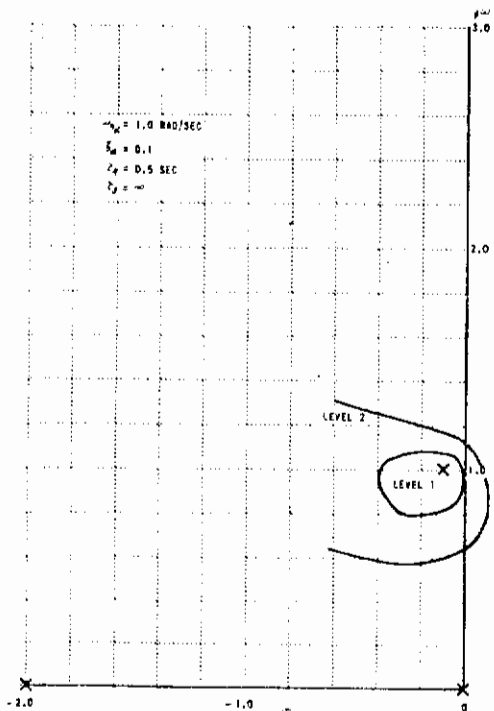


Figure 19 (3.3.2.2)  
 AREAS OF  $p/\delta_{AS}$  TRANSFER FUNCTION  
 ZERO LOCATIONS FOR FLIGHT PHASE  
 CATEGORIES A AND C

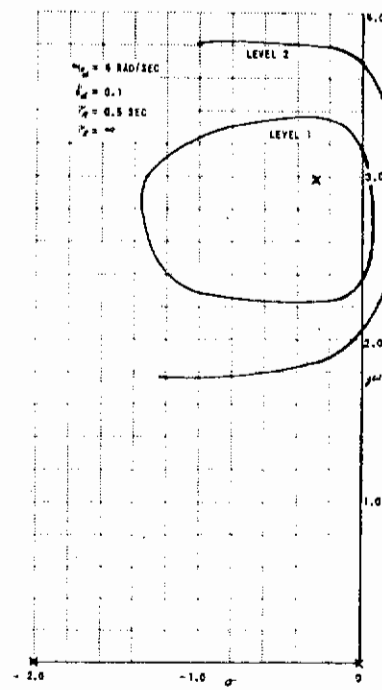


Figure 20 (3.3.2.2)  
 AREAS OF  $p/\delta_{AS}$  TRANSFER FUNCTION  
 ZERO LOCATIONS FOR FLIGHT PHASE  
 CATEGORIES A AND C

Figure 104. Data for Handling-Quality Parameters  $s_6$  and  $s_7$   
 (Taken from Ref. 2)

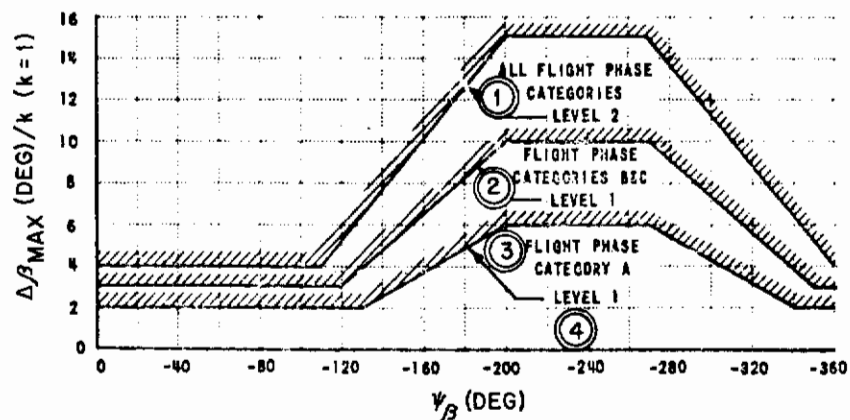


Figure 6 SIDESLIP EXCURSION LIMITATIONS

Figure 105. Data for Handling-Quality Parameter  $s_8$   
Sideslip Specification (Taken from Ref. 1)

APPENDIX II

EVALUATION OF  $\frac{\partial J}{\partial K^1}$ ,  $\frac{\partial^2 J}{\partial K^1 \partial K^{1T}}$ , AND  $\frac{\partial^2 J}{\partial K^1 \partial \lambda}$

The computational algorithm advanced in Section III involves repeated evaluation of first and second partial derivatives of the total cost,  $J$ . Equations for these partials are derived here. Since the performance index,  $J$ , of Equation (21) is a linear sum of individual plant indices,  $J(i)$ , however, the derivations need to be carried out for only one plant. This is done below with all  $i$ -dependence suppressed.

FIRST PARTIALS

Let  $X$  denote the steady-state covariance matrix of Equation (26) with the controller  $u = Kx = [(K^1 + K^3) M + \lambda K^2] x$ :

$$(F + GK) X + X (F + GK)^T + \Gamma \Gamma^T = 0 \quad (73)$$

Corresponding to  $X$ , define an adjoint matrix,  $S$ , as follows:

$$(F + GK)^T S + S (F + GK) + W + K^T R K = 0 \quad (74)$$

Then the performance index,  $J(K)$ , of Equation (28) is given by<sup>25</sup>

$$J(K) = \text{Tr} (W + K^T R K) X = \text{Tr} S \Gamma \Gamma^T \quad (75)$$

---

<sup>25</sup>This identity is a consequence of the following adjoint property of  $X$  and  $S$  (Ref. 30):

If

$$AX + XA^T + Q = 0$$

$$A^T S + SA + R = 0$$

Then

$$\text{Tr} RX = \text{Tr} SQ \quad (76)$$

Proof:

$$\begin{aligned} \text{Tr} RX &= \text{Tr} (-A^T S - SA) X \\ &= \text{Tr} S(-AX - XA^T) = \text{Tr} SQ \end{aligned}$$



The first partials of J can now be computed as follows:

$$\frac{\partial J}{\partial K_{ij}^1} = \text{Tr} \left[ 2K^T_R E^{ij} X + (W + K^T_R K) \frac{\partial X}{\partial K_{ij}^1} \right]$$

where  $E^{ij} \triangleq \frac{\partial K}{\partial K_{ij}^1}$  and  $\frac{\partial X}{\partial K_{ij}^1}$

are defined by

$$(F + GK) \frac{\partial X}{\partial K_{ij}^1} + \frac{\partial X}{\partial K_{ij}^1} (F + GK)^T + GE^{ij} X + X (GE^{ij})^T = 0 \quad (77)$$

Using Equation (76), we get

$$\begin{aligned} \frac{\partial J}{\partial K_{ij}^1} &= \text{Tr} \{ 2K^T_R E^{ij} X + S [GE^{ij} X + X (GE^{ij})^T] \} \\ &= 2 \text{Tr} [(K^T_R + SG) E^{ij} X] \end{aligned} \quad (78)$$

Thus, to evaluate all first partials of J we need only evaluate the two covariance-type equations, Equations (73) and (74), and the algebraic equations, Equation (78). This convenient property was first discovered by T. L. Johnson (Ref. 30).

## SECOND PARTIALS

The second partials are obtained in a similar manner:

$$\begin{aligned} \frac{\partial^2 J}{\partial K_{ij}^1 \partial K_{\ell m}^1} &= \text{Tr} \left[ 2E^{\ell m}_R E^{ij} X + 2K^T_R E^{ij} \frac{\partial X}{\partial K_{\ell m}^1} \right. \\ &\quad \left. + 2K^T_R E^{\ell m} \frac{\partial X}{\partial K_{ij}^1} + (W + K^T_R K) \frac{\partial^2 X}{\partial K_{ij}^1 \partial K_{\ell m}^1} \right] \\ &\quad (F + GK) \frac{\partial^2 X}{\partial K_{ij}^1 \partial K_{\ell m}^1} + \frac{\partial^2 X}{\partial K_{ij}^1 \partial K_{\ell m}^1} (F + GK)^T + GE^{\ell m} \frac{\partial X}{\partial K_{ij}^1} \\ &\quad + \frac{\partial X}{\partial K_{ij}^1} (GE^{\ell m})^T + GE^{ij} \frac{\partial X}{\partial K_{\ell m}^1} + \frac{\partial X}{\partial K_{\ell m}^1} (GE^{ij})^T = 0 \end{aligned}$$

$$\begin{aligned}
 \frac{\partial^2 J}{\partial K_{ij}^1 \partial K_{\ell m}^1} &= 2 \operatorname{Tr} \left[ E^{\ell m} R E^{ij} X + (K^T R + SG) \left( E^{ij} \frac{\partial X}{\partial K_{\ell m}^1} + E^{\ell m} \frac{\partial X}{\partial K_{ij}^1} \right) \right] \\
 &= 2 \left[ R_{\ell i} X_{jm} + \sum_a (K^T R + SG)_{ai} \left( \frac{\partial X}{\partial K_{\ell m}^1} \right)_{ja} \right. \\
 &\quad \left. + \sum_a (K^T R + SG)_{a\ell} \left( \frac{\partial X}{\partial K_{ij}^1} \right)_{ma} \right] \quad (79)
 \end{aligned}$$

and

$$\begin{aligned}
 \frac{\partial^2 J}{\partial K_{ij}^1 \partial \lambda} &= \operatorname{Tr} \left[ 2K^{2T} R E^{ij} X + 2K^T R E^{ij} \frac{\partial X}{\partial \lambda} + 2K^T R K^2 \frac{\partial X}{\partial K_{ij}^1} \right. \\
 &\quad \left. + (W + K^T R) \frac{\partial^2 X}{\partial K_{ij}^1 \partial \lambda} \right] \\
 (F + GK) \frac{\partial^2 X}{\partial K_{ij}^1 \partial \lambda} + \frac{\partial^2 X}{\partial K_{ij}^1 \partial \lambda} (F + GK)^T + GK^2 \frac{\partial X}{\partial K_{ij}^1} + \frac{\partial X}{\partial K_{ij}^1} (GK^2)^T \\
 + GE^{ij} \frac{\partial X}{\partial \lambda} + \frac{\partial X}{\partial \lambda} (GE^{ij})^T &= 0 \\
 \frac{\partial^2 J}{\partial K_{ij}^1 \partial \lambda} &= 2 \operatorname{Tr} \left[ K^{2T} R E^{ij} X + (K^T R + SG) \left( K^2 \frac{\partial X}{\partial K_{ij}^1} + E^{ij} \frac{\partial X}{\partial \lambda} \right) \right] \quad (80)^{26}
 \end{aligned}$$

So the second partials can be computed by solving  $(\ell + 3)$  covariance-type equations for the variables  $X$ ,  $S$ ,  $\partial X / \partial K_{ij}^1$ , and  $\partial X / \partial \lambda$ , where  $\ell$  is the number of free components of  $K^1$ . In addition, the algebraic equations (Equations (79) and (80)), must be evaluated.

## AN INTERPRETATION OF THE MATRICES $\partial X / \partial K_{ij}^1$ , REDUCED COMPUTATION TIME

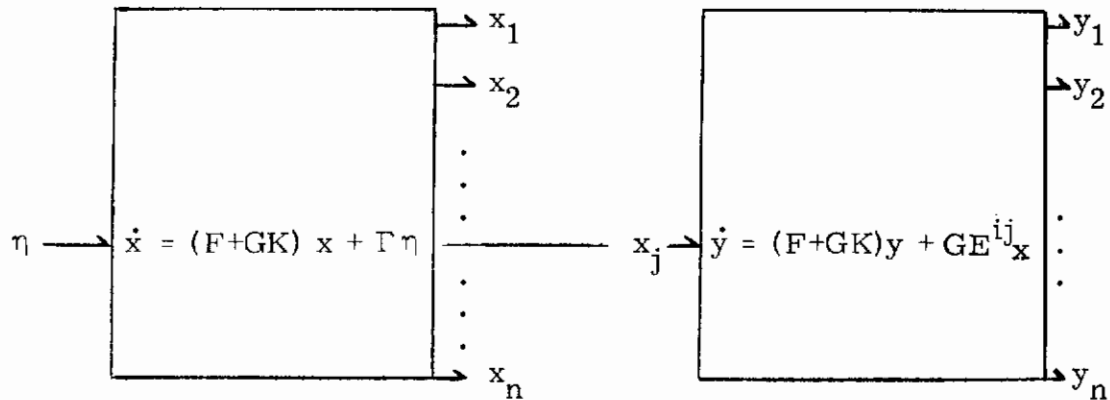
Recall that  $X$  is defined as the state covariance matrix of the controlled system i. e. ,

$$X(t) \triangleq E[x(t) x^T(t)], \text{ when } E[x(t)] = 0$$

<sup>26</sup>  $\partial X / \partial \lambda$  is defined by Equation (77) with  $E^{ij}$  replaced by  $K^2$ .

# Contrails

Then the matrix  $\frac{\partial X}{\partial K_{ij}^1}$  tells us how the covariances change as the feedback gain,  $K_{ij}^1$ , is changed. Aside from this "gradient" interpolation,  $\frac{\partial X}{\partial K_{ij}^1}$  can also be interpreted as a cross-correlation of states in the following 2n-dimensional system:



Original system with controller  $u = Kx$  driven by white noise,  $\eta$ .

Duplicate of original system with controller  $u = Kx$ , but driven by  $GE^{ij}x$ .

where

$$\frac{\partial X}{\partial K_{ij}^1} \equiv E [x(t) y^T(t) + y(t) x^T(t)] \quad (81)$$

The validity of this interpretation can be readily shown by evaluating the overall covariance matrix, call it  $X_{2n}$ , of the 2n-dimensional system. This matrix is the solution of

$$\begin{bmatrix} F + GK & GE^{ij} \\ \hline 0 & F + GK \end{bmatrix} X_{2n} + X_{2n} \begin{bmatrix} F + GK & GE^{ij} \\ \hline 0 & F + GK \end{bmatrix}^T + \begin{bmatrix} 0 & 0 \\ \hline 0 & \Gamma \Gamma^T \end{bmatrix} = 0$$

Let the term  $X_{2n}$  be partitioned as follows:

$$X_{2n} = \begin{bmatrix} E(yy^T) & E(yx^T) \\ E(xy^T) & X \end{bmatrix}$$

Then the (12)-element of the equation is

$$(F+GK) E(yx^T) + GE^{ij}X + E(yx^T) (F+GK)^T = 0$$

# Contrails

and the (21)-element is

$$(F+GK) E(xy^T) + E(xy^T) (F+GK)^T + X(GE^{ij})^T = 0$$

Adding these yields

$$(F+GK) E(xy^T + yx^T) + E(xy^T + yx^T) (F+GK)^T + GE^{ij}X \\ + X(GE^{ij})^T = 0$$

But this is the defining equation for  $\partial X / \partial K_{ij}^1$ , as given by Equation (77).

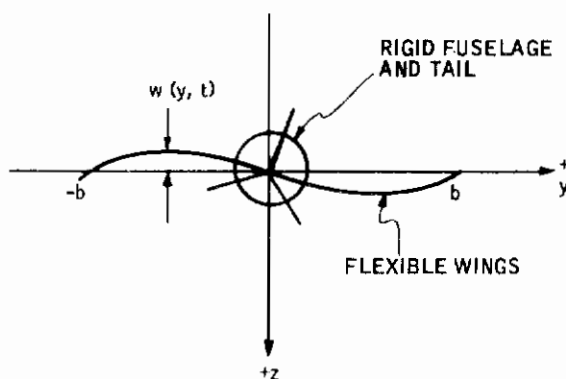
Looking at the structure of the  $2n$ -dimensional system, it is now evident that if some of the states are unaffected by control, then some of the  $y$ 's will be zero, and correspondingly, some elements of  $\partial X / \partial K_{ij}^1$  will be zero for all  $ij$ . For the case of the F4C lateral-axes problem, there are 20 states, 6 of which are unaffected by control (model states, wind states, and command model states). This means that each of the matrices,  $\partial X / \partial K_{ij}^1$ , can be computed by solving a  $(14 \times 14)$  and a  $(14 \times 6)$  covariance-like equation, as opposed to a single  $(20 \times 20)$  equation. The reduction in computing time is proportional to

$$\frac{2(14)^3}{(20)^3} = 0.68$$

## APPENDIX III BENDING MODE EQUATIONS

This appendix provides a derivation of approximate equations for the first asymmetric flexure mode of the F4 aircraft. The symbols used here are not all defined in the list of symbols and some do not correspond to the notation in the rest of the report; they are defined below as needed. All new definitions apply to this appendix only.

The approximate equations were derived by assuming that aircraft flexure consists of wing bending only, with rigid fuselage and tail. This type of flexure is illustrated in the sketch below:



Let  $w(y, t)$  denote the vertical deflection of the wing from the rigid-body axes. This deflection can be expressed as an infinite sum of products of ortho-normal mode shapes,  $\eta_i(y)$ , and mode amplitudes,  $\xi_i(t)$ , i. e.,

$$w(y, t) = \sum_{i=1}^{\infty} \xi_i(t) \eta_i(y) \quad (82)$$

If the mode shapes are known, then the energy methods of LaGrange can be used to derive differential equations for the amplitudes. The following steps are involved [ the details can be found in Bisplinghoff, pages 114-124 (Ref. 31)]:

1) Kinetic energy (T):

$$T = 1/2 \int_{-b}^b m(y) [\dot{w}(y, t)]^2 dy + 1/2 I [\dot{w}'(0, t)]^2 \quad (83)^{27}$$

<sup>27</sup> ( $\dot{\phantom{x}}$ ) denotes time differentiation and ( $\phantom{x}$ )' denotes differentiation with respect to  $y$ .

where

$m(y)$  = Mass distribution along the wing  
 $I$  = Aircraft-less-wing moment of inertia about the x-axis

$$T = \frac{1}{2} \sum_{j=1}^{\infty} M_j \dot{\xi}_j^2 + \frac{1}{2} I \sum_{j=1}^{\infty} \sum_{k=1}^{\infty} \dot{\xi}_j \dot{\xi}_k \eta_j'(0) \eta_k'(0) \quad (84)$$

$$M_j = \int_{-b}^b m(y) \eta_j^2(y) dy \quad (85)$$

2) Potential energy (U, strain energy in the distorted wing):

$$U = \frac{1}{2} \int_{-b}^b \ell(y) \frac{\partial^2 w}{\partial y^2} dy \quad (86)$$

where

$\ell(y)$  = Moment acting on the wing cross section at y

$\frac{\partial^2 w}{\partial y^2} dy$  = Incremental displacement due to  $\ell$

$$U = \frac{1}{2} \sum_{i=1}^{\infty} \sigma_i^2 M_i \xi_i^2 \quad (87)$$

$\sigma_i$  = eigenvalue associated with the mode shape  $\eta_i(y)$

3) Apply Lagrange's Equation:

$$\frac{d}{dt} \left( \frac{\partial T}{\partial \dot{\xi}_i} \right) - \frac{\partial T}{\partial \xi_i} + \frac{\partial U}{\partial \xi_i} = Q_i \quad i = 1, 2, \dots \quad (88)$$

where

$Q_i$  = Generalized force satisfying

$$\text{Incremental work} = \sum_i Q_i \delta \xi_i$$

yields

$$M_i \ddot{\xi}_i + I \sum_{k=1}^{\infty} \dot{\xi}_k \eta_k'(0) \eta_i'(0) + \sigma_i^2 M_i \xi_i = Q_i \quad (89)$$

$$Q_i = \int_{-b}^b F(y, t) \eta_i(y) dy + L \eta_i'(0) \quad (90)$$



where

$L$  = Total rolling moment about the x-axis

$F(y, t)$  = Distributed force acting along the wing

- 4) Finally, if only the first asymmetric bending mode is assumed to be significant, the mode equations become

$$\{M_1 + I[\eta_1'(0)]^2\} \ddot{\xi}_1 + \sigma_1^2 M_1 \xi_1 = Q_1 \quad (91)$$

with

$$Q_1 = Q_{1\xi} \dot{\xi} + Q_{1p} p + Q_{1r} r + Q_{1\beta} \beta + Q_{1\delta AS} \delta AS + Q_{1\delta R} \delta R \quad (92)$$

The coefficients of the last equation are given approximately by the expressions below. Implicit in these formulas are the assumption of aerodynamic strip theory, the neglect of unsteady aerodynamics, and various other cold-blooded approximations:

$$Q_{1\xi} = -q \int_{-b}^b C_{l\alpha}(y) c(y) \frac{\eta_1(y)}{U_0} \eta_1(y) dy \quad (93)$$

(neglecting tail effects and structural damping)

$$\begin{aligned} Q_{1\beta} = & -q \int_{-b}^b C_{l\alpha}(y) c(y) \gamma(y) \eta_1(y) dy + \\ & -q \int_{-b}^b C_{l\alpha}(y) c(y) \alpha_0 \frac{M^2}{1-M^2 \cos^2 \Lambda(y)} \cos \Lambda(y) \sin \Lambda(y) \eta_1(y) dy + \\ & + L_\beta \eta_1'(0) \end{aligned} \quad (94)$$

$$Q_{1p} = -q \int_{-b}^b C_{l\alpha}(y) c(y) \frac{y}{U_0} \eta_1(y) dy + L_p \eta_1'(0) \quad (95)$$

$$Q_{1r} = q \int_{-b}^b C_{l\alpha}(y) c(y) \frac{\alpha_0}{U_0} y \eta_1(y) dy + L_r \eta_1'(0) \quad (96)$$

$$Q_{1\delta AS} = L_{\delta AS} [\eta_1'(0) + \eta_1(y_{AS})/y_{AS}] \quad (97)$$

$$Q_{1\delta R} = \eta_1'(0) L_{\delta R} \quad (98)$$

where

- $L_u$  = Partial derivative of total rolling moment with respect to the variable,  $u$
- $c(y)$  = Wing aerodynamic chord
- $C_{l\alpha}(y)$  = Lift coefficient
- $U_o$  = Nominal velocity
- $\alpha_o$  = Nominal angle of attack
- $q$  = Dynamic pressure
- $\Lambda(y)$  = Sweep angle of the  $\frac{1}{4}$  chord line
- $\gamma(y)$  = Dihedral angle
- $y_{AS}$  = Position of aileron/spoiler center of pressure

In addition, the bending mode itself influences the rigid-body equations through the derivatives

$$\frac{Y_{\xi}}{mU_o}, \quad \frac{Y'_{\xi}}{mU_o}, \quad \frac{L_{\xi}}{I_x}, \quad \frac{L'_{\xi}}{I_x}, \quad \frac{N_{\xi}}{I_z}, \quad \frac{N'_{\xi}}{I_z}$$

These are given by the following approximate expressions:

$$\frac{Y_{\xi}}{mU_o} \approx \frac{q}{mU_o} \int_{-b}^b C_{l\alpha}(y) c(y) \alpha_o \eta_1'(y) dy \quad (99)$$

$$\frac{Y'_{\xi}}{mU_o} \approx \frac{Y_p}{mU_o} \eta'(0) \quad (\text{assuming tail and fuselage effects predominate}) \quad (100)$$

$$\frac{L_{\xi}}{I_x} \approx 0 \quad (101)$$

$$\frac{L'_{\xi}}{I_x} \approx -\frac{q}{I_x} \int_{-b}^b C_{l\alpha}(y) c(y) y \frac{\eta_1(y)}{U_o} dy \quad (102)$$

$$\frac{N_{\xi}}{I_z} \approx 0 \quad (103)$$

$$\frac{N'_{\xi}}{I_z} \approx \frac{N_p}{I_z} \eta'(0) \quad (\text{assuming tail and fuselage effects predominate}) \quad (104)$$

# Contrails

where

$m$  = Total aircraft mass

$I_x, I_y, I_z$  = Total aircraft moments of inertia about x, y, z axes

$Y_u$  = Partial of total side force with respect to u

$N_u$  = Partial of total yawing moment with respect to u

Equations (93) through (104) were evaluated for flight condition 8, which exhibits the low aerodynamic damping usually associated with flexure problems. The following F4 data and additional assumptions were used (Refs. 22, 32, and 33):

- 1) Assumed cubic mode shape

$$\eta_1(y) = -3.1 \cdot 10^{-4} y^2 (|y| - 14.2) \quad (105)$$

This shape is normalized on  $-b \leq y \leq b$ , where  $2b$  is the wing-span (38.4 ft), and it leaves the principal body axes of the aircraft unaltered.

- 2) Assumed elliptic load distribution

$$C_{\ell}(y) c(y) = \frac{\pi S}{b} C_L \sqrt{1 - y^2/b^2} = 86.8 C_L \sqrt{1 - y^2/368} \quad (106)$$

where

$C_L$  = Average lift coefficient

$S$  = Wing area (530 ft<sup>2</sup>)

- 3) Sweep angle

$$\Lambda(y) = \text{sgn}(y) 45 \text{ deg}$$

- 4) Dihedral angle

$$\gamma(y) = \begin{cases} 0 \text{ deg} & |y| < 13.3 \\ \text{sgn}(y) 12 \text{ deg} & |y| > 13.3 \end{cases}$$

- 5) Modal mass

$$\bar{M}_1 = M_1 + I [\eta_1'(0)]^2$$

$$= 2 \int_4^{19.2} 0.4(23.4 - y) \eta_1^2(y) dy = 3.02 \text{ slug-ft}^2$$

6) Experimentally-observed mode frequency

$$\omega_1 = \left\{ \frac{\sigma_1^2 M_1}{M_1 + I[\eta_1'(0)]^2} \right\}^{\frac{1}{2}} = (10.5) 2\pi = 66 \text{ rad/sec}$$

Both (5) and (6) assume wing tanks empty.

7) Aerodynamic data at  $M = 0.9$ ,  $h = 45,000$  ft

$$\begin{aligned} U_o &= 870 \text{ ft/sec} \\ q &= 180 \text{ lb/ft}^2 \\ L_\beta &\dot{=} -321,000 \text{ ft-lb/rad} \\ L_p &\dot{=} -18,700 \text{ ft-lb/(rad/sec)} \\ L_r &\dot{=} 9,400 \text{ ft-lb/(rad/sec)} \\ L_{\delta AS} &\dot{=} 151,000 \text{ ft-lb/rad} \\ L_{\delta R} &\dot{=} 23,800 \text{ ft-lb/rad} \\ Y_p/mU_o &\dot{=} 0.0006 \text{ (rad/sec)/(rad/sec)} \\ N_p/I_z &\dot{=} 0.0240 \text{ (rad/sec}^2\text{)/(rad/sec)} \\ \alpha_o &= 0.108 \text{ rad (wing angle of attack)} \\ C_{L\alpha} &= 3.87/\text{rad} \end{aligned}$$

The resulting mode amplitude equation is

$$\ddot{\xi} + 10.6\dot{\xi} + 4350\xi = 1800\beta - 27p + 3r + 580\delta_{AS} \quad (107)$$

with

$$\begin{aligned} Y_\xi/mU_o &\dot{=} -0.0027 \\ Y_\dot{\xi}/mU_o &\dot{=} 0 \\ L_\xi/I_x &\dot{=} -0.0033 \\ N_\xi/I_z &\dot{=} 0 \end{aligned}$$

This equation is characterized by a damping ratio of  $\zeta = 0.08$ . Its response to single hardover aileron commands consists of damped

# Contrails

oscillations with initial peak-to-peak magnitude  $\xi_{p-p} = \left(\frac{1160}{4350}\right)\left(\frac{30}{57.3}\right) = 0.14$ . The associated wing-tip oscillation is  $0.14 |\eta_1(19.2)| = 0.96$  inch peak-to-peak. These numbers appear reasonable for the F4 in low-q flight. At higher dynamic pressure, of course, initial oscillation magnitudes will be larger. However, this effect is offset by increased aerodynamic damping which tends to alleviate flexure problems.

APPENDIX IV  
TRANSFORMATION MATRICES,  $T_{rb}$ , FOR THE AIRFRAME

FC(1)

1.01148	0.317678E-01	-0.644542E-03	0.768181E-02
-0.136413E 00	0.622453E 00	0.766012E-02	-0.912952E-01
-0.174003E-01	-0.481583E-01	1.000000	-0.116452E-01
1.19060	3.29518	-0.668564E-01	0.796811E 00

FC(2)

1.00850	0.203526E-01	-0.406079E-02	0.149173E-01
-0.310320E-01	0.		
	0.25717E 00	0.148211E-01	-0.544452E-01
-0.190752E-02	-0.456616E-02	1.000000	-0.334672E-02
0.551170E 00	1.31937	-0.263243E 00	0.967021E 00

FC(3)

1.00121	0.113560E-02	-0.439669E-03	0.326380E-02
-0.889563E-02	0.991653E 00	0.323159E-02	-0.239891E-01
-0.266676E-03	-0.250221E-03	1.000000	-0.719155E-03
0.369511E 00	0.346710E 00	-0.134236E 00	0.996474E 00

FC(4)

1.00224	0.398546E-02	-0.756912E-03	0.499770E-02
-0.147008E-01	0.973851E 00	0.496616E-02	-0.327903E-01
-0.584555E-03	-0.103977E-02	1.000000	-0.130386E-02
0.442980E 00	0.787947E 00	-0.149646E 00	0.988073E 00

FC(5)

1.02631	0.762400E-01	-0.639053E-02	0.181204E-01
-0.744316E-01	0.784299E 00	0.180805E-01	-0.512670E-01
-0.447423E-02	-0.129652E-01	1.000000	-0.308176E-02
1.30802	3.79063	-0.317737E 00	0.900941E 0



# Contrails

## TRANSFORMATION MATRICES, $T_{rb}$ , FOR THE AIRFRAME (CONCLUDED)

FC(6)

1.000000	0.278036E-04	-0.147976E-06	0.555877E-04
-0.115626E-01	0.989622E 00	0.552317E-04	-0.207480E-01
-0.348555E-03	-0.312834E-03	1.000000	-0.625448E-03
-0.554398E 00	0.497581E 00	-0.264822E-02	0.994814E 00

FC(7)

1.001000	0.108766E-02	-0.710568E-04	0.138628E-02
-0.199671E-01	0.978843E 00	0.138221E-02	-0.269662E-01
-0.578226E-03	-0.612695E-03	1.000000	-0.780914E-03
0.732973E 00	0.776666E 00	-0.507397E-01	0.989904E 00

FC(8)

1.008000	0.240450E-01	-0.908134E-03	0.538660E-02
-0.477250E-01	0.857598E 00	0.537825E-02	-0.319011E-01
-0.189804E-02	-0.566337E-02	1.000000	-0.126872E-02
1.392000	4.15371	-0.156878E 00	0.930522E 00

FC(9)

0.998362E 00	-0.905921E-03	-0.180825E-03	-0.166040E-02
-0.149977E-01	0.991705E 00	-0.165561E-02	-0.152024E-01
-0.391222E-03	-0.216365E-03	0.999957E 00	-0.396560E-03
0.981607E 00	0.542876E 00	0.108360E-00	0.995000E 00

FC(10)

1.001212	0.228019E-01	-0.131261E-02	0.657772E-02
-0.605527E-01	0.885733E 00	0.656060E-02	-0.328763E-01
-0.277681E-02	-0.524001E-02	1.000000	-0.150763E-02
1.74552	3.29391	-0.189119E 00	0.947707E 00

FC(11)

1.00281	0.272530E-02	-0.408376E-03	0.371281E-02
-0.253380E-01	0.975435E 00	0.368097E-02	-0.334661E-01
-0.121222E-02	-0.117524E-02	1.000000	-0.160108E-02
0.748912E 00	0.726064E 00	-0.108798E 00	0.989152E 00

## APPENDIX V

### QUALITATIVE CHARACTERISTICS AND FORMAL EXPERIMENTAL TRIALS OF PRACTICAL CONTROLLER 7

This appendix contains analog traces which document qualitative characteristics of practical controller PC7 and show typical formal experimental trials. The traces include the information described in the paragraphs that follow.

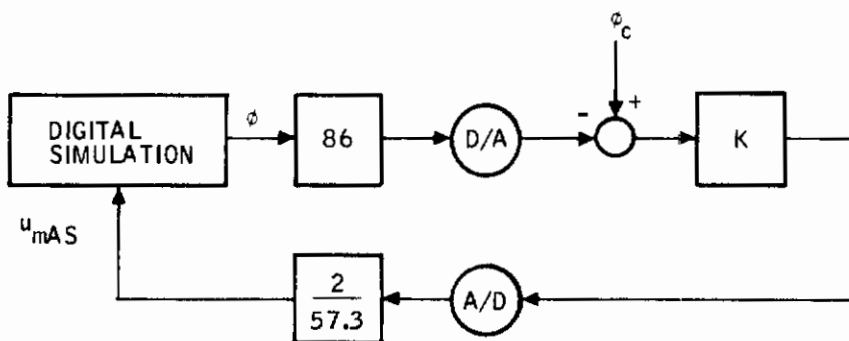
#### DEMONSTRATION FLIGHTS

Figures 106 through 115 are analog traces of piloted demonstration flights taken at Minneapolis with the practical controller. These show that the controller is tolerant of gusts, hardover rudder failures, and engine-out conditions.

The flights were flown at flight conditions 2 through 11 by pilot/experimenter E. D. Skelley. The gust environment was 6-ft/sec lateral gusts with spectral bandwidth  $\omega = U_0/1750$ . All failures were induced from the cockpit by the pilot.

#### AUTOMATIC OUTER LOOPS

Figure 116 shows Minneapolis analog traces of the practical controller with an additional outer bank angle hold loop. This loop consists of bank angle-to-lateral command feedback and was mechanized as follows:



$$K_{\phi} = (86) \left( \frac{2}{57.3} \right) K = 3K$$

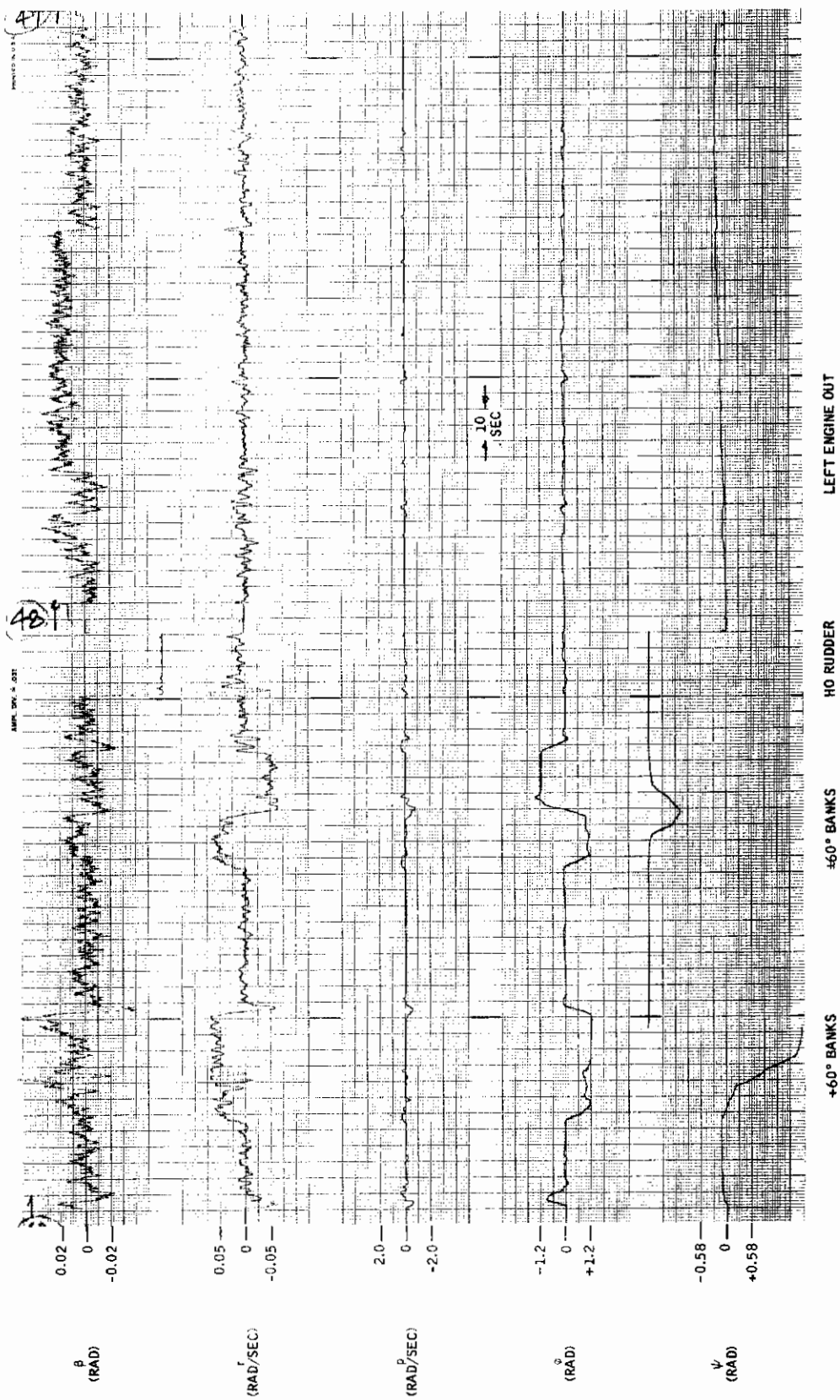


Figure 106. Demonstration Flights -- Flight Condition 2

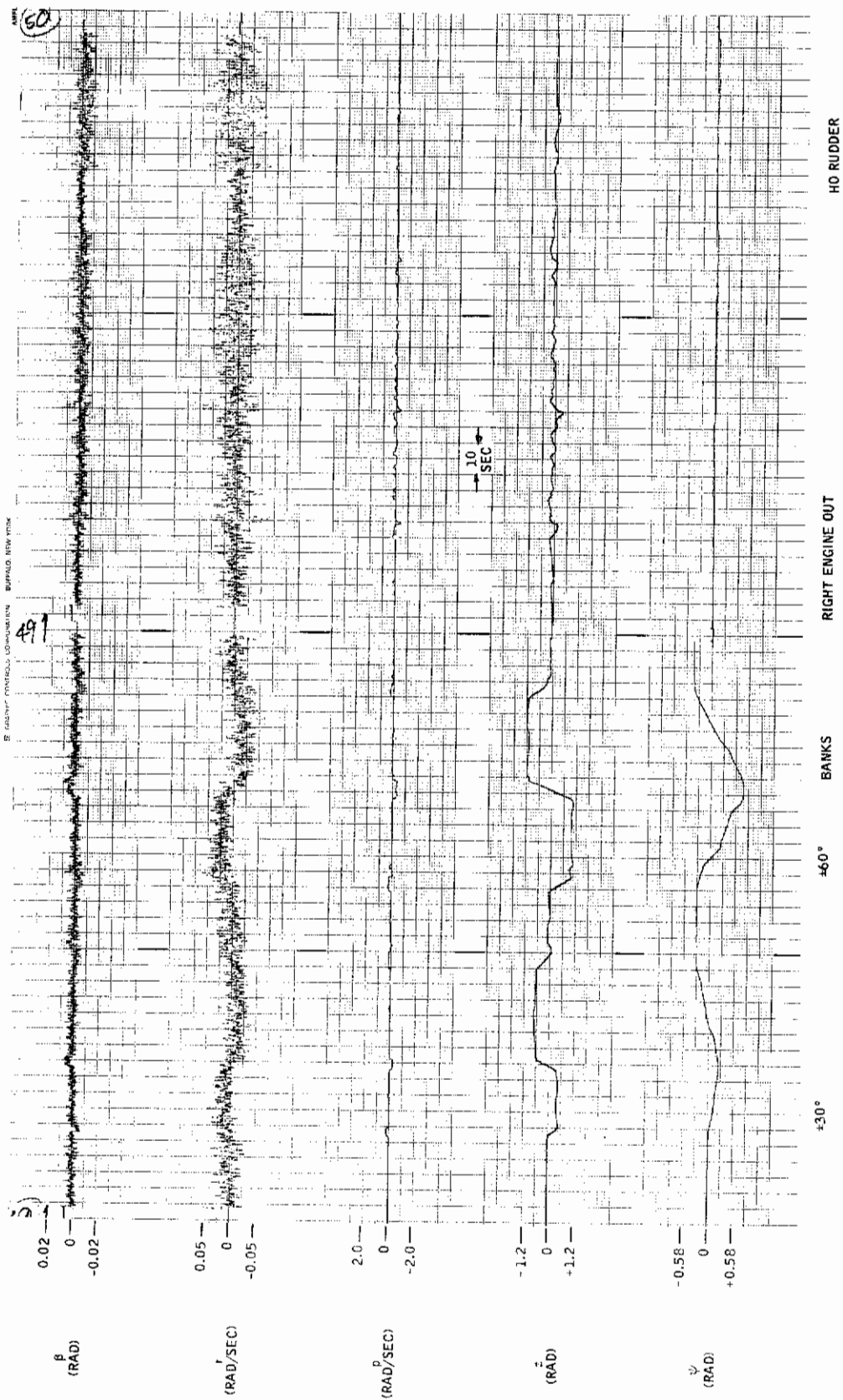


Figure 107. Demonstration Flights -- Flight Condition 3



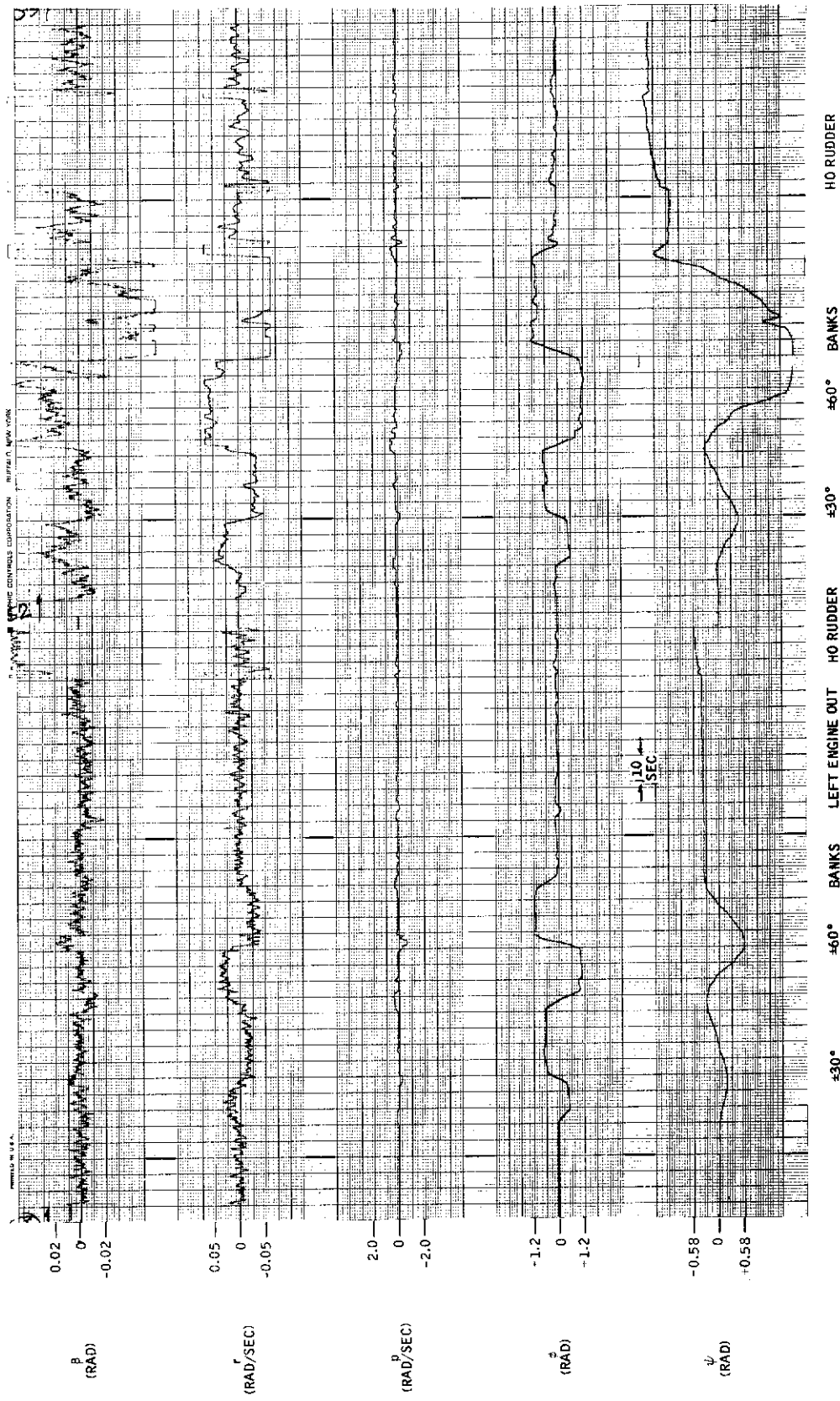


Figure 108. Demonstration Flights --  
Flight Condition 4

Figure 109. Demonstration Flights --  
Flight Condition 5

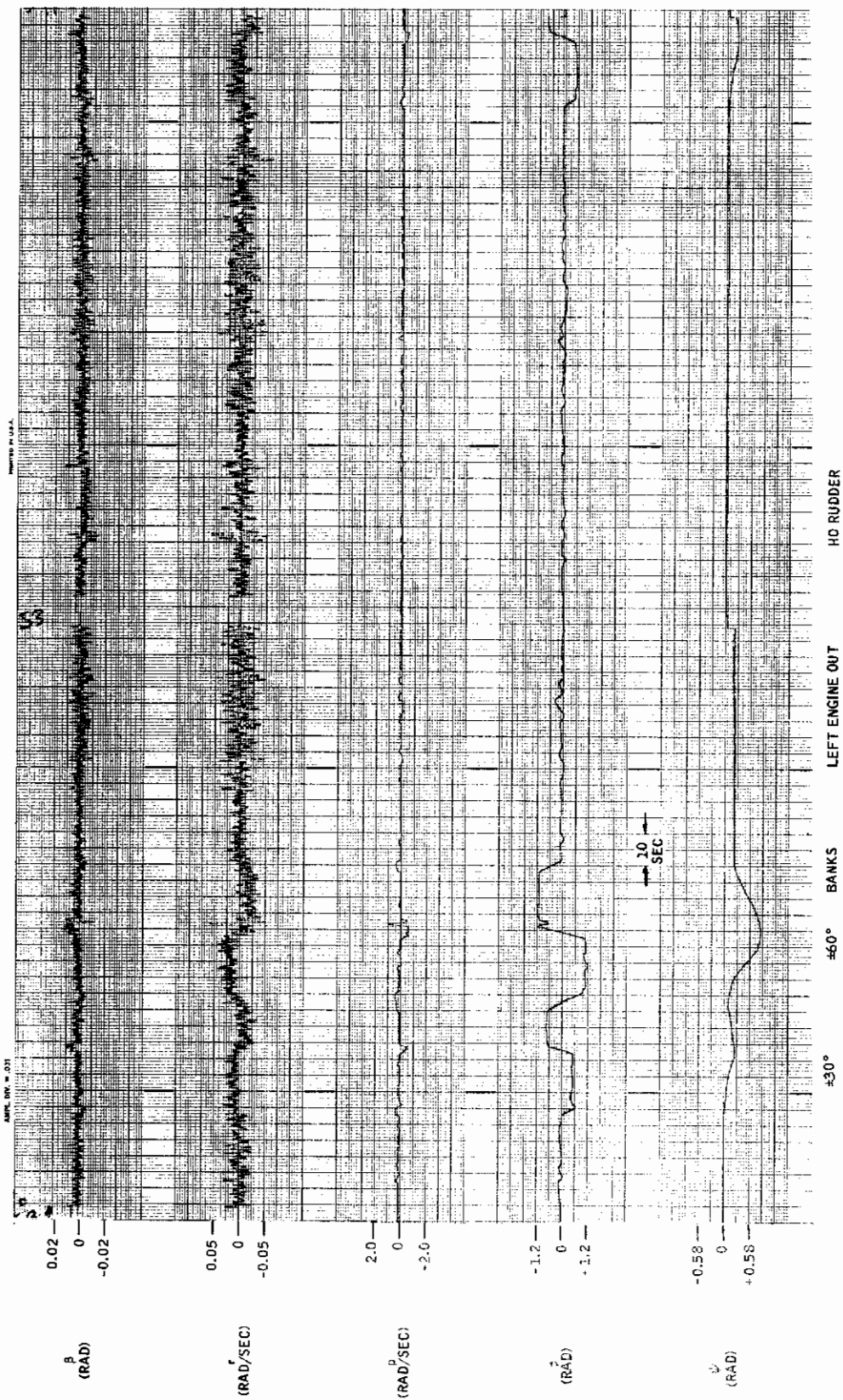


Figure 110. Demonstration Flights -- Flight Condition 6



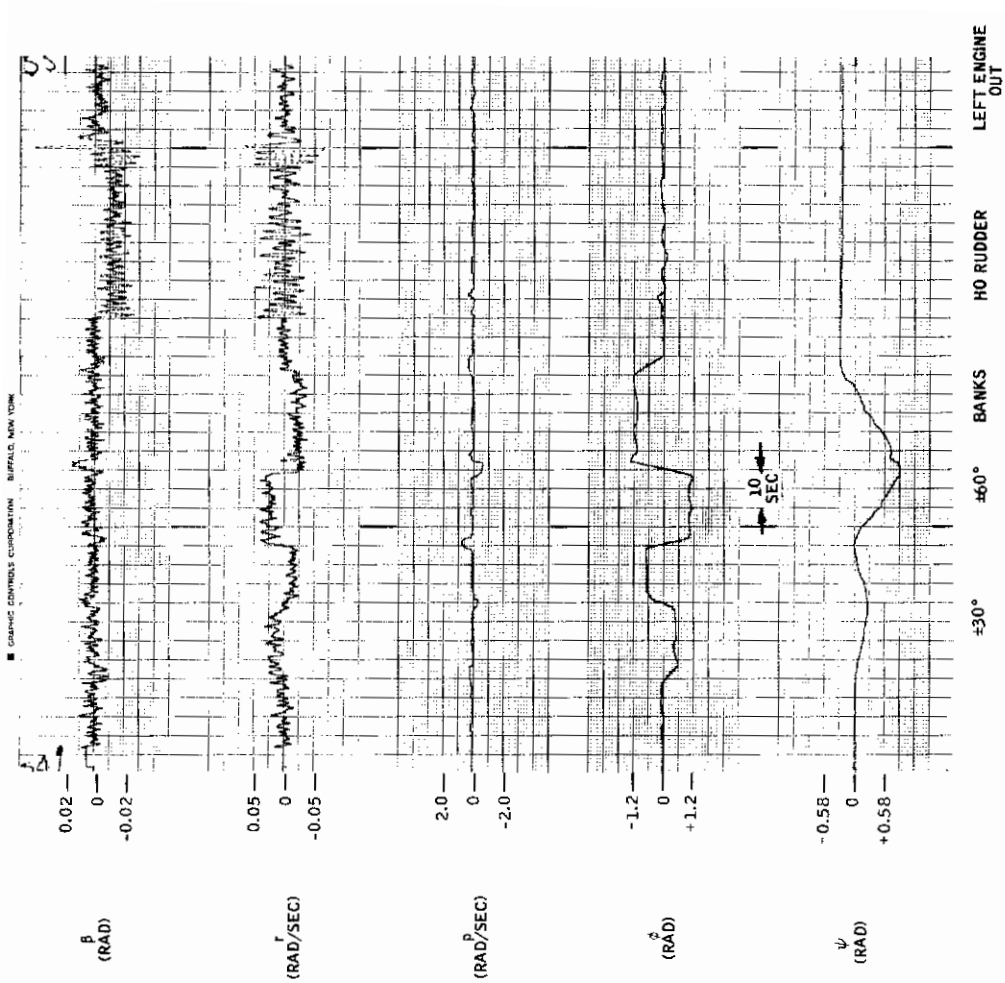


Figure 111. Demonstration Flights -- Flight Condition 7

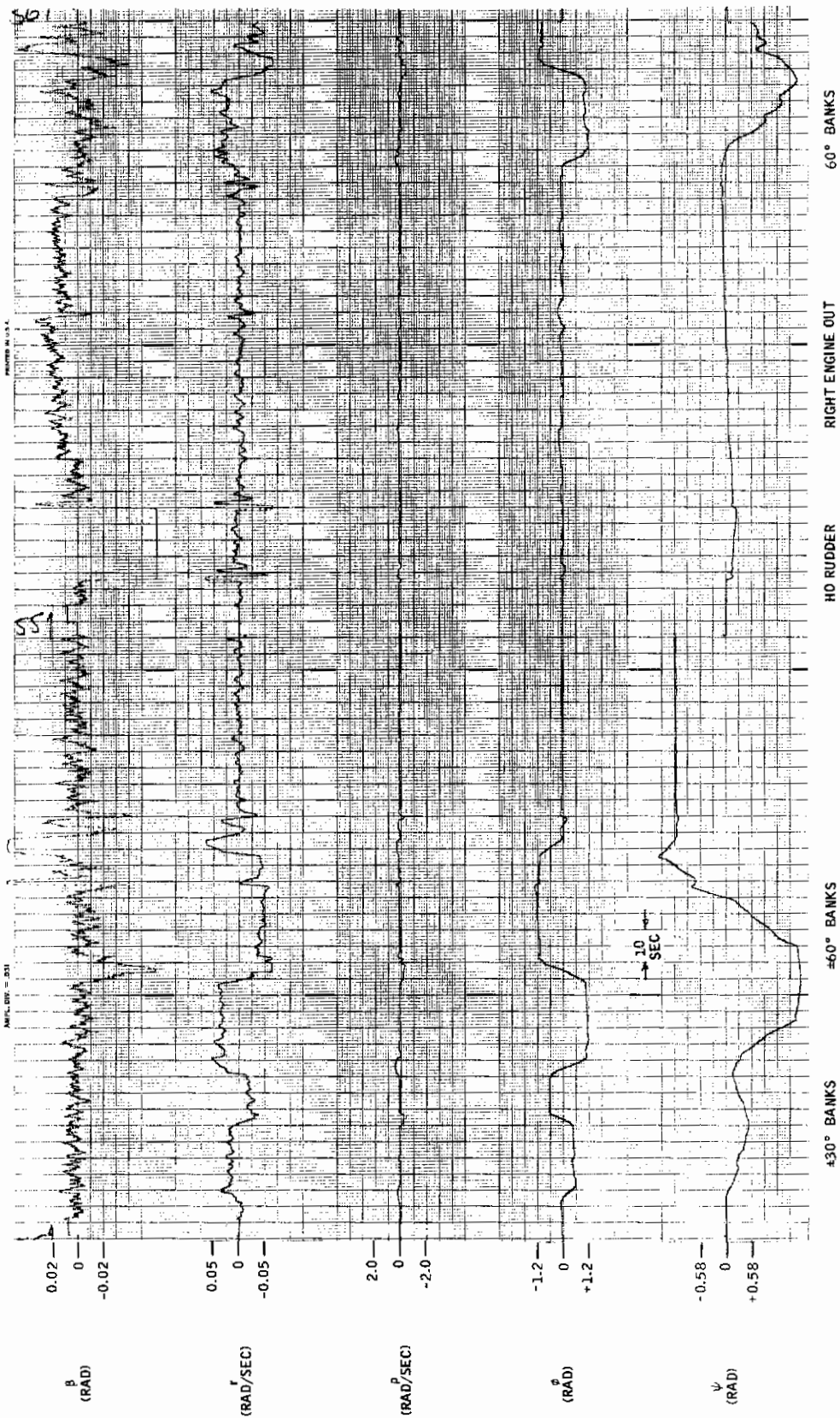


Figure 112. Demonstration Flights -- Flight Condition 8



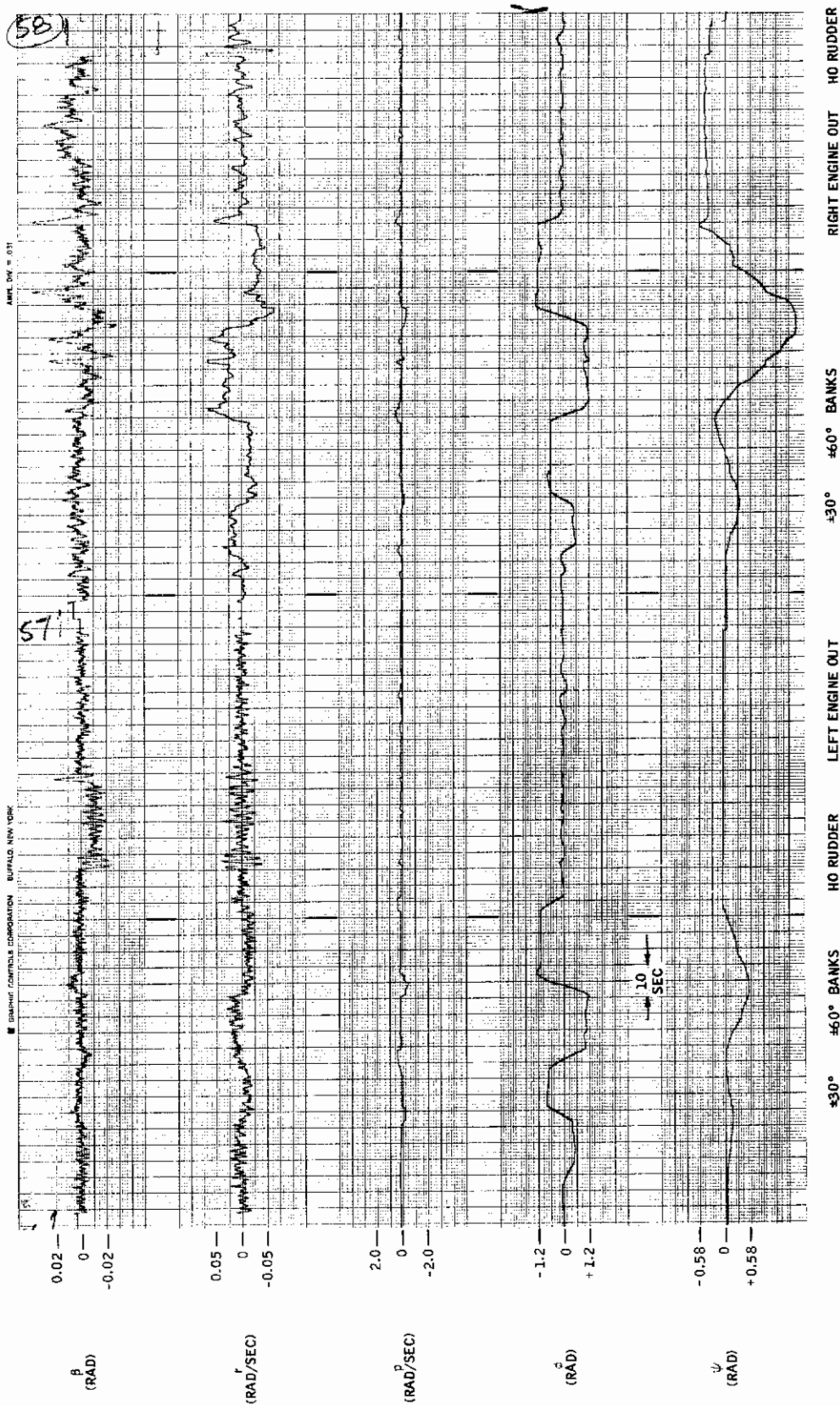


Figure 114. Demonstration Flights -- Flight Condition 10

Figure 113. Demonstration Flights -- Flight Condition 9

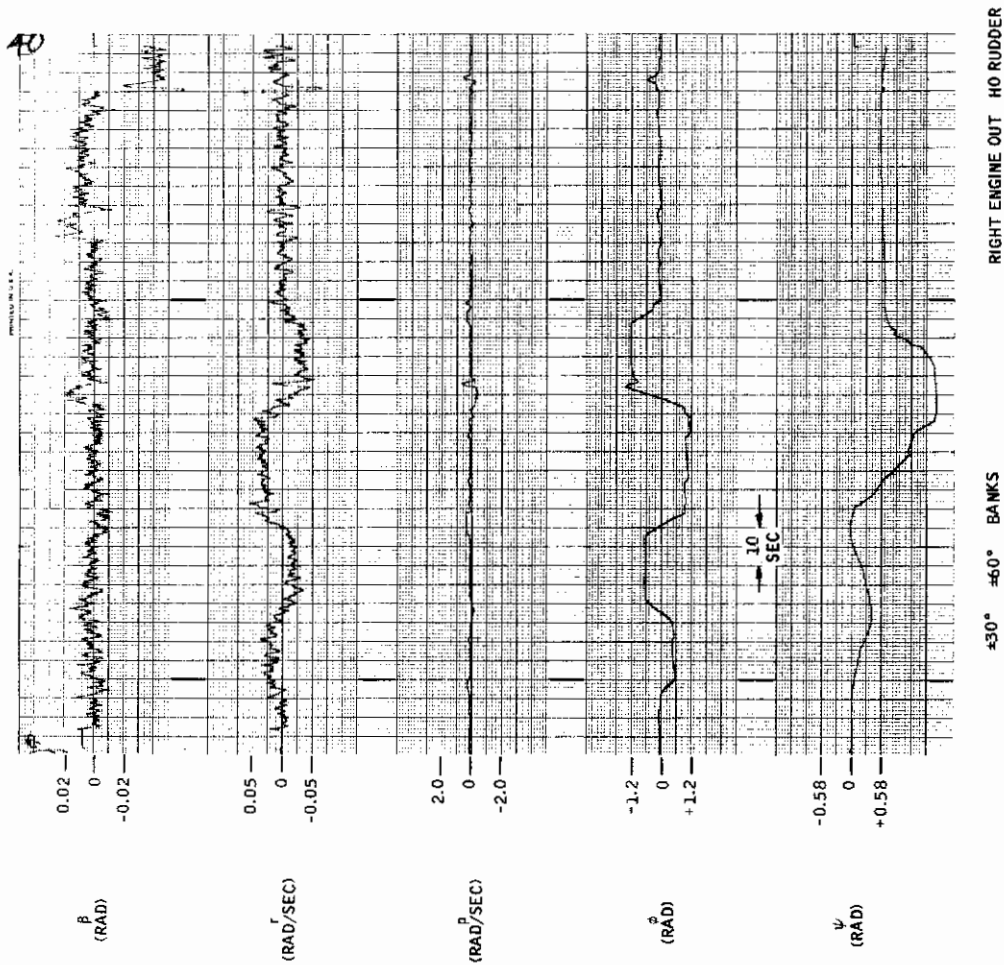


Figure 115. Demonstration Flights -- Flight Condition 11

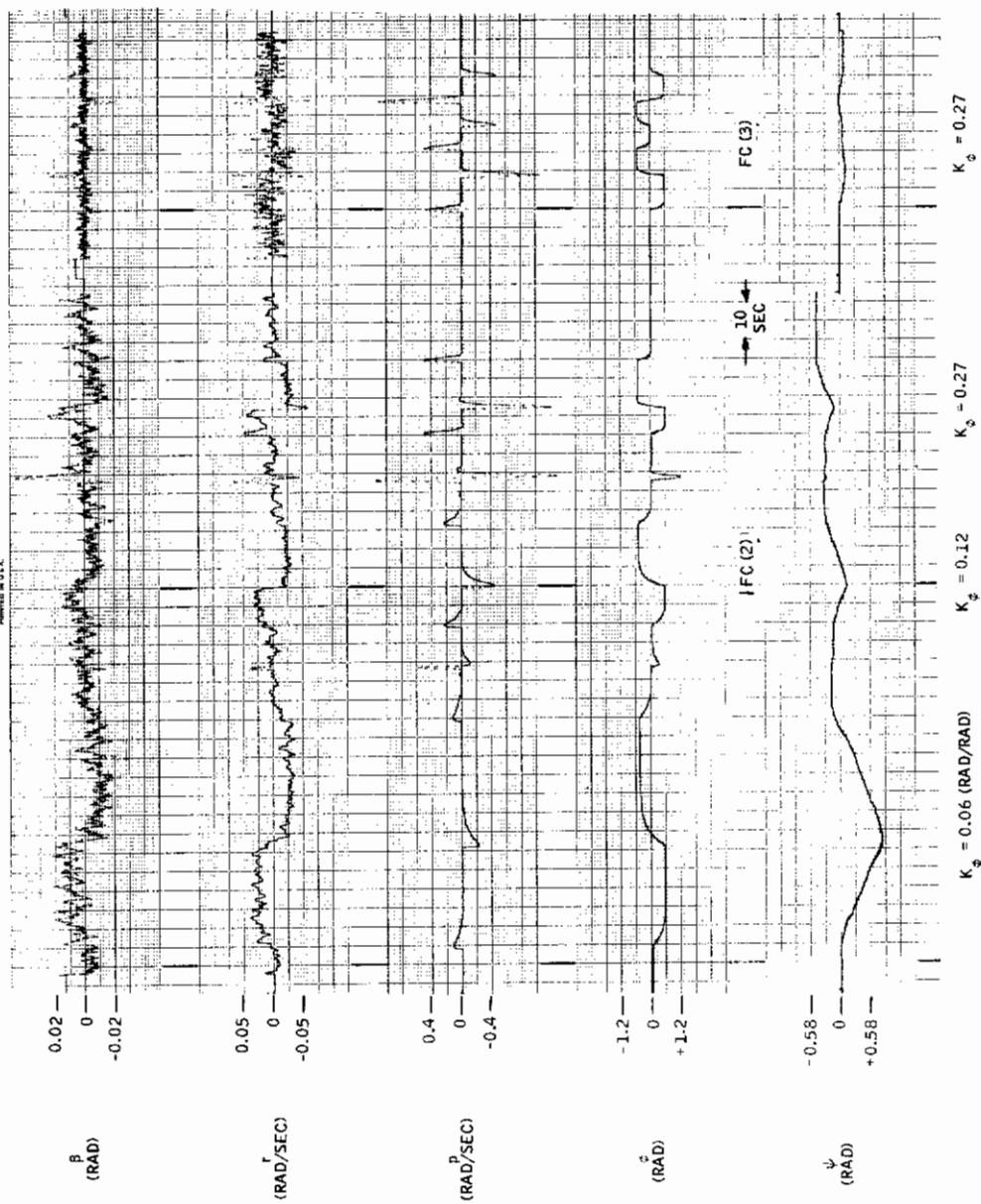


Figure 116. Practical Controller with Bank Angle Hold Loop ( $\pm 30$ -Deg Bank Angle Commands)

## SENSOR NOISE

Figure 117 shows WPAFB traces of the practical controller with sensor noise. The noise levels were 2 ft/sec<sup>2</sup> rms on the accelerometer and 0.05 rad/sec rms on each rate gyro. The noise was mechanized for each instrument by drawing three random numbers ( $\eta_1$ ,  $\eta_2$ ,  $\eta_3$ ) from a uniform (0, 1) digital number generator. These were combined as follows:

$$\eta = 4\sigma (\eta_1 + \eta_2 + \eta_3 - 1.5)$$

where  $\sigma$  is the desired rms level. The variable,  $\eta$ , was then added to the instrument output at each sample time.

## SAMPLE TRIALS OF FORMAL EXPERIMENTS

Typical analog traces of formal data trials for both the Minneapolis and WPAFB simulations are shown in Figures 118 through 129. These show various lateral-directional variables and the displayed error signals for each trial. The lateral error is unique in that it was not displayed directly but transformed by the following equation:

$$\left. \begin{array}{l} \text{Displayed} \\ \text{Lateral error} \end{array} \right\} = K \tan^{-1} (0.0004 E_y)$$

where  $E_y$  is in feet. The constant,  $K$ , was adjusted such that the maximum value of the  $\tan^{-1}(\cdot)$  function would just saturate the localizer display [i. e., for a 100-volt instrument  $K = 100/(\pi/2) = 63.7$ ].

This procedure eliminates saturation of the localizer display for all finite errors.



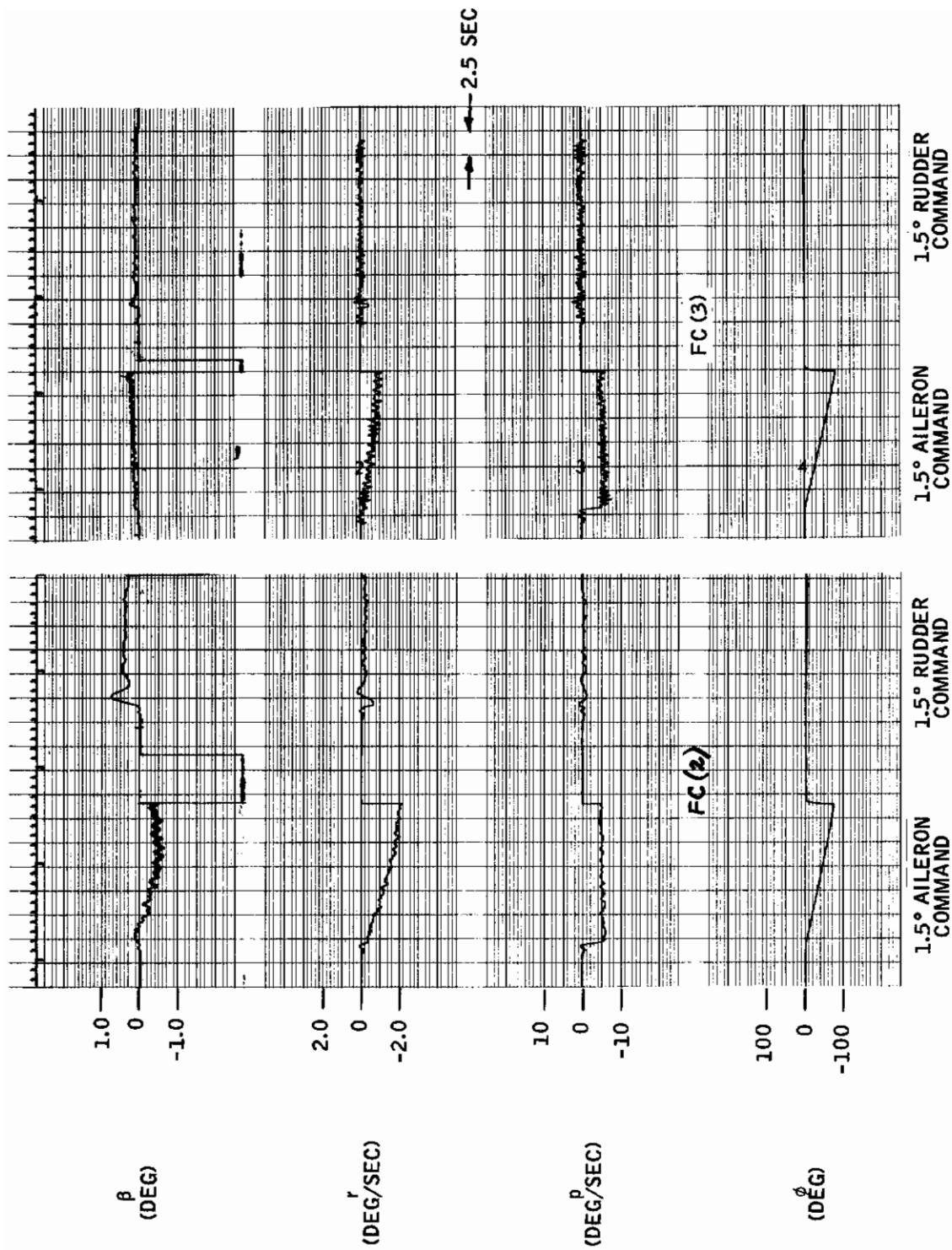


Figure 117. Practical Controller with Sensor Noise  
 (2 Ft/Sec<sup>2</sup> RMS Accelerometer, 0.05  
 Rad/Sec RMS Rate Gyros) -- WPAFB

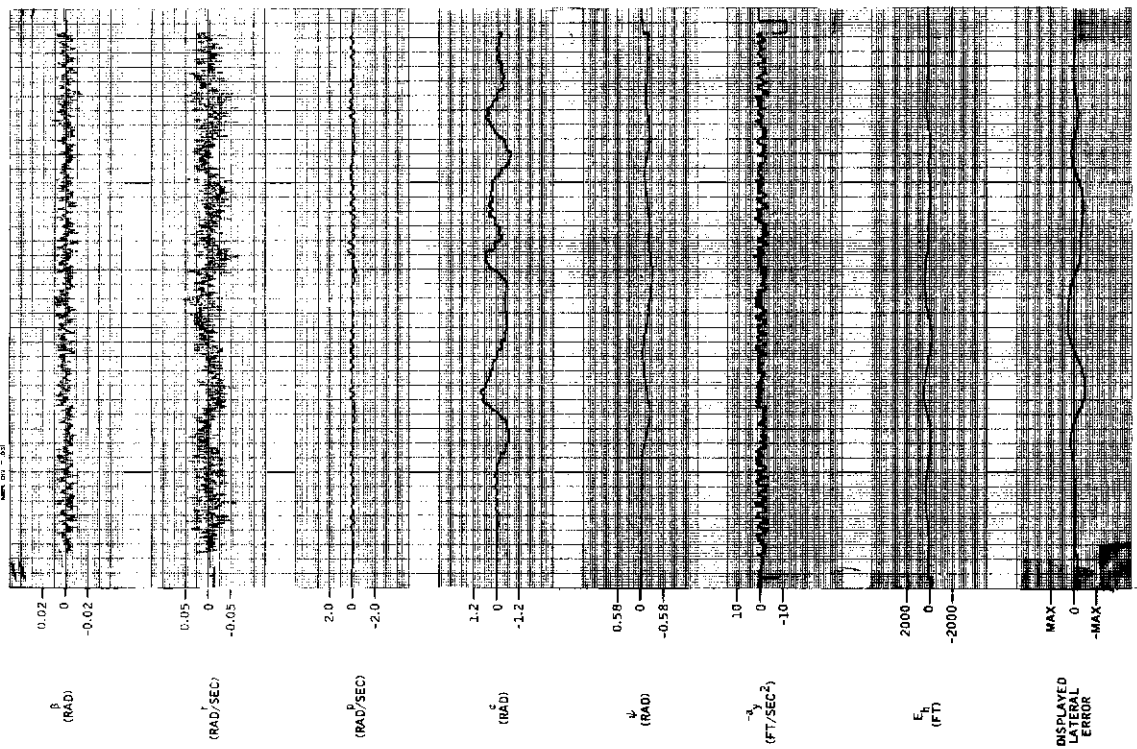


Figure 119. Formal Data Trials -- Subject D.S. at Minneapolis, Model 1, High Speed

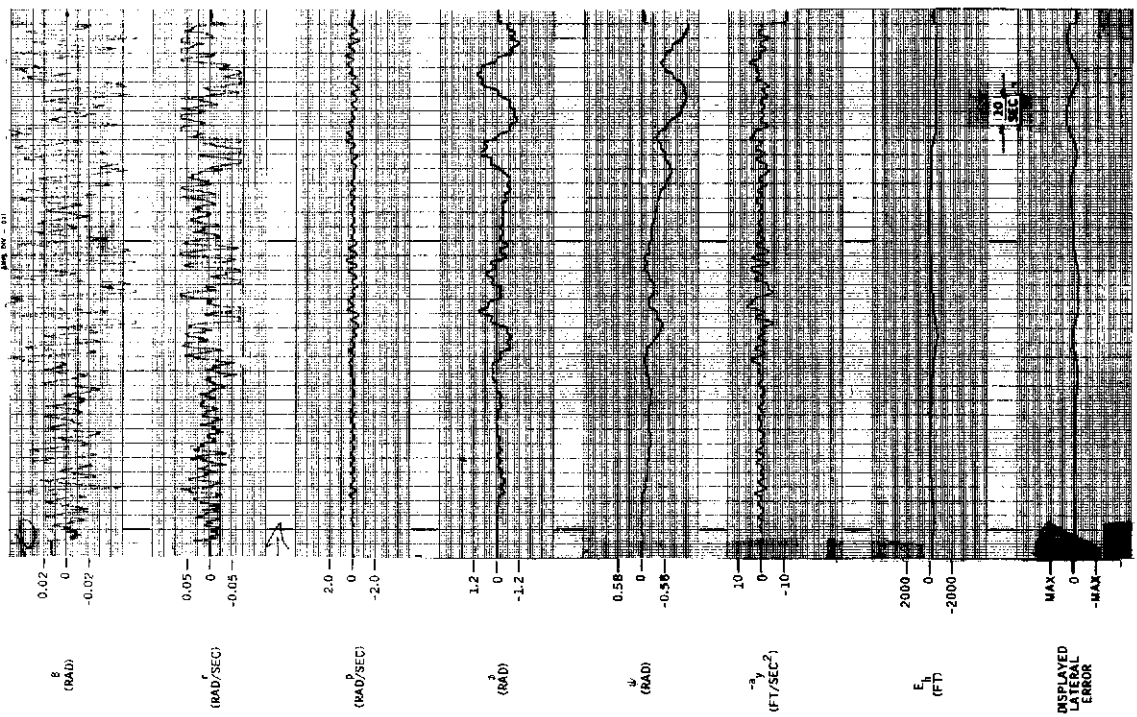


Figure 118. Formal Data Trials -- Subject D.S. at Minneapolis, Model 1, Low Speed



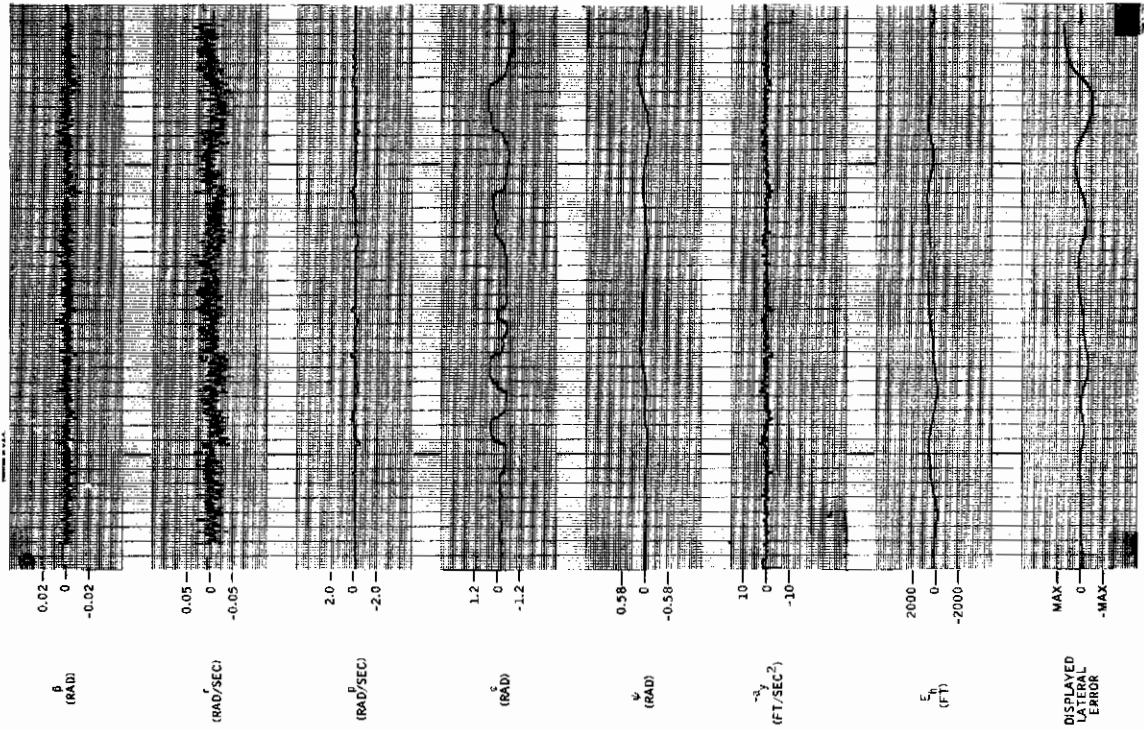


Figure 121. Formal Data Trials -- Subject D.S. at Minneapolis, Model 5, High Speed

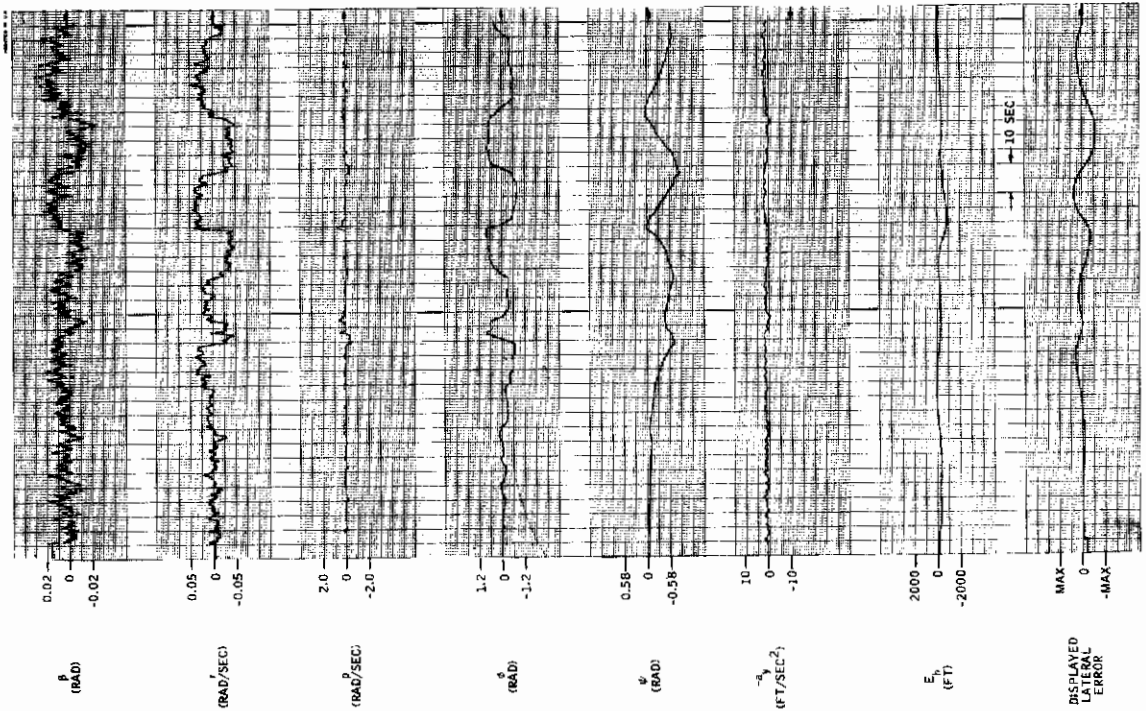


Figure 120. Formal Data Trials -- Subject D.S. at Minneapolis, Model 5, Low Speed



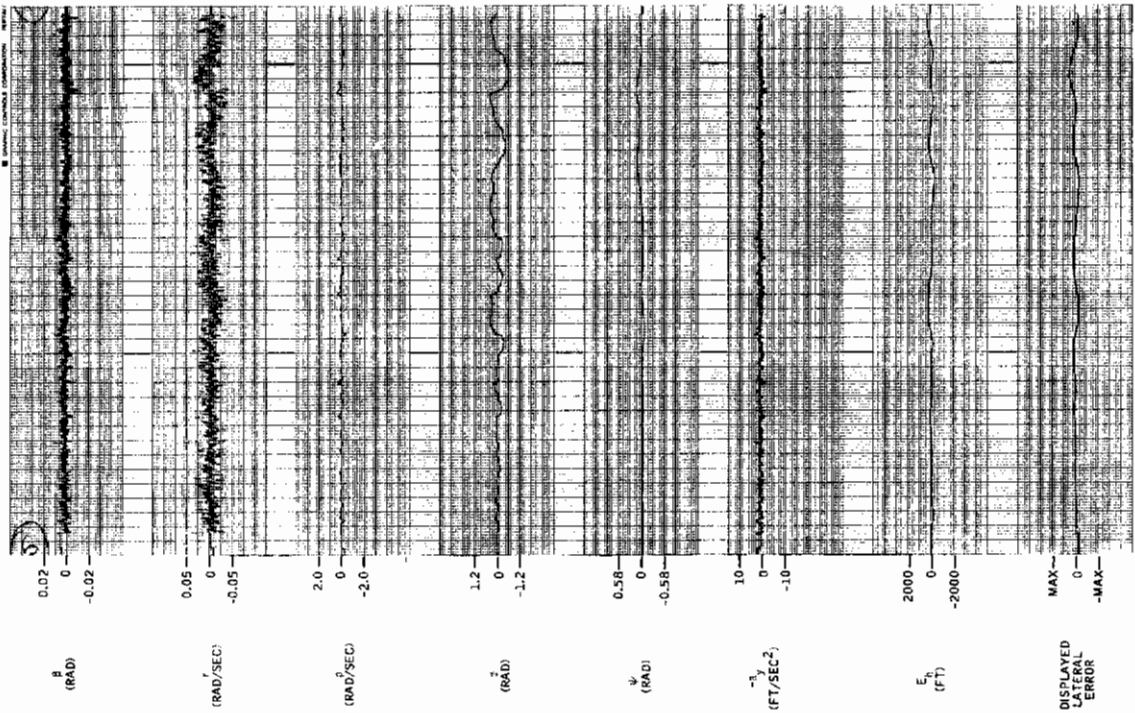


Figure 123. Formal Data Trials -- Subject D.S. at Minneapolis, Model 3, High Speed

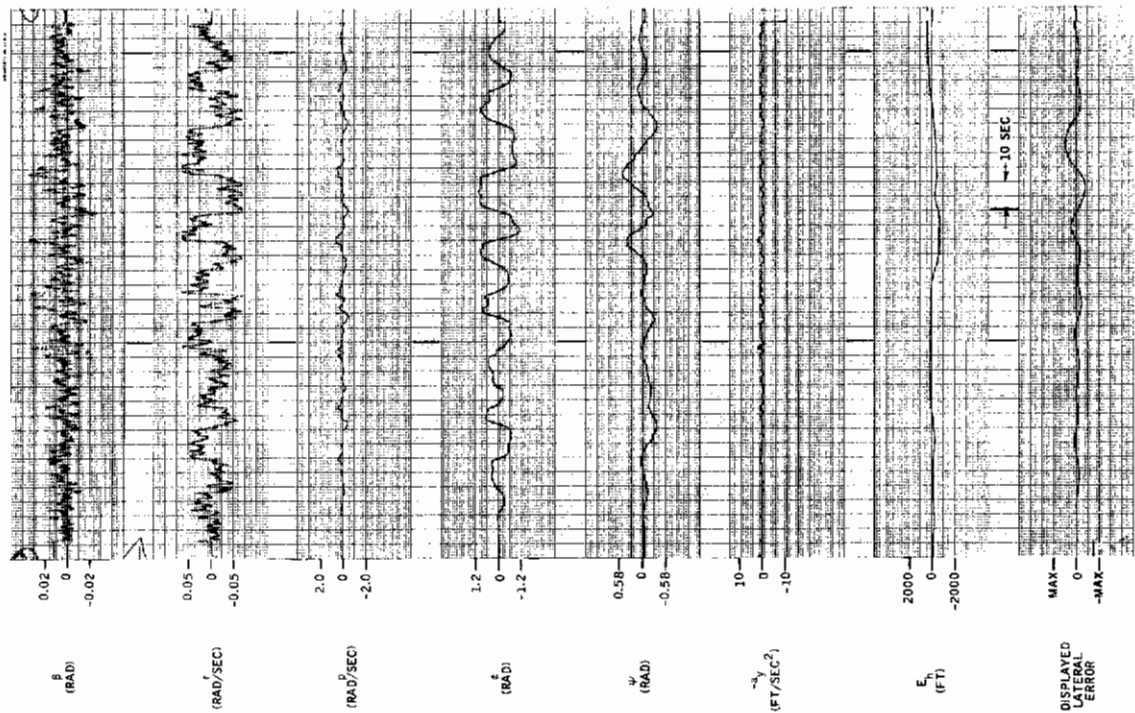


Figure 122. Formal Data Trials -- Subject D.S. at Minneapolis, Model 3, Low Speed

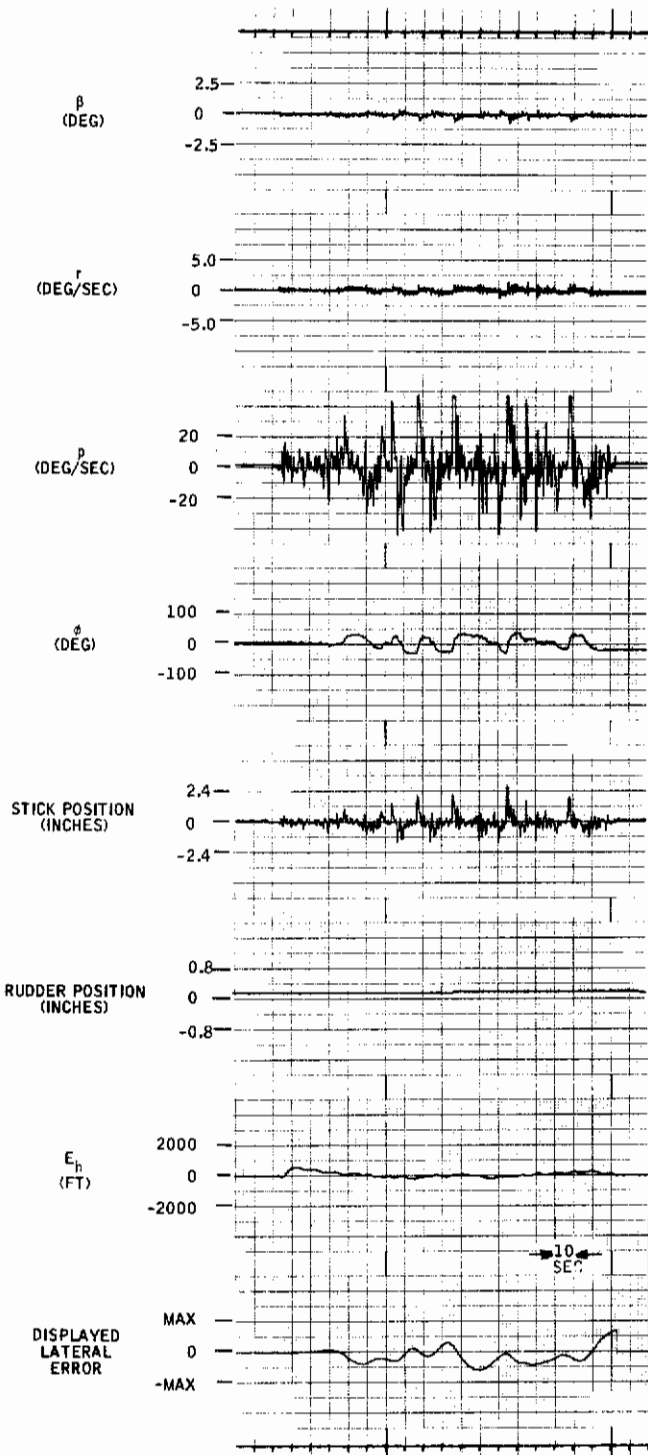


Figure 124. Formal Data Trials -- Subject R.K. at WPAFB, Model 5, High Speed

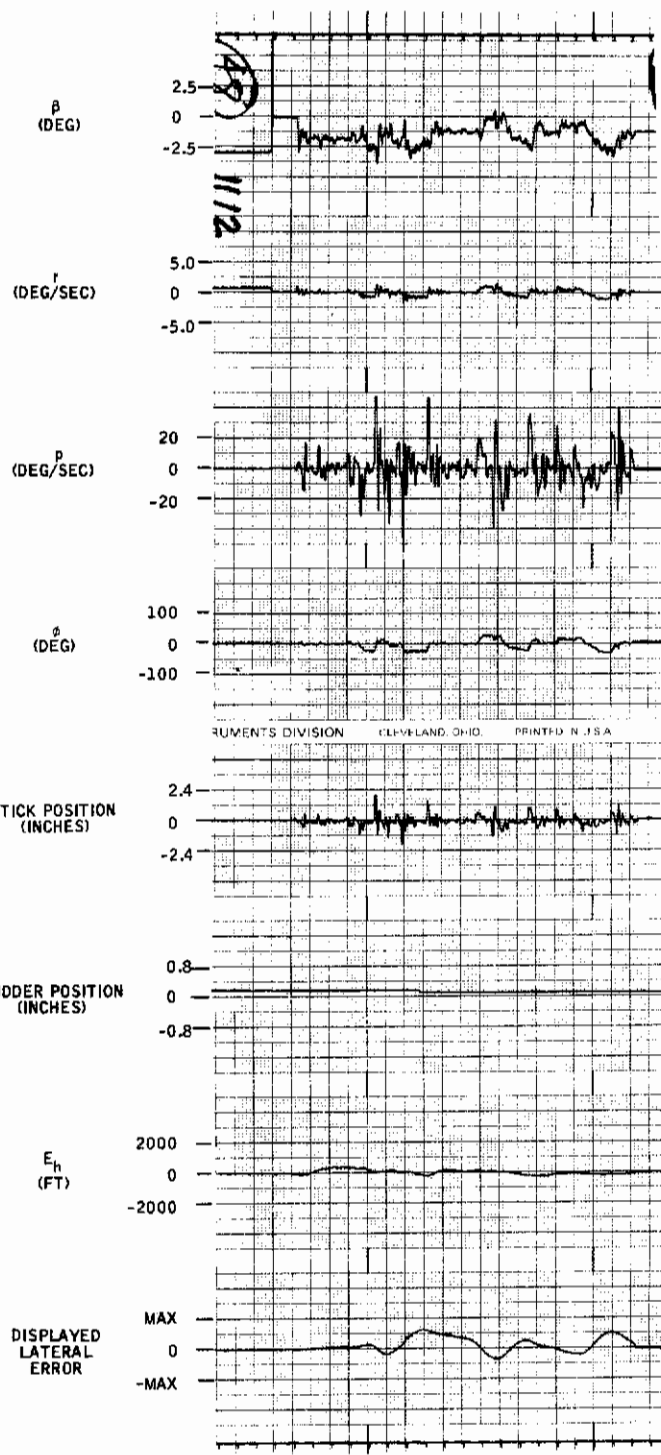


Figure 125. Formal Data Trials -- Subject R.K. at WPAFB, Model 5, Low Speed

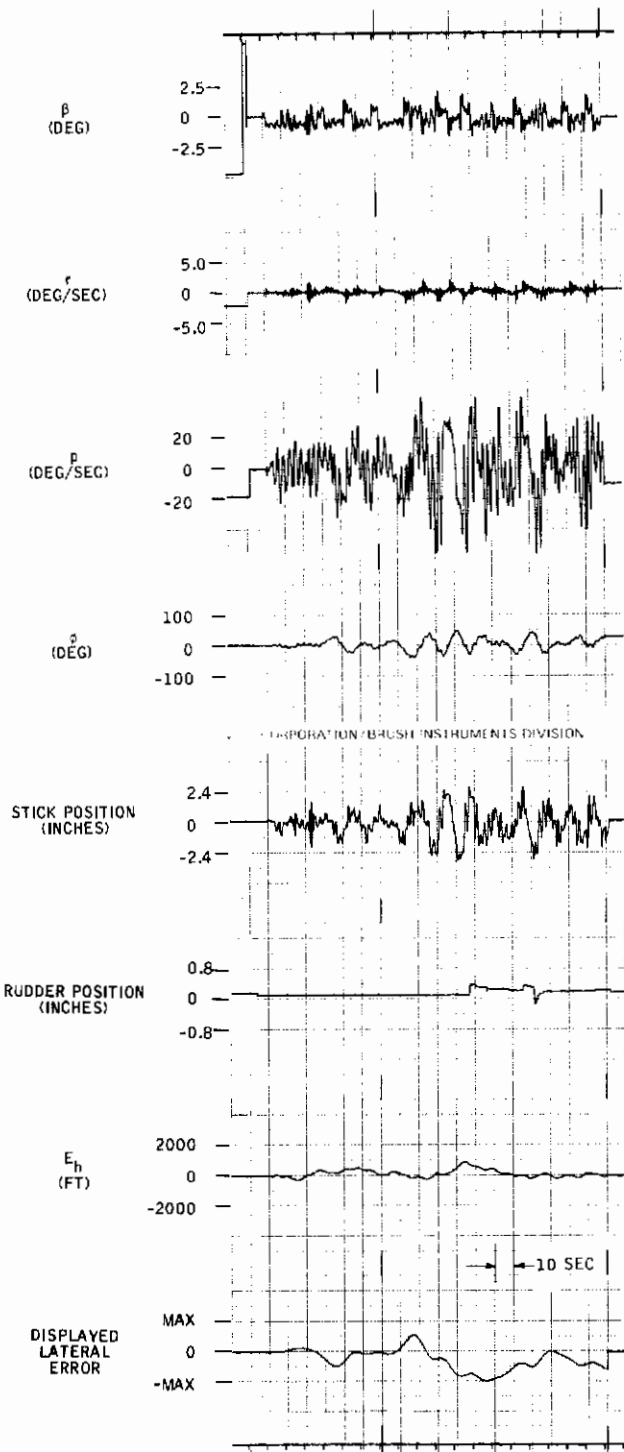


Figure 126. Formal Data Trials -- Subject R.K. at WPAFB, Model 1, High Speed

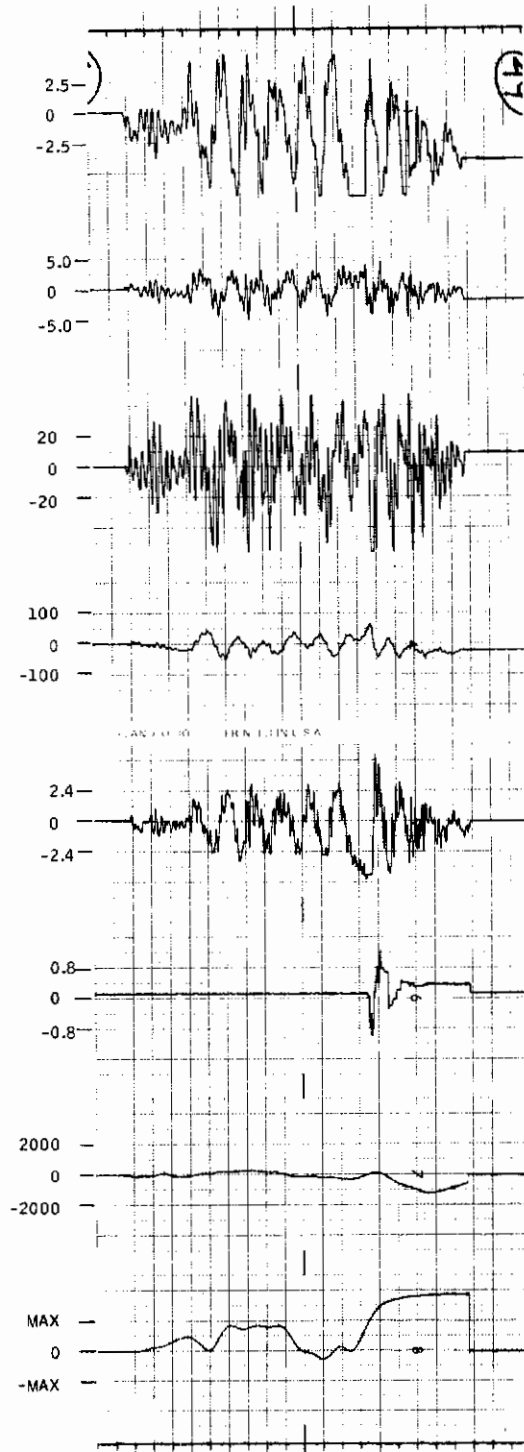


Figure 127. Formal Data Trials -- Subject R.K. at WPAFB, Model 1, Low Speed



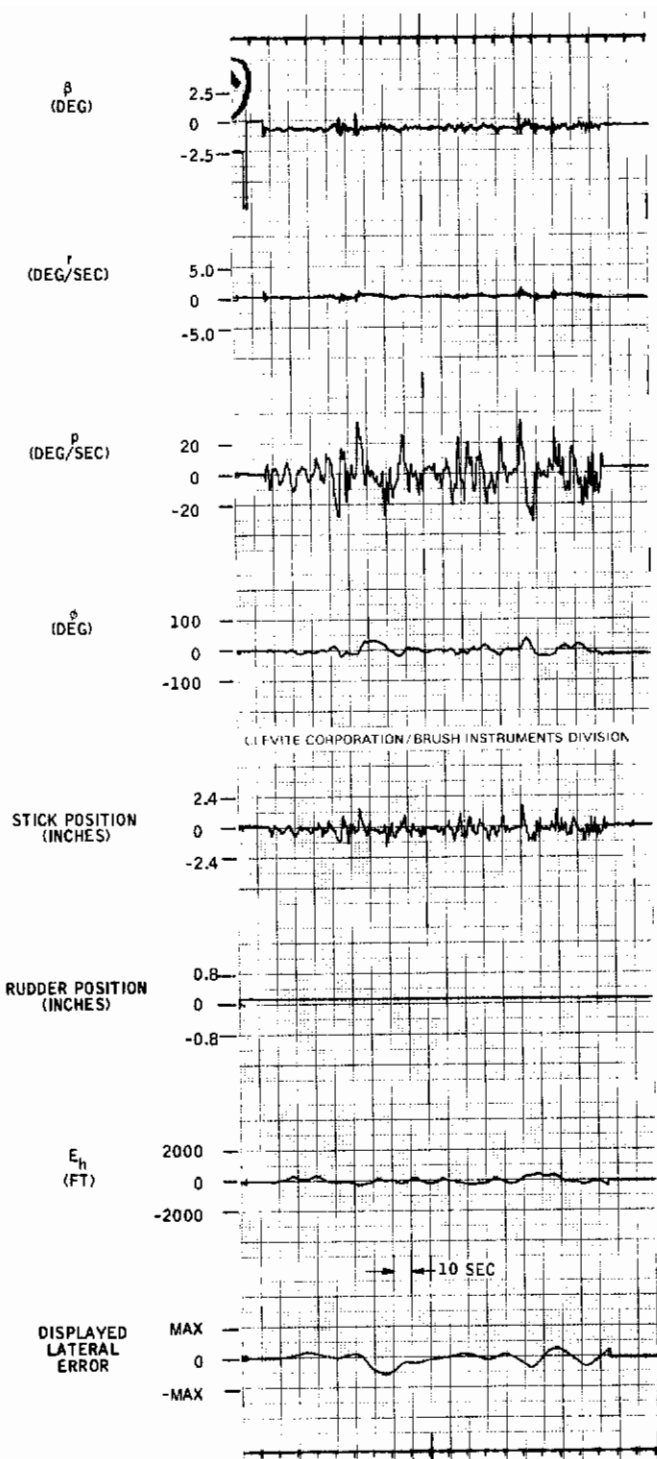


Figure 128. Formal Data Trials -- Subject R.K. at WPAFB, Model 3, High Speed

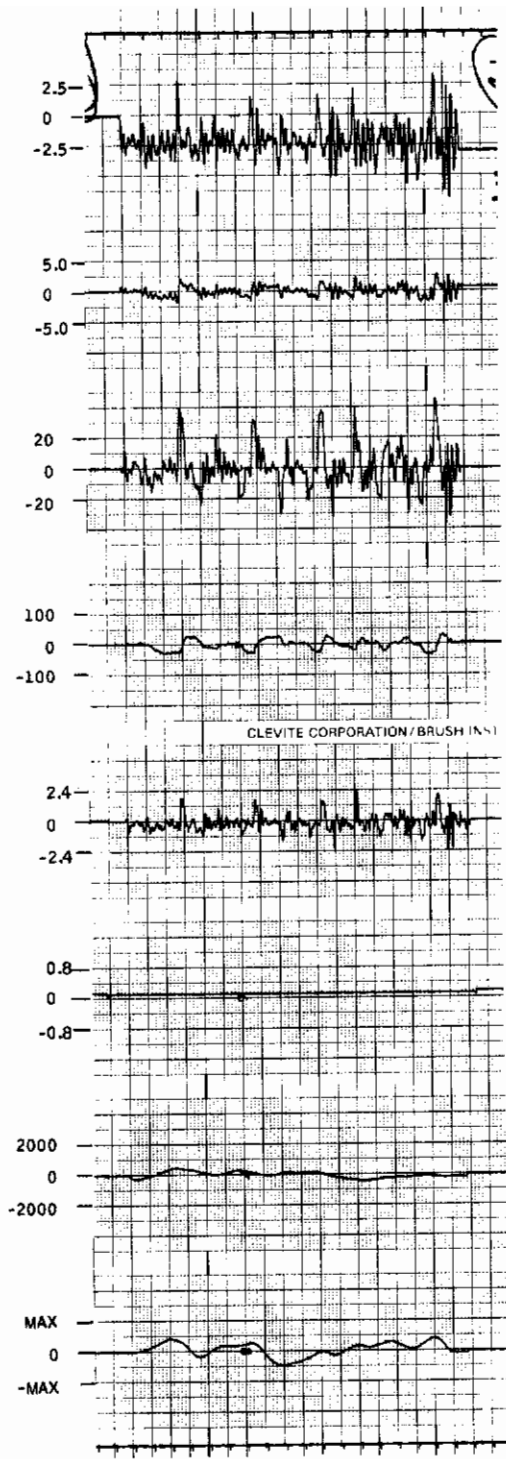


Figure 129. Formal Data Trials -- Subject R.K. at WPAFB, Model 3, Low Speed

## APPENDIX VI

### GENERATION OF FLIGHT PROFILES, LONGITUDINAL-LATERAL COMMAND EQUATIONS, AND LISTING OF FLIGHT PROFILES

#### GENERATION OF FLIGHT PROFILES

Each flight profile consisted of 12 fifteen-second intervals which were individually characterized by one of the following bank angles:

-15, -12.5, -10, -7.5, -5, 0, 5, 7.5, 10, 12.5, 15 deg

The angle for each interval was selected randomly by drawing independent samples from a discrete probability distribution defined by

$$\text{Prob}(\phi = x) = \begin{cases} 0.5 & \text{for } x = 0 \\ 0.05 & \text{for all other bank angles} \end{cases} \quad (108)$$

This means that a flight profile consisted of an average of 90 seconds of straight-and-level flight. The remaining time was taken up with steady turns at assorted bank angles.

Once a sequence of 12 bank angles  $\{\phi_j, j = 1, 2, \dots, 12\}$  was determined by the above sampling procedure, the profile was found by solving the following equations.

Define:

$U_0$  = Aircraft speed  
 $X(t)$  = Downrange position  
 $Y(t)$  = Crossrange position (positive right)  
 $\psi(t)$  = Heading angle (positive right)

and let  $x(0) = y(0) = \psi(0) = 0$ .

Then, for  $\phi_j = 0$ ,

$$\left. \begin{aligned} \psi(t) &= \psi[15(j-1)] \\ X(t) &= X[15(j-1)] + U_0[t-15(j-1)] \cos \psi[15(j-1)] \\ Y(t) &= Y[15(j-1)] + U_0[t-15(j-1)] \sin \psi[15(j-1)] \end{aligned} \right\} \quad (109a)$$

$15(j-1) \leq t \leq 15j$

# Contrails

and for  $\phi_j \neq 0$

$$\left. \begin{aligned}
 \psi(t) &= \psi[15(j-1)] + \frac{U_0}{R_j} [t-15(j-1)] \\
 X(t) &= X[15(j-1)] + R_j \cos \{ \psi[15(j-1)] + 90 \} - \cos [\psi(t) + 90] \\
 Y(t) &= Y[15(j-1)] + R_j \sin \{ \psi[15(j-1)] + 90 \} - \sin [\psi(t) + 90] \\
 15(j-1) &\leq t \leq 15j
 \end{aligned} \right\} \quad (109b)$$

where  $R_j = U_0^2 / g \tan \phi_j$ .

Approximately 40 such trajectories were generated before the experiments were conducted. The first set of 20 flight profiles were calculated using bank angles of  $\pm 5, \pm 10, \pm 15, \pm 20, \pm 25$  and  $\pm 30$  deg. This set of profiles proved to be a very difficult task. Because of the reaction time of the pilot and the error display, it was necessary for the pilot to correct the deviations from lateral center with extreme bank angles (60 deg to 90 deg). This produced a situation where the lateral needle would remain pegged to the limit of the display until the course was intercepted at a high deflection angle whereupon the needle would rapidly swing to the limit on the opposite side. No straight segments were detected by the pilots. To correct this situation we reduced all bank angles by one-half and set the lowest value ( $\pm 2.5$  deg) to zero. The task was then reasonable.

Each trajectory was stored on punched cards in the form of a 3 x 12 array of floating-point constants. These numbers are defined below. They function as lateral/longitudinal display drives, as explained in the subsection which follows this one.

To define profile arrays, let  $[T(i, j)]$  be a (3 x 12) array of numbers. Let the column index (j) correspond to the 12 fifteen-second time intervals of the profile and let the row index (i) identify three numbers which characterize each interval. Then

$$\left. \begin{aligned}
 T(1, j) &= \psi[15(j-1)] \\
 T(2, j) &= X[15(j-1)] \\
 T(3, j) &= Y[15(j-1)]
 \end{aligned} \right\} \text{if } \phi_j = 0 \quad (110a)$$

$$\left. \begin{aligned}
 T(1, j) &= R_j \\
 T(2, j) &= X[15(j-1)] + R_j \cos \{ \psi[15(j-1)] + 90 \} \\
 T(3, j) &= Y[15(j-1)] + R_j \sin \{ \psi[15(j-1)] + 90 \}
 \end{aligned} \right\} \text{if } \phi_j \neq 0 \quad (110b)$$

## LATERAL/LONGITUDINAL DISPLAY EQUATIONS

Altitude errors ( $E_h$ ) and lateral course deviations ( $E_y$ ) were defined in terms of the actual aircraft positions  $X(t)$ ,  $Y(t)$ ,  $h(t)$  (downrange, cross-range, and altitude, respectively) and in terms of the profile array,  $T(i, j)$ . The following equations were used to evaluate the errors:

$$j = \left[ \frac{t}{15} \right]_I + 1 \quad (111)^{28}$$

$$E_h = h(t) - 2000 + 33.3t \quad (112)$$

$$E_y = \begin{cases} -[X(t) - T(2, j)] \sin T(1, j) + [Y(t) - T(3, j)] \cos T(1, j) \\ \quad \text{if } |T(1, j)| < 1000 \\ |T(1, j)| - \sqrt{[X(t) - T(2, j)]^2 + [Y(t) - T(3, j)]^2} \\ \quad \text{if } |T(1, j)| \geq 1000 \end{cases} \quad (113)$$

Lateral and longitudinal displays were driven by scaled values of these errors. Scale factors were determined after a few trial experiments.

## LISTING OF FLIGHT PROFILES

Low-speed and high-speed flight profiles are presented in Tables XXXII and XXXIII, respectively.

---

<sup>28</sup>  
 $[x]_I$  denotes the integer part of  $x$ .

Table XXXII. Low-Speed Flight Profiles

Profile									
1	2	3	4	5	6	7	8	9	10
0	0	0	0	0	0	0	0	0	0
0	- 7.5	0	0	12.5	0	-10.0	-10.0	0	-15.0
- 5.0	7.5	0	-15.0	0	12.5	0	0	-10.0	0
-15.0	0	-15.0	12.5	0	-15.0	0	0	-12.5	0
-10.0	-12.5	7.5	0	-10.0	15.0	-10.0	0	10.0	15.0
0	0	10.0	0	0	0	7.5	7.5	5.0	12.5
12.5	0	0	12.5	0	7.5	0	0	0	0
- 5.0	15.0	-12.5	0	0	-15.0	-15.0	0	0	0
0	0	0	- 7.5	-15.0	-12.5	-10.0	0	0	0
10.0	0	-12.5	0	5.0	0	-15.0	0	15.0	7.5
-15.0	15.0	10.0	0	10.0	0	0	- 7.5	12.5	0
0	7.5	0	0	0	0	0	0	0	5.0
Ratio: Straight and level/bank									
5/7	6/6	6/6	8/4	7/5	6/6	6/6	9/3	6/6	7/5

Table XXXIII. High-Speed Flight Profiles

Profile									
11	12	13	14	15	16	17	18	19	20
0	0	0	0	0	0	0	0	0	0
0	0	-12.5	12.5	0	0	0	15.0	0	0
0	15.0	- 5.0	0	0	0	0	10.0	-15.0	0
15.0	0	0	0	0	0	-12.5	0	0	15.0
0	-10.0	10.0	- 7.5	0	0	5.0	0	0	0
-10.0	-12.5	0	5.0	0	-10.0	10.0	- 5.0	-12.5	0
0	15.0	0	0	0	0	0	0	0	0
0	0	10.0	7.5	15.0	- 5.0	15.0	0	7.5	0
0	15.0	- 5.0	0	0	0	-15.0	0	0	7.50
5.0	0	- 5.0	15.0	0	12.5	15.0	5.0	0	- 5.00
-15.0	0	0	7.5	0	-10.0	12.5	5.0	0	12.50
-12.5	-15.0	12.5	15.0	- 7.5	0	0	0	0	- 7.50
Ratio: Straight and level/bank									
7/5	6/6	5/7	5/7	10/2	8/4	5/7	7/5	9/3	7/5



APPENDIX VII  
TRANSIENT RESPONSES OF THE WPAFB  
AND MINNEAPOLIS SIMULATIONS

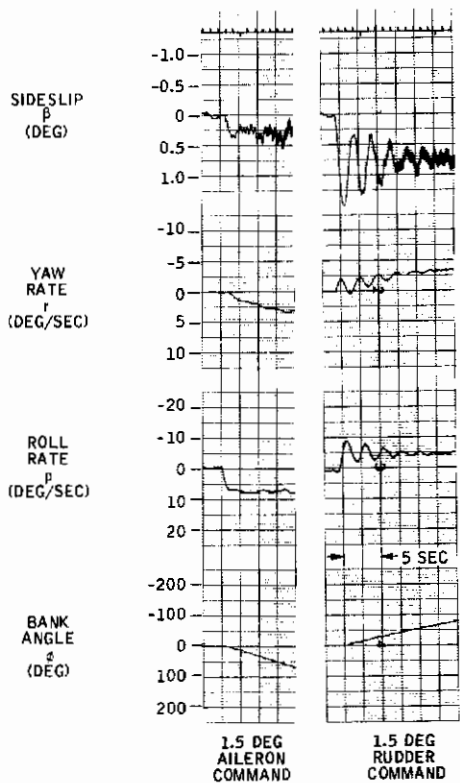


Figure 130. WPAFB Simulation -- Free Aircraft, Flight Condition 2

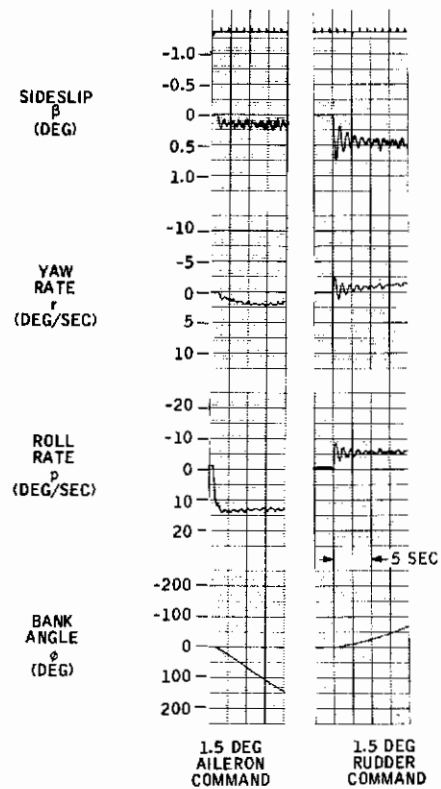


Figure 131. WPAFB Simulation -- Free Aircraft, Flight Condition 3

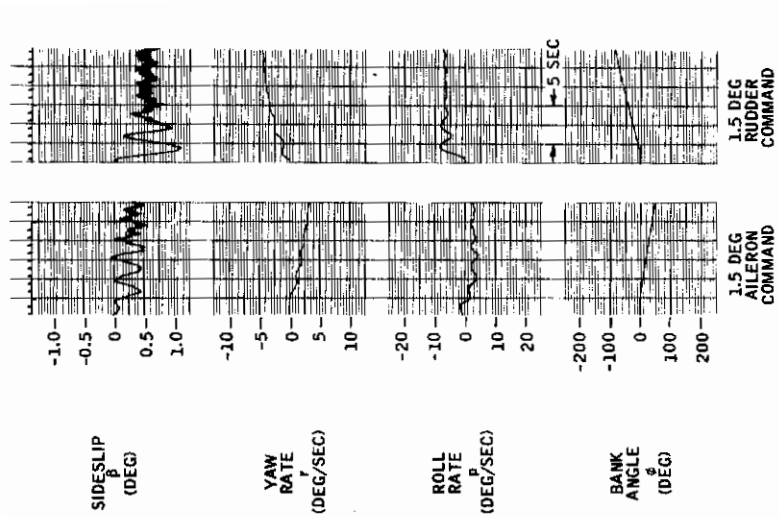


Figure 132. WPAFB Simulation -- Free Aircraft, Flight Condition 4

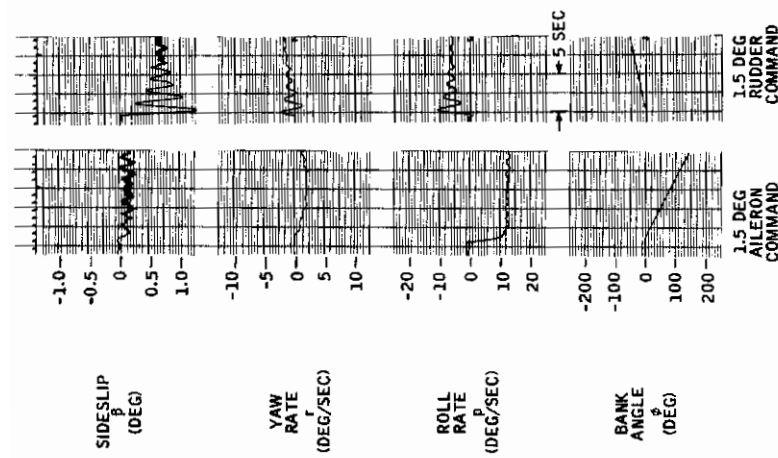


Figure 133. WPAFB Simulation -- Free Aircraft, Flight Condition 5

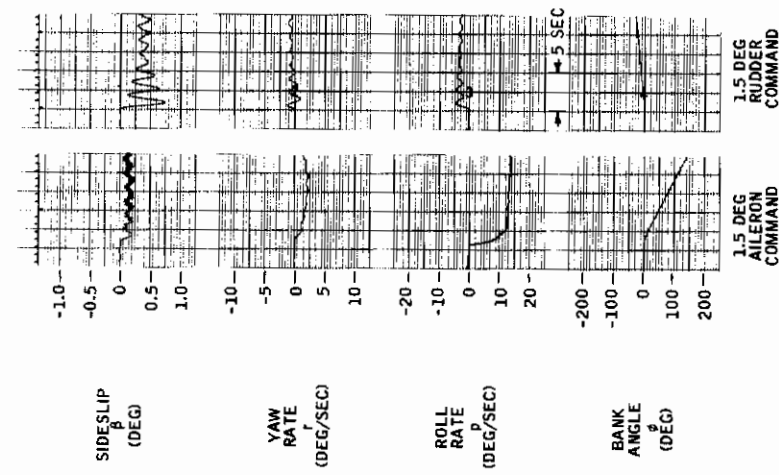


Figure 134. WPAFB Simulation -- Free Aircraft, Flight Condition 6

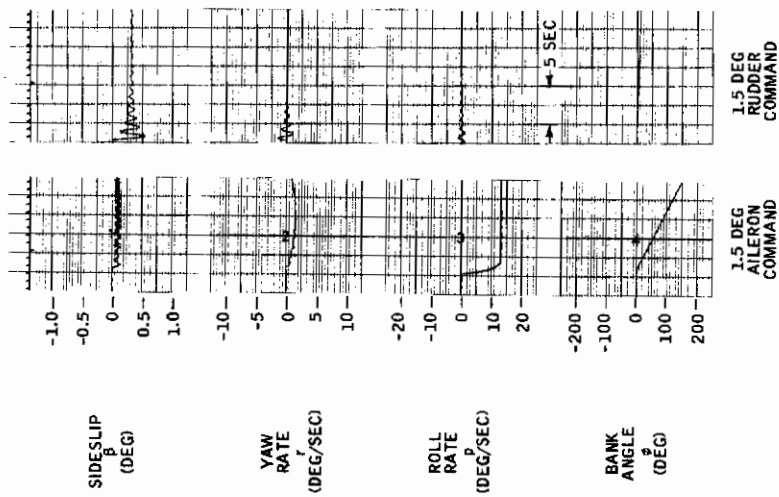


Figure 135. WPAFB Simulation -- Free Aircraft, Flight Condition 7

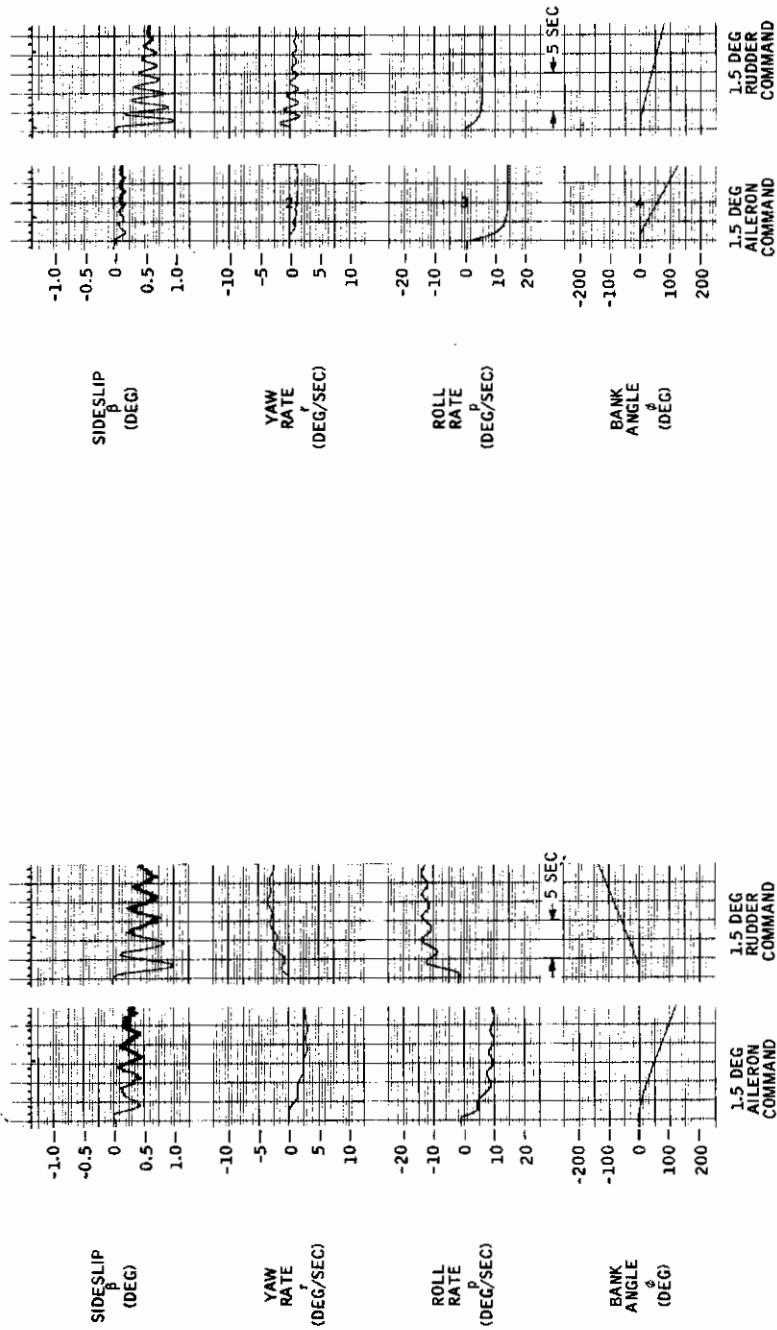


Figure 137. WPAFB Simulation -- Free Aircraft, Flight Condition 9

Figure 136. WPAFB Simulation -- Free Aircraft, Flight Condition 8

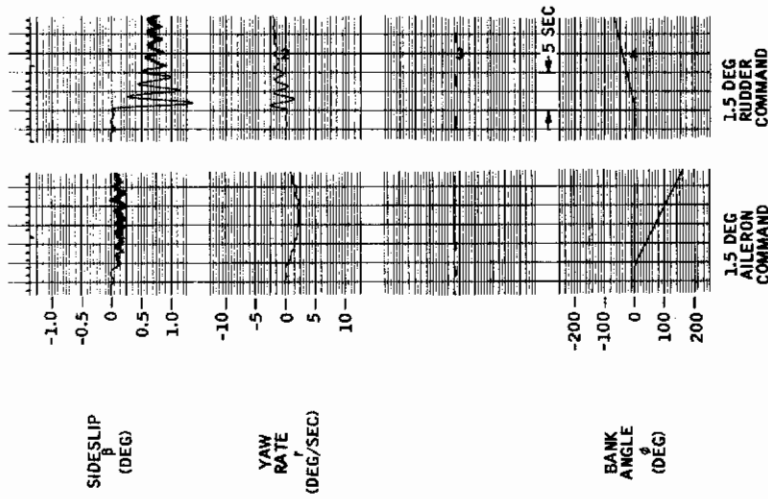


Figure 138. WPAFB Simulation -- Free Aircraft, Flight Condition 10

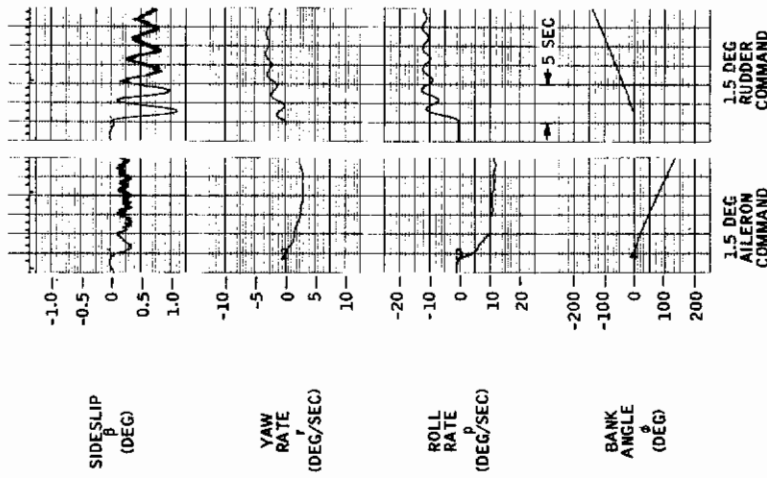


Figure 139. WPAFB Simulation -- Free Aircraft, Flight Condition 11



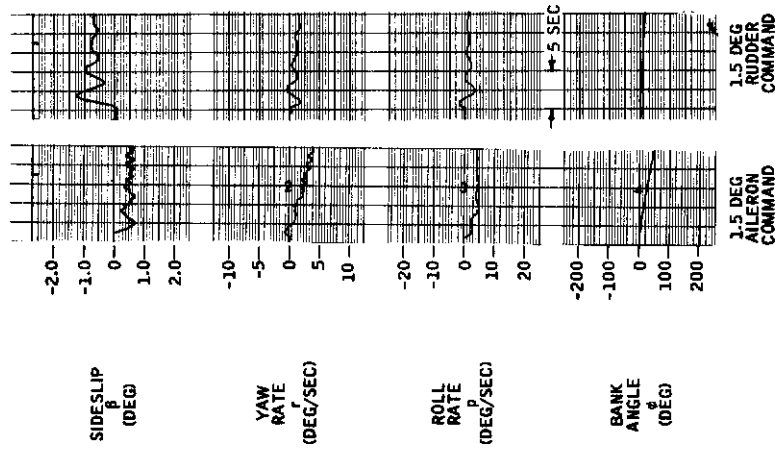


Figure 140. WPAFB Simulation --  
Controlled Aircraft,  
Flight Condition 2,  
Model 1

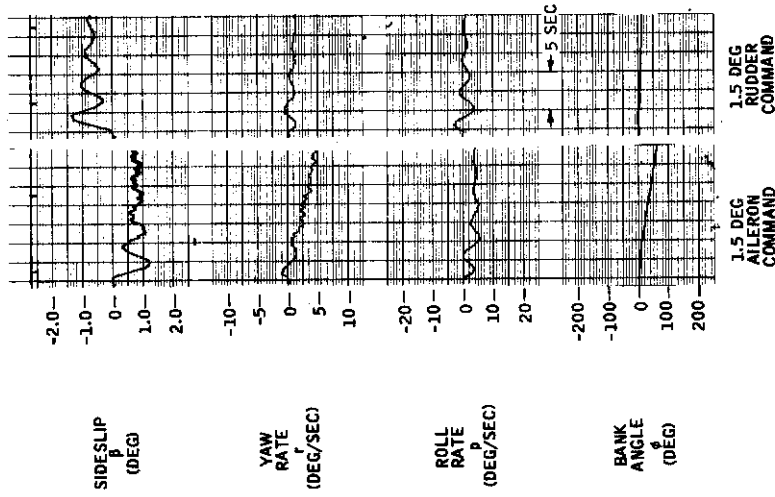


Figure 141. WPAFB Simulation --  
Controlled Aircraft,  
Flight Condition 2,  
Model 2

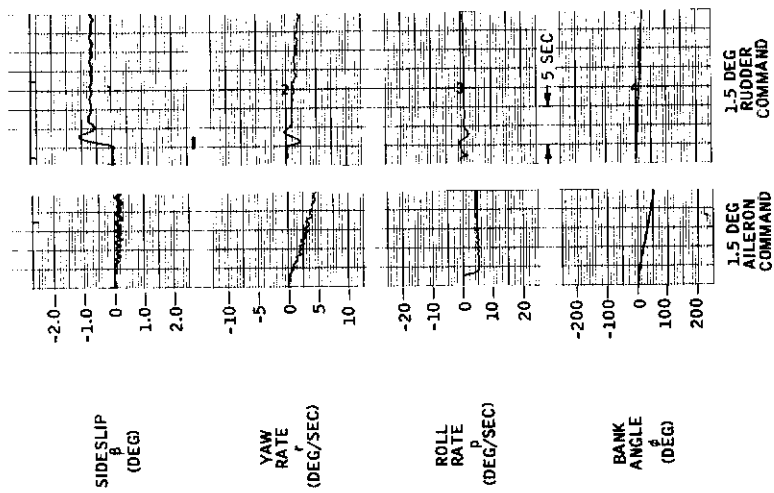


Figure 142. WPAFB Simulation --  
Controlled Aircraft,  
Flight Condition 2,  
Model 3

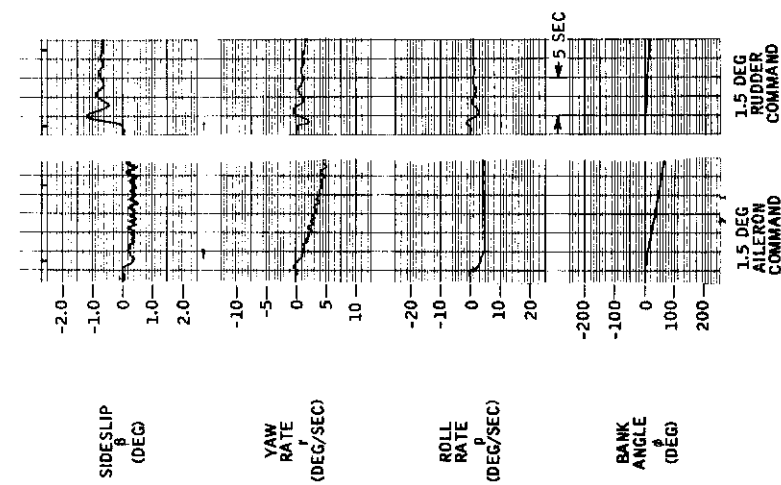


Figure 143. WPAFB Simulation --  
Controlled Aircraft,  
Flight Condition 2,  
Model 4

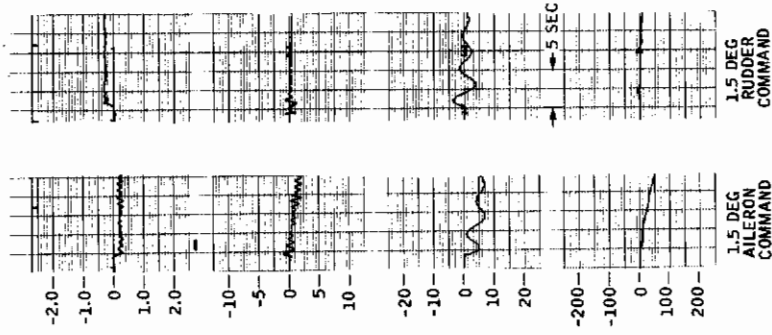


Figure 144. WPAFB Simulation --  
Controlled Aircraft,  
Flight Condition 2,  
Model 4, Practical  
Controller

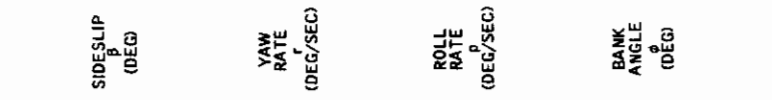


Figure 145. WPAFB Simulation --  
Controlled Aircraft,  
Flight Condition 3,  
Model 1

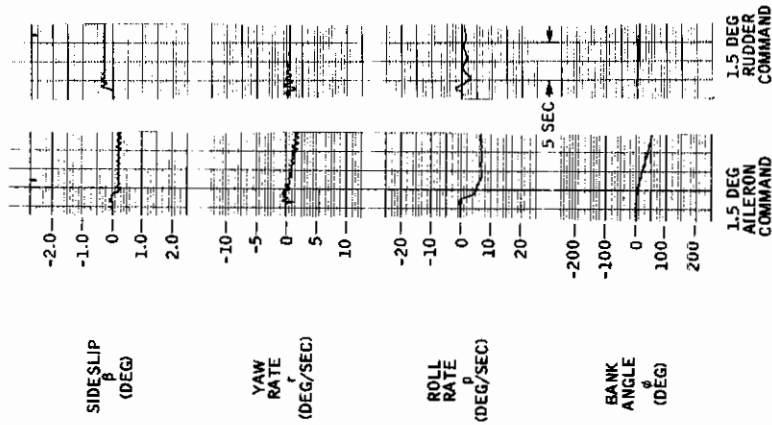


Figure 146. WPAFB Simulation -- Controlled Aircraft, Flight Condition 3, Model 2

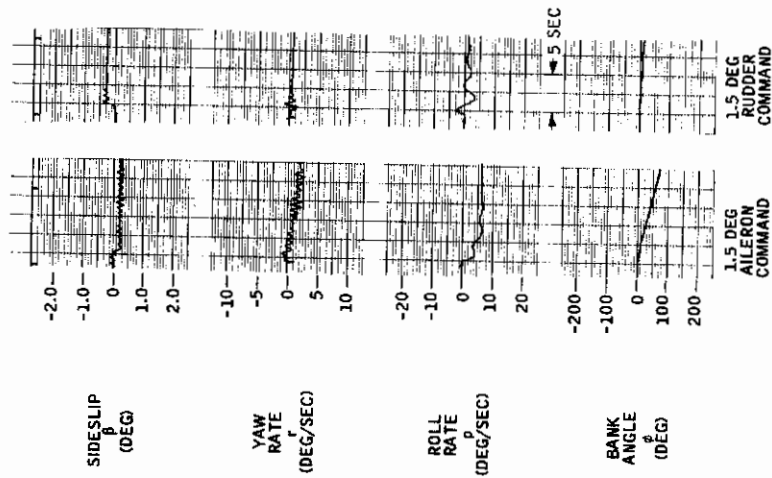


Figure 147. WPAFB Simulation -- Controlled Aircraft, Flight Condition 3, Model 3

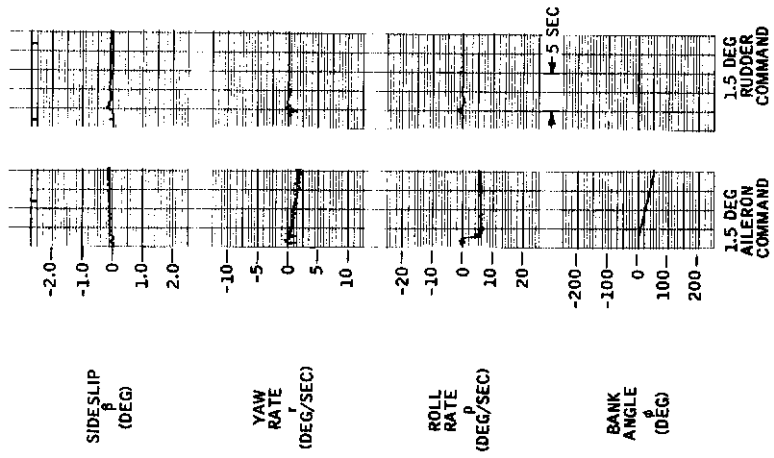


Figure 148. WPAFB Simulation -- Controlled Aircraft, Flight Condition 3, Model 4

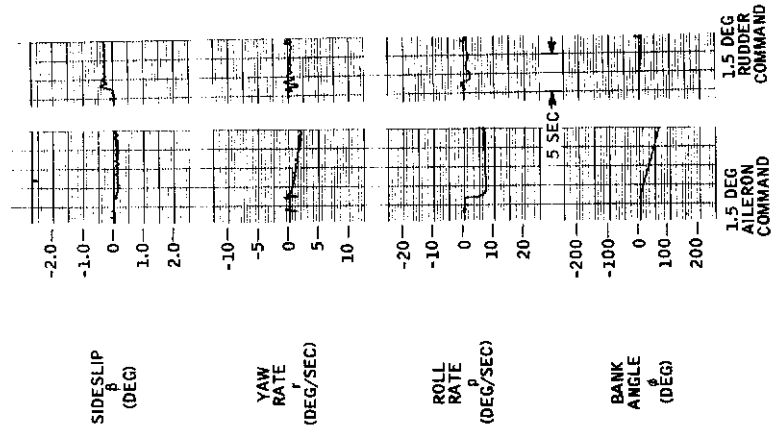


Figure 149. WPAFB Simulation -- Controlled Aircraft, Flight Condition 3, Model 4, Practical Controller



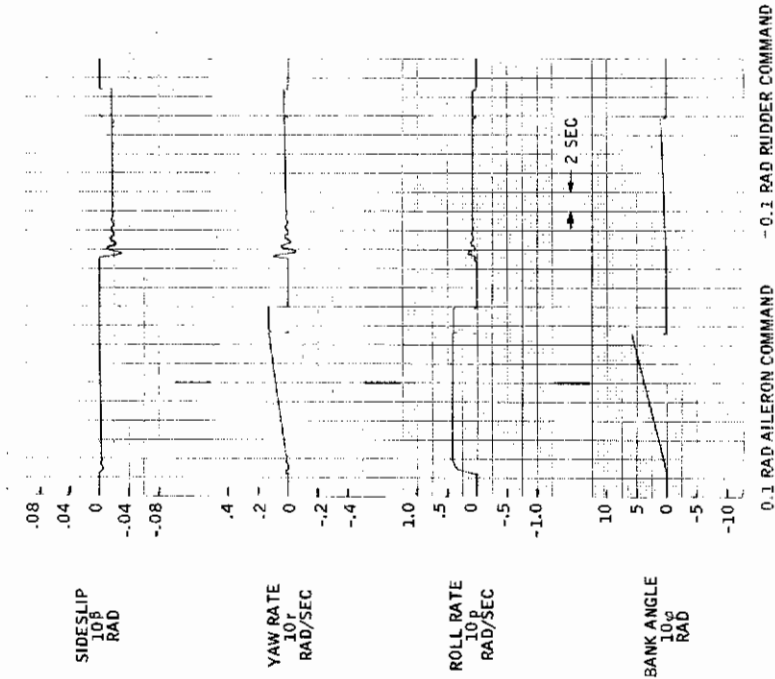


Figure 150. Minneapolis Simulation -- Free Aircraft Flight Condition 2

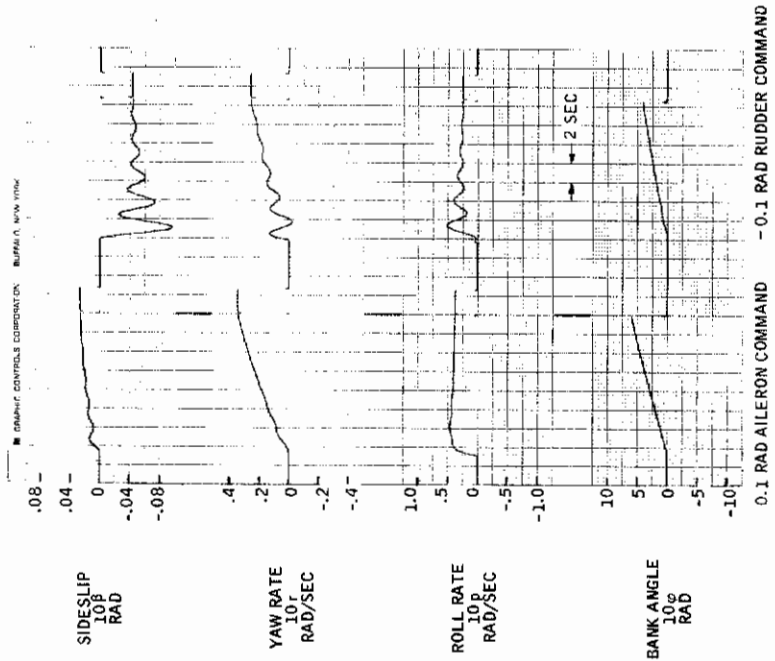


Figure 151. Minneapolis Simulation -- Free Aircraft, Flight Condition 3

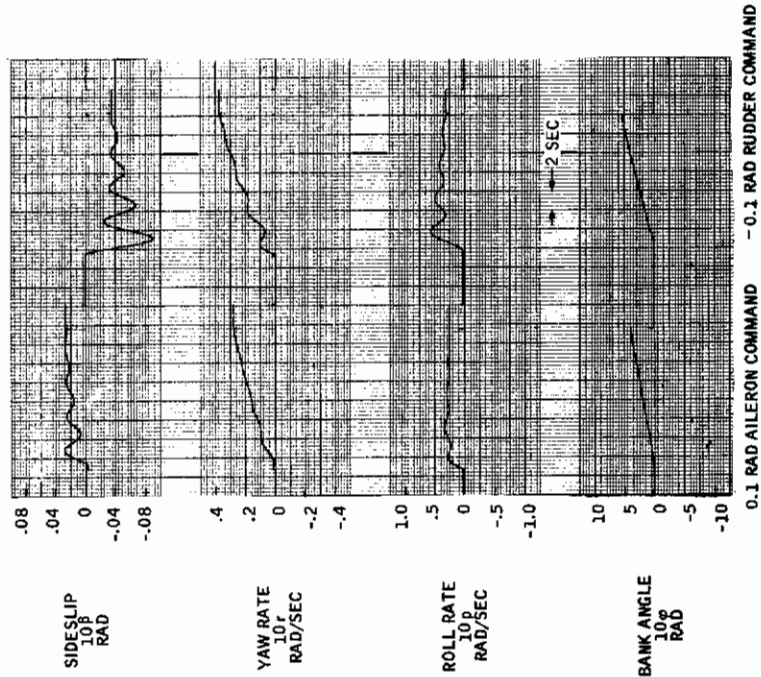


Figure 153. Minneapolis Simulation -- Free Aircraft, Flight Condition 5

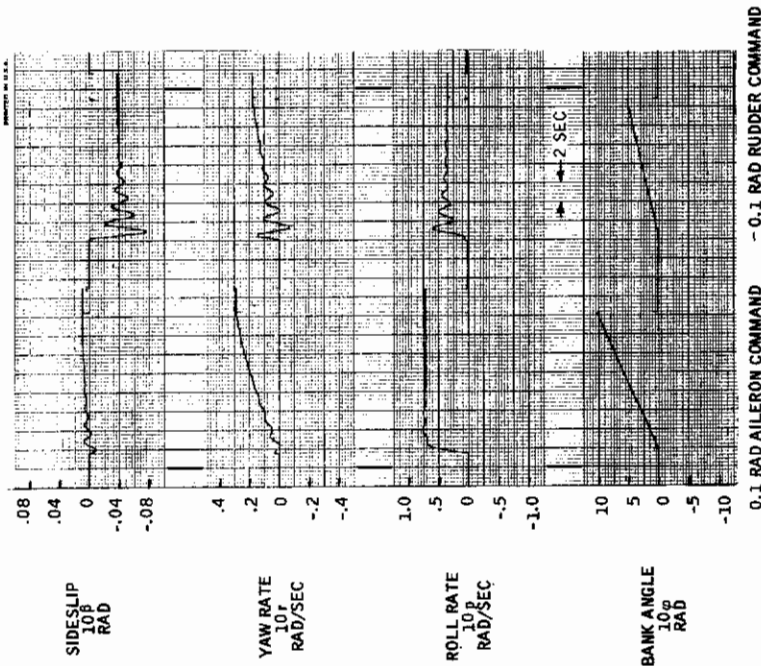


Figure 152. Minneapolis Simulation -- Free Aircraft, Flight Condition 4

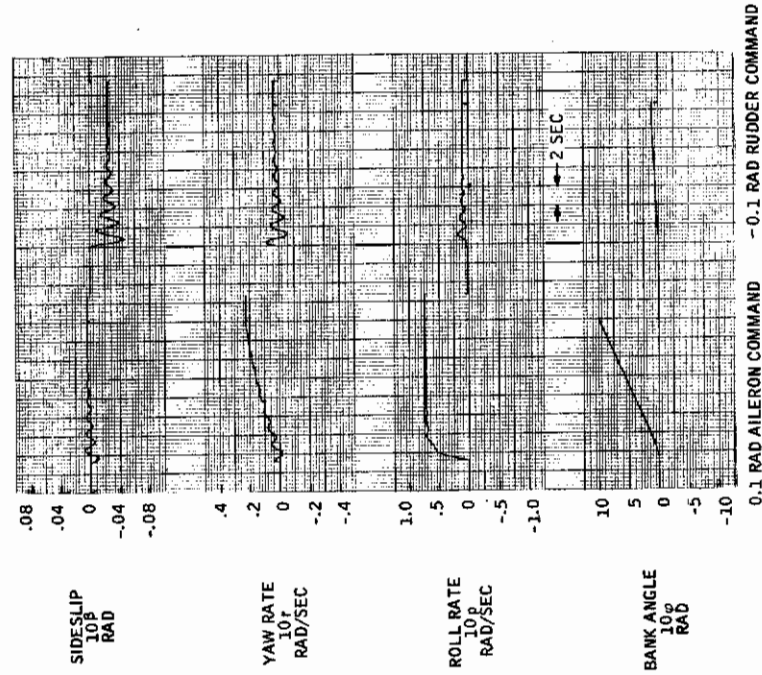


Figure 155. Minneapolis Simulation -- Free Aircraft, Flight Condition 7

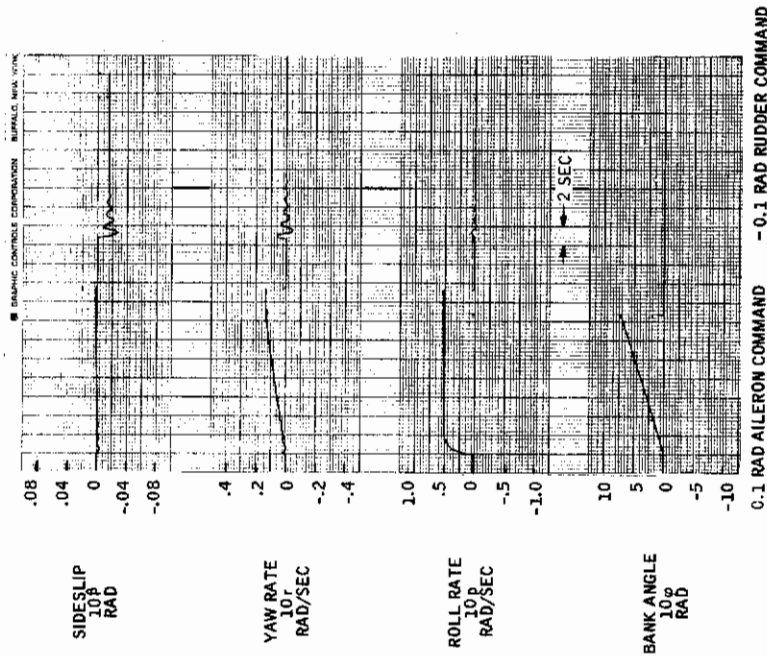


Figure 154. Minneapolis Simulation -- Free Aircraft, Flight Condition 6

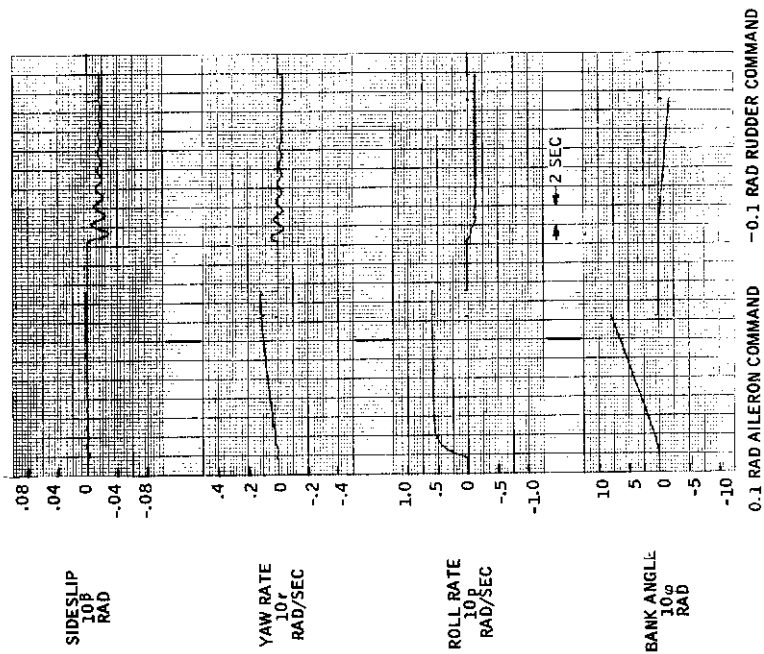


Figure 157. Minneapolis Simulation -- Free Aircraft, Flight Condition 9

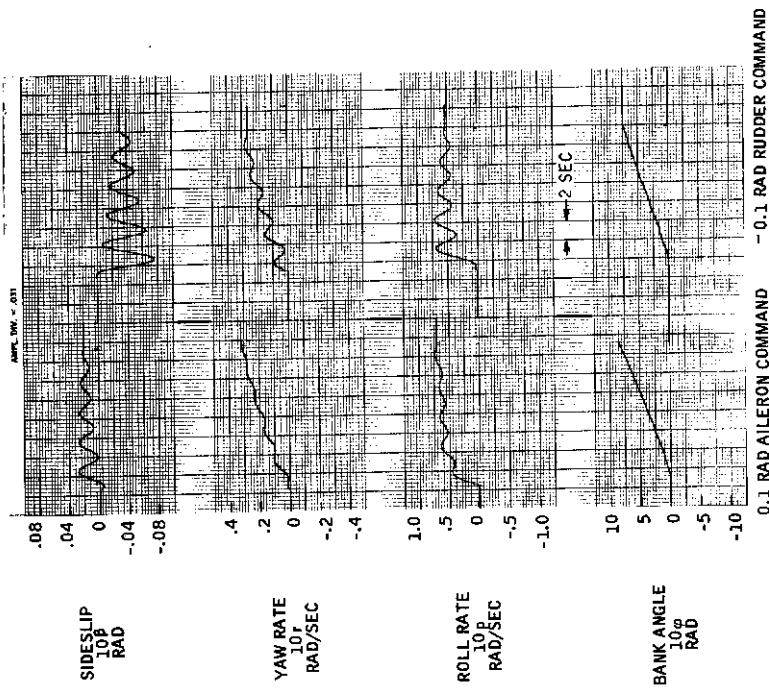


Figure 156. Minneapolis Simulation -- Free Aircraft, Flight Condition 8



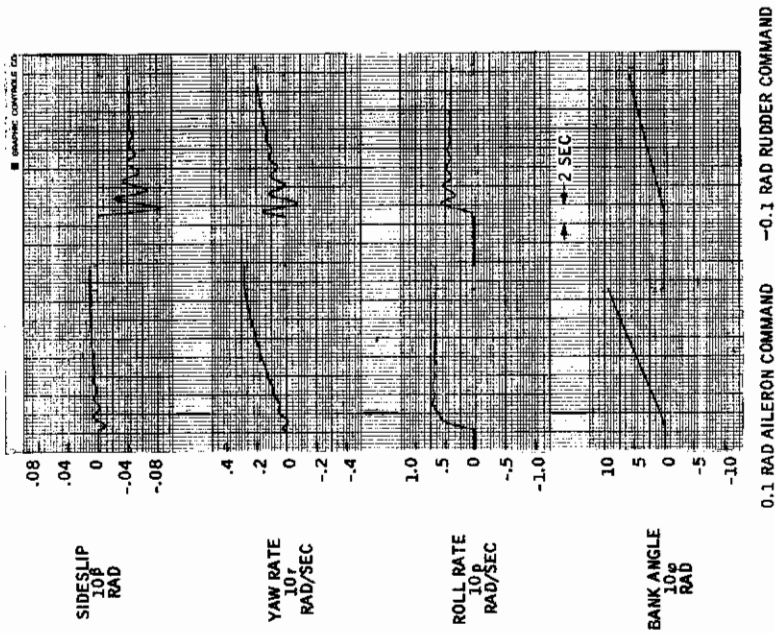


Figure 159. Minneapolis Simulation -- Free Aircraft, Flight Condition 11

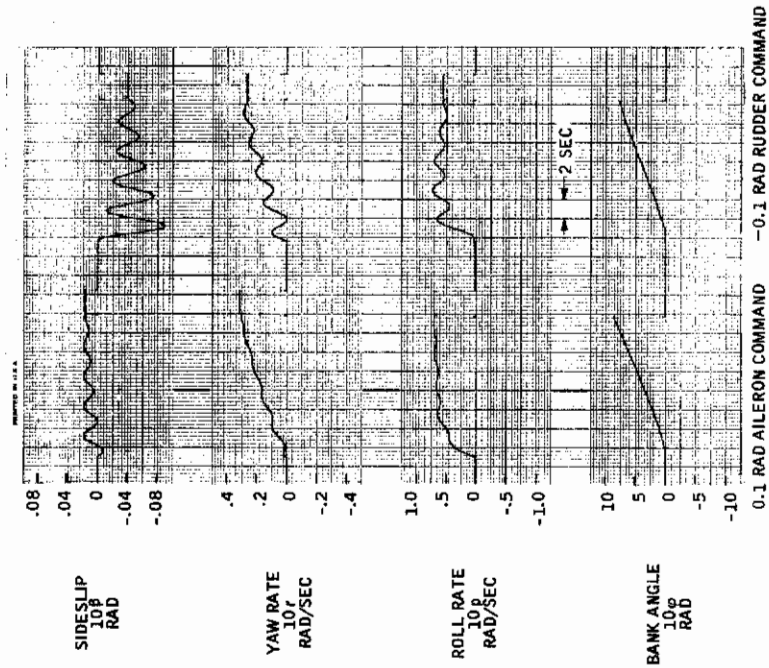


Figure 158. Minneapolis Simulation -- Free Aircraft, Flight Condition 10

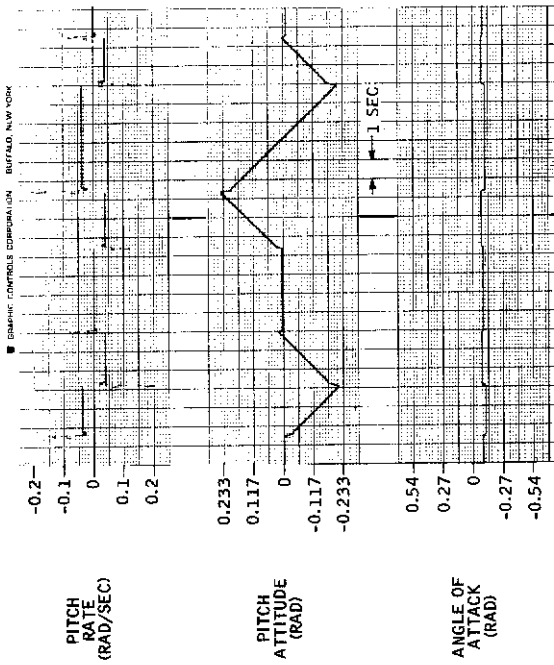


Figure 161. Minneapolis Simulation --  
Controlled Aircraft, Flight  
Condition 3, Pitch Transient  
Response (Stick Input = 1.4  
Deg of Step Stabilator)

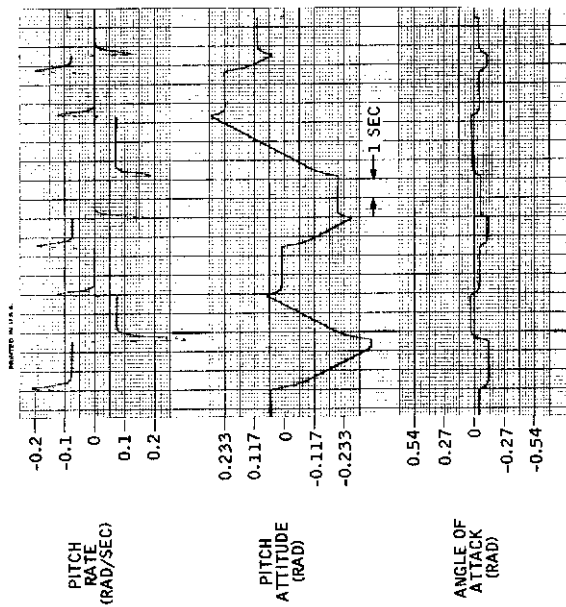


Figure 160. Minneapolis Simulation --  
Controlled Aircraft, Flight  
Condition 2, Pitch Transient  
Response (Stick Input = 1.4  
Deg of Step Stabilator)



APPENDIX VIII  
 TRAINING TRIAL SEQUENCES FOR MINNEAPOLIS  
 AND WPAFB (3 SUBJECTS)

Table XXXIV. Training Trial Sequences for  
 Minneapolis

Trial	Subject D. S.			Subject T. H.			Subject R. P.		
	Cell	Profile	Gust	Cell	Profile	Gust	Cell	Profile	Gust
1	10	6	5	23	19	11	36	1	17
2	13	17	19	26	9	5	39	13	11
3	15	13	14	28	1	20	31	19	6
4	19	15	16	22	10	2	35	11	8
5	11	20	15	24	3	1	37	16	7
6	14	8	6	27	15	12	30	3	18
7	16	7	4	29	17	10	32	2	16
8	12	10	10	25	12	16	38	5	2
9	17	12	12	20	7	18	33	18	4
10	18	4	20	21	14	6	34	9	12
11	18	1	17	21	20	3	35	14	9
12	11	18	7	24	4	13	38	6	19
13	13	14	18	26	8	4	30	10	10
14	17	16	8	20	2	14	34	4	20
15	19	11	3	22	6	9	36	8	15
16	12	5	9	25	16	15	39	20	1
17	14	9	11	27	18	17	31	12	3
18	10	3	1	23	13	7	37	17	13
19	15	20	13	28	5	19	32	7	5
20	16	2	2	29	11	8	33	15	14

Table XXXV. Training Trial Sequences for  
 WPAFB

Trial	Subject D. S.			Subject R. K.			Subject W. S.		
	Cell	Profile	Gust	Cell	Profile	Gust	Cell	Profile	Gust
1	15	14	16	45	14	15	34	2	15
2	11	19	14	41	19	14	33	16	9
3	10	6	20	40	6	20	32	3	6
4	16	10	2	46	10	2	38	4	4
5	19	11	10	49	11	10	37	12	5
6	14	2	15	44	2	15	35	14	16
7	13	16	9	43	16	9	31	19	14
8	18	4	4	48	4	4	30	6	20
9	12	3	6	42	3	6	36	10	2
10	17	12	5	47	12	5	39	11	10
11	19	15	19	49	15	19	38	7	7
12	15	20	1	45	20	1	37	17	17
13	14	9	11	44	9	11	32	1	8
14	10	8	3	40	8	3	36	5	18
15	13	18	12	43	18	12	31	13	13
16	18	7	7	48	7	7	39	15	19
17	17	17	17	47	17	17	35	20	1
18	12	1	8	42	1	8	34	9	11
19	16	5	18	46	5	18	30	8	3
20	11	13	13	41	13	13	33	18	12

DATA TRIAL SEQUENCES FOR MINNEAPOLIS  
AND WPAFB (3 SUBJECTS)

Table XXXVI. Data Session Sequences for Subject  
W.S. at WPAFB

Trial	Session														
	1			2			3			4			5		
	Cell	Profile	Gust	Cell	Profile	Gust	Cell	Profile	Gust	Cell	Profile	Gust	Cell	Profile	Gust
1	34	10	3	38	9	9	34	3	1	30	6	5	37	18	12
2	33	20	17	37	19	3	39	18	15	33	17	18	36	3	6
3	31	18	12	35	15	18	37	14	10	35	13	14	31	14	1
4	30	2	14	34	1	20	35	16	12	39	15	16	35	16	3
5	39	18	13	33	17	19	33	11	11	31	20	15	30	5	2
6	38	1	4	32	10	10	31	13	2	34	8	6	38	4	13
7	32	4	2	36	3	8	38	5	20	36	7	4	34	7	11
8	35	13	8	39	12	14	36	4	6	32	10	10	33	11	17
9	37	15	10	31	14	16	30	7	8	37	12	12	39	13	19
10	36	8	18	30	7	4	32	1	16	38	4	20	32	1	7
11	36	5	15	37	20	1	36	8	13	38	1	17	33	19	4
12	35	11	5	36	4	11	31	19	3	31	18	7	32	8	14
13	33	17	16	34	8	2	39	15	14	33	14	18	37	15	5
14	32	9	6	33	16	12	37	17	4	37	16	8	31	17	15
15	31	19	1	32	2	7	35	12	19	39	11	3	36	2	10
16	30	3	7	31	18	13	33	20	5	32	5	9	34	6	16
17	34	7	9	35	13	15	30	2	7	34	9	11	30	10	8
18	37	14	19	38	6	5	38	6	17	30	3	1	39	12	8
19	39	12	11	30	5	17	32	10	9	35	20	13	35	11	20
20	38	6	20	39	11	6	34	9	18	36	2	2	38	9	9

Table XXXVII. Data Session Sequences for Subject R.K.  
at WPAFB

Trial	Session														
	1			2			3			4			5		
	Cell	Profile	Gust	Cell	Profile	Gust	Cell	Profile	Gust	Cell	Profile	Gust	Cell	Profile	Gust
1	42	10	10	44	8	17	48	1	4	46	9	5	40	3	18
2	46	3	8	48	1	15	42	4	2	40	2	3	48	2	16
3	49	12	14	41	15	1	45	13	8	43	17	9	48	5	2
4	41	14	16	43	17	3	47	15	10	45	19	11	43	18	4
5	40	7	4	42	5	11	46	8	18	44	6	19	44	9	12
6	48	9	9	40	7	18	44	10	3	42	8	4	46	1	17
7	47	19	3	49	12	10	43	20	17	41	14	18	49	13	11
8	45	15	18	47	18	5	41	16	12	49	20	13	41	19	6
9	44	1	20	46	9	7	40	2	14	48	10	15	45	11	8
10	43	17	19	45	20	6	48	18	13	47	12	14	47	16	7
11	41	18	13	43	11	20	40	3	7	49	13	8	49	20	1
12	45	13	15	47	16	2	44	7	9	43	18	10	41	12	3
13	48	6	5	40	4	12	47	14	19	46	5	20	47	17	13
14	40	5	17	42	3	4	49	12	11	48	4	12	42	7	5
15	49	11	6	41	14	13	48	6	20	47	16	1	43	15	14
16	47	20	1	49	13	8	46	5	15	45	15	16	45	14	9
17	46	4	11	48	2	18	45	11	5	44	3	6	46	6	19
18	44	8	2	46	6	9	43	17	16	42	7	17	40	10	10
19	43	16	12	45	19	19	42	9	6	41	11	7	44	4	20
20	42	2	7	44	10	14	41	19	1	40	1	2	46	8	15

Table XXXVIII. Data Session Sequences for Subject D.S. at WPAFB

Trial	Session														
	1			2			3			4			5		
	Cell	Profile	Gust	Cell	Profile	Gust	Cell	Profile	Gust	Cell	Profile	Gust	Cell	Profile	Gust
1	13	15	11	10	1	19	18	4	13	17	13	8	17	15	12
2	19	20	9	16	4	17	14	7	11	13	18	6	19	17	10
3	18	10	15	15	13	3	13	11	17	12	8	12	15	12	16
4	14	4	17	11	15	5	19	13	19	18	2	14	10	7	18
5	17	12	5	14	8	13	12	1	7	11	20	2	11	14	6
6	12	6	10	19	20	18	17	18	12	16	4	7	13	19	11
7	11	17	4	18	10	12	16	3	6	15	16	1	16	9	5
8	16	8	19	13	16	7	11	14	1	10	6	16	18	1	20
9	10	7	1	17	18	9	15	16	3	14	5	18	12	10	2
10	15	13	20	12	2	8	10	5	2	19	11	17	14	3	1
11	16	9	14	11	19	2	14	6	16	12	7	11	15	16	15
12	12	3	16	17	14	4	10	10	18	18	1	13	17	18	17
13	11	11	6	16	7	14	19	12	8	17	19	3	13	13	7
14	17	19	18	12	6	6	15	11	20	13	17	15	18	5	19
15	10	2	7	15	12	15	18	9	9	16	10	4	19	11	8
16	15	18	2	10	5	10	13	19	4	11	16	19	11	20	3
17	14	1	12	19	11	20	12	8	14	10	9	9	14	4	13
18	19	14	3	14	9	11	17	15	5	15	12	20	16	8	4
19	13	16	13	18	3	1	11	17	15	19	14	10	10	2	14
20	18	5	8	13	17	16	16	2	10	14	3	5	12	6	9

Table XXXIX. Data Session Sequences for Subject D.S. at Minneapolis

Trial	Session														
	1			2			3			4			5		
	Cell	Profile	Gust	Cell	Profile	Gust	Cell	Profile	Gust	Cell	Profile	Gust	Cell	Profile	Gust
1	14	3	1	18	1	2	15	12	19	11	11	8	17	14	13
2	19	18	15	13	13	16	10	7	13	16	5	2	12	8	7
3	17	14	10	11	19	11	18	9	8	14	7	17	10	10	2
4	15	16	12	19	11	13	16	8	10	12	6	19	18	9	4
5	13	11	11	17	16	12	14	1	9	10	8	18	16	2	3
6	11	13	2	15	18	3	12	5	20	18	3	9	14	6	14
7	18	5	20	12	3	1	19	18	18	15	17	7	11	20	12
8	16	4	6	10	2	7	17	20	4	13	19	13	19	12	18
9	10	7	8	14	5	9	11	15	6	17	14	15	13	17	20
10	12	1	16	16	9	17	13	17	14	19	16	3	15	19	8
11	16	8	13	12	6	14	19	13	11	10	10	20	13	15	5
12	11	19	3	17	14	4	14	2	1	15	12	10	18	3	15
13	19	15	14	15	20	15	12	6	12	13	18	1	16	7	6
14	17	17	4	13	12	5	10	10	2	11	20	11	14	1	16
15	15	12	19	11	17	20	18	4	17	19	15	6	12	5	11
16	13	20	5	19	15	6	16	3	3	17	13	12	10	4	17
17	10	2	7	16	10	8	13	19	5	14	4	14	17	11	19
18	18	6	17	14	4	18	11	11	15	12	8	4	15	13	9
19	12	10	9	18	8	10	15	16	7	16	2	16	19	18	1
20	14	9	18	10	7	19	17	14	16	18	1	5	11	16	10

Table XL. Data Session Sequences for Subject R.P.  
at Minneapolis

Trial	Session														
	1			2			3			4			5		
	Cell	Profile	Gust	Cell	Profile	Gust	Cell	Profile	Gust	Cell	Profile	Gust	Cell	Profile	Gust
1	30	7	16	31	11	20	32	8	4	38	9	9	34	10	3
2	39	12	10	30	5	14	31	14	18	37	19	3	33	20	17
3	37	18	5	38	7	9	39	20	13	35	15	18	31	16	12
4	36	9	7	37	17	11	38	10	15	34	1	20	30	2	14
5	35	20	6	36	6	10	37	12	14	33	17	19	39	18	13
6	34	8	17	35	19	1	36	9	5	32	10	10	38	1	4
7	38	1	15	39	14	19	30	2	3	36	3	8	32	4	2
8	31	15	1	32	9	5	33	17	9	39	12	14	35	13	8
9	33	17	3	34	3	7	35	19	11	31	14	16	37	15	10
10	32	5	11	33	16	15	34	6	19	30	7	4	36	8	18
11	39	13	8	33	12	12	35	15	16	37	20	1	36	5	15
12	38	2	18	32	10	2	34	3	6	36	4	11	35	11	5
13	36	6	9	30	4	13	32	7	17	34	8	2	33	17	16
14	35	19	19	39	18	3	31	11	7	33	16	12	32	9	6
15	34	10	14	38	8	18	30	1	2	32	2	7	31	19	1
16	33	11	20	37	20	4	39	13	8	31	18	13	30	3	7
17	37	16	2	31	15	6	33	18	10	35	13	15	34	7	9
18	30	4	12	34	2	16	36	5	20	38	6	5	37	14	19
19	32	3	4	36	1	8	38	4	12	30	5	17	39	12	11
20	31	14	13	35	13	17	37	16	1	39	11	6	38	6	20

Table XLI. Data Session Sequences for Subject T.H.  
at Minneapolis

Trial	Session														
	1			2			3			4			5		
	Cell	Profile	Gust	Cell	Profile	Gust	Cell	Profile	Gust	Cell	Profile	Gust	Cell	Profile	Gust
1	29	20	18	24	2	15	26	4	7	22	6	10	27	18	12
2	28	10	12	23	16	9	25	15	1	21	17	4	26	3	6
3	23	16	7	28	4	4	20	6	16	26	8	19	21	14	1
4	27	18	9	22	3	6	24	5	18	20	7	1	25	16	3
5	22	2	8	27	12	5	29	11	17	25	13	20	20	5	2
6	20	1	19	25	14	16	27	13	8	23	15	11	28	4	13
7	26	4	17	21	19	14	23	18	6	29	20	9	24	7	11
8	25	13	3	20	6	20	22	8	12	28	10	15	23	11	17
9	21	15	5	26	10	2	28	2	14	24	4	17	29	13	19
10	24	8	13	29	11	10	21	20	2	27	12	5	22	1	7
11	20	5	10	28	7	7	21	16	19	25	18	2	23	19	4
12	28	11	20	27	17	17	20	9	9	24	1	12	22	8	14
13	24	9	11	22	1	8	25	12	20	29	14	3	27	15	5
14	28	3	1	26	5	18	29	14	10	23	16	13	21	17	15
15	23	17	16	21	13	13	24	3	5	28	5	8	26	2	10
16	21	19	2	29	15	19	22	7	11	26	9	14	24	6	16
17	27	14	4	25	20	1	28	1	13	22	3	16	20	10	18
18	26	7	14	24	9	11	27	19	3	21	11	6	29	12	8
19	22	6	6	20	8	3	23	17	15	27	19	18	25	11	20
20	25	12	15	23	18	12	26	10	4	20	2	7	28	9	9

APPENDIX X

EXPERIENCE QUESTIONNAIRE, AND GLOBAL AND COOPER-HARPER  
RATING SCALES ADMINISTERED TO ALL SUBJECTS AT MINNEAPOLIS,  
WPAFB (3 SUBJECTS), AND WPAFB (4 SUBJECTS)

Date \_\_\_\_\_

Name \_\_\_\_\_ Age \_\_\_\_\_

Address \_\_\_\_\_ Phone \_\_\_\_\_

\_\_\_\_\_

Highest Military Rank \_\_\_\_\_

Current Job Title \_\_\_\_\_

FLYING HISTORY

Type of Aircraft	No. of Total Hours/ No. of Instrument Hours	Currently Qualified? (Yes/No)
1. _____	_____	_____
2. _____	_____	_____
3. _____	_____	_____
4. _____	_____	_____
5. _____	_____	_____
6. _____	_____	_____



# Contrails

Answer the following questions in order:

## HANDLING QUALITIES

	Yes	No	
1. Is the vehicle controllable during this task?	<input type="checkbox"/>	<input type="checkbox"/>	0 1 - Excellent
2. Is the vehicle acceptable for the task? (May have deficiencies which warrant improvement, but is adequate for the task.)	<input type="checkbox"/>	<input type="checkbox"/>	2 - Highly Desirable 3 - Good, Pleasant
3. Is the vehicle satisfactory for the task? (i.e., adequate for the task without improvement.)	<input type="checkbox"/>	<input type="checkbox"/>	4 - Fair 5 - Bad 6 - Very Bad 7 - Nearly Uncontrollable
			8 9 10 <input type="checkbox"/> Uncontrollable

# Contrails

## RESPONSE CHARACTERISTICS

## CONTROL

- 0
- 1 - Excellent, pure (i.e., no accidental excitation) primary and secondary response characteristics
- 2
- 3
- 4 - Good, relatively pure, primary and secondary response characteristics
- 5
- 6 - { Fair, somewhat impure, primary or secondary response characteristics
- 7 - { Quite sensitive, sluggish, or uncomfortable in primary or secondary responses
- 8 - { Extremely sensitive, sluggish, or uncomfortable in primary or secondary responses
- 9 - Nearly uncontrollable

- 0
- 1 - Extremely easy to control with excellent precision
- 2
- 3 - Very easy to control with good precision
- 4
- 5 - Easy to control with fair precision
- 6 - { Controllable with somewhat inadequate precision
- 7 - { Controllable, but only very imprecisely
- 8 - Difficult to control
- 9 - Very difficult to control

10  Uncontrollable

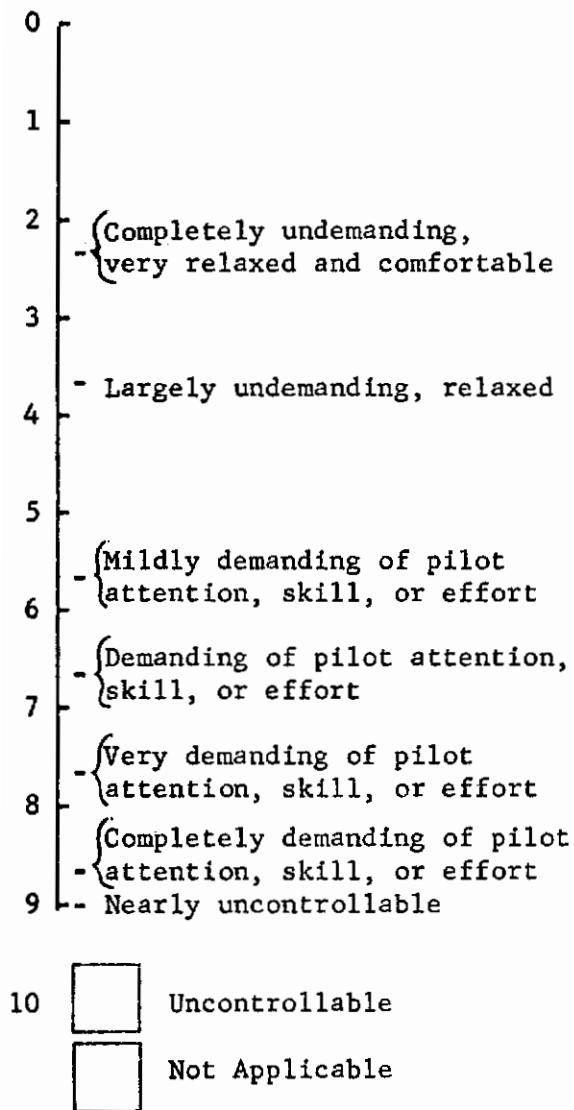
Not Applicable

10  Uncontrollable

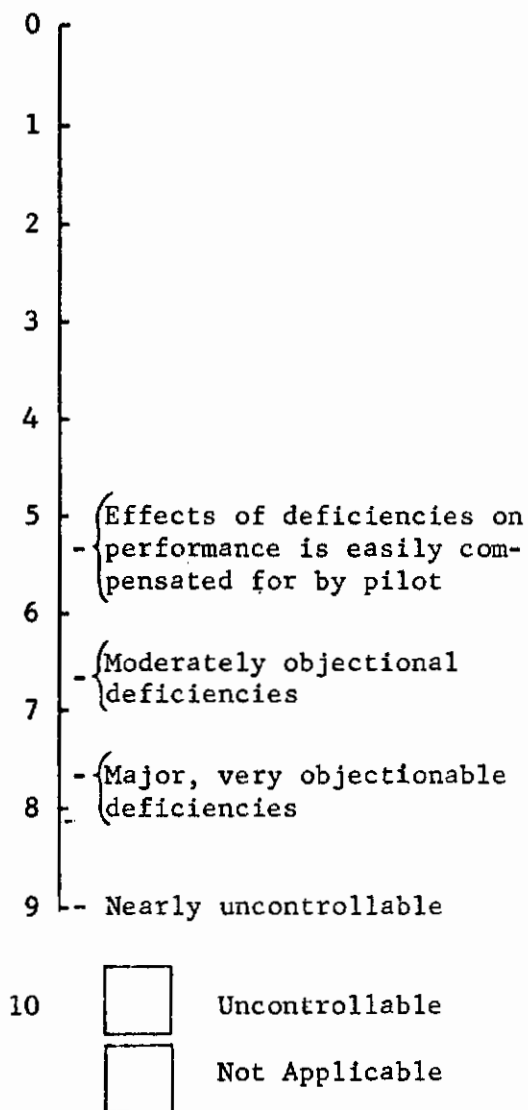
Not Applicable

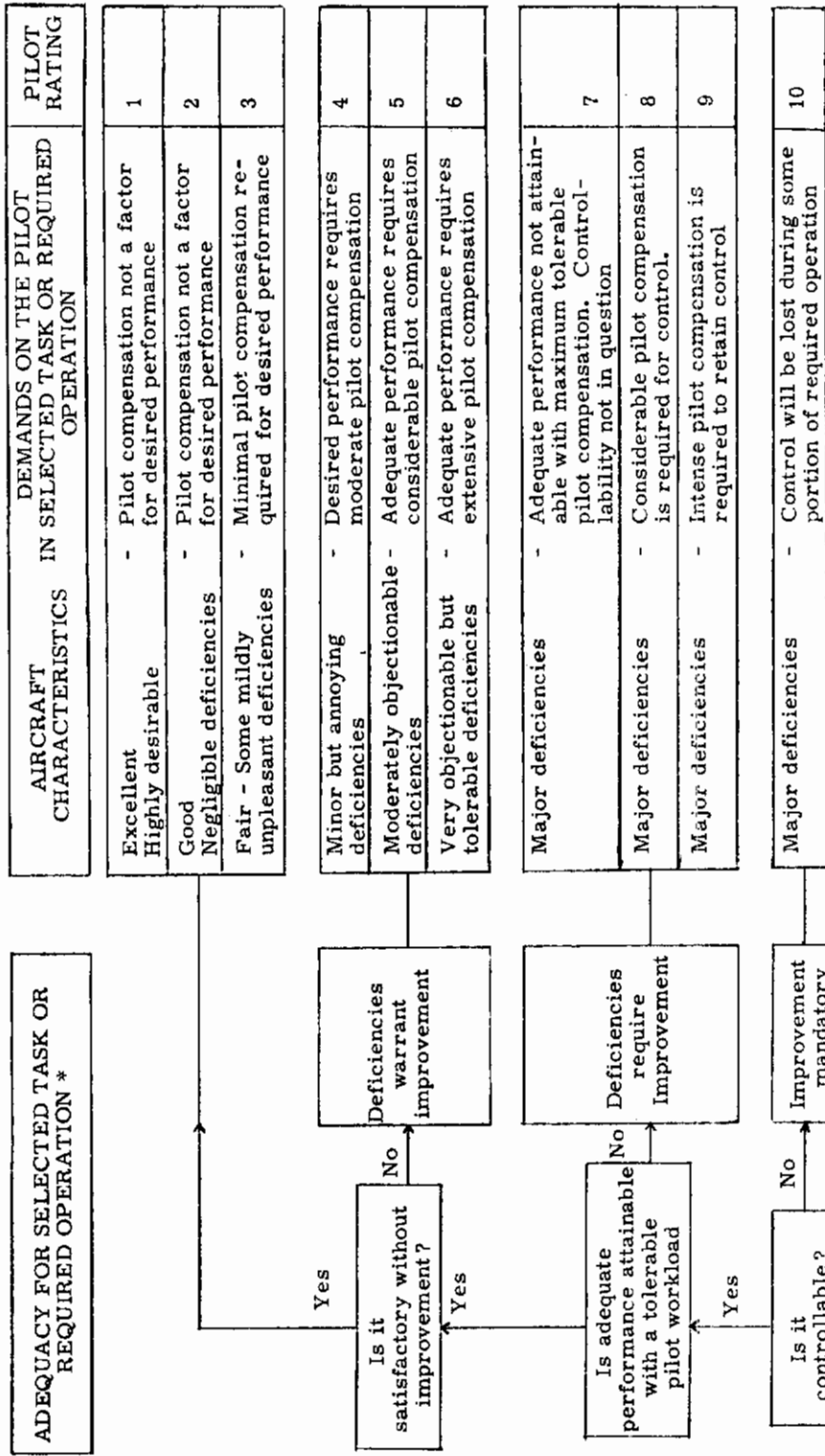
# Contrails

## DEMANDS ON PILOT



## EFFECTS OF DEFICIENCIES





\* Definition of required operation involves designation of flight phase and/or subphases with accompanying conditions.

## APPENDIX XI RAW PILOT RATING DATA

This appendix contains the raw rating data for the Global scale and the Cooper-Harper scale at Minneapolis, WPAFB (3 subjects) and WPAFB (4 subjects). The missing table entries for the Global scale are due to the pilot's lack of response, not misplaced data.

Table XLII. Raw Pilot Rating Data -- WPAFB (3 Subjects)  
(Two Observations/System, Speed, Subject)

System	Speed	Subject	Questions			Handling Qualities	Response Characteristics	Control	Demands on Pilot	Effects of Deficiencies	Cooper-Harper Ratings
			(1) Controllable?	(2) Acceptable?	(3) Satisfactory?						
1	Low	D.S.	Yes	No	No	8.8	8.6	8.9	8.8	8.9	9.0
		R.K.	Yes	No	No	8.9	8.8	8.9	8.9	9.0	9.0
		W.S.	Yes	No	No	6.5	6.7	7.0	6.2	7.0	6.0
		W.S.	Yes	No	No	8.7	7.8	8.0	8.4	8.2	7.6
1	High	D.S.	Yes	No	No	7.7	7.9	8.3	9.7	8.2	9.0
		R.K.	Yes	No	No	8.0	7.8	7.9	8.3	7.8	9.0
		W.S.	Yes	No	No	7.8	7.2	8.0	7.1	7.6	7.0
		W.S.	Yes	No	No	8.0	7.7	7.9	8.6	8.3	7.0
2	Low	D.S.	Yes	No	No	7.6	6.7	7.1	6.8	6.9	6.0
		R.K.	Yes	No	No	5.7	7.0	7.2	7.2	7.2	6.0
		W.S.	Yes	No	No	6.8	6.7	6.5	5.9	6.8	6.0
		W.S.	Yes	Yes	No	7.7	6.7	6.8	6.6	7.4	6.0
2	High	D.S.	Yes	Yes	No	5.3	5.2	4.7	5.5	4.7	3.0
		R.K.	Yes	Yes	Yes	3.7	4.3	5.2	6.2	5.3	4.0
		W.S.	Yes	No	No	6.6	7.0	7.0	6.3	7.0	6.0
		W.S.	Yes	No	No	7.7	7.0	7.0	7.4	7.6	7.0
3	Low	D.S.	Yes	No	No	6.9	6.5	6.5	6.9	7.1	5.0
		R.K.	Yes	Yes	No	7.7	7.7	7.8	8.5	7.6	7.0
		W.S.	Yes	Yes	No	5.2	6.7	6.3	5.7	4.4	4.0
		W.S.	Yes	Yes	Yes	5.3	4.9	5.2	4.7	4.4	4.0
3	High	D.S.	Yes	Yes	No	1.8	1.0	0.9	2.4	2.2	1.0
		R.K.	Yes	Yes	Yes	2.5	1.5	1.8	3.7	3.5	2.0
		W.S.	Yes	Yes	Yes	5.3	6.4	6.1	5.0	5.8	5.0
		W.S.	Yes	Yes	No	3.6	5.2	4.7	4.0	3.2	3.0
4	Low	D.S.	Yes	Yes	Yes	5.3	5.2	6.3	6.1	5.3	4.0
		R.K.	Yes	Yes	Yes	1.2	1.1	1.6	2.0	2.5	2.0
		W.S.	Yes	Yes	No	4.0	4.3	5.0	4.5	5.2	4.0
		W.S.	Yes	Yes	Yes	6.7	6.1	6.4	5.9	5.8	4.0
4	High	D.S.	Yes	Yes	Yes	3.2	3.2	3.1	3.6	4.8	3.0
		R.K.	Yes	Yes	Yes	4.2	3.8	4.7	4.2	5.0	4.0
		W.S.	Yes	Yes	Yes	2.4	2.0	1.9	2.8	2.8	2.0
		W.S.	Yes	Yes	Yes	1.9	1.2	1.5	1.8	1.6	1.6
5	Low	D.S.	Yes	Yes	Yes	3.2	3.2	3.2	3.3	3.3	2.0
		R.K.	Yes	Yes	Yes	2.3	1.8	1.2	1.8	2.3	1.0
		W.S.	Yes	Yes	No	3.7	5.2	4.7	4.3	4.3	3.0
		W.S.	Yes	Yes	Yes	3.9	4.0	4.7	3.7	4.0	4.0
5	High	D.S.	Yes	Yes	Yes	3.0	3.0	2.7	3.5	3.0	3.0
		R.K.	Yes	Yes	Yes	3.0	3.0	3.7	3.7	10.0	3.0
		W.S.	Yes	Yes	Yes	4.3	3.9	4.7	5.5	4.7	3.0
		W.S.	Yes	Yes	Yes	3.5	3.9	3.8	3.8	5.2	3.0
5	Low	D.S.	Yes	Yes	Yes	2.0	2.0	2.0	2.5	3.0	2.0
		R.K.	Yes	Yes	Yes	2.3	1.7	1.7	2.3	2.0	2.0
		W.S.	Yes	Yes	Yes	4.3	5.0	4.4	5.0	5.0	4.0
		W.S.	Yes	Yes	Yes	3.0	3.0	2.7	3.7	10.0	2.5

**Table XLIII. Raw Pilot Rating Data -- Minneapolis  
(3 Subjects) (Two Observations/System,  
Speed, Subject)**

System	Speed	Subject	Questions			Handling Qualities	Response Character- istics	Control	Demands on Pilot	Effects on Deficiencies	Cooper- Harper Ratings
			(1) Controllable ?	(2) Acceptable ?	(3) Satisfactory ?						
1	Low	D. S.	Yes	No	No	8.9	8.6	8.3	8.7	8.8	9.0
		T. H.	Yes	No	No	8.9	8.8	9.0	9.0	9.0	9.0
		R. P.	Yes	No	No	7.7	7.3	7.2	7.7	7.8	8.0
			Yes	No	No	7.7	7.7	7.7	7.7	7.7	8.0
			Yes	No	No	7.6	7.4	8.3	7.3	9.8	8.0
Yes	No	No	7.7	8.6	8.7	9.0	9.2	10.0			
1	High	D. S.	Yes	No	No	8.9	8.9	8.9	8.9	8.9	9.0
		T. H.	Yes	No	No	9.0	8.8	8.8	8.9	8.9	9.0
		R. P.	Yes	No	No	8.7	8.0	8.0	8.7	8.6	9.0
			Yes	No	No	7.0	6.6	7.5	7.2	7.5	7.0
			No	No	No	10.0	8.9	9.0	8.7	8.9	10.0
No	No	No	8.7	8.7	10.0	9.0	9.0	10.0			
2	Low	D. S.	Yes	No	No	8.7	8.0	8.3	8.7	7.9	8.0
		T. H.	Yes	Yes	No	6.3	6.9	6.8	7.3	7.5	6.0
		R. P.	Yes	No	No	6.6	6.7	6.0	6.7	7.0	7.0
			Yes	No	No	5.3	5.7	6.2	5.7	7.0	5.0
			Yes	Yes	Yes	2.3	2.4	2.5	3.6	4.8	3.0
Yes	No	No	7.0	6.7	7.2	7.5	6.8	7.0			
2	High	D. S.	Yes	Yes	Yes	3.9	4.9	4.2	4.1	4.8	3.0
		T. H.	Yes	Yes	---	5.3	6.6	7.2	6.9	7.2	7.0
		R. P.	Yes	Yes	No	5.3	5.7	4.7	5.7	8.7	4.0
			Yes	Yes	No	5.3	5.7	6.3	6.7	7.0	5.0
			Yes	Yes	No	5.3	6.6	6.1	6.6	6.6	6.0
Yes	No	No	8.6	7.6	8.3	7.9	8.0	8.0			
3	Low	D. S.	Yes	Yes	Yes	4.7	5.5	6.1	6.1	8.3	5.0
		T. H.	Yes	Yes	No	5.7	5.9	5.8	5.9	8.1	4.0
		R. P.	Yes	Yes	Yes	4.0	3.7	3.7	5.0	5.3	3.0
			Yes	Yes	Yes	2.3	3.0	2.7	3.0	2.0	2.0
			Yes	Yes	Yes	1.1	0.7	0.7	1.4	1.5	1.0
Yes	Yes	Yes	5.5	5.2	6.3	6.6	5.9	4.0			
3	High	D. S.	Yes	Yes	Yes	4.9	6.0	6.3	6.7	8.9	4.0
		T. H.	Yes	Yes	Yes	4.6	4.9	6.2	5.9	5.3	3.0
		R. P.	Yes	Yes	Yes	4.0	4.5	3.6	5.0	5.3	3.0
			Yes	Yes	Yes	3.7	4.0	3.0	3.8	5.3	3.0
			Yes	Yes	Yes	2.9	4.3	2.3	3.0	4.5	3.0
Yes	Yes	Yes	2.3	3.4	2.6	3.4	5.3	3.0			
4	Low	D. S.	Yes	Yes	No	5.2	6.2	6.5	7.2	7.1	4.0
		T. H.	Yes	Yes	Yes	7.5	6.8	7.5	7.2	7.2	6.0
		R. P.	Yes	Yes	Yes	3.7	3.7	2.7	3.7	4.7	3.0
			Yes	Yes	Yes	3.7	5.3	4.7	5.7	5.7	3.0
			Yes	Yes	Yes	2.7	2.7	1.8	4.8	4.6	3.0
Yes	Yes	Yes	0.3	0.2	0.1	0.4	0.2	1.0			
4	High	D. S.	Yes	Yes	Yes	2.9	3.2	2.3	3.5	4.8	2.0
		T. H.	Yes	Yes	Yes	5.5	6.7	6.4	5.6	8.0	5.0
		R. P.	Yes	Yes	Yes	1.0	0.7	1.0	2.0	2.0	1.0
			Yes	Yes	Yes	3.0	4.0	3.5	4.0	4.0	3.0
			Yes	Yes	Yes	1.1	0.8	0.5	1.7	1.5	1.0
Yes	Yes	No	3.6	5.7	6.1	6.6	6.3	4.0			
5	Low	D. S.	Yes	Yes	No.	5.3	5.7	6.6	5.7	6.8	5.0
		T. H.	Yes	Yes	Yes	1.4	1.3	1.2	2.2	2.7	1.0
		R. P.	Yes	Yes	Yes	3.0	3.7	3.4	4.7	6.0	4.0
			Yes	Yes	Yes	3.0	5.0	3.6	5.0	4.0	3.0
			Yes	Yes	Yes	0.2	0.2	0.2	0.3	0.3	1.0
Yes	Yes	Yes	0.8	1.2	1.0	2.0	1.8	1.0			
5	High	D. S.	Yes	Yes	Yes	2.3	2.7	6.2	6.7	4.9	1.0
		T. H.	Yes	Yes	No	4.7	4.5	2.6	3.3	6.3	5.0
		R. P.	Yes	Yes	Yes	2.0	2.0	2.7	3.0	4.0	2.0
			Yes	Yes	Yes	3.0	4.0	3.0	3.7	3.0	2.0
			Yes	Yes	Yes	1.3	2.2	1.2	2.3	2.3	2.0
Yes	Yes	Yes	0.3	1.0	0.6	1.9	0.4	1.0			



**Table XLIV. Raw Pilot Rating Data -- WPAFB (4 Subjects)  
(Two Observations/System, Speed, Subject)**

System	Speed	Subject	Questions			Handling Qualities	Response Characteristics	Control	Demands on Pilot	Effects of Deficiencies	Cooper-Harper Ratings
			(1) Controllable?	(2) Acceptable?	(3) Satisfactory?						
1	Low	R. E.	Yes	Yes	No	5.0	6.3	6.8	7.4	6.3	5.5
		T. H.	Yes	Yes	No	5.0	7.0	6.0	7.0	6.0	6.0
		D. Z.	Yes	Yes	No	8.7	8.3	8.6	8.5	8.1	8.5
		J. S.	No	No	No	9.9	10.0	10.0	9.0	10.0	10.0
		J. S.	Yes	Yes	Yes	5.8	6.3	6.3	5.6	7.2	8.0
J. S.	Yes	Yes	---	7.0	7.0	7.0	7.0	7.0	7.0	6.0	
1	High	R. E.	Yes	Yes	No	5.0	6.3	6.6	6.0	6.0	5.0
		T. H.	Yes	Yes	No	4.5	5.7	5.5	6.4	5.8	5.5
		D. Z.	Yes	Yes	Yes	5.8	6.0	6.2	6.2	6.6	5.0
		J. S.	Yes	Yes	Yes	6.4	6.3	6.2	6.3	6.8	5.0
		J. S.	Yes	No	No	7.0	6.8	7.1	7.7	7.6	8.0
J. S.	Yes	No	No	7.7	7.6	8.0	8.2	8.0	9.0		
J. S.	Yes	Yes	---	5.0	5.7	5.7	6.3	6.3	7.0		
J. S.	Yes	Yes	---	6.0	7.0	6.7	6.4	7.0	7.8		
2	Low	R. E.	Yes	Yes	No	5.0	6.0	6.0	6.0	6.0	5.0
		T. H.	Yes	Yes	Yes	3.0	4.0	3.5	4.4	2.3	3.0
		D. Z.	Yes	Yes	Yes	4.0	3.8	4.3	4.8	5.0	3.0
		J. S.	Yes	Yes	Yes	4.6	5.2	5.4	5.5	5.9	3.0
		J. S.	Yes	No	No	7.4	7.7	7.9	8.4	7.9	9.0
J. S.	Yes	Yes	No	6.0	6.7	6.6	6.5	6.8	7.0		
J. S.	Yes	---	Yes	3.0	5.0	4.0	5.0	6.0	4.0		
J. S.	Yes	Yes	---	4.5	4.0	4.0	4.0	5.0	3.0		
2	High	R. E.	Yes	Yes	Yes	4.0	4.0	5.0	4.0	2.0	3.5
		T. H.	Yes	Yes	Yes	4.0	5.0	5.0	6.0	5.0	5.0
		D. Z.	Yes	Yes	Yes	5.2	5.7	5.6	5.3	6.1	4.0
		J. S.	Yes	Yes	Yes	5.0	5.4	6.0	6.7	6.2	4.0
		J. S.	Yes	No	No	7.0	7.5	7.0	6.9	7.7	8.0
J. S.	Yes	Yes	Yes	5.4	5.8	6.0	5.9	6.1	4.0		
J. S.	Yes	Yes	---	3.8	3.0	4.0	3.7	6.0	3.0		
J. S.	Yes	---	Yes	3.5	3.0	3.0	4.0	4.0	2.0		
3	Low	R. E.	Yes	Yes	No	4.0	5.0	5.0	3.0	5.0	4.0
		T. H.	Yes	Yes	No	4.5	5.7	5.0	5.0	3.0	5.0
		D. Z.	Yes	Yes	Yes	3.8	3.5	3.0	3.8	4.4	2.0
		J. S.	Yes	Yes	Yes	2.3	2.0	2.3	2.3	4.5	1.0
		J. S.	Yes	Yes	Yes	4.3	5.5	5.0	5.6	5.0	3.0
J. S.	Yes	Yes	Yes	3.9	4.0	4.0	4.0	4.0	3.0		
J. S.	Yes	---	Yes	1.6	2.5	1.2	2.0	5.0	2.0		
J. S.	Yes	---	Yes	3.0	3.0	2.5	2.0	3.0	2.0		
3	High	R. E.	Yes	Yes	Yes	3.0	2.5	2.0	2.0	4.0	2.0
		T. H.	Yes	Yes	No	4.2	5.0	5.0	5.0	3.0	5.0
		D. Z.	Yes	Yes	Yes	3.0	3.3	2.9	3.8	4.8	2.0
		J. S.	Yes	Yes	Yes	3.4	3.1	3.0	3.5	4.3	3.0
		J. S.	Yes	Yes	Yes	4.3	4.0	5.0	5.7	5.3	3.0
J. S.	Yes	Yes	Yes	5.0	5.5	6.0	5.7	5.7	4.0		
J. S.	Yes	---	Yes	3.7	4.0	3.8	3.7	6.0	4.0		
J. S.	Yes	Yes	Yes	5.0	5.0	4.0	5.0	4.0	2.0		
4	Low	R. E.	Yes	Yes	Yes	2.0	3.0	3.0	2.3	1.0	2.0
		T. H.	Yes	Yes	Yes	2.0	2.0	2.0	2.0	1.0	2.0
		D. Z.	Yes	Yes	Yes	5.3	5.2	5.7	5.5	6.2	4.0
		J. S.	Yes	Yes	Yes	2.1	1.6	1.4	2.7	4.2	1.0
		J. S.	Yes	Yes	Yes	4.0	4.5	4.9	5.0	5.0	3.0
J. S.	Yes	Yes	Yes	4.2	4.0	4.5	5.0	5.0	4.0		
J. S.	Yes	---	Yes	1.0	1.0	1.0	2.0	5.0	1.0		
J. S.	Yes	---	Yes	2.0	2.0	1.0	2.0	2.0	3.0		
4	High	R. E.	Yes	Yes	Yes	3.0	3.0	3.0	3.0	1.0	2.5
		T. H.	Yes	Yes	Yes	1.0	1.0	1.0	2.0	0.4	1.0
		D. Z.	Yes	Yes	Yes	5.3	5.2	5.6	5.4	6.0	4.0
		J. S.	Yes	Yes	Yes	4.3	4.3	4.5	4.1	5.8	3.0
		J. S.	Yes	Yes	No	5.3	5.7	6.3	6.0	6.8	5.0
J. S.	Yes	Yes	Yes	5.0	5.2	5.7	5.3	5.2	3.0		
J. S.	Yes	---	Yes	2.0	2.0	2.7	3.0	5.0	2.0		
J. S.	Yes	Yes	---	3.7	4.7	4.0	4.0	6.0	4.0		
5	Low	R. E.	Yes	Yes	Yes	2.0	2.0	2.0	2.0	1.0	2.5
		T. H.	Yes	Yes	Yes	4.0	5.0	4.0	3.7	2.0	3.0
		D. Z.	Yes	Yes	Yes	3.6	3.7	4.7	4.8	5.0	3.0
		J. S.	Yes	Yes	Yes	2.2	2.2	2.3	2.8	4.0	2.0
		J. S.	Yes	Yes	Yes	4.0	5.0	5.0	5.0	5.0	4.0
J. S.	Yes	Yes	Yes	3.8	4.0	4.6	4.5	4.0	3.0		
J. S.	Yes	---	Yes	3.0	3.0	2.7	3.0	5.0	3.0		
J. S.	Yes	---	Yes	1.6	2.0	2.0	2.0	3.0	2.0		
5	High	R. E.	Yes	Yes	Yes	4.0	3.0	5.0	4.0	2.0	3.0
		T. H.	Yes	Yes	Yes	3.0	4.0	4.0	4.5	2.0	4.0
		D. Z.	Yes	Yes	Yes	2.3	2.3	2.2	2.7	4.9	2.0
		J. S.	Yes	Yes	Yes	3.0	3.2	2.7	3.0	3.8	2.0
		J. S.	Yes	Yes	Yes	3.8	4.2	4.7	5.1	5.1	3.0
J. S.	Yes	Yes	Yes	4.0	4.0	4.0	4.0	4.0	3.0		
J. S.	Yes	Yes	---	4.1	4.0	4.0	3.8	6.0	4.0		
J. S.	Yes	Yes	---	3.0	4.0	4.0	5.0	5.0	4.0		

## REFERENCES

1. Anon., "Military Specification -- Flying Qualities of Piloted Airplanes," MIL-F-8785B (ASG), 7 August 1969.
2. Chalk, C.R.; Neal, T.P.; Harris, T.M.; Pritchard, F.E.; and Woodcock, R.J. Background Information and User Guide for MIL-F-8785B (ASG) "Military Specification -- Flying Qualities of Piloted Airplanes," Air Force Flight Dynamics Laboratory Technical Report No. AFFDL-TR-69-72, Wright-Patterson Air Force Base, Ohio, August 1969.
3. McRuer, D., et al., "Human Pilot Dynamics in Compensatory Systems," Air Force Flight Dynamics Laboratory Technical Report No. AFFDL-TR-65-15, Wright-Patterson Air Force Base, Ohio, July 1965.
4. McRuer, D., et al., "New Approaches to Human-Pilot/Vehicle Dynamic Analysis," Air Force Flight Dynamics Laboratory Technical Report No. AFFDL-TR-67-150, Wright-Patterson Air Force Base, Ohio, February 1968.
5. Stapleford, R.L., et al., "A Practical Optimization Design Procedure for Stability Augmentation Systems," Air Force Flight Dynamics Laboratory Technical Report No. AFFDL-TR-70-11, Wright-Patterson Air Force Base, Ohio, October 1970.
6. Ashkenas, I.L., "A Study of Conventional Airplane Handling-Quality Requirements, Part II: Lateral-Directional Oscillatory Handling Qualities," Air Force Flight Dynamics Laboratory Technical Report No. AFFDL-TR-65-138, Wright-Patterson Air Force Base, Ohio, November 1965.
7. Asseo, S.J., "Application of Optimal Control to Perfect Model-Following," J. Aircraft, Vol. 7, No. 4, July-August 1970.
8. Tyler, Jr., J.S. and Tuteur, F.B., "The Use of a Quadratic Performance Index to Design Multivariable Control Systems," IEEE Trans. on Automatic Control, Vol. AC-11, No. 1, January 1966.
9. Winsor, C.A. and Roy, R.J., "The Application of Specific Optimal Control to the Design of Desensitized Model-Following Control Systems," IEEE Trans. Auto. Control, Vol. AC-15, No. 3, June 1970.

## REFERENCES -- CONTINUED

10. Yore, E. E., "Application of Mark III-SOC to Multivariable Control Problems, Part IV. Optimal Decoupling Control Applied to the Lateral-Directional Axes of a Sweep-Wing Aircraft," Air Force Flight Dynamics Laboratory Technical Report No. AFFDL-TR-68-10, Wright-Patterson Air Force Base, Ohio, February 1968.
11. Athans, M., and Falb, P. L., Optimal Control. McGraw Hill, New York, N. Y., 1966, Chapter 9.
12. Ward, M. D., "Quadratic Computer Program Documentation," Research Memo No. MR10924, Honeywell Systems and Research Center, Minneapolis, Minnesota, June 1970.
13. Burris, P. M., and Bender, M. A., "Aircraft Load Alleviation and Mode Stabilization (LAMS)," Air Force Flight Dynamics Laboratory Technical Report No. AFFDL-TR-68-158, Wright-Patterson Air Force Base, Ohio, December 1968.
14. Axsater, S., "Suboptimal Time-Variable Feedback Control of Linear Dynamical Systems with Random Inputs," Int. J. Control, Vol. 4, No. 6, pp. 549-566, 1966.
15. Levine, W. S., and Athans, M., "On the Determination of the Optimal Constant Output Feedback Gains for Linear Multivariable Systems," IEEE Trans. Auto. Control, Vol. AC-15, No. 1, February 1970.
16. Skelton, G. B., "Best Fixed Gains for Several Plants," Research Memo No. MR 10668, Honeywell Systems and Research Center, Minneapolis, Minnesota, July 1969.
17. Ward, M. D. and Stein, G., "A Gradient Iteration Method for Fixed-Form Control," Research Memo No. MR10829, Honeywell Systems and Research Center, Minneapolis, Minnesota, October 1969.
18. Courant, Differential and Integral Calculus, New York: Interscience, 1947.
19. Scharmack, D. K., "An Initial Value Method for Trajectory Optimization," Advances in Control Systems, Vol. 5, C. T. Leondes, Editor, New York, Academic Press, 1967.
20. Konar, A. F., "Improved Iterative Algorithm for Solving the Lyapunov Equation," Honeywell Research Memo No. MR 10702, Honeywell Systems and Research Center, Minneapolis, Minnesota, June 1962.
21. Stein, G., "A Note on High-Speed Computation of Steady-State Solutions to Linear Differential Equations," Research Memo No. MR 10033, Honeywell Systems and Research Center, Minneapolis, Minnesota, July 1967.

## REFERENCES -- CONTINUED

22. Bridges, B.C., "Calculated Lateral-Directional Stability and Performance Characteristics of the F-4B/C/D/J and RF-4B/C Aircraft Plus the AN/ASA-32H Automatic Flight Control System," Report F935, McDonnell Aircraft Corp., May 1968 (revised September 1968).
23. Anon., McDonnell Aircraft Corp., Report F144, November 1966 (revised January 1967).
24. Edwards, A.L., Experimental Design in Psychological Research. New York: Holt, Rinehart and Winston, 1964.
25. Mudd, S.A., "The Treatment of Handling-Qualities Rating Data," Human Factors, 1969, 4, 321-330.
26. Ridgeway, J.E., "Analysis of Rating Scale Data," Human Factors, 1970, 1, 103-104.
27. Barrett, G.V.; Cobe, P.A.; Thornton, C.L.; and Kerber, H.E., "Barrett et al. Reply," Human Factors, 1970, 1, 104.
28. Winer, B.J., Statistical Principles in Experimental Design. New York: McGraw-Hill, 1962.
29. Scheffé, H.A., The Analysis of Variance, New York: Wiley, 1960.
30. Johnson, T.L., "The Aerodynamic Surface Location Problem in Optimal Control of Flexible Aircraft," Report ESL-R-387, Massachusetts Institute of Technology, June 1969.
31. Bisplinghoff, Ashley, Halfman, Aeroelasticity. Addison-Wesley Publishing Co. Inc., Reading, Massachusetts, 1955.
32. Wogtech, A.H. et al., "Model RF4C Calculated Moments of Inertia," Report 9803, McDonnell Douglas Aircraft Corp., April 1967.
33. Bovine, W.J. et al., "Model F/RF-4B/C Aerodynamic Derivatives," Report 9842, McDonnell Douglas Aircraft Corp., February 1964 (revised August 1968).
34. Yore, E. E., "Requirements of Minimum Backup Flight Control Systems," Air Force Flight Dynamics Laboratory Technical Report No. AFFDL-TR-70-48, Wright-Patterson Air Force Base, Ohio, October 1970.
35. O'Brien, P. D., "Application of Frequency Domain Optimization to Improve the Lateral Stability of the F-4 Aircraft," MS Thesis GGC/EE/69-12, School of Engineering, Air Force Institute of Technology, June 1969.

## REFERENCES -- CONCLUDED

36. Bryson, A.E. and Y.C. Ho, Applied Optimal Control, Waltham, Massachusetts: Blaisdell Publishing Co., 1969.
37. Zadeh, L.A., and C.H. Desoer, Linear Systems Theory, New York: McGraw-Hill Book Co., 1963.
38. Papoulis, A. Probability, Random Variables and Stochastic Processes, New York: McGraw-Hill Book Co., 1965.
39. Cooper, G.E. and Harper, R.P., Jr., "The Use of Pilot Rating in the Evaluation of Aircraft Handling Qualities." NASA TND-5153, April 1969.
40. McDonnell, J.D., "Pilot Rating Techniques for the Estimation and Evaluation of Handling Qualities." Air Force Flight Dynamics Laboratory Technical Report No. AFFDL-TR-68-76, Wright-Patterson Air Force Base, Ohio, December 1968.
41. Tobie, H.N., et al., "A New Longitudinal Handling Quality Criterion," presented at the 18th Annual National Aerospace Electronics Conference, 16-18 May 1966.



# *Contrails*



**DOCUMENT CONTROL DATA - R & D**

*(Security classification of title, body of abstract and indexing annotation must be entered when the overall report is classified)*

1. ORIGINATING ACTIVITY (Corporate author) Honeywell Inc., Systems and Research Center Research Department 2345 Walnut Street, Roseville, Minnesota 55113		2a. REPORT SECURITY CLASSIFICATION Unclassified	
		2b. GROUP N/A	
3. REPORT TITLE A DESIGN PROCEDURE AND HANDLING-QUALITY CRITERIA FOR LATERAL-DIRECTIONAL FLIGHT CONTROL SYSTEMS			
4. DESCRIPTIVE NOTES (Type of report and inclusive dates) Final Report - 17 October 1969 through 17 October 1970			
5. AUTHOR(S) (First name, middle initial, last name) Gunter Stein and Allen H. Henke			
6. REPORT DATE May 1971	7a. TOTAL NO. OF PAGES 273	7b. NO. OF REFS 40	
8a. CONTRACT OR GRANT NO. F33615-70-C-1190	9a. ORIGINATOR'S REPORT NUMBER(S) 12212-FR		
b. PROJECT NO. 8219			
c.	9b. OTHER REPORT NO(S) (Any other numbers that may be assigned this report) AFFDL-TR-70-152		
d.			

Approved for public release; distribution unlimited.

11. SUPPLEMENTARY NOTES	12. SPONSORING MILITARY ACTIVITY Air Force Systems Command Air Force Flight Dynamics Laboratory Flight Control Division Wright-Patterson AFB, Ohio 45433
-------------------------	--

13. ABSTRACT

This program develops a practical design procedure for aircraft augmentation systems based on quadratic optimal control technology and handling-quality-oriented cost functionals. The procedure is applied to the design of a lateral-directional control system for the F4C aircraft. The design criteria, design procedure, and final control system are validated with a program of formal pilot evaluation experiments. These use 5 x 2 x 3 mixed-design analysis of variance. A reformulated optimal model-following control problem is used as the cornerstone for the procedure. Design criteria are expressed as model differential equations satisfying available handling-quality data. The reformulation includes optimality over multiple flight conditions and constant gain and measurement realizability constraints. A computational algorithm is developed to solve the new optimization problem. The algorithm successfully handled 20th-order F4C lateral-axes dynamics and optimized five flight conditions simultaneously. The results of the validation experiments were fully positive with strong correlation between performance and pilot opinion data.

14. KEY WORDS	LINK A		LINK B		LINK C	
	ROLE	WT	ROLE	WT	ROLE	WT
Aircraft augmentation systems Practical controller optimal controller Quadratic optimal control technology Handling-quality criteria Lateral-directional control system F4C aircraft Analysis of variance Validation experiments Moving-base simulator Pilot opinion Cooper-Harper rating scale Global rating scale						